ASSESSING ATMOSPHERIC STABILITY IN THE LJUBLJANA BASIN AND VIPAVA VALLEY REGIONS USING RADON-222

Dafina Kikaj

Doctoral Dissertation
Jožef Stefan International Postgraduate School
Ljubljana, Slovenia

Supervisor: Prof. Dr. Janja Vaupotič, Jožef Stefan Institute, Ljubljana, Slovenia
Co-Supervisor: Dr. Scott Dudley Chambers, Australian Nuclear Science and Technology Organisation, Sydney, Australia

Evaluation Board:
Prof. Dr. Aleksander Zidanšek, Chair, Jožef Stefan International Postgraduate School and Jožef Stefan Institute, Ljubljana, Slovenia
Prof. Dr. Klemen Bergant, Member, Slovenian Environment Agency and University of Nova Gorica, Nova Gorica, Slovenia
Prof. Dr. Atsuyuki Sorimachi, Member, Fukushima Medical University, Fukushima, Japan

MEDNARODNA PODIPLOMSKA ŠOLA JOŽEFA STEFANA
JOŽEF STEFAN INTERNATIONAL POSTGRADUATE SCHOOL



Dafina Kikaj

ASSESSING ATMOSPHERIC STABILITY IN THE LJUBLJANA BASIN AND VIPAVA VALLEY REGIONS USING RADON-222

Doctoral Dissertation

DOLOČANJE STABILNOSTI OZRAČJA V LJUBLJANSKI KOTLINI IN VIPAVSKI DOLINI Z UPORABO ^{222}Rn

Doktorska disertacija

Supervisor: Prof. Dr. Janja Vaupotič

Co-Supervisor: Dr. Scott Dudley Chambers

Ljubljana, Slovenia, October 2020

To Aleksandra

"Protect our Earth today for her generation tomorrow"

Acknowledgments

I would like to express my appreciation for the guidance, support, and especially patience, to both my mentors Prof. Dr. Janja Vaupotič and Dr. Scott D. Chambers, over the four years of our academic adventure. Dear Janja, thank you for the dozens of hours that you spent teaching me from science to whatever. You were a great mentor on how to balance all the demands of professional life, and your cheerful "you can do it" moments kept me focused on the goal. Dear Scott, thank you for all your positive energy in each moment of these four years, thank you for constantly pushing me to expand the view of science, and finally thank you for being kind and making me feel important, at all times. I am especially grateful that we live in different time zones – it is great to write about concerns in the evening and get an answer already in the early morning. I also would like to thank the committee members: Prof. Dr. Aleksander Zidanšek, Prof. Dr. Klemen Bergant as well as Prof. Dr. Atsuyuki Sorimachi for evaluation of the thesis and all the suggestions to improve the final version of the dissertation.

I would like to express my gratitude to the head of Department of Environmental Sciences Prof. Dr. Milena Horvat and all my colleagues. I am grateful to Katarina Marković for our pleasant chats by the coffee machines. Big gratitude goes to Dr. Bor Kranjc and Dr. David Kocman for all the brainstorming, laughs and suggestions.

I would like to thank the staff of Institute of Radiochemistry and Radioecology at the University of Pannonia in Veszprém, Hungary for the collaborations, brainstorming and suggestions, especially Prof. Dr. Tibor Kovács.

I am very grateful to Prof. Dr. Klemen Bergant, Filip Štucin, Mateja Gjerek and Neva Pristov from the National Meteorological Service at the Slovenian Environment Agency (ARSO) for sharing the meteorology and air quality data of Ljubljana and Ajdovščina. I appreciate the permission and the assistance, provided by ARSO, by installing the weather instrument shelter for radon monitoring on their land.

Many thanks also to Dr. Matjaž Kobal from Aerosol d.o.o. for sharing the knowledge about the black carbon data and sharing results of their measurements in Ljubljana.

This work was conducted within the Department of Environmental Sciences at Jožef Stefan Institute and has been financially supported by the Slovenian Research Agency (research core funding No. P1-0143 and research project STRAP - Sources, transport and fate of persistent air pollutants in the environment of Slovenia, No. J1-1716) and from the Public Scholarship, Development, Disability and Maintenance Fund of the Republic of Slovenia (contract No. 11011-44/2016-18).

A special thanks goes to my dormitory friends: Tina Šegota, Jožef Šimenko, Melisa & Adnan Bekan, Dušan Sadiković, Jovan Ristov, and Sreten Davidov for their patience and kindness. Many matters – research and private ones – are always solved easily when you have someone who is ready to discuss it with you.

Finally, I would like to say a big thanks to two boys who were there always for me, in the happiest and the worst moments of my Ph.D. life: Adem Kikaj (my brother) and Marijan Bajić (my life partner). Nena and Adelina thanks for all the morning/evening phone chats and help without criticism. Last but not least, I would like to dedicate special

thanks to my baby girl Aleksandra for being there with me in time of completing Ph.D. thesis – your kicks made me the happiest human, you made it possible to finish the last stage of Ph.D. adventure with a lot of smiles.

Abstract

The atmospheric mixing state (or "stability") is of considerable interest because it is among the largest factors influencing air pollution variability, which has become a major global environmental issue. Diurnal timescale changes in the atmospheric mixing state, associated with daytime convection and the formation of nocturnal inversion layers, are known to strongly influence air quality in urban settings, which are home to 54% of the global population. However, the atmospheric mixing state in regions of complex topography (e.g. basin/valley environments) can also change on longer timescales (e.g. synoptic), as evident by persistent temperature inversion (PTI) conditions in non-summer months. PTI events can cause periods of high pollution concentrations that persist for many consecutive days. Common conventional meteorological techniques (e.g. Pasquill-Gifford schemes), more sophisticated stability classification methods (e.g. Richardson Number, Monin-Obukhov similarity), and even more recently-developed diurnal atmospheric stability classification techniques based on near-surface observations of the natural radioactive noble gas radon (^{222}Rn), are not capable of reliably identifying synoptic timescale changes of atmospheric stability in complex terrain for separate analysis.

Consequently, the emphasis of this research was placed on developing a novel radon-based technique to identify synoptic timescale changes in the atmospheric mixing state, and combining this with the existing diurnal radon based technique, to better characterise and understand the comparative atmospheric mixing states of two complex terrain environments in Slovenia (Ljubljana, an urban subalpine basin and Ajdovščina, a sub-Mediterranean town within Vipava Valley) on diurnal, synoptic, and seasonal timescales. This Ph.D. thesis consists of three main investigations.

Firstly, a novel radon-based tool is developed for identifying PTI conditions in topographic basin/valley environments, which is demonstrated to be more reliable in its characterization of meteorology and air quality during PTI events than the conventional pseudo-vertical temperature gradient method. Secondly, a contemporary diurnal radon-based technique was used to investigate relative changes in summer atmospheric stability at two selected sites. The obtained results showed that radon-based stability classification can consistently distinguish between subtle changes in atmospheric mixing state at the two observation sites with strongly contrasting topographic settings. Thirdly, PTI conditions identified by the new radon-based tool were assigned a new (separate) mixing class within the framework of the contemporary diurnal radon-based stability classification method. The combined diurnal and synoptic timescale radon-based mixing classification technique separated, for the first time, "uncontrollable" influences on pollution variability (i.e. meteorology, geographic setting, topographic effects, and cross boundary pollution) from controllable influences (e.g. source distributions and strength) in the urban Ljubljana Basin. The technique developed is universally applicable to non-coastal urban centers throughout Europe, as well as to other continental mid- to high-latitude regions (e.g. central North America).

Results of this Ph.D. study have demonstrated that radon-based methods of atmospheric mixing state classification in urban regions (of either simple or complex topographic settings) is simpler and more effective than pure meteorological approaches. Furthermore, they have provided a novel and consistent tool with which to account for both diurnal and synoptic timescale changes in the atmospheric mixing state of complex terrain, and how this impacts air quality. Based on the consistency and accuracy of novel radon-based atmospheric classification method developed, it is expected that it will prove to be a powerful tool for improved assessment of pollution mitigation measures, evaluating the performance of urban pollution models, and informing public health studies.

Povzetek

Premešanost ozračja ("stabilnost") spada med dejavnike, ki so najbolj odgovorni za nihanja onesnaženosti zraka, zato je predmet številnih raziskav, saj je onesnažen zrak pomembno globalno vprašanje. Znano je, da dnevne (24-urne) spremembe premešanosti ozračja, povezane z dnevno konvekcijo in tvorbo nočnih inverznih plasti, močno vplivajo na kakovost zraka v mestnih okoljih, kjer živi 54% svetovnega prebivalstva. Pri bolj kompleksnih topografijah (na primer kotlina/dolina) pa na premešanost ozračja vplivajo tudi daljše spremembe (sinoptične), kot lahko vidimo na pojavu dolgotrajne temperaturne inverzije (PTI) v ne-poletnih mesecih, ko so lahko v ozračju več dni visoke koncentracije onesnažil. Z različnimi tehnikami za klasifikacijo stabilnosti ozračja, od običajnih meteoroloških (na primer "Pasquill-Gifford schemes"), bolj izpopolnjenih (na primer "Richardson Number", "Monin-Obukhov similarity") ali novejših, ki temeljijo na dnevnih nihanjih koncentracije naravnega radioaktivnega žlahtnega plina radona (^{222}Rn), pri analizah ne moremo zanesljivo prepoznati sinoptičnih sprememb stabilnosti ozračja.

Zato je bil poudarek te raziskave na razvoju nove tehnike, ki bi na osnovi radona omogočila identifikacijo tudi sinoptičnih časovnih sprememb premešanosti ozračja, in jo združiti z obstoječo tehniko identifikacije premešanosti ozračja na osnovi dnevnih nihanj koncentracije radona. Da bi bolje opisali in razumeli stanje premešanosti ozračja na dnevni, sinoptični in sezonski časovni lestvici, smo izbrali dve kompleksni mesti v Sloveniji (Ljubljano – v kotlini pod Alpami z zmernim celinskim podnebjem in Ajdovščino – v Vipavski dolini s submediteranskim podnebjem), kjer smo izvedli meritve. Doktorska disertacija sestoji iz treh glavnih raziskav.

Prvič, na osnovi radona smo razvili povsem novo orodje za prepoznavanje pojava PTI v topografskih okoljih kotlina/dolina, ki se je pokazalo kot bolj zanesljivo od običajnega orodja psevdo-vertikalnega temperaturnega gradienta pri ovrednotenju meteoroloških dejavnikov in kakovosti zraka med obdobji PTI. Drugič, sodobno tehniko na osnovi dnevnih nihanj koncentracije radona smo uporabili za raziskovanje relativnih sprememb v stabilnosti ozračja na obeh izbranih mestih v poletnem času. Dobljeni rezultati so pokazali, da lahko s klasifikacijo stabilnosti na osnovi radona najdemo razlike med komaj opaznimi spremembami v mešanju ozračja na mestih, ki imata povsem različne topografske značilnosti. Tretjič, z novim orodjem smo za obdobja PTI določili dodaten (ločen) razred premešanosti ozračja v okviru sodobne tehnike klasifikacije stabilnosti, zasnovane na dnevnih koncentracijah radona. Na osnovi združenih dnevnih in sinoptičnih sprememb v radonski tehniki klasifikacije premešanosti ozračja smo prvič lahko ločili "nenadzorovane" vplive na spreminjanje onesnaženja (to je meteorološke dejavnike, geološke značilnosti, topografske učinke in čezmejno onesnaževanje) od nadzorovanih vplivov (na primer porazdelitev in moč vira onesnaženja) v Ljubljanski kotlini. Ta na novo razvita tehnika je splošno uporabna za ne-obalna urbana središča po vsej Evropi, pa tudi za druga srednje in visoko ležeča celinska področja (na primer osrednji del Severne Amerike).

Rezultati doktorske študije so pokazali, da smo s to dopolnjeno radonsko tehniko klasifikacije premešanosti ozračja v urbanih okoljih (z enostavno in kompleksno topografijo) dobili novo in učinkovito orodje, ki upošteva tako dnevne kot sinoptične spremembe

premešanosti ozračja na kompleksnih področjih in nam pove, kako te spremembe vplivajo na kakovost zraka. Pričakujemo, da bo ta tehnika na osnovi opazovanja dnevnih in sinoptičnih sprememb koncentracije radona, koristno in uspešno orodje pri načrtovanju in uvajanju ukrepov za zmanjšanje onesnaženosti zraka in pri oceni uspešnosti modelov onesnaževanja v mestih.

Contents

List of Figures **xvii**

List of Tables **xix**

Abbreviations **xxi**

1 Introduction **1**
1.1 Composition of the Urban Atmosphere ... 2
1.1.1 Gaseous Pollutants ... 2
1.1.2 Particulate Pollutants ... 4
1.1.3 Air Quality in Slovenia: Overview ... 6
1.2 Dynamics in the Atmospheric Boundary Layer ... 6
1.2.1 Atmospheric Stability ... 9
1.3 Radon as a Tracer of Atmospheric Stability ... 12
1.3.1 Origin, Chemistry and Physics of Radon ... 12
1.3.2 Temporal and Spatial Variability of Radon Concentration ... 14
1.3.3 Radon-based Atmospheric Stability Classification ... 15

2 Aims and Hypothesis **17**

3 Methods **19**
3.1 Experimental Sites ... 19
3.1.1 Ljubljana Basin ... 19
3.1.2 Vipava Valley ... 20
3.2 Measurements ... 20
3.2.1 Radon Measurements ... 20
3.2.2 Meteorology Observations ... 21
3.2.3 Air Quality Observations ... 22
3.3 Development of Radon-based PTI Identification Method, and Implementation of Existing Radon-based Stability Classification ... 22
3.3.1 Diurnal Radon-based Stability Classification ... 22
3.3.2 Synoptic Timescale Radon-based Classification ... 25

4 Publications **27**
4.1 Development of a New Radon-based Method for Identification of Synoptic Timescale PTI Events in Complex Terrain ... 27
4.2 Comparison of Atmospheric Dispersion in Two Contrasting Topographic Regions using Radon-based Mixing Classification ... 53
4.3 Combining Diurnal and Synoptic Timescale Radon-based Mixing Classification Methods and Testing Their Applicability to Urban Pollution Studies ... 65
4.4 Influence of Meteorological Parameters on Radon Time Series ... 107
4.5 Radon Effective Doses at a Mediterranean Site ... 129

5 Conclusions **137**

Appendix A Radon Data and Stability Analysis **139**
A.1 Ljubljana Basin 139
A.2 Vipava Valley 147

Appendix B Radiosonde Vertical Profiles within Radon Atmospheric Mixing Classes **153**
B.1 Winter Season 154
B.2 Spring Season 155
B.3 Summer Season 156
B.4 Autumn Season 157

References **159**

Bibliography **175**

Biography **177**

List of Figures

Figure 1.1: Characteristic atmospheric residence times for air pollutants....4
Figure 1.2: Diurnal evolution of the atmospheric boundary layer....7
Figure 1.3: Illustration of the different atmospheric mixing conditions in basin....9
Figure 1.4: Three conditions of idealised atmosphere....10
Figure 3.1: Topographic map of Slovenia....20
Figure 3.2: Methodological steps for development of radon-based classification....24
Figure A1.1: Time series of hourly radon concentration observations in Ljubljana....139
Figure A1.2: Diurnal composite plots of observed radon concentrations....140
Figure A1.3: Diurnal composite plots of local radon by season and mixing classes....140
Figure A1.4: Composite plots of time rate changes of radon by mixing classes....141
Figure A2.1: Time series of hourly radon concentration observations in Ajdovščina....147
Figure A2.2: Diurnal composite plots of observed radon concentrations....147
Figure A2.3: Diurnal composite plots of local radon by season and mixing classes....148
Figure B1: Sonde vertical profile within six radon mixing classes in winter....154
Figure B2: Sonde vertical profile within six radon mixing classes in spring....155
Figure B3: Sonde vertical profile within six radon mixing classes in summer....156
Figure B4: Sonde vertical profile within six radon mixing classes in autumn....157

List of Tables

Table 1.1: Air quality standards for the protection of health. 2
Table 1.2: Meteorological conditions defining the Pasquill stability classes.....11
Table 1.3: Description of the 24-hour six radon-based mixing classes 24
Table A1.1: Daily mean radon values within six radon mixing classes in Ljubljana 143
Table A1.2: Threshold values defining six radon mixing classes in Ljubljana 145
Table A2.1: Daily mean radon values within six radon mixing classes in Ajdovščina ...149
Table A2.2: Threshold values defining six radon mixing classes in Ajdovščina. 151

Abbreviations

ABL	... Atmospheric Boundary Layer
a.g.l.	... Above Ground Level
ARL	... Air Resources Laboratory
ARSO	... Slovenian Environmental Agency
a.s.l.	... Above Sea Level
BC	... Black Carbon
CO	... Carbon Monoxide
CO_2	... Carbon Dioxide
CH_4	... Methane
E	... East
EU	... European Union
GDAS	... Global Data Assimilation System
H_2O_2	... Hydrogen Peroxide
H_2SO_4	... Sulphuric Acid
HYSPLIT	... Hybrid Single Particle Lagrangian Integrated Trajectory
LLD	... Lower Limit of Detection
MBR	... Mediterranean Basin Region
N	... North
NBL	... Nocturnal Boundary Layer
NE	... North-East
NNE	... North-North-East
NOAA	... National Oceanic and Atmospheric Administration
NO	... Nitric Oxide
NO_2	... Nitrogen Dioxide
NO_x	... Nitrogen Oxide
N_2O	... Nitrous Oxide
O_3	... Ozone
OH	... Hydroxide
PG	... Pasquill-Gifford
PM	... Particulate Matter
$PM_{2.5}$	... PM – aerodynamic diameter $\leq$2.5 μm
PM_{10}	... PM – aerodynamic diameter $\leq$10 μm
ppmv	... Parts per Million by Volume
PTI	... Persistent Temperature Inversion
^{226}Ra	... Radium
^{222}Rn	... Radon
^{220}Rn	... Thoron
^{219}Rn	... Actinon
S	... South
SIL	... Synoptic Inversion Layer
SNBL	... Stable Nocturnal Boundary Layer

SO_2	... Sulphur Dioxide
^{232}Th	... Thorium
^{235}U	... Uranium
^{238}U	... Uranium
UFP	... Ultrafine Particle
VOCs	... Volatile Organic Compounds
W	... West
WHO	... World Health Organization
α	... Alpha
δ	... Adiabatic Lapse Rate

Chapter 1

Introduction

Urban environments cover only 2–3% of global land areas (Mills et al., 2010; Cleugh & Grimmond, 2012; Pandey et al., 2012) but in 2015, 54% of the world's population (4 billion people) lived in urban areas; by 2050, 66% of the world's population is expected to be urban (Bolay, 2020). Today, the most urbanized regions include North America (82%) and Europe (73%) (Bolay, 2020). This concentration of population in urban centers has increased the demand for vehicles (transportation in general), energy consumption and industrialization, which contributed to the degradation of urban air quality (Karanasiou & Mihalopoulos, 2013; EEA, 2018). Consequently, urban regions make a disproportionately large contribution to global pollution, and urban air pollution has become one of the main environmental health risks (WHO, 2014; EEA, 2019). Air pollution derives from a combination of gaseous and particulate pollutants, which may be emitted directly into the atmospheric boundary layer (ABL) from surface- or near-surface-based sources, or formed there as a result of precursor reactions. Air pollution is associated with many health impacts, including chronic obstructive pulmonary disease, and acute lower respiratory illness, cerebrovascular disease, ischaemic heart disease, and lung cancer (Cohen et al., 2005; Griffin, 2005; Pope & Dockery, 2006; Goudie, 2014; Lelieveld et al., 2015). Air pollution contributes to 3.3 million premature deaths worldwide per year and it is estimated that the number of deaths will double by 2050 if the issue remains unattended (Lelieveld et al., 2015). However, air quality is not simply related to emission sources and strengths, it varies in response to a complex interplay between numerous factors such as meteorology (e.g. dilution, advection, venting), geographic setting (e.g. proximity to coastlines or lakes), topographic effects (e.g. ridges, valleys, basins), and cross-boundary pollution transport. Based on instantaneous measurements, depending on the spatial and temporal variability of sources and the relative location of observations, pollution concentration can vary strongly with wind direction and speed. However, on average, the largest factor influencing pollutant concentration is the mixing volume into which the pollutant is released. This mixing volume is largely dictated by the depth of the ABL, a quantity that is closely related to its mixing state (or "stability"), which can change on diurnal, synoptic and seasonal timescales. In urban regions of complex topography (e.g. the Mediterranean Basin Region; MBR), poor air quality can also be exacerbated by other factors (e.g. mesoscale circulations or stagnation events) leading to pollution events of potentially life-threatening duration and intensity (Rakovec, Merše, Jernej, & Paradiž, 2002; Silcox et al., 2012; Wang et al., 2016; Largeron & Staquet, 2016; Baasandorj et al., 2017).

Consequently, it is very important in urban regions to understand the dominant factors that influence changes in air quality on various temporal and spatial scales, in order to improve the assessment of pollution mitigation measures and understanding of health impacts.

1.1 Composition of the Urban Atmosphere

The composition of the atmosphere is determined by gases and aerosols of natural and anthropogenic origin, and the energy balance within the atmosphere (Oke, Mills, Christen, & Voogt, 2017). In the urban atmosphere, concentrations of some particular gases and aerosols are quite variable and can build up to levels that may cause harm to human health and surrounding ecosystems. Consequently, the World Health Organization (WHO) and European Union (EU) recommended Air Quality Standards (AQS) for the four most notorious gaseous pollutants: carbon monoxide (CO); nitrogen dioxide (NO_2); sulphur dioxide (SO_2); and tropospheric ozone (O_3), as well as for particulate matter (PM) (**Table 1.1**). These gases and aerosols are known as "criteria pollutants", and either originate directly through primary emission from urban sources, or are formed in situ through chemical transformation reactions of their precursor species. Apart from the criteria pollutants, there are other species common in the urban atmosphere (e.g. black carbon; BC) that are not yet regulated by WHO or EU, despite evidence that exposure to even small concentrations of BC is linked with cardiorespiratory diseases (Janssen et al., 2011; Dons et al., 2012).

In the following sections CO, NO_2, SO_2, O_3, PM and BC are discussed in terms of their abundance, sources and sinks in the urban atmosphere and their health effects.

Table 1.1: Air quality standards for the protection of health, given by European Union (EU) and World Health Organization (WHO). Air quality standards in brackets represent those stipulated by the WHO (adapted from EEA (2018)).

	CO ($mg\ m^{-3}$)	NO_2 ($\mu g\ m^{-3}$)	SO_2 ($\mu g\ m^{-3}$)	O_3 ($\mu g\ m^{-3}$)	PM_{10} ($\mu g\ m^{-3}$)	$PM_{2.5}$ ($\mu g\ m^{-3}$)
Max daily			125 (20)		50 (50)	25 (25)
Max daily 8-hour mean	10 (10)			120 (100)		
Max hourly	(30)	200	350	240 (200)		

PM_{10} – aerodynamic diameter ≤10 μm; $PM_{2.5}$ – aerodynamic diameter ≤2.5 μm.

1.1.1 Gaseous Pollutants

Carbon monoxide is produced as a primary pollutant from oxygen-limited (incomplete) combustion of organic materials (e.g. gasoline, natural gas, oil, coal and wood). Overall, the main natural sources of CO are volcanoes and forest fires, while the main anthropogenic sources are motor vehicles and some industrial processes (Badr & Probert, 1994).

The major atmospheric sink of CO is chemical conversion to carbon dioxide (CO_2). It can also be lost by deposition to soils and ice caps, or by dissolution in ocean water. Since it is relatively insoluble, however, its dissolution rate is slow (Saxena & Sonwani, 2019).

CO is not an important component with respect to stratospheric ozone reduction or acid deposition. However, with a lifetime of several months or more (Seinfeld & Pandis, 2006), it can be a major contribution to air pollution at local (urban) and regional to global scales (**Figure 1.1**). The effects of severe exposure to CO are well understood, e.g. exposure to 300 ppmv of CO for one hour causes headaches; exposure to 700 ppmv of CO for one hour causes death. The mechanism by which CO poisoning occurs is that when it dissolves in blood it replaces oxygen as an attachment to hemoglobin [Hb(aq)], thereby disrupting the oxygen supply to muscles and vital organs. By contrast, the health effects of prolonged low level exposure to CO are unclear (Jacobson, 2002). The EU and WHO short-term

(8-hour mean and max hourly) guideline values of CO exposure for protection of health are presented in **Table 1.1.**

Nitrogen dioxide is produced mainly as a secondary pollutant through the oxidation of nitric oxide (NO). It has several natural sources including atmospheric oxidation of ammonia, denitrification in soils and plants, and lightning. Anthropogenic sources of NO_2 relating to the burning of fossil fuels, industrial processes, and motor vehicles are more significant to urban pollution than natural sources because they are more concentrated in urban areas (**Figure 1.1**) (Thurston, 2008).

The removal of NO_2 from the atmosphere happens through oxidation into nitric acids or nitrates which are then lost to the surface through dry or wet deposition (rain washout or in-cloud scavenging) processes.

As one of the urban atmospheric criteria pollutants, a limit value for short-term (max hourly) exposure to NO_2 has also been set by the EU and WHO (**Table 1.1**). There is growing evidence linking NO_2 with a cardiovascular disease such as congestive heart failure (Atkinson et al., 2013) and acute myocardial infarction (Tonne et al., 2007; Madrigano et al., 2013).

Sulphur dioxide in the global atmosphere is predominantly (about 70%) of anthropogenic origin (Smith et al., 2011; Zhang et al., 2017). The main anthropogenic sources are coal-fired power plants (Li et al., 2010; Fioletov et al., 2016), industrial activities (metal smelting (Garg, Shukla, Bhattacharya & Dadhwal, 2001), mineral ore processing), and also motor vehicles. Major natural SO_2 sources include oxidation of biogenic dimethyl sulfide (Davis et al., 2001) and volcanic eruptions (Carn, Yang, Prata & Krotkov, 2015; Ge et al., 2016).

The three most important pathways for removing SO_2 from the atmosphere are: (i) oxidation (gas-phase homogeneous photo-chemical reaction with other minor components in cloud droplets), (ii) wet deposition of SO_2 (in-cloud scavenging or below-cloud scavenging), and (iii) direct deposition of SO_2 to the land surface. In the atmosphere, SO_2 is predominantly oxidized by reactions with the OH radical in the gas phase, or by hydrogen peroxide (H_2O_2) and O_3 in the aqueous phase, to form sulfuric acid (H_2SO_4), the latter of which can lead to acid rain formation and particulate sulfate (Seinfeld & Pandis, 2006). SO_2 is a major contribution to air pollution at local (urban) scales (**Figure 1.1**).

Exposure to SO_2 affects human health by increasing respiratory (Chen et al., 2007; Chen et al., 2012; Rodriguez-Villamizar, Magico, Osornio-Vargas & Rowe, 2015) and cardiovascular morbidity (Chen et al., 2012). Therefore, due to its profound impacts on human health and aquatic and terrestrial ecosystems (through acid rain), limit values have also been set for SO_2 (**Table 1.1**). In addition, SO_2 emission has been regulated in the power plant and transport sectors though the use of reduction techniques (scrubbers, flue gas desulfurization, and the use of low sulphur coal). With the implementation of these techniques in developed countries, after 1990 a significant improvement in the air quality, in regard to SO_2 emissions, has been observed (EEA, 2016, 2018).

Ozone is found in both the troposphere and stratosphere. Stratospheric O_3 (also known as "good" ozone), is the planet's naturally-occurring "protective jacket" against harmful ultra-violet radiation (Dessler, 2000). Tropospheric O_3 is known as "bad" ozone due to its significant role in the formation of photochemical pollution ("smog") and its oxidizing nature in the atmosphere. The formation of tropospheric O_3 is a complex and non-linear process. Tropospheric O_3 is produced when sunlight reacts with various precursors such as

nitrogen oxides (NO_x), volatile organic compounds (VOCs) and hydrocarbons emitted by anthropogenic sources (combustion of coal and petroleum fuels) (Monks et al., 2015).

Sinks of tropospheric O_3 include photochemical reactions, reactions with the OH radical, titration by NO, direct transfer to soils and ice caps through dry and/or wet deposition, and (slow) dissolution in ocean waters.

Tropospheric O_3 is recognized as a threat to human health (WHO, 2003; Lim et al., 2012). It has been estimated that about 5–20% of all deaths related to air pollution are attributable to O_3 (Brauer et al., 2011; Silva et al., 2013). It is also an important tropospheric greenhouse gas (IPCC, 2007; Stevenson et al., 2013).

While O_3 has a relatively short atmospheric lifetime (**Figure 1.1**), in polluted urban regions where concentrations of its precursors are high, its lifetime in the free troposphere is of the order of several weeks (Stevenson et al., 2006; Hsu & Prather, 2009; Young et al., 2013), sufficiently long for it to be transported over intercontinental scales e.g., precursor emissions from Italy and France can impact O_3 concentrations in Spain (Millán et al., 1997); long-range transport of O_3 and its precursors has been seen to influence the background O_3 concentrations in Europe (UNECE, 2010); or urban emissions resulting in O_3 episodes in surrounding rural areas (Querol et al., 2016). However, Querol et al. (2016, 2018) has found that in the MBR, local-regional emissions play a key role in exceeding target values of O_3 (**Table 1.1**).

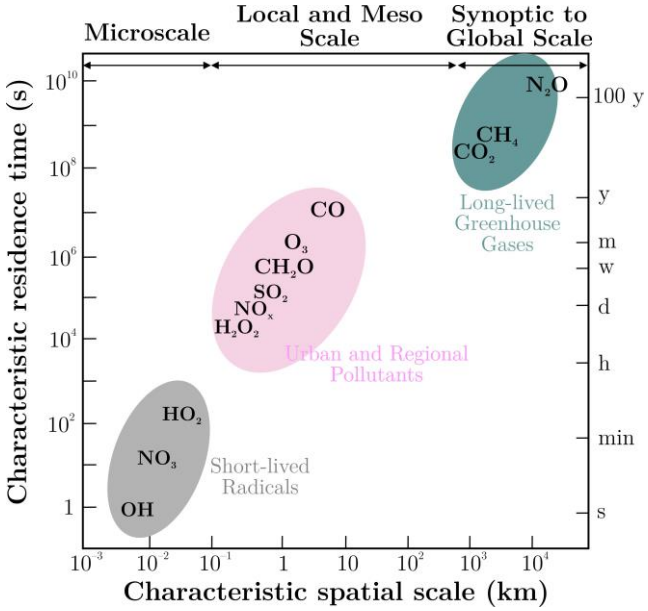


Figure 1.1: Characteristic atmospheric residence times for selected gaseous air pollutants along with the characteristic horizontal scale of dispersion (adapted from Seinfeld & Pandis (2006), and Hobbs (2000)).

1.1.2 Particulate Pollutants

Particulate matter is a complex mixture of solid and liquid particles that can be of either natural or anthropogenic origin. It can be directly emitted (as a primary pollutant) or formed in the atmosphere (as a secondary pollutant) and contain a wide range of inorganic and organic components (Tomasi & Lupi, 2017). Direct natural emissions come mainly from wildfires, sea spray and the resuspension of organic matter. Mineral dust has both natural and anthropogenic origins: it is lofted from arid and semiarid regions and can be mobilized by agricultural, construction or mining activities. The largest anthropogenic sources of PM, however, are through the combustion of fossil fuels and biofuels.

Environmental effects and lifetimes of particles vary with their size; therefore, PM is classified by its aerodynamic diameter. The label "PM_{10}" is used to represent particulate matter with diameter ≤10 μm, "$PM_{2.5}$" or "fine particles" represents the fraction of PM with aerodynamic diameter ≤2.5 μm, and particles with diameter ≤0.1 μm are denoted as "$PM_{0.1}$" or ultrafine particles (UFP)(Sun et al., 2018).

Public health policy, in terms of establishing guidelines or standards for acceptable levels of ambient PM pollution, has focused only on the mass concentrations of PM_{10} and $PM_{2.5}$ (**Table 1.1**). However, the size of PM is directly linked to its potential for causing health problems, since smaller particles penetrate further down the respiratory tract and may even transfer directly to extrapulmonary organs, including the central nervous system (Peled et al., 2005; Middleton et al., 2008; Kumar et al., 2014). Routine measurement of PM_{10} or $PM_{2.5}$ mass concentrations cannot adequately represent UFP since they contribute only a minor fraction to the overall particle mass. Particle size, however, directly influences residence time (through the settling velocity), such that the finer (more hazardous) particles remain airborne for much longer (Seinfeld & Pandis, 2006; Mohan, 2016). The question, therefore, is whether the size or the mass of PM is more important to consider? To date, this question is still unresolved. Further, in addition to PM size and mass number concentrations, their volatility, morphology and chemical composition are critical factors to be considered in the assessment of risk. Most of the urban cities in the world have PM_{10} levels above the WHO and EU standards (**Table 1.1**; WHO, 2016; EAA, 2019).

With lifetimes on the order of days to weeks, PM can undergo long-range transport, resulting in local, regional and global impacts (**Figure 1.1**) (Hobbs, 2000). Due to its location, the MBR serves as a crossroad for polluted air masses originating from North Africa (Kallos et al., 2006), the North Atlantic Ocean and Mediterranean Sea (He et al., 2018). North African dust is mobilized year-round, but its transport pathways vary seasonally. Transport to the MBR is maximized in spring due to intensification of westerly winds and development of Sharav cyclones (Kaskaoutis et al., 2019a; Kaskaoutis, et al., 2019b). In addition to sea-salt, shipping emissions are considered an important contributor to primary PM in the MBR and Europe in general.

Black carbon is a small, dark particle resulting from combustion. The four main sources of BC in the atmosphere are: (i) diesel engines used for transport, (ii) residential solid fuels, namely wood and coal, (iii) forest and savanna burning (natural), and (iv) industrial processes (Bond, 2007). Over two thirds of BC emissions derive from anthropogenic sources, attributable to the rapid increase use of fossil fuels and biofuel. During these burning processes, small carbon spherules of diameters <10 nm up to 50 nm are formed. Soon after emission the BC particles become mixed (aggregated) with other aerosol components in the atmosphere. Their number and size distributions are therefore a function of atmospheric processes during transport.

BC has a unique and important role in Earth's climate system because it absorbs solar radiation, influences cloud processes, and changes the surface albedo after deposition over the surface of snow or ice (Bond et al., 2013). According to a systematic assessment, the total radiative forcing of BC is +1.1 W m^{-2} (Bond et al. 2013), which is 59% of that of CO_2 (Stocker et al. 2013). While a number of studies have examined the climate impacts of BC emissions, few have focused on the associated health impacts of BC exposure (Anenberg et al., 2011). Being comprised of small particles, BC has a higher chance to penetrate deep into lungs and may translocate to the brain (Oberdörster et al., 2005; WHO, 2012; Kumar et al., 2014). Most of the time BC health impacts are associated with those of $PM_{2.5}$ (since BC is considered to be a component of $PM_{2.5}$) (Saikawa et al., 2009; Anenberg et al., 2011, Anenberg et al., 2012; Shindell et al., 2012). However, the health effects directly attributable to BC alone are not yet well understood. Sun et al. (2019)

argued that due to higher number concentrations and smaller diameters BC has a higher surface area per unit mass, and is therefore more readily able to absorb toxic materials than larger particles.

1.1.3 Air Quality in Slovenia: Overview

Air quality in Slovenia is influenced by a combination of local and remote sources, the relative contributions of which depend on the characteristics of Slovenian terrain (Pucer & Štrumbelj, 2018; Glojek, Gregorič & Ogrin, 2019), and prevailing meteorology. South-west Slovenia has a Mediterranean climate, which increases the chances of high O_3 levels in summer. Most central-Slovenian cities are located in valleys and basins that are prone to stagnation events, thus increasing the contribution of locally produced pollutants (e.g. PM, NO_2, BC). Since there are no large industries, the dominant local pollution sources are traffic and, in the colder months, domestic heating, which has increased by 17% in recent years (Energy Balance of City of Ljubljana, 2019). In terms of remote pollution sources, due to its location Slovenia serves as a "crossroads" for polluted air masses originating from Africa (Kallos et al., 2006); across Europe from the North Atlantic Ocean and across Italy from the Mediterranean Sea (He et al., 2018); the northern Balkan Peninsula, and Eastern Europe (Poberžnik & Štrumbelj, 2016; He et al., 2018).

Currently, the main air quality issues in Slovenia are PM_{10}, $PM_{2.5}$, BC and O_3. Within the EU, Slovenia has one of the largest emissions of PM_{10} per capita and per surface area (Gjerek, 2018). In 2018 the total number of PM_{10} exceedances surpassed the number allowed in EU countries (35) at six monitoring sites: Zagorje (55), Ljubljana Center (51), Murska Sobota Cankarjeva (46), Celje Mariborska (45), Celje Gaji (43) and Trbovlje (37). Most of the exceedances occurred during winter. The WHO recommendation for the annual average of PM_{10} and $PM_{2.5}$ (20 µg m^{-3} and 10 µg m^{-3}, respectively) were exceeded at all monitoring sites across Slovenia. The trend of PM_{10} levels from 2002 to 2018 does not show a significant improvement (Pucer & Štrumbelj, 2018). An improved understanding of natural (meteorological) influences on PM concentrations in urban regions of Slovenia would assist the development of mitigation measures.

In recent years the maximum daily 8-hour mean O_3 value recommended for the protection of human health was exceeded at almost every measuring site. The highest annual average concentrations were measured at high-altitude monitoring sites (e.g. Krvavec) (Gjerek, 2018; 2019).

1.2 Dynamics in the Atmospheric Boundary Layer

Earth's atmosphere is a complex system. This complexity is primarily attributable to interactions between thermodynamic processes that, in turn, affect our lives. Consequently, understanding atmospheric processes and how they modulate concentrations of natural and anthropogenic pollutants to which we are exposed is of great importance.

The atmosphere is divided into four main layers: the troposphere (from the surface to 8–16 km above sea level a.s.l.), stratosphere (between 8 and 50 km a.s.l.), mesosphere (between 50 and 80 km a.s.l.) and thermosphere (between 80 and 700 km a.s.l.). These layers are characterised by alternating decreases and increases of air temperature with height. Temporal changes in air temperature near the surface of the earth are caused at a range of temporal scales by the alternation of night and day, traveling synoptic weather systems, and changing seasons (Stull, 1988). The focus of this thesis is on the troposphere.

In the troposphere, three types of lapse rates are used to express the rate of temperature with height ($\Delta T/\Delta z$): (i) the dry adiabatic lapse rate (–9.8 ℃ km^{-1}), and (ii) the saturated adiabatic lapse rate (from –5.5 to –3.5 ℃ km^{-1}), representing the extremes, and (iii) the "standard" (or average) atmospheric lapse rate (–6.5 ℃ km^{-1}). When layers of air within the troposphere have a lapse rate greater than the saturated adiabatic lapse rate they are stable, and sometimes called *temperature inversions*. The four most common inversion types are known as: (i) radiation, (ii) persistent (anticyclonic, large-scale subsidence), (iii) marine, and (iv) frontal (Jacobson, 2002).

The specific part of the troposphere that this thesis will focus on is its lowest part, typically referred to as atmospheric boundary layer (ABL). This is the region directly in contact with the surface that supports and most directly impacts life on the planet. Importantly, it is also the layer into which most pollution is emitted.

Typically, the ABL constitutes 10–20% of the thickness of the troposphere during the day, but its thickness is quite variable in space and time. Stull (1988) defines the ABL as the part of the troposphere that is directly influenced by the presence of the earth surface, and responds to surface forcing with a time scale of about one hour or less. At night, when only mechanical mixing is active, its thickness can be as low as a few tens of meters. During the day, however, when convective and mechanical mixing combine, the thickness can easily reach 1–2 km (**Figure 1.2**) (Stull, 1988). The combined intensity of all vertical mixing process in the ABL, sometimes referred to as the mixing state, is closely related to the depth of the ABL, which in turn affects the dilution of pollution emitted from the surface. At any given location, there are a number of factors that may directly affect the local ABL mixing state, including: diurnal changes in solar elevation, seasonal changes in solar elevation, latitudinal changes in solar elevation, the passage of synoptic systems (cyclones and anti-cyclones), topographic elevation (the height a.s.l.), continentally (the distance from the sea) and orography (presence of mountains). Local meteorological factors most closely related to changes in the mixing state (or "stability") are the vertical air temperature gradient and wind speed (e.g. Ivey et al. (2019) and references therein).

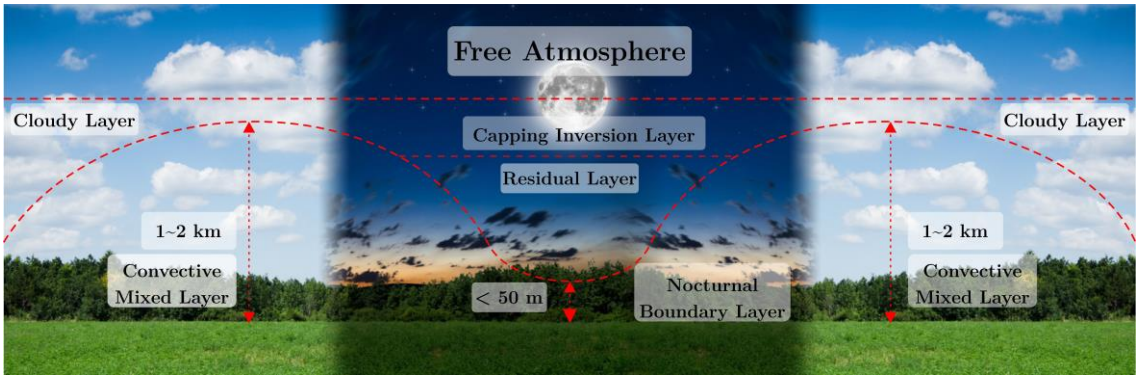


Figure 1.2: Diurnal evolution of the atmospheric boundary layer (inspired by Stull (1988)).

In complex topographies (e.g. basins and valleys), both thermal and mechanical boundary conditions are different compared to those of flat terrain, and mesoscale motions result in the daily cycle of ABL mixing being more complex (Stull, 1988). Two good examples of sites where complex orography as well as passing synoptic systems can influence the local mixing state and air flows are: (i) Ljubljana, a subalpine urban site situated within a topographic basin (Petkovšek, 1978; Rakovec et al., 2002), and (ii) Ajdovščina, a sub-Mediterranean town of Vipava Valley at the foothills of Trnovski gozd barrier only 25 km from the Adriatic coast (Grisogono & Belušić, 2009; Mole et al., 2017).

In mountainous terrain (basins and valleys), radiation and persistent temperature inversions (PTI) are the most common inversions. During nights with fair weather conditions (i.e. in the presence of high-pressure systems; slow surface winds and clear-sky), strong radiative cooling of the surface results in the formation of a shallow, poorly mixed inversion layer – radiation inversion or stable nocturnal boundary layer (SNBL) (**Figure 1.3a**). Pollutants emitted at or near the surface are usually trapped within this layer. Such pollution events usually end abruptly each morning shortly after the onset of convective mixing as a result of intense sunlight heating the surface (**Figure 1.3a**). In such cases, concentrations of primary pollutants drop to ~ 50% from peak values by midmorning and reach their minimum values in the early afternoon when the ABL is deep and uniformly mixed. In summer, particularly during anticyclonic conditions, daytime pollution events are also common as a result of rapid secondary-pollutant formation (O_3). During winter and autumn, however, day lengths are shorter, sun angels lower, and surfaces wet or frozen, so in topographically complex regions PTIs can occur within anticyconlic systems. Over the MBR, PTI events are usually attributable to the presence of the persistent "Siberian High", well-known for producing a large-scale subsidence inversion. Usually anticyclonic regimes persist for several days, leading to the development of a synoptic subsidence inversion layer (SIL). The height of this layer can coincide with the average elevation of the mountain summits surrounding the basin/valley (Whiteman, 1982; Largeron & Staquet, 2016a). In such a system, air descends, compressing and warms adiabatically. Over land at night (**Figure 1.3b**), air in a large-scale high-pressure system can descend and warm on top of near-surface air that has been cooled radiatively thus creating a SNBL (height $\leq$50 m) within the SIL. **Figure 1.3b** show that during the day (between morning and afternoon) the SNBL eroded, so what remained was only the synoptic SIL.

The elevated inversions (PTIs), which effectively decouple much of the basin/valley atmosphere from the free troposphere above, serves as a lid to confine the high pollution beneath it (Petkovšek, 1985; Rakovec et al., 2002; Silcox et al., 2012; Lareau et al., 2013; Whiteman, Hoch, Horel & Charland, 2014; Anisimov et al., 2017; Largeron & Staquet, 2016a; Baasandorj et al., 2017; Fiorella et al., 2018; Wang et al., 2019) for several consecutive days. Once decoupled from the free troposphere, the lower atmosphere of the basin/valley is free to develop a local dynamic of its own (Largeron & Staquet, 2016b), including diurnal valley and mountain flows. In Alpine regions, diurnal thermal (katabatic/anabatic) winds result due to the strong diurnal cooling and heating associated with anticyclonic conditions. In this region also the downslope winds appear, mainly in two groups – warm winds "foehn", and cold winds "Bora". Bora is observed on the lee side of Dinaric Alps – in Ajdovščina, and usually is classified according to the synoptic situation (Yoshino, 1976). It commonly appears in the presence of a high pressure system over Central Europe or a cyclonic system over or close to Adriatic Sea or combination of both (Jurčec, 1981; Poje, 1992). On the other hand, when anticyclonic conditions dominate over the mountains surrounding Ljubljana, there are anabatic winds that blow *up* the slopes during the day and katabatic winds that flow *down* the slope at night. The anabatic/katabatic winds are also common in Ajdovščina.

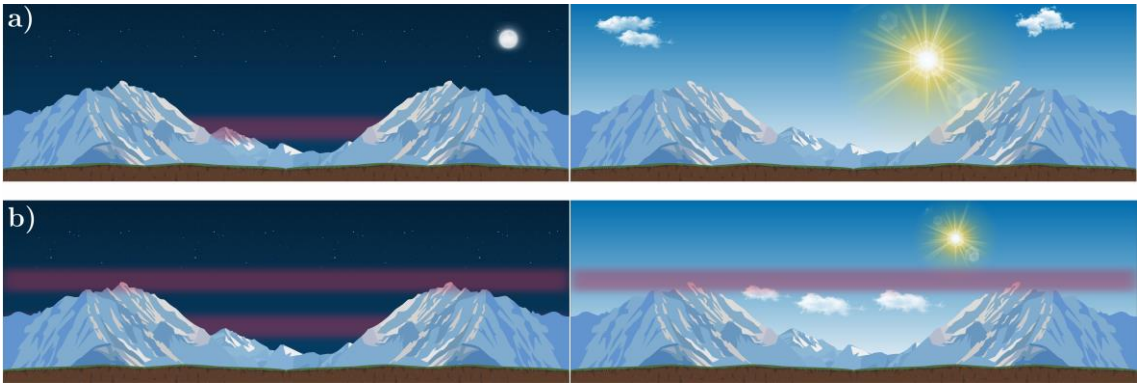


Figure 1.3: Illustration of the different atmospheric mixing conditions over the basin terrain: a) night (formed stable nocturnal boundary layer), day (eroded stable nocturnal boundary layer), and b) night (formed stable nocturnal boundary layer within synoptic inversion layer), day (only synoptic inversion layer) (inspired by Knox & Ackerman (2010)).

It is not just anticyclonic conditions that result in high levels of pollution, another synoptic-timescale influence on pollution concentrations (typically under cyclonic conditions) arises through cross-boundary advection. Low-pressure (cyclonic) systems are characterized by moderate-to-strong gradient wind conditions, the most effective conditions for transporting pollution. Long-range transport events of both anthropogenic and natural pollution are often experienced by many countries of the MBR region (Salvador et al., 2014), such as Portugal (Russo, Trigo, Martins & Mendes, 2014; Conceição et al., 2018), Spain (Díaz et al., 2017), Italy (Gobbi et al., 2019), Slovenia (Beeston et al., 2011), Croatia (Čanić et al., 2009), and Greece (Kaskaoutis et al., 2019a, 2019b).

To this end, it seems that formulating a better understanding the influence of changing atmospheric mixing state (or "atmospheric stability") over diurnal, synoptic and seasonal timescales on pollutant concentrations that urban residents are exposed to is very important.

1.2.1 Atmospheric Stability

Historically, atmospheric stability has been described in one of two different ways: (i) treating stability as a continuum, with a threshold value, or range of values, that separates atmospheric mixing conditions (e.g. Richardson Number approach (Williams et al 2013), or Monin-Obukhov similarity theory (Nieuwstadt, 1984)), or (ii) categorical, with discrete values that fall into several classes; classes describe the degree to which vertical mixing in the ABL is suppressed or enhanced over a specific site under certain meteorological conditions. The mixing classes at any given time will depend on *static* (related to the change in temperature with height) and *dynamic* (a function of wind speed and surface roughness) stability.

In broad general terms, atmospheric stability can be characterized by three categories:

(i) **unstable** atmosphere – is one that encourages continual vertical motion of the air, upwards or downwards (**Figure 1.4a**);

(ii) **neutral** atmosphere – is one that neither discourages nor encourages vertical motion of the air (**Figure 1.4b**);

(iii) **stable** atmosphere – is one that discourages vertical motion (**Figure 1.4c**).

The conditions of stability and instability of the air depend on the *lapse rate* and is defined as follows:

$$\delta = -\frac{\mathrm{d}T}{\mathrm{d}z} \tag{1.1}$$

where T is the temperature and z the vertical coordinate.

A layer of the atmosphere is considered unstable if it has a lapse rate less than the dry adiabatic lapse rate (i.e. $\delta < -9.8$ ℃ km^{-1}). A layer of the atmosphere is considered stable if its lapse rate is greater than saturated adiabatic lapse rate (i.e. $\delta > (-5.5) - (-3.5)$ ℃ km^{-1}). Between these two lapse rate extremes, the layer of air may be conditionally stable/unstable (depending upon its water content), or it may be considered neutral (neither stable or unstable).

Figure 1.4 shows the mixing conditions of an idealised "standard" atmosphere (i.e. lapse rate = –6.5 ℃ km^{-1}), which is associated with an observed atmospheric sounding. On average, temperature gradients more negative than the "standard" adiabatic lapse rate (i.e. super-adiabatic lapse rates; **Figure 1.4a**), are indicative of an unstable basin atmosphere, whereas gradients less negative than the "standard" adiabatic lapse rate (sub-adiabatic; **Figure 1.4c**) are indicative of an atmosphere that is stable, or tending toward stability. When observed temperature gradients are the same as the "standard" adiabatic lapse rate, the atmosphere is considered neutral (**Figure 1.4b**).

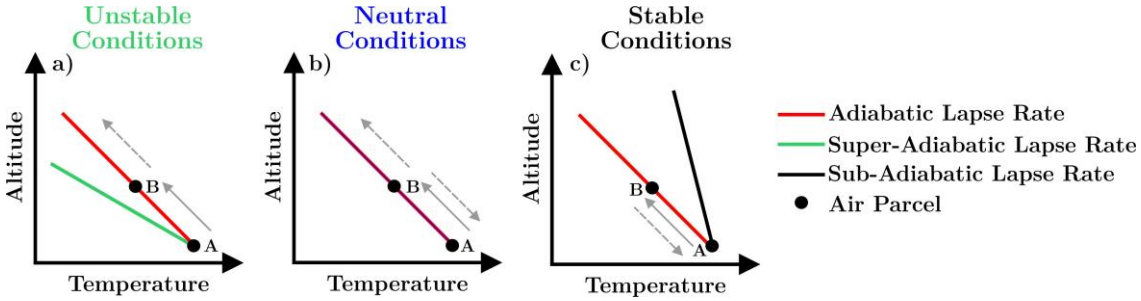


Figure 1.4: Three conditions of an idealised "standard" atmosphere: a) unstable (encourages continual vertical motion of the air), b) neutral (neither discourages nor encourages vertical motion of the air), and c) stable (discourages vertical motion).

One of the simplest, and therefore most widely used, approaches to assess atmospheric stability is the Pasquill-Gifford (PG) technique, which has both turbulence and radiation-based schemes (Pasquill, 1961; Turner, 1964; Pasquill & Smith, 1983). This approach is so commonly adopted because it makes use of routinely available surface-based measurements of either wind speed and wind direction, or wind speed, cloud cover and insolation. The categorical PG stability classes range from A (extremely unstable) to F (moderately stable), with D representing neutral conditions (**Table 1.2**). An additional class G was added by later authors to represent low-wind nocturnal conditions (Hasse & Weber, 1985).

There are, however, a number of reasons why PG schemes might be expected to provide unsatisfactory characterization of atmospheric stability. The PG method does not consider variations in surface roughness (Bowen, 1994; Panofsky & Dutton, 1984) and does not specify the height of the required "surface" wind speed measurement, an important detail which can affect the assignment of stability category (Venkatram, 1996). Especially, since topography can have a significant influence on the atmospheric mixing state, the PG turbulence scheme is often poorly applicable in basin/valley settings due to consistently low wind speeds (Chambers et al., 2015; Wang et al., 2016; Kahl & Chapman, 2018). While

the Pasquill classes are elegant in their simplicity, they ignore important processes affecting atmospheric stability including air mass fetch (Crawford et al., 2016), synoptic weather conditions (Luna & Church, 1972), and variations in thermal properties of soils (Gifford, 1976). The non-categorical atmospheric stability methods (e.g. Richardson Number (Galperin, Sukoriansky & Anderson, 2007), Monin-Obukhov similarity (Foken, 2006)), however, do not require only routinely measured meteorological data but also fundamental parameters that describe atmospheric dispersion (e.g. friction velocity, boundary layer height). The required fundamental dispersion parameters can only be derived from highly-sensitive, rapidly responding meteorological sensors that are expensive to buy, and require considerable maintenance and effort in data pre-processing. Furthermore, results derived from such measurements are challenging to apply to regions that are not large, flat and homogeneous.

Table 1.2: Meteorological conditions defining the Pasquill stability classes (after Pasquill (1961)).

	Daytime Insolation			Nighttime Conditions	
Surface Wind Speed ($m\ s^{-1}$)	Strong	Moderate	Slight	Thin overcast or >4/8 low cloud	<=4/8 cloudiness
<2	A	A–B	B	E	F
2–3	A–B	B	C	E	F
3–5	B	B–C	C	D	E
5–6	C	C–D	D	D	D
>6	C	D	D	D	D

A–Extremely unstable; **B**–Moderately Unstable; **C**–Slightly Unstable;
D–Neutral; **E**–Slightly Stable; **F**–Moderately Stable; **G**–Extremely Stable.

However, a fundamental assumption of these stability classification methods is that changes of atmospheric mixing state occur only on diurnal timescales. In complex terrain under PTI conditions this assumption is violated, since the bulk of the basin/valley atmosphere can be stagnant for several consecutive days (synoptic timescales), with restricted diurnal changes happening near the surface within this deeper layer. Consequently, PTI conditions are typically studied as a separate event. Unfortunately, however, there are only a few observational studies of PTIs (Clements, Whiteman & Horel, 2003; Dorninger et al., 2011; Silcox et al., 2012; Lareau et al., 2013; Lehner et al., 2015). One of the first European field campaigns to target PTI events took place in the Chamonix-Mont-Blanc valley, in January–February 2015. This study was motivated by the anomalously high pollution concentrations frequently recorded there. The comprehensive suite of meteorological and chemical observations made throughout the campaign has been described by Chemel et al. (2016).

To date, this lack of observational PTI studies has mainly been due to the difficulty in making the necessary meteorological measurements within the topographically challenging regions (Yao & Zhong, 2009). Such studies often require the deployment of sophisticated instrumentation (e.g. radiosondes, tethered balloons, masts, or aircraft). These instruments are typically expensive and labor intensive to operate (Baasandorj et al., 2017) e.g. radiosondes are launched usually between 1–4 times per day, depending on the site. However, many sites do not have the facilities to conduct operational radiosonde launches. Consequently, Whiteman, Eisenbach, Pospichal & Steinacker (2004) proposed a meteorological approach to identify PTI conditions using only surface measurements for which differences between air temperatures at various elevations on the sidewalls of a valley

or basin are calculated (the so-called "pseudo-vertical temperature gradient" method). This method was employed by Largeron & Staquet (2016a) in the French Alps to detect PTI events throughout the cold season (November 2006 to February 2007). There are, however, a variety of mesoscale processes that have the potential to disrupt this pseudo-vertical temperature profile and the assumed horizontal atmospheric homogeneity (including local drainage flows or mesoscale motions, nocturnal jets, and intermittent turbulence) (Whiteman, Eisenbach, Pospichal & Steinacker, 2004; Williams, Chambers & Griffiths, 2013). Such influences can complicate the interpretation of pseudo-vertical temperature gradients derived from stations of contrasting elevations on valley or basin walls, depending on their particular spatial locations.

By contrast to the methods so far described to assess changes in the mixing state on diurnal or synoptic timescales, measurement of a surface-emitted atmospheric tracer with appropriate physical properties (e.g. simple source and sink characteristics), which responds directly to atmospheric mixing processes, has the potential to provide a more consistent and representative method by which to account for both diurnal and synoptic changes in the atmospheric mixing state. The naturally occurring radioactive gas radon (^{222}Rn) is an ideal candidate for this task.

1.3 Radon as a Tracer of Atmospheric Stability

Radon is a unique naturally-occurring element in being a gas, noble, radioactive, and having relatively simple source and sink characteristics. ^{222}Rn (hereafter referred as "radon") originates in the ^{238}U (uranium) decay chain and has a half-life ($t_{1/2}$) of 3.82 days, ^{220}Rn (thoron) is in the ^{232}Th (thorium) chain with $t_{1/2}$=55.6 s and, ^{219}Rn (actinon) is in the ^{235}U (uranium) series with its $t_{1/2}$=3.9 s. All are alpha particle emitters. The most important isotope is, by far, radon because its half-life allows it to migrate long enough and travel long distances. This collection of properties makes radon a very useful tool for investigating a number of atmospheric processes.

In order to properly address the question of radon's suitability for use as a tool in atmospheric research, its origin, processes of transport, and basic physical and chemical characteristics will first be characterized. Following this, the temporal and spatial variability of radon will be highlighted, and finally a summary will be presented of the research done in the field of radon as a tracer for atmospheric mixing studies.

1.3.1 Origin, Chemistry and Physics of Radon

Radon is an α–decay product of ^{226}Ra (radium), a member of the ^{238}U (uranium) chain. ^{226}Ra ($t_{1/2}$ =1602 y) is ubiquitous to rocks and soils all over the Earth's crust. Release of radon from the soil grains to the atmosphere takes place by a series of processes (Nazaroff & Nero, 1988):

> **Emanation** – radon atoms formed from the decay of radium escape from the grains (mainly because of recoil) into the interstitial space between grains. Emanation depends mainly on the distribution of radium in the grains (Sakoda et al., 2010a), the kind of mineral (Abumurad & Al-Tamimi, 2001; Jobbágy et al., 2009; Kardos et al., 2015), the grain size/surface area (Breitner et al., 2010; Sakoda et al., 2010b), the content of clay and organic matter (Greeman & Rose, 1996), the moisture content in grains (Bossew, 2003), the temperature of the grains (Iskandar et al., 2004; Lee et al., 2012), and weathering of the grains (Schumann & Gundersen, 1996).

Transport – the emanated radon atoms in the soil pore spaces can move through the ground by diffusion (driven by concentration gradients) and convection/advective flow (driven by pressure gradients) (Etiope & Martinelli, 2002). In general, radon transport is dependent on the soil type, its pore size distribution, its water content, and permeability (Schumann & Gundersen, 1996). Because of the large difference between the radon diffusion coefficient in air (1.2×10^{-5} $m^2\ s^{-1}$) and in water (1.4×10^{-9} $m^2\ s^{-1}$), soil moisture effects generally dominate other physical factors. At high water contents (near saturation), the pores become blocked by water and diffusion decreases (Papachristodoulou et al., 2007).

Exhalation – after radon is emitted from the grains and transported through the soil, a fraction of it enters the atmosphere through an exhalation process. The depth at which soil grains can contribute to the radon being exhaled from the surface depends on the type of soil, its moisture content, the isotope half-life and underlying geology and/or lithology. For radon (^{222}Rn) the depth is generally about 1–2 m in unsaturated soils, more for sands and less for saturated and compacted soils (Tanner, 1980; Akber & Holdsworth, 2004). The magnitude of the exhalation process is usually called the exhalation rate, which is defined as the number of radon atoms leaving a unit surface area of the soil per unit time (e.g. atoms $m^{-2}\ s^{-1}$).

Once emitted to the atmosphere radon is directly influenced by the meteorological processes that regulate turbulent mixing, namely, vertical and horizontal components of dispersion. The radon exhalation rate from the land is typically 2–3 orders of magnitude higher than that from the open ocean (exhalation rate: 1300–1800 Bq m^{-2} d^{-1} from continents as opposed to ~17 Bq m^{-2} d^{-1} from oceanic areas; Nazaroff, 1992; Schery & Huang, 2004).

Being an inert gas, radon does not chemically react with other atmospheric constituents and its low solubility makes it unlikely to be scavenged in clouds or washed out by rainfall. Consequently, it is eliminated from the atmosphere predominantly by radioactive decay ($t_{1/2} = 3.82$ d). Its half-life, conveniently between the timescales of diurnal and synoptic events, is ideal for characterizing a wide range of meteorological events (Zahorowski, Chambers & Henderson-Sellers, 2004; Williams, Chambers & Griffiths, 2013). While radon's relatively short half-life prevents it from accumulating in the atmosphere greater than synoptic timescales, with a sufficiently sensitive detector it is possible to track air masses containing radon for 2–3 weeks, enabling them to carry important geophysical information over long distances. In particular, the large gradient in the concentrations of radon between oceanic and terrestrial air masses aids in identifying the sources of air masses (continental versus maritime) so that radon can serve as an unambiguous indicator of recent terrestrial influence on oceanic air masses (Rao & Desai, 1969; Lambert, Polian & Taupin, 1970; Wilkening & Clements, 1975; Carvalho, 1995; Chambers, Zahorowski, Matsumoto & Uematsu, 2011; Chambers et al., 2009; 2016a; 2018). Since radon's half-life is much greater than mixing timescales of the ABL (<1 h), and since radon is still relatively conservative (within 5–10%) over the course of a whole night, radon is an appropriate atmospheric tracer for near-surface mixing studies from hourly to nightly timescales. Combined, these characteristics make radon unique and powerful indicator of atmospheric stability.

1.3.2 Temporal and Spatial Variability of Radon Concentration

In the ABL, radon concentrations exhibit a high degree of temporal variability on hourly to seasonal timescales. The majority of this variability is attributable to atmospheric processes occurring at seasonal, synoptic, and diurnal timescales.

Seasonal variability – (timescale≤3 months) of radon concentrations is contributed to by long-term changes in (i) air mass fetch, (ii) radon source function, (iii) day length, and (iv) mean ABL depth (deep in summer, shallow in winter), brought about by the annual solar cycle. In addition, a significant variation of radon from one season to another can be caused also by mean soil moisture content, snow cover, or soil freezing (Szegvary, Leuenberger & Conen, 2007; Zhuo, Guo, Chen & Cheng, 2008; Szegvary, Conen & Ciais, 2009; Chambers, Zahorowski, Matsumoto & Uematsu, 2011; Mazur & Kozak, 2014; Karstens, Schwingshackl, Schmithüsen & Levin, 2015; Salzano et al., 2016, 2018) that directly affects the exhalation process.

Synoptic variability – (timescale≤2 weeks) is mainly attributable to short-term changes in air mass fetch, boundary layer depth, advection, and ventilation of the boundary layer, brought about by the passage of synoptic weather systems. In this case, variability of the radon source function over the air masses' recent fetch can have a greater influence on atmospheric radon concentrations than the local radon source function at the measurement site.

Diurnal variability – (timescale≤24 hours) is primarily attributable to changes in the atmospheric mixing state, and the strength of the local radon source function (which, on synoptic timescales and above, depends primarily on the lithology at measurement site). Depending on season (specifically, the duration and intensity of solar radiation), the timing and duration of the diurnal maximum and minimum concentration periods may change by several hours. The diurnal cycles are characterized by peak concentrations near sunrise, when near-surface mixing is usually suppressed, and minimum values in the mid-afternoon, when the ABL is deep (typically ~1 km) and uniformly mixed. However, diurnal variability also includes sub-diurnal changes (e.g. changes in wind speed, in atmospheric pressure, individual rainfall events); these changes are of secondary significance and random in nature, so they typically average out in long-term (seasonal) statistics (see **in sub-chapter 3.2**).

The seasonal and diurnal radon cycles at Ljubljana Basin and Vipava Valley are shown in Appendix A (**Figures A1.2 and A2.2**).

Spatial variability – of near-surface radon activity concentrations is primarily dependent on the radium content of the soil (Dueñas, Perez, Fernandez & Carretero, 1996; Ielsch et al., 2001) and its permeability (Etiope & Martinelli, 2002). The variability of radium content and degree of permeability are caused by the most important geologic characteristics: lithology and the presence of faults. A recent European radon exhalation map (Karstens et al., 2015) shows some areas of very high radon exhalation, which coincide with areas in Europe where the radium activity concentration in the upper soil layer is very high (e.g. Massif Central in southern France, the Iberian Peninsula, areas in central Italy, and south-western of Slovenia). Based on this map, radon exhalation rates can differ by a factor of two over distances as small as 50 km, e.g. in Slovenia radon exhalation in the Ajdovščina region is around twice that in Ljubljana. Lithology is expected to have the largest influence on variability of local radon source between these two sites (Kovács et al., 2013). The higher radon exhalation rates in Slovenia are expected from flysch and carbonates (Ajdovščina), compared to other lithologies (e.g. sea and lake sediments, Ljubljana) (Kardos et al., 2015). However, compared to other gases emitted from the land surface, such as biogenically-produced CO_2, N_2O and CH_4, the radon source function is

fairly uniformly distributed on local to regional scales (1 atom cm^{-2} s^{-1} ±25%; Jacob et al., 1997; Karstens et al., 2015) and is emitted at constant rate.

1.3.3 Radon-based Atmospheric Stability Classification

Soon after its discovery in 1900, pioneering studies using radon as an atmospheric tracer began (Elster & Geitel, 1901; Satterly, 1910). Its popularity as a tool for indicating atmospheric stability increased markedly from the 1960s (Jacobi & André, 1963; Moses, Lucas & Zerbe, 1963; Pearson & Jones, 1965; Turekian, Nozaki & Benninger, 1977), and more recently it has become quite well-accepted by the scientific community generally as an atmospheric tracer (Balkanski et al., 1993; Dueñas, Perez, Fernandez & Carretero, 1996; Jacob et al., 1997; Zahorowski, Chambers & Henderson-Sellers, 2004; Zahorowski et al., 2005; Desideri et al., 2006; Szegvary, Conen & Ciais, 2009; Williams, Chambers & Griffiths, 2013; Williams et al., 2016). This has happened because, if radon emissions are spatially homogeneous and venting from the ABL can be ignored, changes in near surface radon concentrations are directly related to the net effect of near-surface vertical mixing processes. In practice, as already mentioned above (**sub-chapter 1.3.2**), air mass time over land and the spatial distribution of the radon source function are rarely uniform. Because of radon's half-life, air masses retain a "memory" of radon emissions from upwind regions (Sesana, Caprioli & Marcazzan, 2003; Galmarini, 2006; Chambers, Williams, Crawford & Griffiths, 2015). Consequently, an observed radon time series is a combination of two signals: a local contribution (determined by the local radon flux and ABL depth), and a fetch effect (determined by the upwind source distribution). The fetch effect needs to be accounted for radon to be used as a quantitative indicator of atmospheric mixing. Measuring vertical radon gradients, or calculating time rates of change in radon concentration, are some ways of accounting for fetch effects.

So far, the main obstacles to the wider use of radon as a quantitative indicator of atmospheric stability have been a lack of continuous radon gradient measurements, which are ideal for this purpose, or failure to properly calculate and remove the non-local radon contributions from single height radon measurements. Some landmark studies in this field in recent decades include: the findings of Sesana, Caprioli & Marcazzan (2003), Sesana, Ottobrini, Polla & Facchini (2006) and Perrino, Pietrodangelo & Febo (2001), which clearly demonstrated good correlation between diurnal variations of radon concentrations with primary urban pollutants (accumulated at night and diluted during the day); direct measurements of radon concentration gradients and their relationship to near-surface atmospheric mixing by Moses, Lucas & Zerbe (1963), Cohen, Barr, Krablin & Newstein (1972), Butterweck, Reineking, Kesten & Porstendorfer (1994), Chambers et al. (2011), and Williams, Chambers & Griffiths (2013); and the technique of Chambers et al. (2015) to estimate and remove non-local contributions (or "fetch effects") to measured radon time series. Together, the results of these studies helped lead to the development of a method that reliably provides a "relative measure" of nocturnal mean near-surface mixing at a site (by way of classes of atmospheric mixing state) that is based on near-surface single-height radon measurements (Chambers et al. (2019), and references therein).

The radon-based stability classification approach introduced by Chambers et al. (2015) is a comparatively new method for characterizing relative changes in the nocturnal average atmospheric mixing state at a site for a range of scientific purposes. Williams et al. (2016) used four mixing classes derived from radon observations 15 m a.g.l. to accurately characterize CO and benzene concentrations across the diurnal cycle throughout all seasons in Bern, Switzerland. Pal et al. (2015) used the same method applied to radon concentrations recorded at 180 m a.g.l., to improve understanding of the daytime behavior of trace gases in the lower atmosphere of rural site in France. Further, Chambers et al.

(2016b) and Melintescu et al. (2018) used radon observations from 10 m a.g.l., to investigate the influence of atmospheric stability on anthropogenic and natural atmospheric radioisotopes in the vicinity of a decommissioned nuclear research reactor in Romania near Bucharest. The radon-based technique for stability classification was also applied to radon observations 2 m a.g.l., to assess urban heat island intensity in the relatively flat region of Łódź in central Poland (Chambers, Podstawczyńska, Williams & Pawlak, 2016c; Podstawczyńska & Chambers, 2018; Chambers et al., 2019), and to see the influence of atmospheric mixing on canopy-level climate between the urban centre Łódź and the surrounding agricultural land in Ciosny, Poland (Podstawczyńska, 2016).

However, in complex terrain where PTI conditions can readily occur, contemporary radon-based atmospheric stability methods alone are not sufficient to assess all stability influences on urban pollution. PTI events result in atmospheric conditions that violate important assumptions of the radon-based stability assessment tool introduced by Chambers et al. (2015) since the basin atmosphere can stagnate for several days, allowing radon to continually accumulate between the surface and synoptic inversion. Under these conditions a SNBL may also develop, but it would be weaker than if the overlying persistent synoptic inversion was not present (see **Appendix A, Figure A1.4**). When this surface inversion breaks down the following morning, it mixes with the already high-radon air beneath the persistent synoptic inversion. In these situations, if "non-local processes" are removed as described by Chambers et al. (2015), the multi-day accumulation of radon under the synoptic inversion is incorrectly removed as a "fetch effect", and the affected measurement days are incorrectly assigned to an intermediate stability class due to weaker surface inversion conditions.

Chapter 2

Aims and Hypothesis

It is important to improve current understanding of atmospheric controls on air quality in regions of complex topography in order to better assess pollution mitigation measures, evaluate the performance of urban pollution models, and inform public health studies (Chambers et al., 2019). However, contemporary radon-based atmospheric stability tools alone are not sufficient to assess stability influences on urban pollution in complex topographies where PTI conditions can occur. These heterogeneous environments also prove challenging for the more sophisticated meteorological stability assessment methods (e.g. Richardson Number, Monin-Obukhov similarity). Since PTI conditions cause periods of dangerously high pollution concentrations that persist for many consecutive days, it is very important to better understand natural (uncontrollable) influences on urban air quality on various temporal and spatial scales in order to develop and revise mitigation measures and health guidelines.

While much evidence already exists in the literature regarding the control that atmospheric stability and topography can have over urban air quality that people are exposed to, this thesis demonstrates the superiority of radon over conventional approaches to efficiently and accurately assess the nocturnal mean mixing state. However, there is currently a lack of ongoing radon measurements in and around urban areas globally, which has led to inadequate interpretation of data. In order to help reduce this knowledge gap, we provided examples of long-term radon data sets in urban regions suitable for characterising seasonal changes in the atmospheric mixing state. To go one step further, in an effort to showcase the versatility of radon as a convenient and reliable tracer of near-surface atmospheric mixing and transport, in this study we have chosen two experimental sites with strongly contrasting topographic features: an enclosed basin environment (Ljubljana Basin with subalpine climate), and an open valley region (Ajdovščina, a rural town in the Vipava Valley with sub-Mediterranean climate). The topographic features of these respective sites result in similarly contrasting seasonal meteorological conditions. Nevertheless, we are able to demonstrate that radon can be applied equally well in both settings as a tool for the characterisation of the nocturnal mean atmospheric mixing state.

In this study three main goals are considered:

- to develop and test a novel radon-based tool to identify PTI conditions in topographic basin/valley environments,
- to use an existing radon-based stability method (under non-PTI conditions) to compare the atmospheric dispersion characteristics of two contrasting topographic regions: a basin environment and a valley region prone to katabatic drainage flows, and

- to combine, for the first time, the existing radon-based stability classification method with the newly-developed radon-based tool from this study for identification of PTIs, in order to (i) better characterize natural influences on urban pollution variability in the city of Ljubljana; and (ii) to separately use the radon-based stability classification tool to better constrain remote pollution transport into the Ljubljana basin region.

Within the presented thesis the following hypotheses are tested:

in **Chapter 4.1**

- comparing the relative magnitudes of synoptic- and diurnal-timescale influences on near-surface radon concentration enables the identification of PTI events in basin/valley environments for separate analysis;
- radon-based identification of PTI events is more reliable than the conventional pseudo-vertical temperature gradient method, and enables superior characterization of meteorology and air quality across the diurnal cycle during PTI events;

in **Chapter 4.2**

- radon-based atmospheric stability classification is superior to conventional techniques for understanding how relative changes in mixing state between contrasting topographic settings may impact air quality;

in **Chapter 4.3**

- if seasonal changes in the radon source function are accounted for, radon-based stability classification of the ABL is a more effective class-typing tool than meteorological approaches for all seasons in topographic basin settings;
- combining the new radon-based PTI classification method with the existing radon-based stability classification approach enables superior characterization of meteorological controls on air quality in Ljubljana city than conventional approaches;

in **Chapter 4.4**

- comparing diurnal radon cycles between sites under a range of atmospheric mixing conditions each season helps to explain the effects of changing lithology and soil moisture/freezing on radon exhalation at each site;

in **Chapter 4.5**

- at sites with moderate to high radon exhalation changes in the atmospheric mixing state can increase radon activity concentrations in the "zone of habitation" (≤2 m a.g.l.) by two orders of magnitude.

Chapter 3

Methods

3.1 Experimental Sites

In order to study the use of radon as an indicator of atmospheric stability in complex terrains, Ljubljana Basin and Vipava Valley were selected as experimental sites (Vaupotič, Kobal & Križman, 2010). These two sites differ substantially in terms of topography, climate and lithology.

3.1.1 Ljubljana Basin

The Subalpine Basin site (46.05° N, 14.51° E; 299 m a.s.l.) is in Ljubljana, the capital city of Slovenia, which had a population of around 280 000 at the time of this study. The city's climate, classified as temperate and continental, is typical of southern European subalpine regions. Air temperatures exhibit a distinct seasonal cycle, with daily means reaching a maximum of 22 ℃ in summer and a minimum of 0 ℃ in winter. Prevailing winds for the region are NE, NNE, and ENE, and the rainfall distribution is irregular, peaking in summer (ARSO, 2017).

The basin is surrounded by peaks of the Julian and Kamnik–Savinje alps (Vrhovec, 1990). To the north the region is bounded by the Julian and Kamnik–Savinje Alps (highest peaks: Grintovec 2558 m and Krvavec 1742 m), to the west the Šmarna Gora and Rašica hills connect to the Polhov Gradec hills (highest peak: Pasja Ravan, 1019 m), and to the east there are the Posavje hills (highest peak: Kum, 1211 m) (**Figure 3.1**). Immediately to the south is Ljubljansko barje (Šajn et al., 2011), a drained ancient moor that was frequently a lake during the ice ages (Pak, 1992). Ljubljana is located in a shallow sedimentary basin filled with heterogeneous Quaternary deposits. The basin was first covered with gravel deposits by the Sava River and then with sea and lake sediments. Within the gravelly Ljubljana Basin, most water goes underground (Gregorič et al., 2013).

The air quality of Ljubljana is affected by a combination of local and remote influences, the relative contributions of which are dictated by prevailing synoptic processes. The geographic location of Slovenia is such that remote influences on air quality, when they occur, are mainly the result of pollution transport from northern Africa (Kallos et al., 2006), from the North Atlantic Ocean, and across Italy from the Mediterranean Sea (He et al., 2018), the northern Balkan Peninsula, or eastern Europe (Poberžnik & Štrumbelj, 2016). Drag associated with the complex topography of the surrounding region retards synoptic-scale winds, resulting in a mean near-surface annual wind speed of only 1.3 m s^{-1}. Extended periods of anticyclonic conditions are also common for the region.

Combined with the unique concave shape of the Ljubljana Basin (**Figure 3.1**), this results in comparatively calm conditions in the colder months, with frequent foggy days and PTIs (120 d y^{-1}), favoring the buildup of locally sourced emissions.

3.1.2 Vipava Valley

Ajdovščina (98 m a.s.l. ~6800 inhabitants) is a small rural town in the Vipava Valley, Slovenia. The terrain surrounding the valley rises from southwest (the Adriatic coast, 0 m a.s.l.) to the northeast (Karst plateau, 500 m a.s.l), over a distance of less than 20 km. Continuing in this direction, the elevation then falls into the Vipava Valley (100 m a.s.l.) before rising again to the Trnovski gozd barrier (up to 1500 m a.s.l.) (**Figure 3.1**). Due to the location and topography, strong downslope winds (known as 'Bora' wind) can occur as a result of synoptically driven flow over the mountains (Mole et al., 2017; R. Smith, 1985). Although the Bora wind can be observed year-round, it is most vigorous and frequent in the winter, when it can persist for several days, often reaching speeds of more than 28 m s^{-1} in gusts (Grisogono & Belušić, 2009). The prevailing wind directions at this site are: N-NE during Bora wind events, moderate (<5 m s^{-1}) SW flow from the coast, or SE winds that usually follow Bora wind events (typically <20 m s^{-1}). The climate of Ajdovščina is sub-Mediterranean. The mean air temperature is 24 °C in summer and 4 °C in winter. Annual rainfall in the valley is 1500 mm, peaking in autumn (ARSO, 2017).

The valley is situated on flysch, with carbonates at a distance of less than a few km in the NE and SW directions.

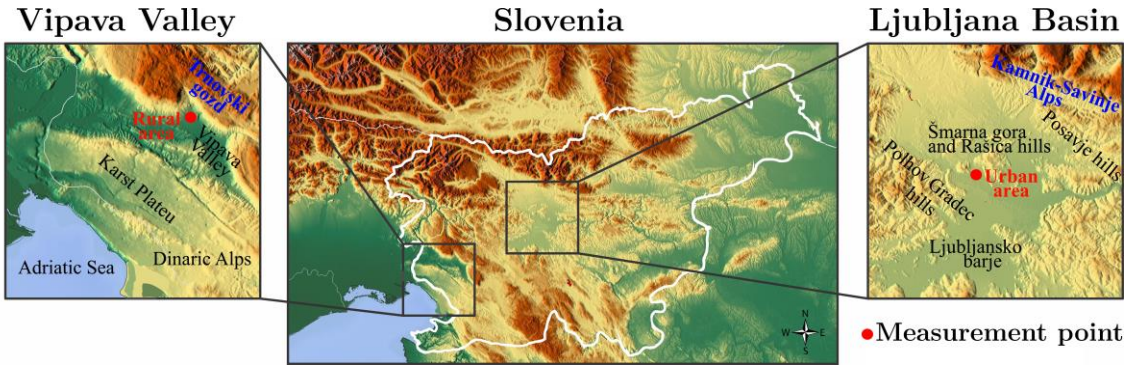


Figure 3.1: Topographic map of Slovenia with the locations of the sub-Mediterranean valley and subalpine basin sites indicated.

3.2 Measurements

3.2.1 Radon Measurements

Atmospheric radon measurements were made for 3 years (14 Dec 2016–30 Nov 2019) at the Ljubljana Bežigrad automatic weather station in the central part of the city, and for 2 and a half years (8 Aug 2017–30 Nov 2019) at Dolenje pri Ajdovščini automatic weather station (see **Appendix A: Figures A1.1 and A2.1** – time series of radon concentrations at the two sites). The measurements were conducted using an AlphaGUARD PQ2000 PRO (Bertin Instruments) ionization chamber operating in diffusion mode with a 1 h integration time. The instrument was mounted 1.5 m above ground level (m a.g.l.), within a Stevenson Screen instrument shelter. It should be mentioned that this type of AlphaGUARD does not differentiate ^{222}Rn and ^{220}Rn. However,

based on following factors, we can conclude that more than 95% of the observed radon concentrations with AlphaGUARD PQ2000 PRO represent the isotope ^{222}Rn: (i) 90% of radon in the atmosphere is ^{222}Rn, and only 9% is ^{220}Rn (less than 1% is ^{219}Rn and other isotopes of radon), (ii) considering that ^{220}Rn and ^{219}Rn are short half-lives (55.6 s and 3.9 s, respectively) and with the instrument mounted in 1.5 m a.g.l., inside an enclosure, operating in diffusion mode (not flow mode), there would be no contribution at all from ^{219}Rn and possible contribution from ^{220}Rn would be less than 5% (Kochowska et al., 2009).

Calibration of the radon devices owned by the Radon Center (Department of Environmental Sciences, Jožef Stefan Institute) is performed regularly either by the company who supplied the instrument, or by exposing the device to known concentration of radon in a radon chamber. The data quality assurance and control are also checked regularly by intercomparison (Murn & Stepišnik, 2019).

AlphaGUARD PQ2000 PRO monitors have a lower limit of detection (LLD) of around 2 Bq m^{-3} (AlphaGUARD Manual: Bertin Instruments). Over the measurement period only about 1% of ambient atmospheric radon activity concentrations at either measurement site were at or below the LLD, which justifies the use of the AlphaGUARD at this site as a suitable tool for air quality assessment.

3.2.2 Meteorology Observations

The Ljubljana Bežigrad and Dolenje pri Ajdovščini weather stations, operated by the National Meteorological Service at the Slovenian Environment Agency (ARSO), have a comprehensive suite of meteorological sensors. The following parameters, recorded at 2 m a.g.l., with 10–30 min time resolution were used in this study: air pressure (hPa), air temperature (°C), relative humidity (%), wind speed (m s^{-1}), wind direction (°), and precipitation (mm). To supplement these observations, total cloud cover (%) and ABL height (m) with 3-hour time resolution were obtained from the Global Data Assimilation System (GDAS) model of NOAA ARL (National Oceanic and Atmospheric Administration Air Resources Laboratory). All the observations are aggregated (or linearly interpolated) to hourly temporal resolution and are reported on local time (UTC+1). The Northern Hemisphere seasonal convention has been adopted (i.e. winter: December–February; spring: March–May; summer: June–August; autumn: September–November).

In addition to the Ljubljana Bežigrad air temperature measurements near the bottom of the Ljubljana Basin (299 m a.s.l.), ARSO air temperature observations were also retrieved from a number of weather stations on the sidewalls of the basin at a range of elevations from 268 to 1742 m (Litija – 268 m, Letališče Jožeta Pučnika Ljubljana – 364 m, Sevno – 556 m, Topol – 695 m, Pasja Ravan – 1019 m, Kum – 1211 m, Krvavec – 1742 m). These air temperature data were used for calculating the pseudo-vertical temperature gradient.

Vertical profiles of the Ljubljana Basin atmosphere (ARSO sounding observations to ~20 km a.g.l.) were also available but are only conducted daily at 4–6 a.m. local time. For the purposes of this study we focused only on the profile information from the lower part of the troposphere (0–2 km a.s.l.) during the period Dec 2016 to Feb 2018 (see **Chapter 4.3 and Appendix B**).

Backward trajectory analysis for air mass fetch analysis was performed using the NOAA/ARL HYSPLIT (Hybrid Single Particle Lagrangian Integrated Trajectory) model (Draxler & Rolph, 2011).

3.2.3 Air Quality Observations

Air quality parameters (PM_{10}, CO, NO_2, SO_2, and O_3) were obtained for the same time period as the radon measurements, but only from the Ljubljana Bežigrad site. PM_{10} concentrations were measured with a continuous direct mass measurement for particulate matter utilizing a tapered element oscillating microbalance (TEOM). NO_2 was measured by chemiluminescence, SO_2 by ultraviolet fluorescence, and O_3 by ultraviolet photometry (Gjerek et al., 2017). In addition, BC was measured with a Magee Scientific Aethalometer AE-33 and the data were provided by Aerosol d.o.o., Ljubljana, Slovenia. The total reported concentration of BC represents the sum of traffic (BC_{tr}) and biomass burning (BC_{bb}) sources (Sandradewi et al., 2008).

3.3 Development of Radon-based PTI Identification Method, and Implementation of Existing Radon-based Stability Classification

The ABL of complex terrain environments changes on synoptic and diurnal scales. After determining that the contemporary radon-based method for assessing the atmospheric mixing state misclassified conditions during PTI events, we adapted this method such that it might also be able to accommodate changes in observed radon concentrations brought about by changes in the atmospheric mixing state on greater than diurnal timescales. The result was a radon-based method that could identify and isolate PTI events from a long-term record prior to assigning the usual diurnal atmospheric mixing classification so that all mixing categories could be investigated separately.

Both the new and contemporary methods are based on continuous, near-surface, single-height observations of atmospheric radon concentrations (**Appendix A: Figures A1.1 and A2.1**, time series of measured radon in Ljubljana Basin and Vipava Valley). As outlined in **sub-chapter 1.3.2** numerous factors contribute to the observed natural variability in radon concentrations at different timescales. Consequently, prior to implementing the methods described above it is necessary to appropriately curate the measured radon data. To account for seasonality in the regional radon exhalation rate, the radon-based class-typing techniques need to be performed separately for each season. Therefore, the seasonality of radon exhalation rates does not adversely affect the efficacy of the technique, making it seasonally independent. The principle of both radon-based methods (synoptic and diurnal) is described in detail in **Chapters 4.1 and 4.2**. However, a brief summary of the methodological steps (1–6) is outlined in the following sub-chapters.

3.3.1 Diurnal Radon-based Stability Classification

1. Minimizing instrument uncertainty and sub-diurnal radon variability

Since afternoon radon concentrations can be close to the instruments' detection limit, measurement uncertainty cannot be neglected. Furthermore, to minimize the impact of sub-diurnal timescale contributions on our estimation of diurnal minimum radon concentrations, we started by performing a *3-h running mean smoothing* on the measured radon values.

2. Identification of the synoptic variability ("fetch-related") and isolation of diurnal variability ("mixing-related")

Measured radon concentrations represent a combination of local (mixing-related) and non-local (fetch-related, brought by synoptic processes) signals. Since only the mixing-related radon signal can be used as an indicator of the changing diurnal atmospheric mixing state, it is important to identify non-local radon signal and exclude them. Although, the principle of the diurnal radon-based stability classification is presented with Ljubljana summer season (**Figure 3.2**) the same approach was used for all seasons in both sites.

In order to do so, firstly, the period of the diurnal cycle at which the lowest radon values usually occurred (between 12:00–18:00 h) was identified (see **Figure 3.2a**). This period of the day is characterized by the strongest atmospheric mixing, therefore there is usually very little difference in radon concentrations measured near the surface (e.g. 1.5 m a.g.l.) and those measured much further from the surface (e.g. ~500 m a.g.l.) near the middle of the ABL. At night, however, radon accumulates near the surface in the SNBL (usually only a few 10s or 100s of m thick), whereas the radon concentrations in the residual layer above (including around 500 m a.g.l.) remain similar to that of the previous day. Therefore, in the absence of vertical radon gradient measurements, as in our case, it is possible to *approximate* a radon measurement at a second height far from the surface (which better represents non-local contributions to radon values), by *linearly interpolating* between consecutive daily minimum radon concentrations (from one afternoon to the next) of near-surface measurements (see **Figure 3.2b**). Calculating the difference between the measured radon concentrations (C_{Rn}) (**Figure 3.2b** – black line) and the interpolated non-local radon contributions ($C_{\mathrm{Rn\text{-}fetch}}$) (**Figure 3.2b** – red line), the local radon contribution ("mixing-related radon concentration" - $C_{\mathrm{Rn\text{-}mix}}$) (**Figure 3.2c**) is obtained:

$$C_{\mathrm{Rn}} - C_{\mathrm{Rn\text{-}fetch}} = C_{\mathrm{Rn\text{-}mix}} \tag{3.1}$$

The difference is analogous to calculating a radon gradient measurement.

3. Calculating the mean nocturnal mixing-related radon

The next step was to define a nocturnal window (**Figure 3.2d**) over which to assess the near-surface radon accumulation. The timing and duration of this window was based on the longest day of the year in summer (approximately sunset to sunrise, 19:00–05:00 h; **Figure 3.2d**). Since the non-local radon values have been removed, the mixing-related radon concentration averaged over this nocturnal window will be directly related to the average net near-surface vertical mixing processes that night. To minimize seasonal effects, predominantly changing day length, on the absolute magnitude of these nocturnal mean radon concentrations, each nocturnal mean value is referenced to the corresponding 19:00 h radon concentration (Chambers et al., 2019), such that:

$$C_{\mathrm{Rn}_{19:00\text{-}05:00}} = \left(\frac{\sum_{i=11}^{11} C_{\mathrm{Rn}}}{11} \right) - C_{\mathrm{Rn}_{19:00}} \tag{3.2}$$

4. Definition of the five diurnal radon-based atmospheric mixing classes

A cumulative histogram of these nocturnal-mean diurnal radon values ($C_{\mathrm{Rn\text{-}noc}}$) was then calculated for each season and site (e.g. summer cumulative frequency in Ljubljana Basin – **Figure 3.2e**). Quartiles of the nocturnal-mean diurnal radon were used to denote threshold values for the five diurnal relative atmospheric mixing classes (**Table 3.1**: expected meteorological conditions for each class): "mixed-fetch" (class #1), "near-neutral"

(class #2), "weakly stable" (class #3), "moderately stable" (class #4) and "most stable" (class #5). It is important to note that while the nocturnal mixing classes have been clearly defined through measurements, the daytime mixing classes are only implied, assuming short-term atmospheric persistence (**Table 3.1**) (Chambers et al., 2019; Podstawczyńska & Chambers, 2018).

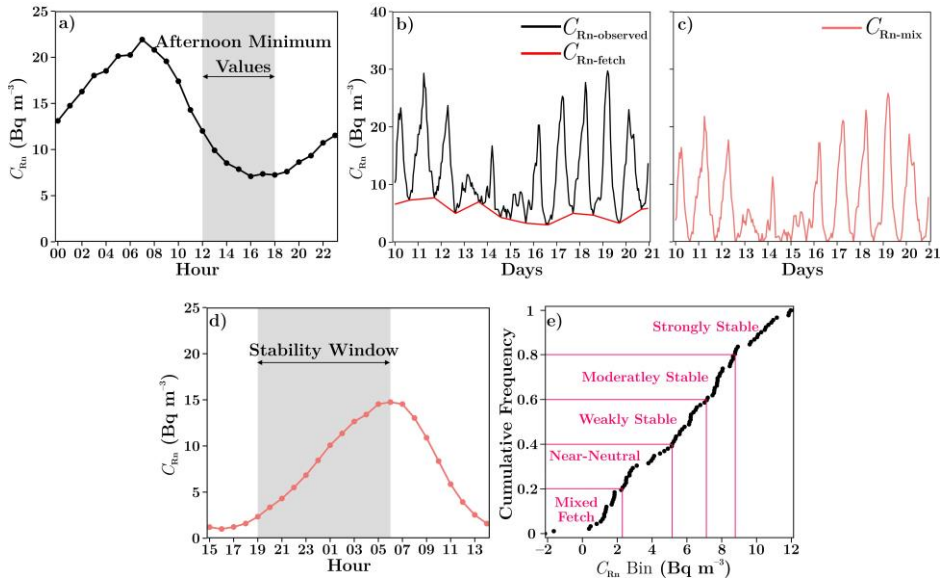


Figure 3.2: Illustration of the methodological steps for development of diurnal radon-based stability classification: a) diurnal cycle of observed radon concentration (period at which the lowest radon values occur is highlighted), b) few days of observed radon concentration and interpolated radon fetch component, c) few days of mixing-related radon concentration (difference between observed radon concentration and fetch-related radon concentration), d) diurnal cycle of mixing-related radon concentration (nocturnal stability window is highlighted), e) cumulative frequency distribution of nocturnal mean mixing-related radon within the nocturnal stability window. All data refers to the summer season (Jun–Aug 2019).

Table 3.1: Description of the 24-hour six radon-based atmospheric mixing classes.

24-h mixing class	Night-time mixing conditions	Daytime mixing conditions	Expected meteorological conditions
#1	Mixed fetch	Mixed fetch	Moderate-strong gusty winds, cloudy, fronts, precipitation
#2	Near-neutral	Near-neutral	Moderate-strong winds, overcast, precipitation
#3	Weakly stable	Weakly unstable	Light-moderate winds, broken cloud/overcast, precipitation
#4	Moderately stable	Moderately unstable	Light winds, scattered clouds, precipitation uncommon
#5	Strongly stable	Strongly unstable	Calm-light wind, clear sky, typically no precipitation
#6	Persistent temperature inversion	Persistent temperature inversion	Calm gradient wind, foggy/low-level clouds, no precipitation

The quartile ranges of the cumulative frequency histogram for each season and site, used to define five radon-based diurnal mixing classes, are presented in **Appendix A** (**Tables A1.2 and A2.2**). The tables also provide a relative breakdown of the number of events in each mixing class experienced in each season. The daily mean measured radon values (containing the non-local and local radon signals) for the six radon-based mixing classes are also tabulated in **Appendix A** (**Tables A1.1 and A2.1**). In addition, diurnal composites of the mixing-related radon component within each mixing class for all seasons and each site are illustrated in **Appendix A** (**Figures A1.3 and A2.3**).

In some cases, more often at Ajdovščina which is closer to the coast, the nocturnal-mean diurnal radon values become negative (see **Tables A1.2 and A2.2**). This is a result of nocturnal radon concentrations occurring that are below "afternoon minimum" values, which usually indicates synoptic non-stationarity (e.g. a frontal system) or change in air mass fetch from land to recently oceanic (see Figure 2 in Chambers et al. (2019).

3.3.2 Synoptic Timescale Radon-based Classification

1. Isolation of synoptic timescale radon variability

Variability on greater than synoptic timescales was evident in the radon time series, which needed to be minimized prior to attempting to identify PTI events. The first step was to characterize typical synoptic timescale variability at the two chosen sites. We did this by performing a *spectral analysis* of the hourly Ljubljana and Ajdovščina atmospheric pressure observations for each season. Throughout winter and autumn, the analysis indicated a synoptic timescale of 5–8 d, whereas in spring and summer the synoptic timescale was typically 6–7 d. A *running-minimum* radon concentration using a window derived from the spectral analysis of atmospheric pressure (7-d window for all seasons) was calculated. Lastly, this running-minimum concentration ($C_{\mathrm{Rn-subtracted}}$) was subtracted from the $C_{\mathrm{Rn-fetch}}$ (fetch-effect) derived in (step 2) above, in order to isolate the synoptic timescale contributions to the radon observations ($C_{\mathrm{Rn-syn}}$).

2. Definition of synoptic radon-based atmospheric mixing class (PTI class)

Having isolated the synoptic timescale contribution to the measured radon time series, the next steps to develop the PTI identification tool were to:

(i) identify periods when synoptic timescale variability of radon dominates diurnal variability of radon

For this purpose, we chose the seasonal standard deviation ($+\sigma$) of the mixing-related radon contribution as a measure of the significance of diurnal radon variability each season. The values of ($+\sigma\ C_{\mathrm{Rn-mix}}$) for all seasons at each site are presented in **Appendix A** (class #6 in **Tables A1.2 and A2.2**).

(ii) decide on a minimum length of time that this needs to occur for the event to be considered a PTI.

The duration threshold on these exceedances for an event to be classified as a PTI was chosen to be 48 consecutive hours.

So, a PTI event is considered to have occurred when the synoptic contribution to the radon signal exceeds the standard deviation of the diurnal contribution for that season for a period of at least 48 h:

$$C_{\mathrm{Rn-syn}} > +\sigma\ C_{(\mathrm{Rn\text{-}mix})\mathrm{season}} \geq 48\ \mathrm{h} \tag{3.3}$$

Chapter 4

Publications

4.1 Development of a New Radon-based Method for Identification of Synoptic Timescale PTI Events in Complex Terrain

The aim of this study was to determine a reliable and seasonally-independent radon-based method to identify PTI events in topographic basin environments, such that they can be separately grouped as a new atmospheric mixing class of the contemporary diurnal radon-based stability classification method. The results of this study are presented in the peer-reviewed article entitled "Identifying persistent temperature inversion events in a subalpine basin using radon-222".

Development of the radon-based PTI identification tool required an understanding of the various timescales contributing to variability in the hourly radon time series (sub-diurnal, diurnal, synoptic, and greater than synoptic). The method is applied in four steps: (i) minimize sub-diurnal radon variability, (ii) identify the fetch-related (synoptic-scale) radon variability, (iii) isolate the synoptic-scale from larger timescale variability, and (iv) identify PTI events using the seasonal standard deviation of diurnal timescale radon variability as an event threshold with a $\geq$48 h persistence requirement. The method was applied separately for each season in order to account for seasonal changes in the radon source function, day length, and atmospheric mixing.

By comparing the newly-developed technique with an existing pseudo-vertical temperature gradient method, the radon-based method was shown to be more reliable and seasonally independent. The consistency and accuracy of this method has the potential to significantly increase the understanding of meteorological processes resulting in air pollution episodes. Once a representative number of PTI events have been observed within each season, this technique also has the potential to objectively assess the relative strength of PTI events. As such, the radon method has the potential to become a key tool in urban centers for air quality management and assessing public health risks.

In this scientific article, the candidate developed the research question, performed data collection, curation and formal analysis. She performed all visualization of data, concepts, interpreted the results and wrote the complete original draft of the manuscript.

Atmos. Meas. Tech., 12, 4455–4477, 2019
https://doi.org/10.5194/amt-12-4455-2019
© Author(s) 2019. This work is distributed under
the Creative Commons Attribution 4.0 License.

Atmospheric Measurement Techniques
Open Access
EGU

Identifying persistent temperature inversion events in a subalpine basin using radon-222

Dafina Kikaj[1,2], **Janja Vaupotič**[2], **and Scott D. Chambers**[3]

[1]Jožef Stefan International Postgraduate School, Jamova cesta 39, 1000 Ljubljana, Slovenia
[2]Jožef Stefan Institute, Department of Environmental Sciences, Jamova cesta 39, 1000 Ljubljana, Slovenia
[3]ANSTO, Environmental Research, Locked Bag 2001, Kirrawee DC, NSW 2232, Australia

Correspondence: Dafina Kikaj (dafina.kikaj@ijs.si)

Received: 16 November 2018 – Discussion started: 22 February 2019
Revised: 15 May 2019 – Accepted: 17 July 2019 – Published: 21 August 2019

Abstract. One year of meteorological and atmospheric radon observations in a topographically complex subalpine basin are used to identify persistent temperature inversion (PTI) events. PTI events play a key role in public health due to the accumulation of urban pollutants that they cause. Two techniques are compared: a new radon-based method (RBM), based on single-height ^{222}Rn measurements from a single centrally located station, and an existing pseudo-vertical temperature gradient method (TGM) based on observations from eight weather stations around the subalpine basin. The RBM identified six PTI events (four in winter, two in autumn), a subset of the 17 events identified by the TGM. The RBM was more consistent in its identification of PTI events for all seasons and more selective of persistent strongly stable conditions. The comparatively poor performance of the TGM was attributed to seasonal inconsistencies in the validity of the method's key assumptions (influenced by mesoscale processes, such as local drainage flows, nocturnal jets, and intermittent turbulence influence) and a lack of snow cover in the basin for the 2016–2017 winter period. Corresponding meteorological quantities for RBM PTI events (constituting 27 % of the autumn–winter cold season) were well characterized. PTI wind speeds in the basin were consistently low over the whole diurnal cycle (typically 0.2–0.6 m s^{-1}). Suitability of the two techniques for air quality assessment was compared using hourly PM_{10} observations. Peak PM_{10} concentrations for winter (autumn) PTI events were underestimated by 13 µg m^{-3} (11 µg m^{-3}) by the TGM compared with the RBM. Only the RBM indicated that nocturnal hourly mean PM_{10} values in winter PTI events can exceed 100 µg m^{-3}, the upper threshold of low-level short-term PM_{10} exposure according to World Health Organization guidelines. The efficacy, simplicity, and cost effectiveness of the RBM for identifying PTI events has the potential to make it a powerful tool for urban air quality management in complex terrain regions, for which it adds an additional dimension to contemporary atmospheric stability classification tools. Furthermore, the long-term consistency of the radon source function will enable the RBM to be used in the same way in future studies, enabling the relative magnitude of PTI events to be gauged, which is expected to assist with the assessment of public health risks.

1 Introduction

Urban air pollution is one of the main environmental health risks in Europe (EEA, 2017; WHO, 2014). It derives from aerosols and/or trace gases of natural (e.g., sandstorms, volcanos, forest fires, and ocean spray) or anthropogenic origin (e.g., biomass burning, power generation, transport, and industry) (Beeston et al., 2011; Ferrario et al., 2008; Langmann et al., 2012; Miranda et al., 2015; Pey et al., 2013; Vardoulakis and Kassomenos, 2008). Public health effects can be acute or chronic in nature, and include respiratory illnesses, cardiovascular disorders, conjunctivitis, skin irritations, meningococcal meningitis, valley fever, and even mortality (Goudie, 2014; Griffin, 2005; Highwood and Kinnersley, 2006; Pope and Dockery, 2006). With public health in mind, the World Health Organization (WHO) identified numerous "criteria pollutants" in urban regions for which they have recommended guidelines on concentrations and/or du-

ration (the Air Quality Directive; EEA, 2017). An air pollution event is considered to have occurred when the concentration of one or more of the criteria pollutants exceeds the guideline value for longer than the specified duration threshold. Such pollution events can be of short duration (1–12 h, day or night) or, under certain conditions, they can persist for days to weeks.

Urban air quality can be influenced by remote, regional, or local processes, depending on the prevailing meteorology (Kukkonen et al., 2005). The particular focus of this study is on pollution events arising as a result of local anthropogenic emissions, the effects of which are exacerbated under specific synoptic weather conditions: cold-season anticyclones. Anticyclonic weather conditions are associated with relatively calm winds and clear skies, due to regional-scale subsidence. In summer, anticyclonic conditions can result in daytime pollution events as a result of rapid secondary-pollutant formation, or nighttime pollution events, when strong radiative cooling results in the formation of shallow, poorly mixed inversion layers. Such pollution events usually end abruptly each morning shortly after the onset of convective mixing as a result of intense sunlight on dry surfaces. In such cases, near-surface concentrations of primary emissions drop $\sim 50\,\%$ from peak values by midmorning and reach their minimum values in the early afternoon when the atmospheric boundary layer (ABL) is deep and uniformly mixed (Chambers et al., 2015). In winter, however, day lengths are shorter, sun angles lower, and surfaces wet or frozen. In topographically complex regions, when wind speeds and day length can be even further reduced, and katabatic flows down the basin walls result in the "pooling" of cold air, large-scale subsidence associated with slow-moving or stagnant anticyclonic systems can inhibit the daytime mixing that usually disperses accumulated nocturnal pollution, resulting in air pollution events that can persist for days to weeks (Baasandorj et al., 2017; Cuxart et al., 2006; Kassomenos and Koletsis, 2005). Here we refer to such extended periods of severe air pollution as persistent temperature inversion (PTI) events.

In light of the above, the ability to reliably identify PTI events and objectively quantify their magnitude is important for improved understanding of pollutant concentration variability, assessing potential health impacts on residents, and developing new mitigation measures for air pollution in such complex topographical regions. Unfortunately, there have been relatively few observational studies of PTI events (Clements et al., 2003; Dorninger et al., 2011; Lareau et al., 2013; Lehner et al., 2015; Silcox et al., 2012). To date, this lack of observational studies has mainly been due to the difficulty in making the necessary meteorological measurements within the topographically challenging regions (Yao and Zhong, 2009). Furthermore, such studies often require the deployment of sophisticated instrumentation (e.g., radiosondes, tethered balloons, masts, or aircraft), which is typically expensive and labor intensive to operate (Baasandorj et al., 2017).

The first European field campaign to target PTI events took place in the Chamonix-Mont-Blanc valley, in January–February 2015. This study was motivated by the anomalously high pollution concentrations frequently recorded there. The comprehensive suite of meteorological and chemical observations made throughout the campaign has been described by Chemel et al. (2016). A meteorological approach, based on differences between air temperatures from automatic weather stations at various elevations of the sidewalls of the valley, was used to characterize the stable nocturnal conditions (Dorninger et al., 2011; Whiteman et al., 2004) based on the assumption of horizontally homogenous air temperature. The same pseudo-vertical temperature gradient method was employed by Largeron and Staquet (2016a) in the French Alps to detect PTI events throughout the cold season (November 2006 to February 2007). There are, however, a variety of mesoscale processes that have the potential to disrupt the vertical temperature profile and its horizontal homogeneity (including local drainage flows, nocturnal jets, and intermittent turbulence) (Whiteman et al., 2004; Williams et al., 2013). Such influences can complicate the interpretation of pseudo-vertical temperature gradients derived from stations of contrasting elevations on valley or basin walls, depending on their particular spatial locations.

By contrast, measurement of a surface-emitted atmospheric tracer with appropriate physical properties (e.g., simple source and sink characteristics), which responds directly to atmospheric mixing processes, has the potential to provide a more consistent and representative method by which to identify PTI events. Such a method should be uniformly applicable, allowing seasonal changes in the number and duration of such events to be determined. Furthermore, once a representative number of events have been identified, seasonally dependent threshold concentrations of the tracer could be determined to help gauge the severity of the inversion events and characterize the meteorological conditions with which they are associated. The naturally occurring radioactive gas radon (^{222}Rn) is an ideal candidate for this task. The use of radon as a tracer in atmospheric studies dates back from the early 1900s (Eve, 1908; Satterly, 1910; Wigand and Wenk, 1928; Wright and Smith, 1915). In particular, however, radon has achieved considerable credibility in the field of atmospheric science as an indicator of vertical mixing and transport near the Earth's surface from the 1960s until present (Moses et al., 1960; Kirichenko, 1962; Cohen et al., 1972; Allegrini et al., 1994; Perrino et al., 2001; Sesana et al., 2003; Galmarini, 2006; Avino and Manigrasso, 2008; Chambers et al., 2011, 2015, 2019; Williams et al., 2011, 2013, 2016; Pitari et al., 2014; Wang et al., 2016).

Radon concentrations exhibit a high degree of variability on hourly to seasonal timescales. The majority of this variability is attributable to processes occurring at diurnal, synoptic, and seasonal timescales. Other influences, such as those arising from mesoscale motions, or the effects of geographical variability in soil characteristics, rainfall, wind

speed, and atmospheric pressure on the radon source function (Chambers et al., 2011; Etiope and Martinelli, 2002; Karstens et al., 2015; Levin et al., 2002; Mazur and Kozak, 2014; Salzano et al., 2016, 2018; Szegvary et al., 2007, 2009; Zhuo et al., 2008), are of secondary significance and random in nature, so they typically average out in long-term (seasonal) statistics. The PTI identification technique developed in this study necessitates the ability to characterize and separate the different temporal scales contributing to the variability observed in a radon time series.

Seasonal variability of radon concentrations is contributed to by long-term changes in (i) air mass fetch, (ii) radon source function (through average soil moisture, snow cover, or soil freezing) (Salzano et al., 2016, 2018; Szegvary et al., 2007, 2009; Zhuo et al., 2008), (iii) day length, and (iv) mean atmospheric boundary layer depth (higher in summer, lower in winter), brought about by the annual solar cycle. Synoptic variability (timescale ≤ 2 weeks) is mainly attributable to short-term changes in air mass fetch, boundary layer depth, and ventilation of the boundary layer, brought about by the passage of synoptic weather systems. In this case, variability of the radon source function over the air masses' recent fetch can have a greater influence on observed concentrations than the local radon source function at the measurement site. Diurnal variability, on the other hand, is primarily attributable to changes in the atmospheric mixing state (i.e., mixing depth or "stability"), and the strength of the local radon source function.

The diurnal radon cycle is characterized by a midafternoon minimum (the magnitude of which is related to the air masses' fetch history) and a nocturnal maximum near dawn (when the atmospheric mixing depth is shallowest). The amplitude of the diurnal radon cycle is directly related to the degree to which near-surface turbulent mixing is suppressed each night. Synoptic cycles of the afternoon minimum radon concentrations can be analogous to the diurnal radon cycle, but on longer timescales. These cycles are characterized by minimum values when gradient winds are strong (or terrestrial fetch is limited), and maximum values when gradient winds are low and there is subsidence (or during extended periods of terrestrial fetch, including stagnation episodes). In the warmer months, when days are convective and nights are stable, diurnal cycle amplitudes exceed synoptic cycle amplitudes. In the colder months, however, the amplitude of the synoptic cycle can be comparable to, or even greater than, that of the diurnal cycle. This seasonal change in relative amplitudes of the diurnal and synoptic radon cycles forms the basis of our method to identify PTI events.

The aims of this study are to use the first year of continuous joint atmospheric radon and meteorological measurements in a subalpine basin (Ljubljana, Slovenia) to (i) develop a seasonally independent radon-based method to reliably identify persistent temperature inversion events in complex topographic regions; (ii) compare the performance of the radon-based scheme to that of a previously published pseudo-vertical temperature gradient method for identifying PTI events over the whole year; (iii) investigate the seasonality of PTI event occurrence in the subalpine basin; and (iv) characterize the local meteorological conditions (air temperature, relative humidity, cloud cover, wind speed, wind direction, and precipitation) associated with PTI events, as well as discuss the implications of these conditions for urban air quality using hourly urban PM_{10} observations as an example.

2 Methodology

2.1 Radon as a tracer of atmospheric transport and mixing

^{222}Rn (hereafter radon) is the gaseous decay product of ^{226}Ra (radium), a member of the ^{238}U (uranium) chain, which is ubiquitous all over the Earth's crust. Radon is fairly uniformly distributed on local to regional scales ($1\ \mathrm{atom\ cm^{-2}\ s^{-1}} \pm 25\,\%$; Jacob et al., 1997; Karstens et al., 2015), and has a source function that is 2–3 orders of magnitude greater from unsaturated land surfaces than from the open ocean (Schery and Huang, 2004). Once emitted to the atmosphere radon is directly influenced by the meteorological processes that regulate turbulent mixing, namely, vertical and horizontal components of dispersion. Being an inert gas, radon does not chemically react with other atmospheric constituents and its low solubility makes it unlikely to be washed out by rainfall. Consequently, it is eliminated from the atmosphere predominantly by radioactive decay (half-life 3.82 d). While radon's short half-life prevents it from accumulating in the atmosphere greater than synoptic timescales, it is possible to track air masses that have been in contact with terrestrial surfaces over the ocean, or within the troposphere, for 2–3 weeks, enabling it to carry important geophysical information over long distances. Since radon's half-life is much greater than mixing timescales of the atmospheric boundary layer, and since radon is still relatively conservative (within 5 %–10 %) over the course of a whole night, radon is an appropriate atmospheric tracer for near-surface mixing studies from hourly to nightly timescales. Furthermore, based on the relatively small fraction of terrestrial surfaces occupied by urbanization, at the regional scale radon's terrestrial source function is not significantly affected by human activity.

2.2 Measurement sites and surroundings

The Ljubljana subalpine basin site (SAB; 46.05° N, 14.51° E; 299 m above sea level, m a.s.l.) is in the capital city of Slovenia, which has a population of around 280 000. The city's climate, classified as temperate and continental, is typical of southern European subalpine regions. Air temperatures exhibit a distinct seasonal cycle, with daily means reaching a maximum of 22 °C in summer and a minimum of 0 °C in winter. Prevailing winds for the region are NE, NNE, and

ENE, and the rainfall distribution is irregular, peaking in summer (ARSO, 2017).

The SAB is surrounded by peaks of the Julian and Kamnik–Savinje alps (Vrhovec, 1990). To the north the region is bounded by the Julian and Kamnik–Savinje alps (highest peaks: Grintovec 2558 m and Krvavec 1742 m), to the west the Šmarna Gora and Rašica hills connect to the Polhov Gradec hills (highest peak: Pasja Ravan, 1019 m), and to the east there are the Posavje hills (highest peak: Kum, 1211 m). Immediately to the south is Ljubljansko Marshes (Šajn et al., 2011), a drained ancient moor that was frequently a lake during the ice ages (Fig. 1b) (Pak, 1992).

The air quality of Ljubljana is affected by a combination of local and remote influences, the relative contributions of which are dictated by prevailing meteorology. The geographic location of Slovenia (Fig. 1a) is such that remote influences on air quality, when they occur, are mainly a result of pollution transport from northern Africa (Kallos et al., 2006), from the North Atlantic Ocean, and across Italy from the Mediterranean Sea (He et al., 2018), the northern Balkan Peninsula, or eastern Europe (Poberžnik and Štrumbelj, 2016).

Drag associated with the complex topography of the surrounding region retards synoptic-scale winds, resulting in a mean near-surface annual wind speed of only $1.3\,\mathrm{m\,s^{-1}}$. Extended periods of anticyclonic conditions (low-gradient winds and subsidence) are also common for the region. Combined with the unique concave shape of the subalpine Ljubljana basin (Rakovec et al., 2002), this results in comparatively calm conditions in the colder months, with frequent foggy days and persistent temperature inversions ($120\,\mathrm{d\,y^{-1}}$), favoring the buildup of locally sourced emissions.

2.3 Measurement methods

Atmospheric radon measurements were made for 1 year (14 December 2016 to 30 November 2017) at the Ljubljana Bežigrad (LjB) automatic weather station in the central part of the city (46°07′ N, 14°52′ E; Fig. 1c), and are ongoing. The measurements were conducted using an AlphaGUARD PQ2000 PRO (Bertin Instruments) ionization chamber operating in diffusion mode with a 1 h integration time. The instrument was mounted 1.5 m above ground level (m a.g.l.), within a Stevenson Screen instrument shelter. Setup in this way more than 95 % of the observed radon concentrations represent the isotope ^{222}Rn (Kochowska et al., 2009). Consequently, to a good approximation contributions from the isotopes ^{220}Rn (thoron) and ^{219}Rn (actinon) can be ignored. The AlphaGUARD has a lower limit of detection (LLD) of around $2\,\mathrm{Bq\,m^{-3}}$. Over the year only 1 % of observed radon concentrations were at or below this limit, which justifies the continued use of the AlphaGUARD at this site as a tool for air quality assessment.

The LjB weather station, operated by the National Meteorological Service at the Environmental Agency of the Republic of Slovenia (ARSO), also has a comprehensive suite of meteorological sensors. The following parameters, recorded at 2 m a.g.l. and aggregated to hourly temporal resolution, were used in this study: air temperature (°C), relative humidity (%), wind speed ($\mathrm{m\,s^{-1}}$), wind direction (°), and precipitation ($\mathrm{mm\,h^{-1}}$) as well as the standard air quality parameter PM_{10} ($\mu\mathrm{g\,m^{-3}}$) (ARSO, 2017). To supplement these observations, total cloud cover (%) was obtained from the Global Data Assimilation System (GDAS) model of NOAA ARL (National Oceanic and Atmospheric Administration Air Resources Laboratory).

In addition to the LjB air temperature measurements near the bottom of the Ljubljana basin (299 m a.s.l.), ARSO air temperature observations were also retrieved from a number of weather stations on the sidewalls of the basin at a range of elevations from 268 to 1742 m. A full list of station names, abbreviations, and elevations is provided in Table 1, and their locations relative to LjB are shown in Fig. 1c. To facilitate subsequent analyses, each station was assigned an elevation category (low, medium, or high) according to its elevation relative to the bottom of the basin (Table 1).

The statistical analyses for this study were performed using the ggplot2 (Wickham, 2009) and imputeTS (Moritz, 2017) packages under R 3.3.1 (R Development Core Team, 2008). All reported times are local (local time is UTC+1) and the Northern Hemisphere seasonal convention has been adopted (i.e., winter: December–February; spring: March–May; summer: June–August; autumn: September–November).

2.4 Identifying persistent temperature inversion events

2.4.1 The radon-based method (RBM)

Our method for identifying PTI events is based on continuous, near-surface, single-height observations of atmospheric radon concentrations. The principle of the method is outlined in the following two steps: (i) minimize or separate contributions to the observed radon variability occurring at the four main timescales (sub-diurnal, diurnal, synoptic, and greater-than synoptic), and then (ii) compare the relative magnitudes of variability contributed by the diurnal and synoptic timescales. Since the separation and comparison of different timescale contributions to radon concentration variability is performed separately for each season and year, changes in mean rates of radon emission between seasons or years do not adversely affect the efficacy of the technique.

Although the performance of the method is seasonally independent, the greatest number of PTI events in the SAB occurs in winter, so here we focus only on winter observations for the purpose of demonstrating the method. The processes involved in minimizing or separating contributing timescales to the observed radon time series in order to isolate the syn-

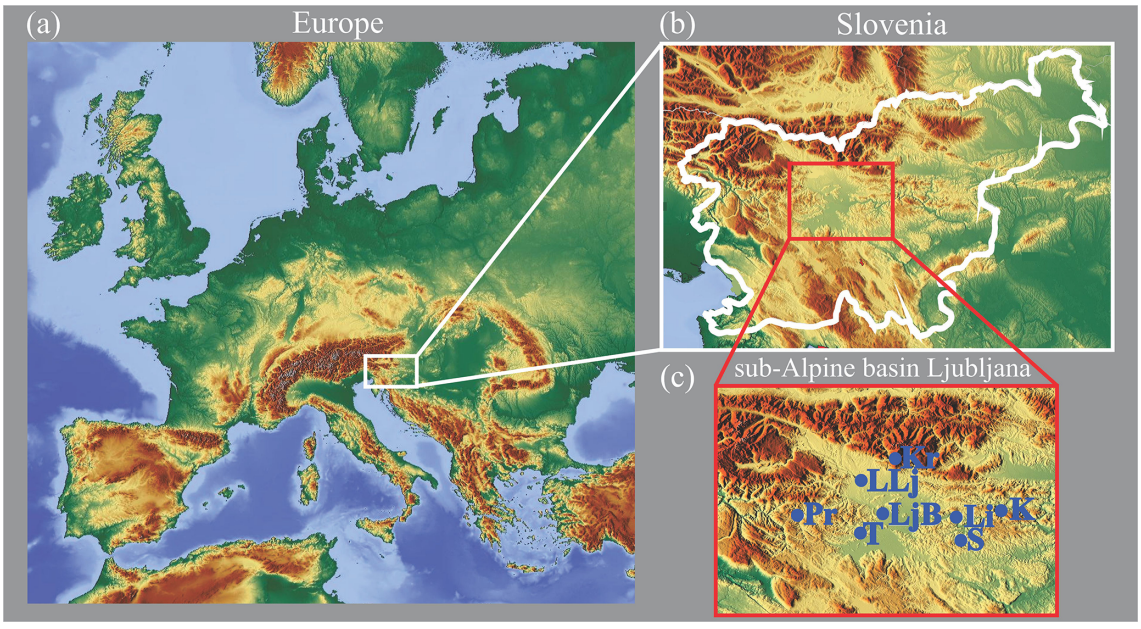


Figure 1. **(a)** Location of Slovenia within Europe, **(b)** topographic map of Slovenia with the location of Ljubljana indicated, and **(c)** topographic map of the Ljubljana basin, with the locations of automatic weather stations indicated. Basemap source: © https://www.openstreetmap.org/copyright, last access: 11 August 2019.

Table 1. Ground-based automatic weather station name, abbreviation, position, elevation, and elevation category.

Station name	Acronym	Latitude (° N)	Longitude (° E)	Elevation (m)	Elevation category
Litija	Li	46°06′	14°81′	268 m	low
Ljubljana-Bežigrad	LjB	46°07′	14°52′	299 m	low
Letališče Jožeta Pučnika Ljubljana	LLj	46°21′	14°47′	364 m	low
Sevno	S	45°98′	14°92′	556 m	medium
Topol	T	46°09′	14°37′	695 m	medium
Pasja Ravan	PR	46°09′	14°22′	1019 m	high
Kum	K	46°08′	15°07′	1211 m	high
Krvavec	Kr	46°29′	14°53′	1742 m	high

optic timescale contributions for further analysis (i.e., Step 1) are outlined below.

1. *Minimizing instrument uncertainty and sub-diurnal radon variability*. Since afternoon radon concentrations can be close to the instruments' detection limit (even in winter), measurement uncertainty cannot be neglected. Furthermore, as outlined in Sect. 1 numerous factors contribute to natural variability in observed radon concentrations at sub-diurnal timescales. To minimize the impact of the above contributions on our estimation of diurnal minimum radon concentrations, we started by performing a 3 h running mean smoothing on the observed radon concentrations (Fig. 3a, black line, $C_{\text{Rn-observed}}$).

2. *Characterization of the synoptic variability ("fetch effect")*. Mean summer and winter diurnal radon cycles at LjB are shown in Fig. 2a. As detailed in Sect. 1, these cycles are characterized by peak concentrations near sunrise, when near-surface mixing is usually suppressed, and minimum values in the midafternoon, when the ABL is deep (typically ≥ 1 km) and uniformly mixed. Depending on season (specifically, the duration and intensity of solar radiation), the timing and duration of the diurnal maximum and minimum concentration periods may change by several hours (Fig. 2a). For a given season, afternoon minimum radon concentrations are primarily influenced by the combined radon emissions along the air masses' recent (two to three radon half-lives) fetch, which changes with the passage of synoptic weather systems. Diurnal variability (driven by changes in mixing depth and the local radon flux) is superimposed on top of this fetch-driven radon variability. As an economical alternative to vertical radon gradient

measurements (which require multiple research-grade detectors), the fetch-related influence (synoptic contribution) to radon concentrations observed at a single height can be approximated by linearly interpolating between successive afternoon minimum values (Chambers et al., 2015; Podstawczyńska and Chambers, 2018). For the purpose of this investigation we derived the daily minimum radon concentrations over the year of observations by identifying the minimum smoothed concentration each afternoon between 14:00 and 19:00 LT. An example of this linearly interpolated approximation of the air mass fetch contribution to the LjB radon concentrations is shown in Fig. 3a (light blue line, $C_{\text{Rn-advected}}$). It should be noted that the assumptions upon which this fetch-effect approximation is based are invalid under severe weather conditions (e.g., during the passage of strong frontal systems, or rapid changes from terrestrial to oceanic fetch).

3. *Isolation of synoptic contribution from longer timescale radon contributions*. Variability on greater than synoptic timescales was evident in the radon time series, which needed to be minimized prior to attempting to identify PTI events. The first step was to characterize typical synoptic timescale variability at LjB. We did this by performing a spectral analysis of the hourly LjB atmospheric pressure observations for each season (Fig. 2b; winter and summer examples). Throughout winter and autumn our analysis indicated a synoptic timescale of 5 to 8 d, whereas in spring and summer the synoptic timescale was typically 6 to 7 d. We then calculated a running-minimum radon concentration using a window derived from the spectral analysis of atmospheric pressure (7 d window for all seasons). Lastly, this running-minimum concentration (Fig. 3a; blue line, $C_{\text{Rn-subtracted}}$) was subtracted from the $C_{\text{Rn-advected}}$ (fetch effect) derived in (2) above, in order to isolate the synoptic timescale contributions to the radon observations (Fig. 3b; red line, $C_{\text{Rn-synoptic}}$). The $\mu \pm \sigma$ of the subtracted radon contribution was 4.2 ± 2.1, 3.1 ± 0.5, 3.8 ± 0.7, and $4.8 \pm 1.3\,\text{Bq m}^{-3}$, for winter, spring, summer, and autumn, respectively.

Having isolated the synoptic-scale contribution to the observed radon time series, the next steps to develop the PTI identification tool were to (i) identify periods when synoptic variability dominates diurnal variability, and (ii) decide on a minimum length of time that this needs to occur for the event to be considered a PTI.

The diurnal (mixing-related) contribution to the LjB radon time series was obtained by subtracting the advected signal from the measured radon concentrations (see Fig. 3a). For the purpose of this study we chose the seasonal standard deviation ($+\sigma$) of the diurnal radon contribution as a measure of the significance of diurnal variability each season. For our winter example, in Fig. 3b we plotted the isolated synoptic radon signal ($C_{\text{Rn-synoptic}}$) and the standard deviation of the winter diurnal radon signal ($+\sigma\,(C_{\text{Rn-diurnal}})$ W). Numerous cases were evident when accumulation of radon due to synoptic processes ($C_{\text{Rn-synoptic}}$) exceeded $+\sigma\,(C_{\text{Rn-diurnal}})$ W. At such times, synoptic controls on the near-surface radon observations are more significant than diurnal controls. The final step is to set a duration threshold on these exceedances for an event to be classified as a PTI.

We consider a persistent temperature inversion event to have occurred when the synoptic contribution to the radon signal exceeds the standard deviation of the diurnal contribution for that season for a period of at least 48 h:

$$(C_{\text{Rn-synoptic}}) > +\sigma\,(C_{\text{Rn-diurnal}})_{\text{season}} \quad \text{for} \quad \geq 48\,\text{h}. \tag{1}$$

Although only a winter example is presented in Figure 3b, the same approach was used for all seasons.

2.4.2 The pseudo-vertical temperature gradient method (TGM)

If distributed ground-based air temperature measurements are available over a wide range of representative elevations within a basin or valley, it is possible to identify PTI events by analyzing pseudo-vertical temperature gradients between stations with significantly different elevations. This method, described by Largeron and Staquet (2016a), relies upon two key assumptions: (1) horizontal homogeneity of air temperature between stations of similar elevations and (2) the existence of significant vertical changes in air temperature between stations at different elevations. The validity of these assumptions can be assessed by calculating correlations between stations within designated elevation groups, and between stations across designated elevation groups. If the assumptions hold, temperature gradients between stations within the designated elevation groups can be calculated, and a threshold value determined to identify PTI events.

As detailed in Table 1, in the case of the Ljubljana basin, air temperature observations were available from eight automatic weather stations representative of three different elevation categories (low ~ 310 m, medium ~ 630 m, and high ~ 1320 m) for detecting PTI events. Firstly, all hourly temperature observations from the eight stations over the December 2016 to November 2017 period were separated by season. Next, seasonal correlation coefficients between each of the eight stations were calculated separately (Table 2). Air temperatures from the three low-elevation stations (Li, LjB, and LLj) were strongly correlated for all seasons, despite a spatial separation of up to ~ 60 km (Fig. 1c). Likewise, air temperatures of the two medium-elevation stations (S and T) were strongly correlated for all seasons. In the case of the high-elevation stations (PR, K, and Kr), however, only moderate correlation coefficients were obtained (Table 2), indicating a degree of non-homogeneity of the horizontal air temperature field near the top of the basin.

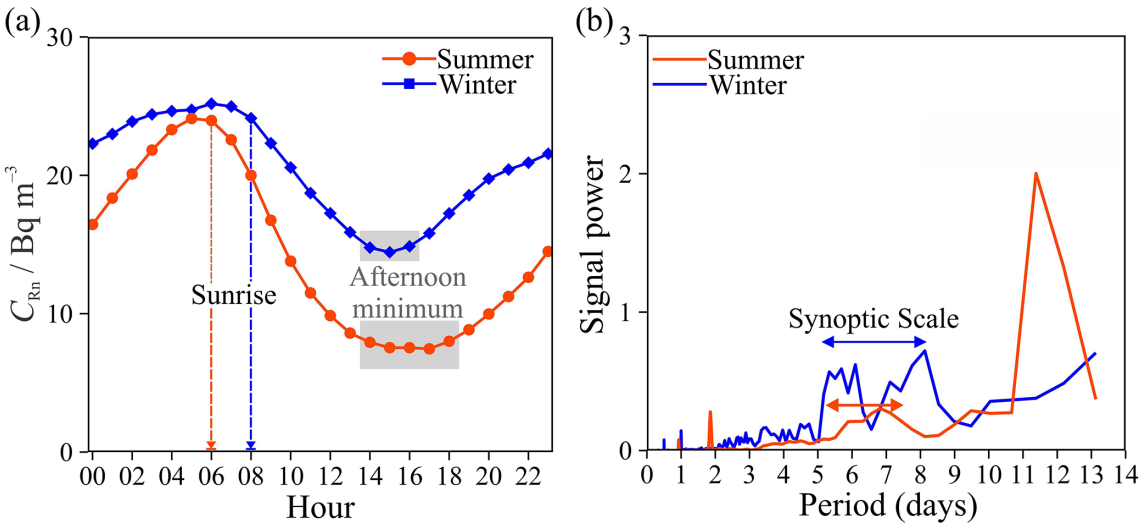


Figure 2. **(a)** Summer and winter diurnal composite hourly radon concentration and **(b)** spectral analysis of the LjB hourly atmospheric pressure data for summer and winter.

Table 2. Air temperature correlation coefficients between each of the eight ground-based automatic weather stations in spring, summer, autumn, and winter.

Winter								
	Li	LjB	LLj	S	T	PR	K	Kr
Li	1	0.96	0.94	0.81	0.74	0.59	0.47	0.27
LjB		1	0.95	0.84	0.78	0.59	0.47	0.26
LLj			1	0.80	0.75	0.59	0.46	0.24
S				1	0.96	0.80	0.69	0.46
T					1	0.85	0.74	0.52
PR						1	0.84	0.75
K							1	0.75
Kr								1

Spring								
	Li	LjB	LLj	S	T	PR	K	Kr
Li	1	0.97	0.97	0.89	0.87	0.87	0.83	0.74
LjB		1	0.96	0.91	0.91	0.80	0.86	0.80
LLj			1	0.88	0.87	0.88	0.83	0.80
S				1	0.97	0.96	0.96	0.90
T					1	0.98	0.96	0.92
PR						1	0.76	0.71
K							1	0.94
Kr								1

Summer								
	Li	LjB	LLj	S	T	PR	K	Kr
Li	1	0.95	0.97	0.87	0.85	0.85	0.81	0.66
LjB		1	0.96	0.91	0.91	0.98	0.83	0.72
LLj			1	0.89	0.89	0.98	0.83	0.68
S				1	0.97	0.96	0.96	0.90
T					1	0.98	0.96	0.92
PR						1	0.76	0.71
K							1	0.94
Kr								1

Autumn								
	Li	LjB	LLj	S	T	PR	K	Kr
Li	1	0.97	0.95	0.88	0.85	0.82	0.80	0.70
LjB		1	0.94	0.90	0.88	0.84	0.81	0.72
LLj			1	0.85	0.83	0.82	0.78	0.70
S				1	0.98	0.96	0.94	0.85
T					1	0.97	0.95	0.86
PR						1	0.77	0.78
K							1	0.73
Kr								1

Vertical temperature gradients between the low- and medium-elevation stations and the medium- and high-elevation stations were not as distinct in spring, summer, or autumn as they were in winter, as indicated by strong correlation coefficients between temperatures from those elevations (Table 2). Thus, according to Whiteman et al. (2004), the actual vertical temperature profile of the basin's atmosphere can only be suitably approximated by pseudo-vertical temperature gradient measurements from the ground-based stations over the whole year at night, when convective mixing is not active. Only in the colder months (winter and some of autumn; under low-gradient wind conditions) can the pseudo-vertical temperature gradient be used effectively over the whole diurnal cycle.

Making the assumption of year-round horizontal homogeneity of the temperature field (Largeron and Staquet,

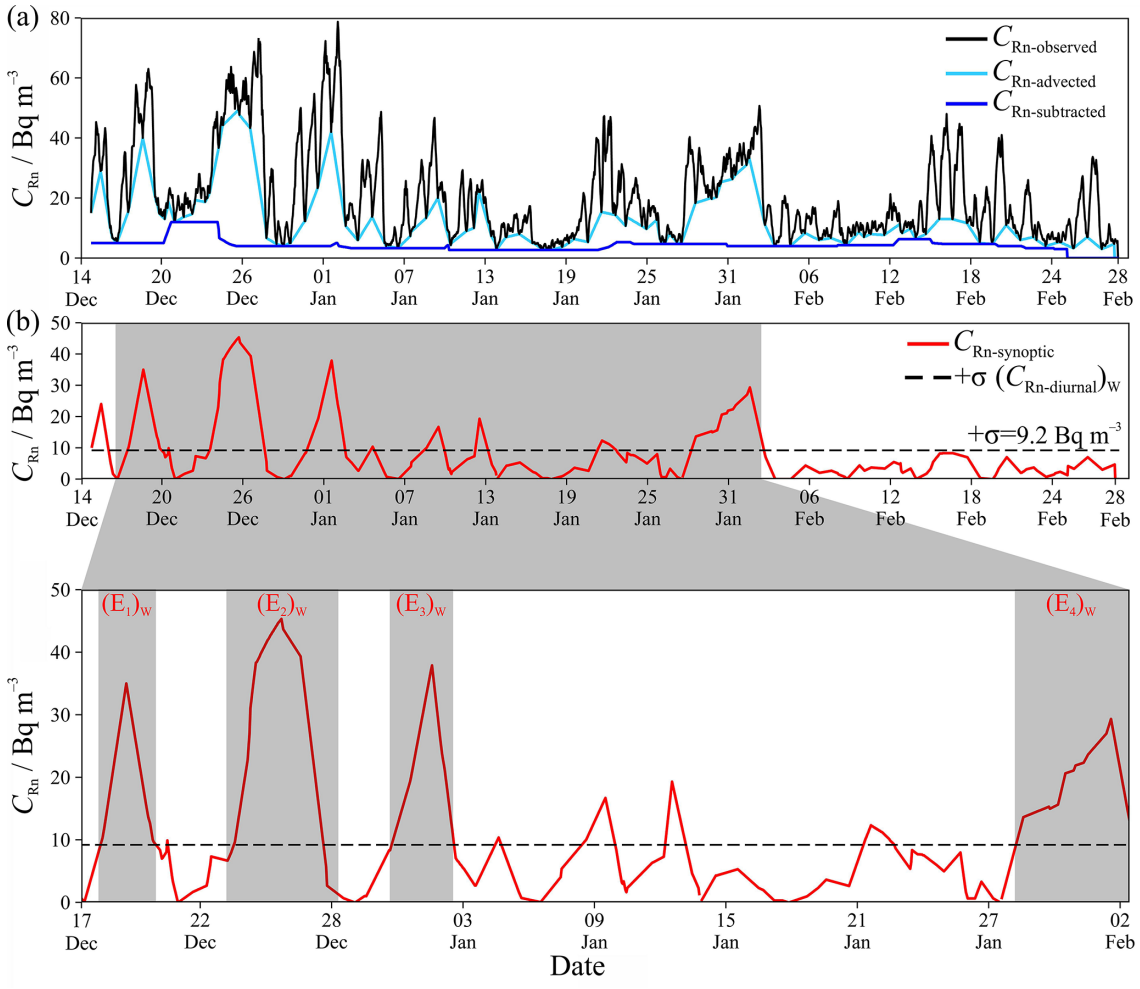


Figure 3. (a) Hourly mean observed radon concentrations, the advected radon contribution with subtracted radon indicated, and **(b)** isolated synoptic timescale radon contribution in winter with the standard deviation ($+\sigma$) of the diurnal contribution indicated. Four persistent temperature inversion events $(E_i)_W$ detected by the RBM are shown in the shaded area and enlarged in the breakout panel beneath; see text in Sect. 2.3.1 for details.

2016a), a relative measure of the degree of stability of the ABL can be made by calculating the vertical temperature gradient between stations of different elevation categories (e.g., high–medium, high–low, or medium–low), $(\Delta T/\Delta z)_i$, where the index i refers to any pair of stations. To this end, following Largeron and Staquet (2016a), we calculated pseudo-vertical temperature gradients for four station pairs. Of the 21 possible gradient combinations we sought to avoid medium–high gradient pairs (since the high stations were not internally well correlated), and avoided the use of station S in the medium height category due to its comparatively high correlation with temperatures of the low stations. Other combinations were chosen to minimize spatial separation. The gradient pairs chosen for this study were as follows:

i. Li and K, $(\Delta T/\Delta z)_1$, 29 km apart, $\Delta z = 943$ m;

ii. LjB and T, $(\Delta T/\Delta z)_2$, 19 km apart, $\Delta z = 396$ m;

iii. LjB and PR, $(\Delta T/\Delta z)_3$, 35 km apart, $\Delta z = 720$ m;

iv. LLj and Kr, $(\Delta T/\Delta z)_4$, 23 km apart, $\Delta z = 1378$ m.

Following Largeron and Staquet (2016a) we derived our basin stability measure (the pseudo-vertical temperature gradient) from the average of the four separate gradients:

$$\frac{\Delta T}{\Delta z}(t) = \frac{1}{4}\sum_{i=1}^{4}\left(\frac{\Delta T}{\Delta z}\right)_i(t). \quad (2)$$

We note, however, that $\Delta T/\Delta z$ and the individual gradients $(\Delta T/\Delta z)_i$ were typically very similar:

$$\frac{\Delta T}{\Delta z}(t) \approx \left(\frac{\Delta T}{\Delta z}\right)_i(t) \quad \text{for } i = 1\ldots4. \quad (3)$$

In order to avoid the detection of successive strong nocturnal-only temperature inversions and isolate persistent

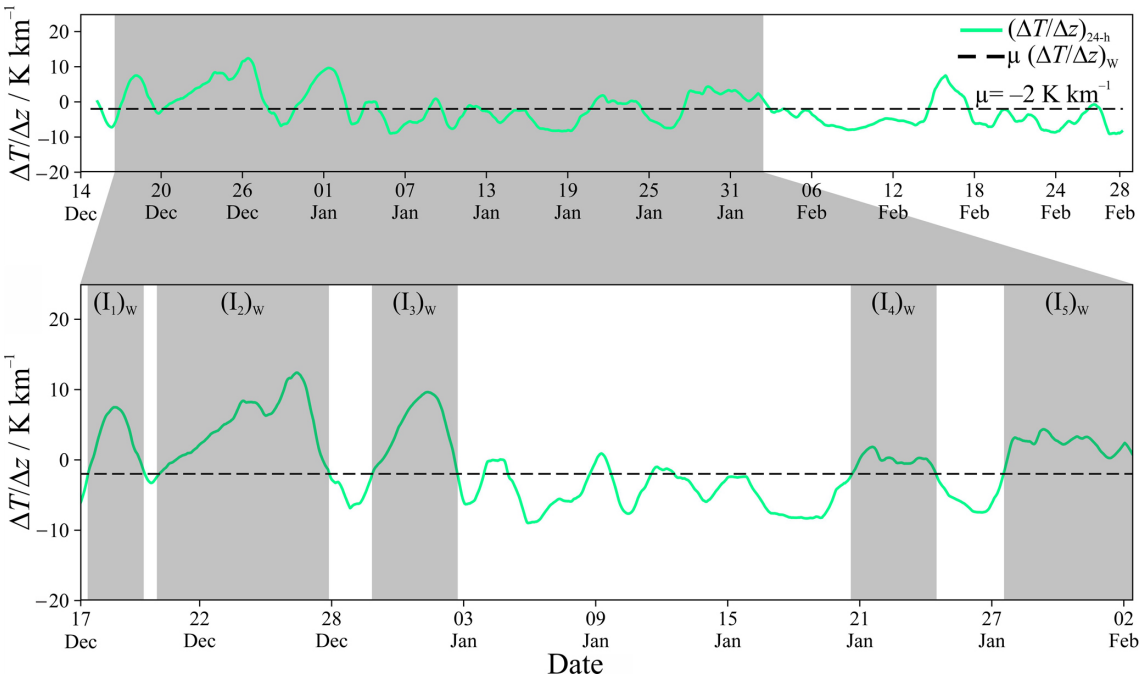


Figure 4. The 24 h running mean pseudo-vertical temperature gradient in winter. Five persistent temperature inversion events $(I_i)_W$ detected by the TGM are shown in the shaded area and enlarged in the breakout panel beneath; see text in Sect. 2.3.2 for details.

temperature inversion events, we applied a 24 h running mean smoothing to the pseudo-vertical temperature gradient ($(\Delta T/\Delta z)_{24\,h}$). Lastly, we calculated seasonal average (μ) values of $\Delta T/\Delta z$ to use as our seasonal thresholds for PTI event identification, a slight deviation from the approach of Largeron and Staquet (2016a), which used the cold season average (November–December).

A persistent temperature inversion event is considered to have occurred when the $(\Delta T/\Delta z)_{24\,h}$ value exceeds the seasonal average value for ≥ 48 h:

$$(\Delta T/\Delta z)_{24\,h} > \mu(\Delta T/\Delta z)_{season} \text{ for } \geq 48\,h. \quad (4)$$

As an example of this technique we present the winter event selection results in Fig. 4. The same approach was used for all seasons.

3 Results and discussion

3.1 Data overview

The time series of hourly average radon concentration at LjB revealed a seasonal cycle, characterized by a winter maximum and summer minimum (Fig. 5a). When monthly averages of the separated synoptic- and diurnal-scale contributions to the radon observations are considered (Fig. 5c) it is clear that the seasonal cycle is mainly controlled by synoptic factors (changes in air mass fetch or time over land).

From October through December monthly mean wind speeds were typically low (Fig. 5c), associated with frequent synoptic stagnation events. These periods resulted in higher radon concentrations (long time over land). In January and February, even though monthly average wind speeds increased, recent air mass fetch was predominantly continental, as indicated by dominant NE–E winds in seasonal wind roses (not shown), resulting in moderate monthly mean radon concentrations. The lowest synoptic contributions to observed radon concentrations occurred in spring and summer. During these times the mean monthly wind speeds were higher (strong mixing), and wind directions were often from the southwest, in the direction of the Gulf of Venice and Adriatic Sea, so terrestrial fetch for air masses was limited. In a few specific cases (e.g., April and August), intense rainfall events appeared to be associated with a reduction in radon concentrations, likely attributable to short-term reductions in the radon flux (Fig. 5b).

From March through September in Fig. 5a the variability in radon concentration appears to be of considerably higher frequency than from October through February. This is further evidence of a change in dominant influences from diurnal to synoptic timescales, associated with changing day length and intensity of solar radiation within the Ljubljana basin. The period of greater synoptic influence (reduced diurnal radon variability) corresponds well with times when mean daily temperatures were close to or below 0 °C, when soil freezing was likely (Fig. 5a and b).

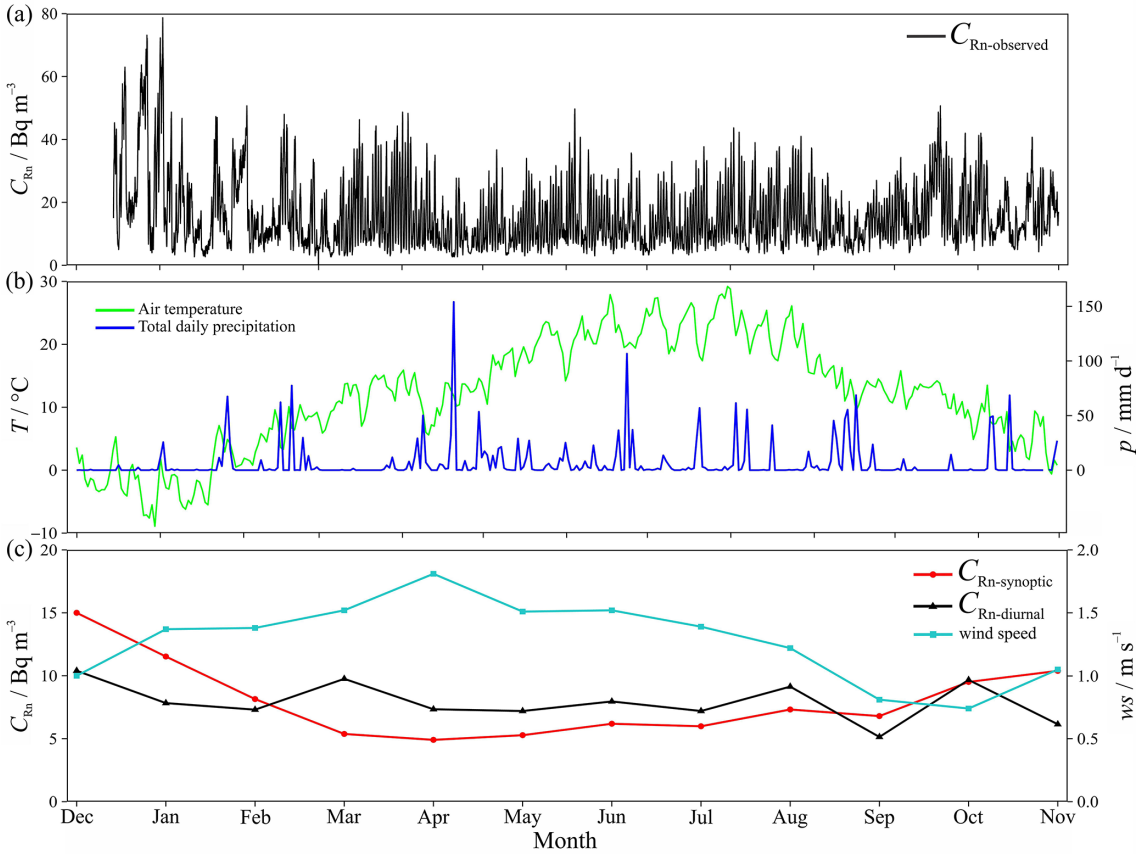


Figure 5. A total of 1 year (December 2016 to November 2017) of **(a)** hourly mean radon concentration, **(b)** hourly mean air temperature and total daily precipitation, and **(c)** monthly mean of synoptic radon, diurnal mixing of radon, and wind speed.

Table 3. Persistent temperature inversion events (E_i) by season (winter, W; spring, Sp; summer, S; autumn, A) detected by the radon-based method (RBM), including time period and duration.

Event	Persistent inversion period	Duration
$(E_1)_W$	17/12/2016–19/12/2016	59 h (2.5 d)
$(E_2)_W$	23/12/2016–27/12/2016	101 h (4.2 d)
$(E_3)_W$	30/12/2016–02/01/2017	72 h (3 d)
$(E_4)_W$	28/01/2017–02/02/2017	131 h (5.5 d)
$(E_1)_A$	14/10/2017–18/10/2017	96 h (4 d)
$(E_2)_A$	19/11/2017–21/11/2017	48 h (2 d)

3.2 Radon-based PTI event selection (RBM)

The radon-based method (RBM) identified six PTI events in the basin over the whole year of measurements. Four events were detected in winter (hereafter $(E_i)_W$) and two in autumn ($(E_i)_A$). Dates, times, and durations of these events are summarized numerically in Table 3 and graphically in Fig. 3b (winter) and Fig. 6b (autumn). The RBM detected no PTI events in spring and summer (see Figs. 7b and 8b).

According to the RBM approximately 20 % of winter experienced persistent strongly stable conditions, associated with anticyclonic synoptic conditions in the basin and surrounding regions. By contrast, the RBM classified only 7 % of autumn as PTI events. Events $(E_1)_A$ and $(E_2)_A$ lasted 4 and 2 d, respectively, and both occurred in the second half of autumn.

3.3 Pseudo-vertical temperature gradient PTI event selection (TGM)

A total of 17 PTI events were detected throughout the measurement year by the TGM. Dates, times, and duration of these events are summarized in Table 4. Five events were detected in winter (hereafter $(I_i)_W$), three in spring ($(I_i)_{Sp}$), two in summer ($(I_i)_S$), and seven in autumn ($(I_i)_A$), as illustrated in Figs. 4, 9, 10, and 11.

Approximately 30 % of winter days experienced persistently stable conditions according to the TGM. All of the TGM-classified events lasted from 3 to 8 d and were associated with strong inversion conditions (based on the mean vertical temperature gradients) with the exception of $(I_4)_W$, which was of lower intensity (Fig. 4). The highest number

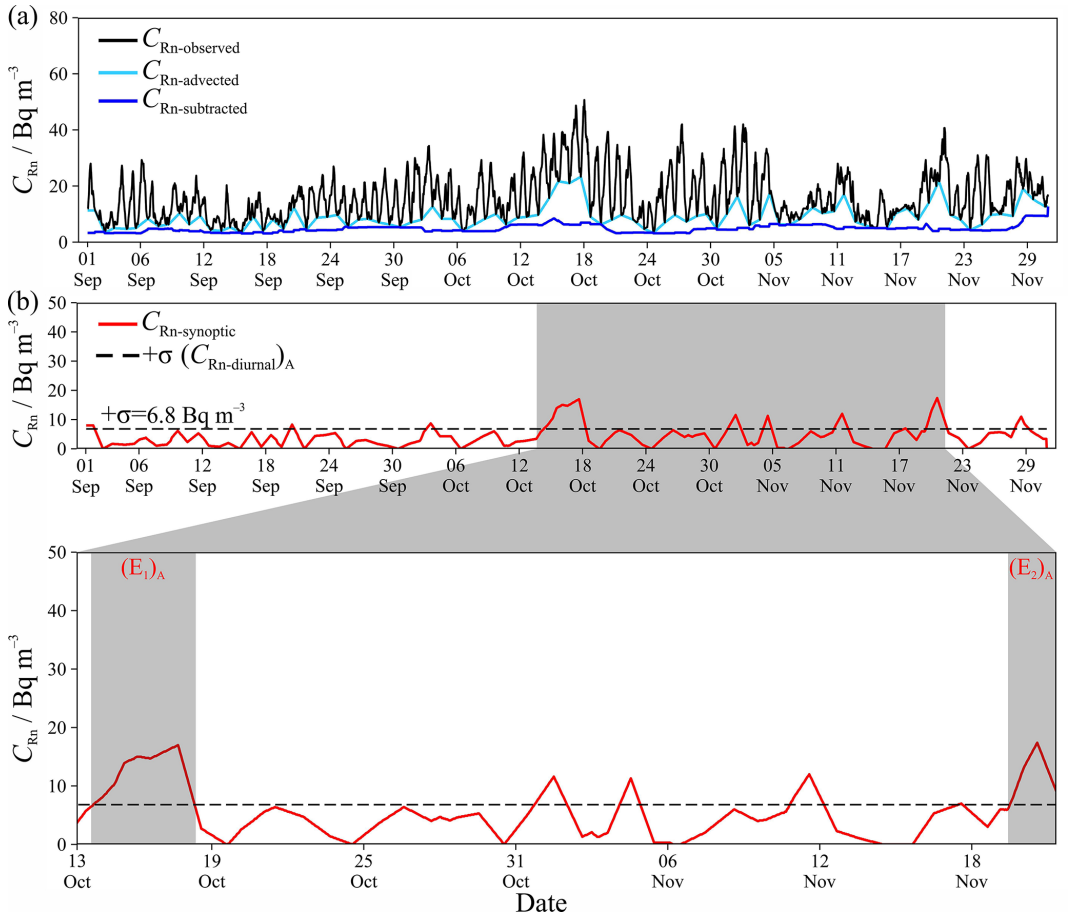


Figure 6. **(a)** Hourly mean observed radon concentrations, the advected radon contribution with subtracted radon indicated, and **(b)** isolated synoptic timescale radon contribution in autumn with the standard deviation ($+\sigma$) of the diurnal contribution indicated. Two persistent temperature inversion events $(E_i)_A$ detected by the RBM are shown in the shaded area and enlarged in the breakout panel beneath; see text in Sect. 2.3.1 for details.

of PTI events identified by the TGM was in autumn (Fig. 9). Around 32 % of this season was classified as PTI conditions. The identified $(I_i)_A$ had durations of 2 to 12 d, with $(I_1)_A$, $(I_2)_A$, and $(I_7)_A$ being the shortest and with the least intense stability. The longest-lasting event with the strongest stability was $(I_3)_A$.

In contrast to the RBM, the TGM also identified PTI events in spring (22 %) and summer (26 %) (Figs. 10 and 11).

3.4 Comparison of the radon-based and temperature gradient methods

Diurnal composites, based on hourly means, of air temperature, relative humidity, cloud cover, wind speed, wind direction, and precipitation for all conditions (winter mean) and for typical PTI event days in winter selected by RBM and TGM are shown in Fig. 12. As evident, winter RBM PTI days were mainly associated with modest diurnal temperature amplitudes ($\sim 5\,^{\circ}$C on average), with morning minimums mostly between 0 and $-4\,^{\circ}$C (Fig. 12a). The diurnal amplitude of relative humidity was ~ 15 % on average (Fig. 12b), with little variability in the extreme ($\mu + 1\sigma$) values (not shown). Wind speeds between sunset and sunrise were low and relatively consistent (on average 0.5–0.7 m s^{-1}), from the ESE (Fig. 12d and e), with around 25 % cloud cover predicted and no measured rainfall (Fig. 12f), all consistent with anticyclonic synoptic conditions. The high variability in NOAA GDAS nocturnal cloud amount (Fig. 12c) may be associated with fog that frequently forms under PTI conditions. There was no snow during the 2016–2017 winter, which would otherwise have led to stronger and longer-lasting persistent temperature inversion conditions. Results from a companion study to this one, still in preparation, indicate that snow cover in the following 2017–2018 winter reduced mean winter rates of radon emission by a factor of 2–3. The mean atmospheric pressure during PTI events was ~ 994 hPa, compared to ~ 986 hPa for non-PTI conditions, confirming the prevalence of anticyclonic conditions.

The mean diurnal temperature amplitude (6 °C) of TGM PTI events was 1 °C larger than that of the RBM events, the

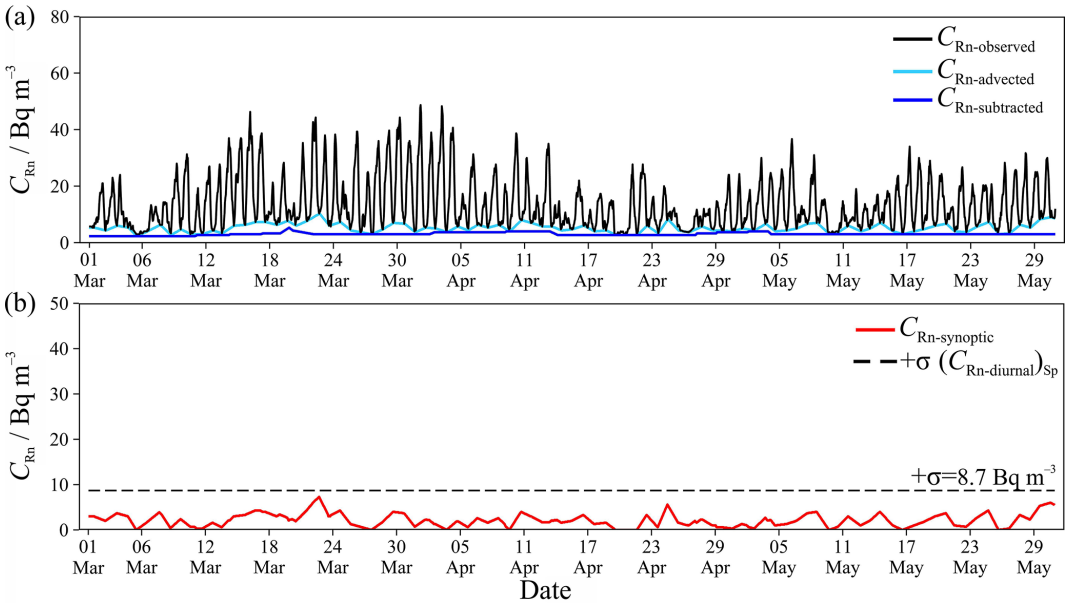


Figure 7. **(a)** Hourly mean observed radon concentrations, the advected radon contribution with subtracted radon indicated, and **(b)** isolated synoptic timescale radon contribution in spring with the standard deviation ($+\sigma$) of the diurnal contribution indicated. No persistent temperature inversion events were detected by the RBM this season.

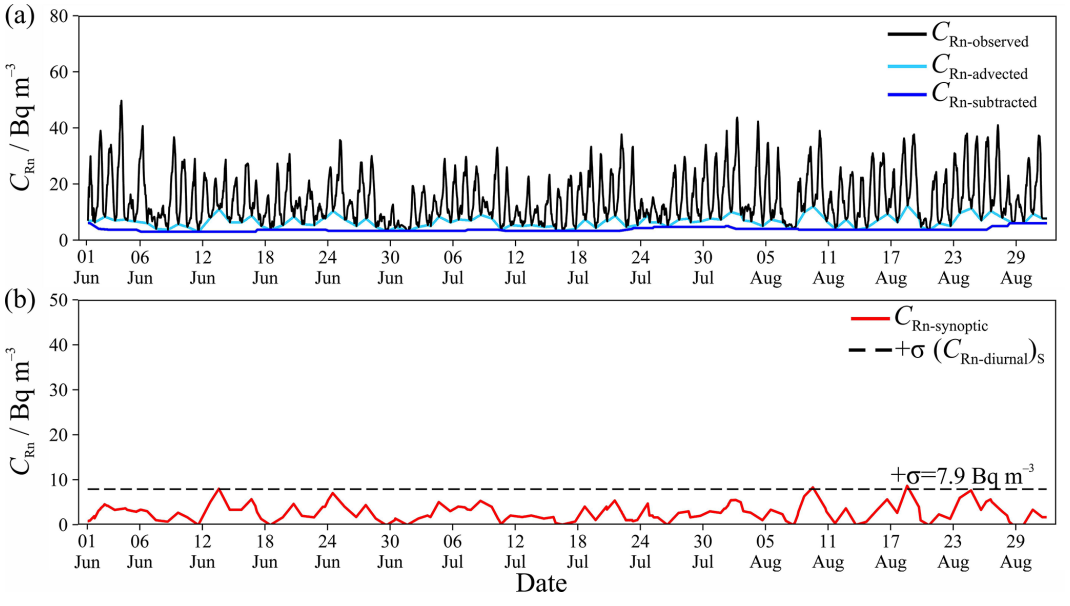


Figure 8. **(a)** Hourly mean observed radon concentrations, the advected radon contribution with subtracted radon indicated, and **(b)** isolated synoptic timescale radon contribution in summer with the standard deviation ($+\sigma$) of the diurnal contribution indicated. No persistent temperature inversion events were detected by the RBM this season.

diurnal amplitude of relative humidity (20 %) was 5 % larger than that of the RBM events, and nocturnal extreme relative humidity values were less consistent (Fig. 12a and b; green vs. red lines). Diurnal minimum wind speeds were slightly higher (0.6–0.7 m s^{-1}), and had a considerably larger diurnal amplitude than that of the RBM events (Fig. 12d). The TGM-selected PTI days had more cloud cover (by 10 %–15 %) and experienced some rainfall (Fig. 12c and f), which is very uncharacteristic of stable (typically anticyclonic) conditions. It should be noted that many of the differences between RBM and TGM PTI events selected in winter can be attributed to the single event $(I_4)_W$, for which the mean temperature gradient indicated a lesser degree of stratification (Fig. 4).

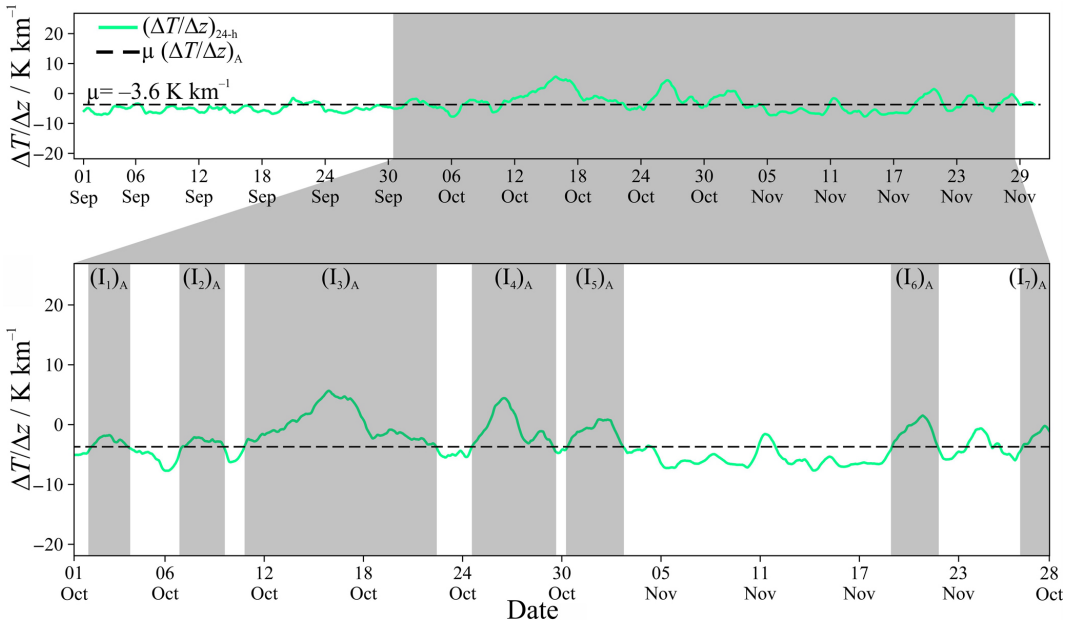


Figure 9. The 24 h running mean of the pseudo-vertical temperature gradient in autumn; seven persistent temperature inversion events $(I_i)_A$ detected by the TGM are shown in the shaded section and enlarged in the breakout panel beneath; see text in Sect. 2.3.2 for details.

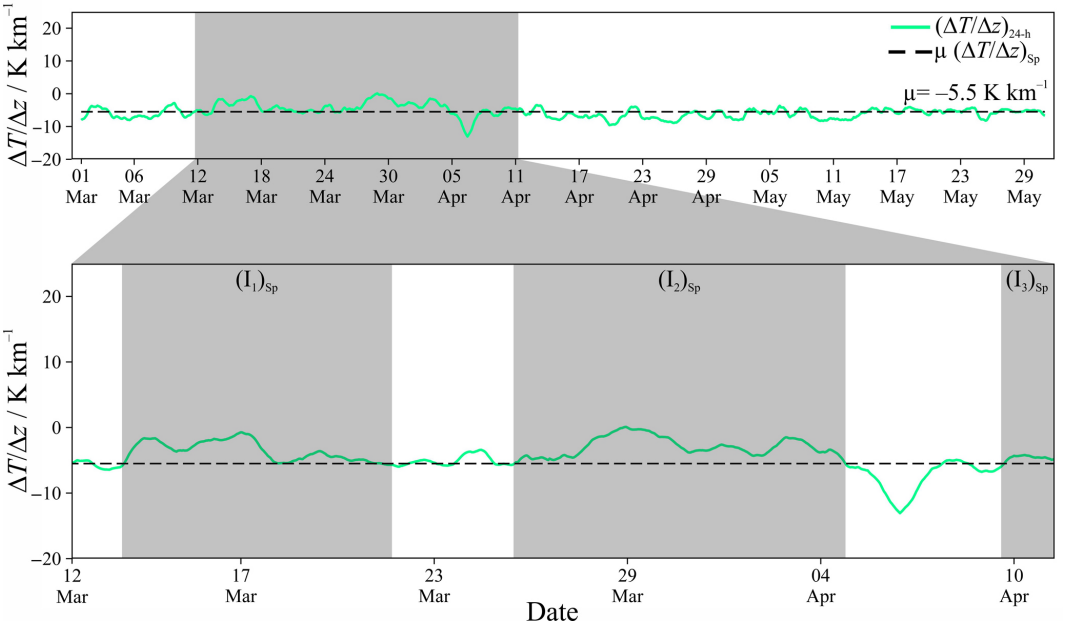


Figure 10. The 24 h running mean of the pseudo-vertical temperature gradient in spring; three persistent temperature inversion events $(I_i)_{Sp}$ detected by the TGM are shown in the shaded area and enlarged in the breakout panel beneath; see text in Sect. 2.3.2 for details.

Atmospheric pressure (not shown) was also elevated for all $(I_i)_W$ except $(I_4)_W$.

The composite diurnal meteorological conditions associated with the autumn PTI events (RBM and TGM) and autumn mean are shown in Fig. 13. Of particular note, wind speeds for the autumn RBM PTI events were even lower than those in winter, with broad $\geq$ 12 h periods of consistently low wind speeds (0.1–0.3 m s^{-1}) throughout the night, but also from the ESE (Fig. 13d and e; red lines). The mean diurnal amplitude of wind speed on autumn PTI days selected by RBM was $\sim$ 0.5 m s^{-1} compared to $\sim$ 2.5 m s^{-1} for non-PTI autumn days (Fig. 13d). By comparison, PTI events identified by the TGM had shorter nocturnal periods of lowest wind speed (5–8 h) (Fig. 13d), with daytime $\mu+1\sigma$ values of

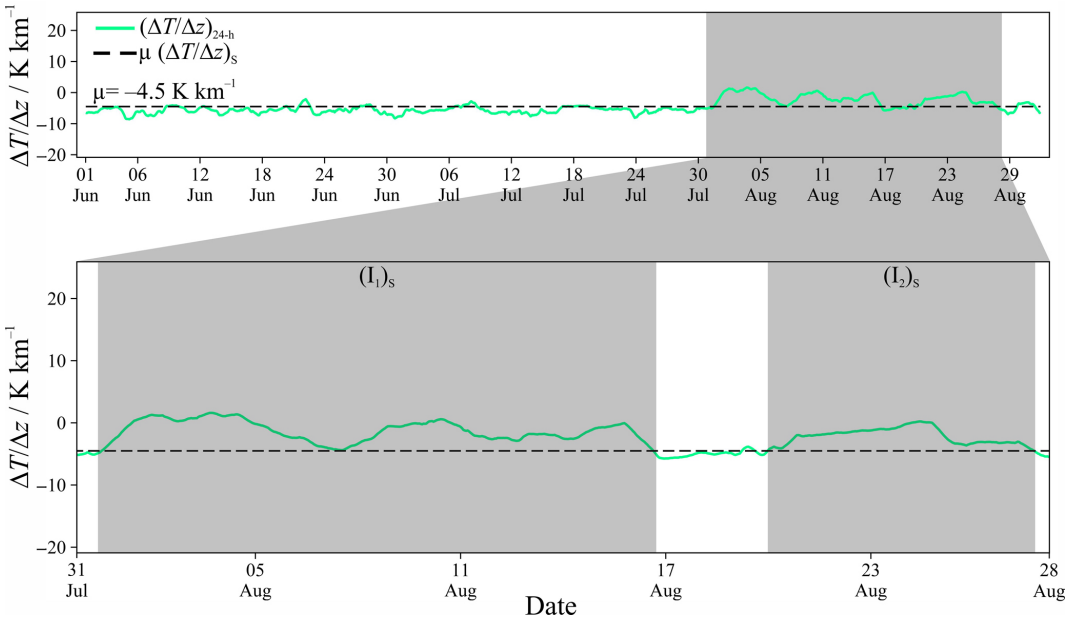


Figure 11. The 24 h running mean of the pseudo-vertical temperature gradient in summer; two persistent temperature inversion events $(I_i)_S$ detected by the TGM are shown in the shaded section and enlarged in the breakout panel beneath; see text in Sect. 2.3.2 for details.

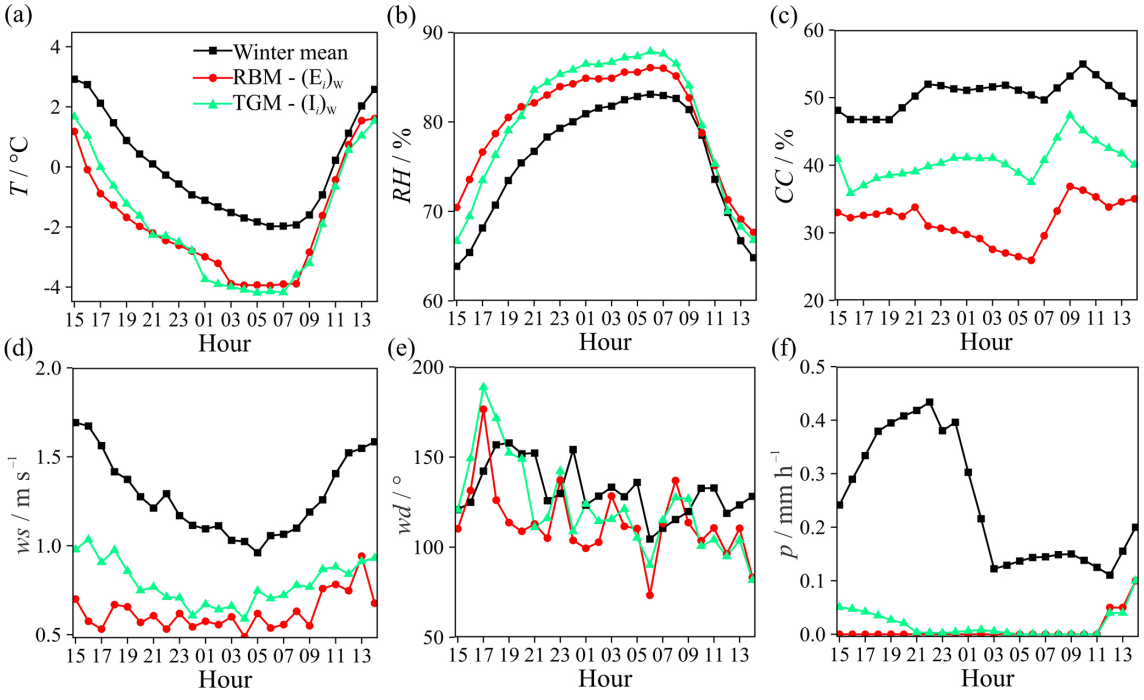


Figure 12. Diurnal composites, based on hourly means, of **(a)** air temperature, **(b)** relative humidity, **(c)** cloud cover, **(d)** wind speed, **(e)** wind direction, and **(f)** precipitation, for winter mean, and persistent temperature inversion events detected in winter by the RBM and TGM.

2–3.2 m s^{-1} (not shown). Between 00:00 and 05:00 LT near-surface air temperature changed very slowly on RBM PTI nights (around −0.1 °C h^{-1}; Fig. 13a) compared with around −0.4 °C h^{-1} for non-PTI nights. On the other hand, diurnal composites of meteorological quantities corresponding to the autumn TGM PTI events showed moderate-amplitude temperature variability (5 to 15 °C), a 37 % amplitude change in relative humidity (with relatively consistent peak values between 01:00 and 06:00 LT) (Fig. 13a, b). Relatively high cloud cover amounts were associated with autumn TGM

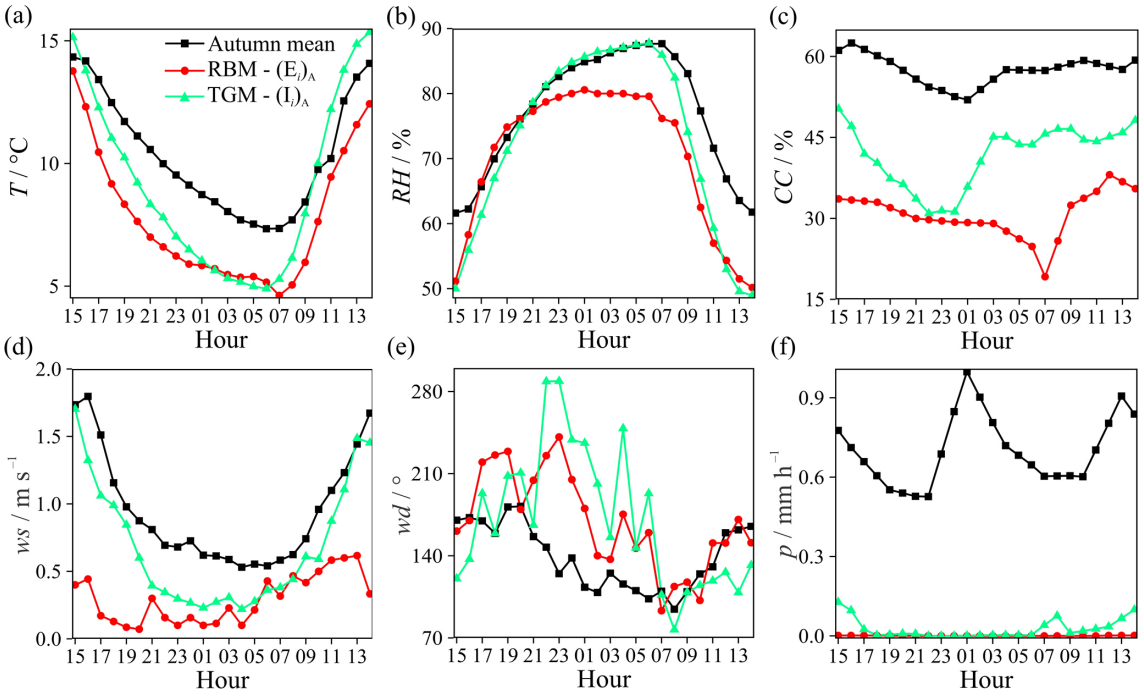


Figure 13. Diurnal composites, based on hourly means, of **(a)** air temperature, **(b)** relative humidity, **(c)** cloud cover, **(d)** wind speed, **(e)** wind direction, and **(f)** precipitation, for autumn mean, and persistent temperature inversion events detected in autumn by the RBM and TGM.

Table 4. Persistent temperature inversion events (I_i) by season (winter, W; spring, Sp; summer, S; autumn, A) detected by pseudo-vertical temperature gradient method (TGM), including time period and duration.

Event	Persistent inversion period	Duration
$(I_1)_W$	**17/12/2016–19/12/2016**	**62 h (2.6 d)**
$(I_2)_W$	**20/12/2016–27/12/2016**	**184 h (7.6 d)**
$(I_3)_W$	**29/12/2016–02/01/2017**	**93 h (3.8 d)**
$(I_4)_W$	20/01/2017–24/01/2017	89 h (3.7 d)
$(I_5)_W$	**27/01/2017–02/02/2017**	**152 h (6.3 d)**
$(I_1)_{Sp}$	13/03/2017–21/03/2017	191 h (8 d)
$(I_2)_{Sp}$	25/03/2017–04/04/2017	246 h (10.3 d)
$(I_3)_{Sp}$	25/03/2017–04/04/2017	48 h (2 d)
$(I_1)_S$	31/07/2017–16/08/2017	386 h (16 d)
$(I_2)_S$	20/08/2017–27/08/2017	186 h (7.8 d)
$(I_1)_A$	01/10/2017–03/10/2017	51 h (2.1 d)
$(I_2)_A$	07/10/2017–09/10/2017	59 h (2.5 d)
$(I_3)_A$	**10/10/2017–22/10/2017**	**277 h (11.5 d)**
$(I_4)_A$	24/10/2017–29/10/2017	117 h (4.9 d)
$(I_5)_A$	30/10/2017–02/11/2017	79 h (3.3 d)
$(I_6)_A$	**19/11/2017–21/11/2017**	**65 h (2.7 d)**
$(I_7)_A$	26/11/2017–28/11/2017	50 h (2.1 d)

Note: the events in bold were also detected by the radon-based method (RBM).

PTI events (around 40 %), with occasional rainfall recorded (Fig. 13c and f). In contrast to results from the TGM, from prior to sunset until several hours after sunrise, while some fog or cloud occurred, no rainfall was recorded at all under PTI conditions identified by the RBM in autumn (Fig. 13c and f).

Diurnal composites of meteorological conditions associated with spring and summer PTI events selected only by TGM and for mean spring and summer seasons are summarized in Figs. 14 and 15. The spring air temperature, relative humidity, and wind speed diurnal composites show gradual and relatively consistent changes throughout the night to brief (not broad) minimum–maximum values around 05:00–06:00 LT, followed by a rapid change after sunrise (Fig. 14a, b, and d). The days identified here as PTI events actually correspond with days on which a strongly stable nocturnal boundary layer has formed, which is then broken up in the morning by strong convection, rather than persistent inversion conditions. Further in support of this observation, only between 00:00 and 05:00 LT on the spring days identified by the TGM as PTI events did the wind direction switch to ESE (Fig. 14e), the expected direction of katabatic drainage at this site. The large mean diurnal amplitudes of temperature ($\sim$ 13 °C), relative humidity ($\sim$ 45 %), and wind speed ($\sim$ 2.5 m s^{-1}) in spring (Fig. 14a, b, and d) were not consistent with characteristics usually associated with PTI events. Similar characteristics were observed within the diurnal composite plots of summer PTI events identified by

the TGM (Fig. 15), indicative of stable nocturnal conditions (though not as strong in summer) that rapidly become convective after sunrise, rather than persisting as stable events throughout the day. Further evidence that the TGM was even less selective of nocturnally stable conditions is the frequent rainfall events observed on the nights in question (Fig. 15f).

By definition, PTI events should not exhibit strong diurnal cycles of temperature and relative humidity, should have consistently light to calm nocturnal wind speeds, and, since little daytime convective mixing is expected, daytime wind speeds should also be relatively light. Furthermore, since they usually occur under anticyclonic synoptic conditions, when regional subsidence prevails, rainfall is not expected.

In summary, while no PTI events identified by the RBM in winter or autumn were missed by the TGM (Tables 3 and 4), it is clear that the TGM is less selective of truly persistently stable conditions than the RBM. However, the TGM classified a number of other periods in winter and autumn as PTI events, and also considered that the $(I_3)_A$ was longer lasting than predicted by the RBM. This shortcoming is likely attributable to the degree of validity of the assumptions on which the TGM is based for the Ljubljana basin. In spring and summer (Figs. 14 and 15) some assumptions of the TGM are less valid (i.e., less distinction between temperatures at different elevations), causing the method to produce misleading results. Large temperature gradients on very stable nights push daily mean values well above the seasonal mean. For consecutive strongly stable nights, under anticyclonic conditions, this is incorrectly interpreted as a PTI event by the TGM.

3.5 Advantages and limitations of radon-based method (RBM)

The RBM relies upon accurate characterization of afternoon minimum radon concentrations. In this regard, measurement quality and time series analysis are important. The lower limit of detection of commercial, portable radon detectors such as the AlphaGUARD (LLD 2–3 Bq m^{-3}) is 2 orders of magnitude poorer than that of research-grade two-filter radon detectors (LLD $\sim$ 0.02 Bq m^{-3}; Chambers et al., 2014). Compared with sub-diurnal variability this necessitates smoothing of radon observations if using a commercial instrument, the extent of which is likely to be application-/site-specific. An alternative, but more expensive, solution would be to make vertical radon gradient measurements using research-grade detectors. This would ensure the most accurate, and simple, separation of diurnal (mixing-related) and synoptic (fetch-related) contributions to observed radon concentrations.

The amount of radon that accumulates over a night or a given synoptic PTI event is directly related to the seasonal average radon flux. By performing the RBM separately for each season and year, long-term (i.e., seasonal mean) changes of the terrestrial radon flux from one season or year to the next (as may be driven by changes in mean soil moisture, snow cover, or soil freezing) do not affect the comparative seasonal efficacy of the technique, making it seasonally independent. However, large spatial variability in the radon source function (as experienced between land and open water bodies) has the potential to prevent this technique from accurately identifying PTI events, but only for study regions located on (or close to, i.e., $\leq$ 10 km) the coast. For non-coastal regions, the longevity of radon's parent (^{226}Ra, half-life 1600 years) ensures that the technique can be applied consistently over long periods and – when enough PTI events have been observed within a given season – provide a means of objectively assessing their severity.

Compared to the pseudo-vertical temperature gradient method, which requires input from multiple ground-based weather stations (Whiteman et al., 2004), single-height radon monitoring, from a single monitoring station near the bottom of the basin/valley, clearly provides a simple, economical, and low-maintenance means by which to identify persistent temperature inversion events with a substantially higher degree of success than some contemporary meteorological approaches.

3.6 Advantages and limitations of the pseudo-vertical temperature gradient method (TGM)

For the Ljubljana basin the TGM was found to not always be a reliable means of detecting PTI events. This was mainly due to limited validity of the necessary assumptions. The assumption of a horizontally homogeneous temperature field was often invalid in the case of the high-elevation sites, where a variety of mesoscale processes, including drainage flows, nocturnal jets, and intermittent turbulence (Whiteman et al., 2004; Williams et al., 2013) limit the ability to derive representative vertical temperature gradients from spatially separated locations at different elevations. Furthermore, the assumption of distinct differences between temperatures of the different elevation groups based on daily means was typically only valid in winter (Table 2).

Consequently, for most of the year the TGM was only able to reliably identify stable conditions in the boundary layer at night, when buoyancy or gravitational effects tend to produce horizontal isotherms (Whiteman et al., 2004). However, pseudo-vertical temperature profiles are useful for identifying extended periods of strongly stable conditions based on 24 h data in winter (Largeron and Staquet, 2016a). According to Whiteman et al. (2004), the TGM tends to be more representative of PTI events when the study region has snow cover. A uniform cover of snow reduces the temperature contrasts usually associated with radiation receipt on different aspect slopes and different types of ground cover, helping to maintain stability over the diurnal cycle (Whiteman et al., 2004). The reduced accuracy of the technique in the SAB during the 2016–2017 winter season may be attributable in part to a lack of snow cover that winter.

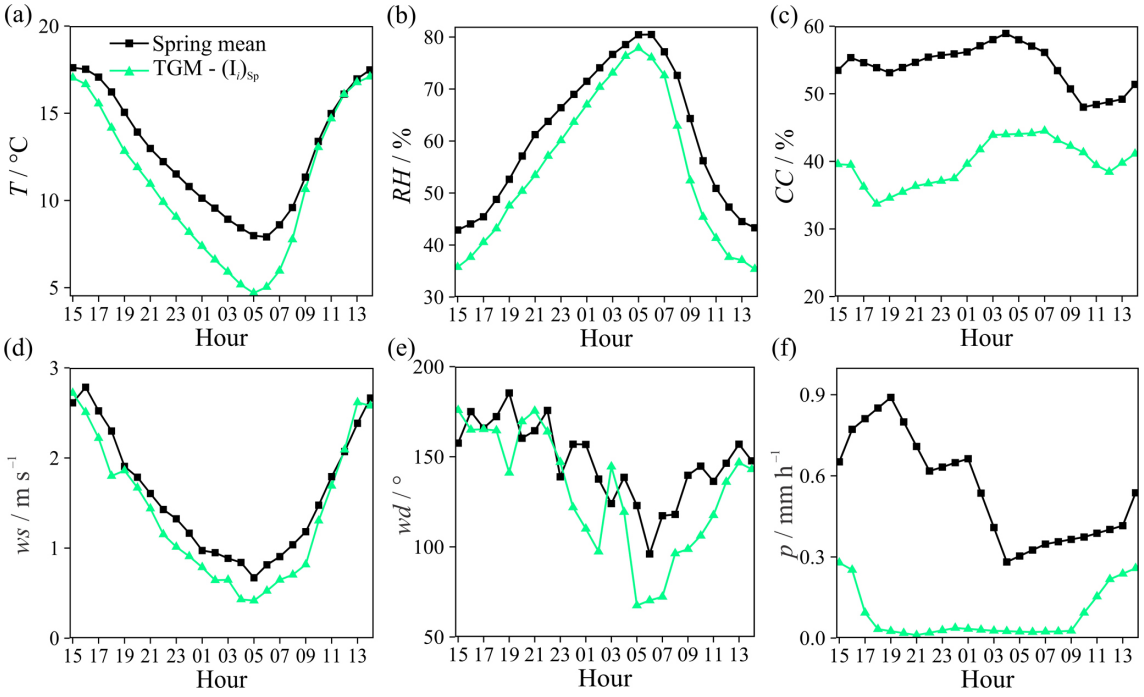


Figure 14. Diurnal composites, based on hourly means, of **(a)** air temperature, **(b)** relative humidity, **(c)** cloud cover, **(d)** wind speed, **(e)** wind direction, and **(f)** precipitation, for spring mean, and persistent temperature inversion events detected in spring by the TGM. No persistent temperature inversion events were detected by the RBM this season.

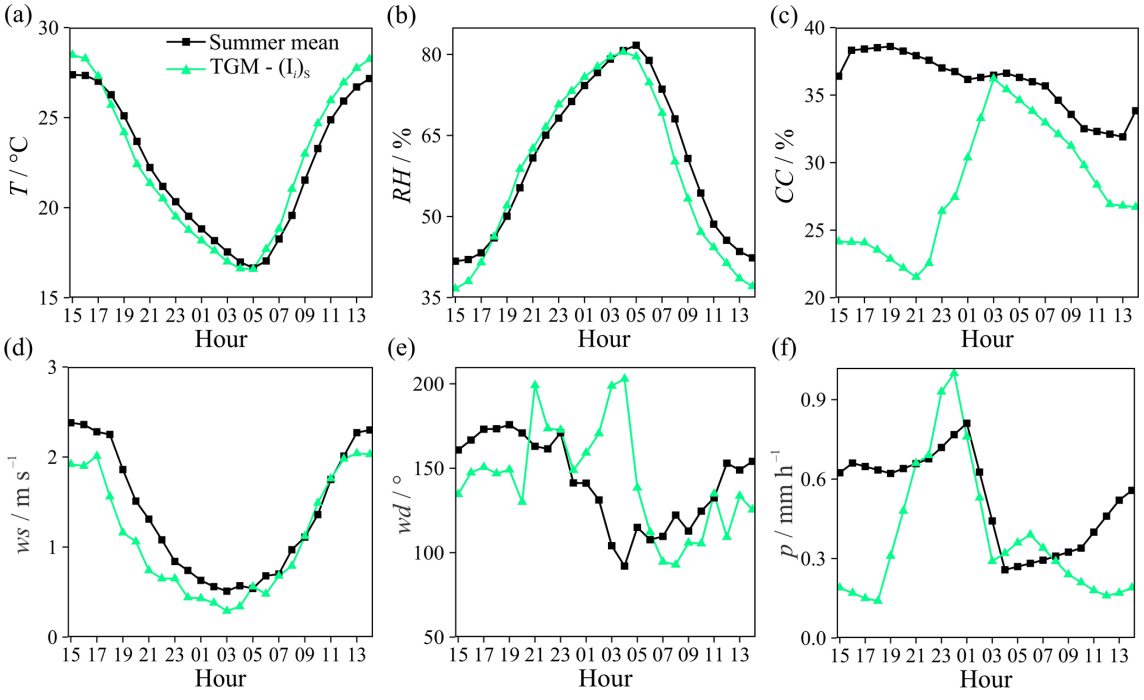


Figure 15. Diurnal composites, based on hourly means, of **(a)** air temperature, **(b)** relative humidity, **(c)** cloud cover, **(d)** wind speed, **(e)** wind direction, and **(f)** precipitation, for summer mean, and persistent temperature inversion events detected in summer by the TGM. No persistent temperature inversion events were detected by the RBM this season.

The number and location of ground-based weather stations are important factors of the TGM; stations should be placed in all directions (north, east, south, and west). The Ljubljana basin automatic weather station network lacked stations in the south, which may have contributed to the poor performance of the technique. Large open regions of complex topography, more exposed to synoptic wind influences, are not well suited to the TGM (Whiteman et al., 2004).

Overall, the inability of the TGM to perform equally well in all seasons and its lack of appropriate selectivity of truly persistent stable conditions (regarding event number, duration, and strength) in winter and autumn compared to the RBM were the most serious limitations.

3.7 Urban air quality during persistent temperature inversion events

In some regions of Europe with complex terrain, urban air quality is strongly influenced by PTI events. For example, of 29 separate air pollution events in the Eordaia mountain basin of northeastern Greece analyzed by Triantafyllou (2001), more than half occurred under PTI conditions. Other European regions in which cold season PTI events have been studied in complex topographical locations include Athens, Greece (Kassomenos and Koletsis, 2005); Cracow, Poland (Bielec-Bąkowska et al., 2011; Jędruszkiewicz et al., 2017); Grenoble (Largeron and Staquet, 2016a) and Chamonix-Mont-Blanc (Chemel et al., 2016), France; Ljubljana (Petkovšek, 1978, 1985, 1992; Rakovec et al., 2002) and Ajdovščina (Longlong et al., 2016), Slovenia; and the Po Valley region, Italy (Marcazzan et al., 2001). The pollution events in each of these studies were characterized by stable stratification and subsidence, suppressing vertical mixing while the confining topography and weak-to-calm-gradient winds prevented advection and favored air stagnation (Kukkonen et al., 2005). Under such circumstances the accumulation of primary pollutants and formation of secondary pollutants not only poses adverse pulmonary and cardiovascular health effects, but also greatly reduces the visibility (Largeron and Staquet, 2016a, b; Reddy et al., 1995; Silcox et al., 2012; Whiteman et al., 2014) and can lead to hazardous episodes of persistent freezing rain, drizzle, or fog (Petkovšek, 1974).

In order to better compare the suitability of the RBM and TGM methods of PTI identification for air quality assessment of subalpine basin cities, hourly observations of PM_{10} in Ljubljana city were analyzed. The diurnal and seasonal variability of PM_{10} in Ljubljana are shown in Fig. 16 for all conditions (seasonal mean), as well as for PTI conditions as determined by the RBM and TGM.

Overall, the annual mean PM_{10} concentration for Ljubljana was $28\,\mu g\,m^{-3}$, and the average daily-maximum PM_{10} concentration for winter was $53\,\mu g\,m^{-3}$, which exceeded the WHO and EEA standard of maximum daily concentration $50\,\mu g\,m^{-3}$ (EEA, 2016, 2017; Ivančič and Vončina, 2015).

Compared with seasonal mean values, there was a significant increase in PM_{10} concentrations under cold season PTI conditions, as a consequence of poor atmospheric mixing over the whole diurnal cycle (Fig. 16a and b). Compared to the RBM, the TGM underestimated peak hourly PM_{10} concentrations of PTI events by 13 and $11\,\mu g\,m^{-3}$, in winter and autumn, respectively. In winter PM_{10} concentrations for PTI events were underestimated across the entire diurnal cycle by the TGM, and for around 18 h of the composite day in autumn. These differences would lead to significantly different levels of daily-mean exposure for residents. The amplitude of the diurnal cycle of PM_{10} for TGM PTI events was $4\,\mu g\,m^{-3}$ larger than that of RBM events; attributable to more mixing at night and slightly stronger daytime atmospheric mixing in the case of TGM PTI events (Fig. 16a and b).

In the warmer months, neither the daily mean PM_{10} values for seasonal mean nor TGM PTI periods exceeded guideline values (Fig. 16c and d). Diurnal cycles of PM_{10} for TGM PTI events at these times were characterized by higher concentrations in the morning (06:00–08:00 LT) and evening (18:00–20:00 LT) rush hours. In the afternoons when the ABL was deepest, concentrations of PM_{10} were the lowest due to typical diurnally changing as opposed to persistent atmospheric mixing conditions.

The seasonal inconsistency of the TGM for PTI identification, in addition to its lack of selectivity of persistently stable conditions in the cold seasons, renders it an unsuitable tool for air quality management purposes in subalpine basin environments.

Our findings, based on the RBM of PTI event identification, indicated that PTI events span 27 % of the cold season (winter and autumn) in the subalpine Ljubljana basin, making it one of the critical European regions with regard to urban air quality issues. Due to domestic heating requirements, the increased use of vehicles, and the production of energy from the thermal power plant, pollutant emissions drastically increase in the cold season. Adverse dispersion conditions as a result of frequent cold season PTI events favor the accumulation of pollutants, leading to severe health issues. For these reasons, improving knowledge about the frequency, duration, intensity, and seasonal variability of PTI events is required for decision makers when considering the need for emission mitigation strategies.

The technique developed in this study adds another dimension to contemporary radon-based methods of characterizing the atmospheric mixing state (Chambers et al., 2015, 2019; Williams et al., 2016) that were developed for less complex topographic regions. Under PTI conditions contributions to radon concentration variability on synoptic timescales can dominate variability on diurnal timescales, thereby violating a fundamental assumption of the approach employed by Chambers et al. (2019). Consequently, nocturnal periods under PTI conditions would be misclassified below their actual degree of atmospheric stability. Applying the RBM of PTI classification to observations in a subalpine basin set-

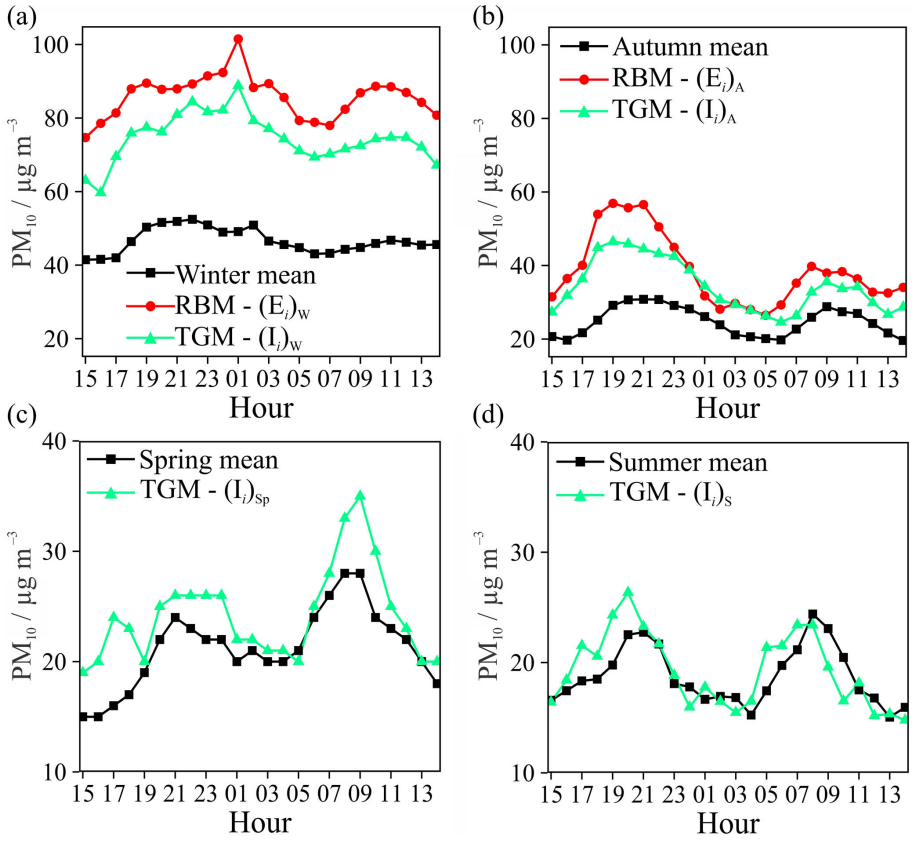


Figure 16. Diurnal PM_{10} composites, based on hourly means, for: **(a)** winter, **(b)** autumn, **(c)** spring, and **(d)** summer, for all conditions (seasonal mean) and for persistent temperature inversion events detected by the RBM and TGM.

ting after first classifying the data according to the scheme of Chambers et al. (2019) would enable clear identification of the misclassified events for separate analysis. The combined application of these two approaches using a complete suite of criteria pollutants in Ljubljana city will be the subject of a separate investigation.

4 Conclusions

The aim of this study was to determine a reliable and seasonally independent method to identify persistent temperature inversion events in the subalpine basin setting of Ljubljana, based on observations over the period December 2016–November 2017. To this end, two methods were compared: (i) a new radon-based method developed and tested in this study and (ii) a previously published pseudo-vertical temperature gradient method.

Development of the radon-based method required an understanding of the various timescales contributing to variability in the 1-year hourly radon time series (sub-diurnal, diurnal, synoptic, and greater than synoptic). The method is applied in four steps: (i) minimize sub-diurnal radon variability, (ii) identify the fetch-related (synoptic-scale) radon variability, (iii) isolate the synoptic-scale from larger timescale variability, and (iv) identify persistent temperature inversion events using the seasonal standard deviation of diurnal timescale radon variability as an event threshold with a ≥ 48 h persistence requirement. The method was applied separately for each season in order to account for seasonal changes in the radon source function, day length, and atmospheric mixing.

The existing pseudo-vertical temperature gradient method to identify PTI events was applied using 1 year of measurements from eight automatic weather stations, within three distinct elevation categories, distributed around the base and on the sidewalls of the basin. The technique considers daily-mean temperature gradients between stations in different elevation categories. The applicability of the technique is contingent upon two key assumptions: (i) horizontal homogeneity of air temperature between stations within the same elevation category, and (ii) clear and consistent distinction of temperature between stations in different elevation categories.

Over the year, the radon-based method identified six PTI events (four in winter, two in autumn). No PTI events were identified in spring or summer. By comparison, the pseudo-vertical temperature gradient method identified 17 PTI events (five in winter, three in spring, two in summer, and seven in

autumn). All six events identified by the radon-based method were also identified by the pseudo-vertical temperature gradient method. Each of the events identified by both methods were associated with persistent strongly stable conditions, light to calm winds (typically 0.2–0.6 $m\,s^{-1}$), modest amplitudes of diurnal temperature and relative humidity cycles, relatively consistent nocturnal conditions, and no precipitation. On the other hand, the additional 11 events detected by the pseudo-vertical temperature gradient method were characterized by somewhat mixed meteorological conditions: larger amplitude diurnal cycles of temperature, humidity, and wind speed, daytime wind speeds of up to 4 $m\,s^{-1}$, and frequent nocturnal rainfall. The comparative suitability of the RBM and TGM of PTI event identification in air quality studies was determined using hourly PM_{10} observations. Peak hourly-mean PM_{10} concentrations of TGM PTI events were 13 (11) $\mu g\,m^{-3}$ lower than those of RBM PTI events in winter (autumn). Only peak hourly-mean values of RBM PTI events exceeded 100 $\mu g\,m^{-3}$, the upper threshold of low-level short-term PM_{10} exposure according to World Health Organization guidelines.

The RBM was found to be more reliable and seasonally independent than the TGM. The inaccuracy and inconsistency of the TGM was thought to be primarily attributable to the requisite assumptions, which were not consistently met throughout the year. We demonstrated that the RBM is a convenient, simple, and economical means of consistently identifying PTI events in complex topographies (e.g., basins or valleys) regardless of season. The consistency and accuracy of this method has the potential to significantly increase the understanding of meteorological processes resulting in air pollution episodes. Once a representative number of PTI events have been observed within each season, this technique also has the potential to objectively assess the relative strength of PTI events. As such, the RBM has the potential to become a key tool in urban centers for air quality management and assessing public health risks.

Data availability. Meteorological and air quality data are collected and supplied by the National Meteorological Service at the Environmental Agency of the Republic of Slovenia (ARSO) (https://meteo.arso.gov.si/, last access: 11 August 2019). Atmospheric radon data will be made available on request.

Author contributions. The investigation was jointly conceptualized by DK, SC, and JV. Radon monitoring instrumentation was deployed and managed by DK and JV. Data collection and curation was performed by DK. Formal data analysis was performed by DK and SC. Acquisition of funding for the research was arranged by JV. The research methodology was jointly developed by DK and SC and investigation jointly conducted by DK and JV. The project was administered by JV, with JV and SC responsible for supervision. All visualization of data, concepts, and results was performed by DK. DK wrote the complete original draft of the paper, which was subsequently edited and reviewed jointly by DK, SC, and JV.

Competing interests. The authors declare that they have no conflict of interest.

Acknowledgements. The authors acknowledge the financial support from the Public Scholarship, Development, Disability and Maintenance Fund of the Republic of Slovenia (contract no. 11011-44/2016-18). The authors also gratefully acknowledge the Environmental Agency of the Republic of Slovenia for the permission provided for and the assistance in installing the weather instrument shelter for radon monitoring on their land and for providing the meteorological and air quality data.

Financial support. This research has been supported by the Slovenian Research Agency (research core funding no. P1-0143).

Review statement. This paper was edited by Robyn Schofield and reviewed by Roberto Salzano and one anonymous referee.

References

Allegrini, I., Febo, A., Pasini, A., and Schiarini, S.: Monitoring of the nocturnal mixed layer by means of particulate radon progeny measurement, J. Geophys. Res., 99, 18765–18777, 1994.

ARSO: Slovenian Environment Agency (Slovenian: Agencija Republike Slovenije za okolje), Climate Characteristics of Ljubljana – Wind Rose for the City of Ljubljana, 2017.

Avino, P. and Manigrasso, M.: Ten-year measurements of gaseous pollutants in urban air by an open-path analyzer, Atmos. Environ., 42, 4138–4148, https://doi.org/10.1016/j.atmosenv.2008.01.024, 2008.

Baasandorj, M., Hoch, S. W., Bares, R., Lin, J. C., Brown, S. S., Millet, D. B., Martin, R., Kelly, K., Zarzana, K. J., Whiteman, C. D., Dube, W. P., Tonnesen, G., Jaramillo, I. C., and Sohl, J.: Coupling between chemical and meteorological processes under persistent cold-air pool conditions: evolution of wintertime $PM_{2.5}$ pollution events and N_2O_5 observations in Utah's Salt Lake Valley, Environ. Sci. Technol., 51, 5941–5950, https://doi.org/10.1021/acs.est.6b06603, 2017.

Beeston, M., Grgić, I., van Elteren, J. T., Iskra, I., Kapun, G., and Močnik, G.: Chemical and morphological characterization of aerosol particles at Mt. Krvavec, Slovenia, during the Eyjafjallajökull Icelandic volcanic eruption, Environ. Sci. Pollut. Res., 19, 235–243, https://doi.org/10.1007/s11356-011-0563-8, 2011.

Bielec-Bąkowska, Z., Knozová, G., Leśniok, M., Matuszko, D., and Piotrowicz, K.: High suspended dust concentrations in Brno, Sosnowiec and Krakow (the year 2009 as an example), Pr. Geogr., 126, 67–84, 2011.

Chambers, S., Williams, A. G., Zahorowski, W., Griffiths, A., and Crawford, J.: Separating remote fetch and local mixing influences on vertical radon measurements in the lower atmo-

sphere, Tellus B, 63, 843–859, https://doi.org/10.1111/j.1600-0889.2011.00565.x, 2011.

Chambers, S. D., Hong, S.-B., Williams, A. G., Crawford, J., Griffiths, A. D., and Park, S.-J.: Characterising terrestrial influences on Antarctic air masses using Radon-222 measurements at King George Island, Atmos. Chem. Phys., 14, 9903–9916, https://doi.org/10.5194/acp-14-9903-2014, 2014.

Chambers, S. D., Williams, A. G., Crawford, J., and Griffiths, A. D.: On the use of radon for quantifying the effects of atmospheric stability on urban emissions, Atmos. Chem. Phys., 15, 1175–1190, https://doi.org/10.5194/acp-15-1175-2015, 2015.

Chambers, S. D., Podstawczyńska, A., Pawlak, W., Fortuniak, K., Williams, A., and Griffiths, A.: Characterising the state of the urban surface layer using Radon-222, J. Geophys. Res.-Atmos., 124, 770–788, 2019.

Chemel, C., Arduini, G., Staquet, C., Largeron, Y., Legain, D., Tzanos, D., and Paci, A.: Valley heat deficit as a bulk measure of wintertime particulate air pollution in the Arve River Valley, Atmos. Environ., 128, 208–215, https://doi.org/10.1016/j.atmosenv.2015.12.058, 2016.

Clements, C. B., Whiteman, C. D., and Horel, J. D.: Cold-air-pool structure and evolution in a mountain basin: Peter Sinks, Utah, J. Appl. Meteorol., 42, 752–768, https://doi.org/10.1175/1520-0450(2003)042<0752:CSAEIA>2.0.CO;2, 2003.

Cohen, L. D., Barr, S., Krablin, R., and Newstein, H.: Steady-state vertical turbulent diffusion of radon, J. Geophys. Res., 77, 2654–2668, 1972.

Cuxart, J., Holtslag, A. A. M., Beare, R. J., Bazile, E., Beljaars, A., Cheng, A., Conangla, L., Ek, M., Freedman, F., Hamdi, R., Kerstein, A., Kitagawa, H., Lenderink, G., Lewellen, D., Mailhot, J., Mauritsen, T., Perov, V., Schayes, G., Steeneveld, G.-J., Svensson, G., Taylor, P., Weng, W., Wunsch, S., and Xu, K.-M.: Single-column model intercomparison for a stably stratified atmospheric boundary layer, Bound.-Lay. Meteorol., 118, 273–303, https://doi.org/10.1007/s10546-005-3780-1, 2006.

Dorninger, M., Whiteman, C. D., Bica, B., Eisenbach, S., Pospichal, B., and Steinacker, R.: Meteorological events affecting cold-air pools in a small basin, J. Appl. Meteorol. Climatol., 50, 2223–2234, https://doi.org/10.1175/2011JAMC2681.1, 2011.

EEA: Air quality in Europe – 2016 report, 2016.

EEA: Air quality in Europe – 2017 report, 2017.

Etiope, G. and Martinelli, G.: Migration of carrier and trace gases in the geosphere: an overview, Phys. Earth Planet. Inter., 129, 185–204, 2002.

Eve, A. S.: On the amount of radium emanation in the atmosphere near the Earth's surface, London, Edinburgh, Dublin Philos. Mag. J. Sci., 16, 622–632, 1908.

Ferrario, M. E., Rossa, A., and Pernigotti, D.: Characterization of PM_{10} accumulation periods in the Po valley by means of boundary layer profilers, in IOP Conference Series: Earth Environ. Sci., 1, 012067, doi:10.1088/1755-1315/1/1/01206, 2008.

Galmarini, S.: One year of ^{222}Rn concentration in the atmospheric surface layer, Atmos. Chem. Phys., 6, 2865–2886, https://doi.org/10.5194/acp-6-2865-2006, 2006.

Goudie, A. S.: Desert dust and human health disorders, Environ. Int., 63, 101–113, https://doi.org/10.1016/j.envint.2013.10.011, 2014.

Griffin, D. W.: Atmospheric movement of microorganisms in clouds of desert dust and implications for human health, Clin. Microbiol. Rev., 20, 459–477, https://doi.org/10.1128/CMR.00039-06, 2005.

He, T., Chen, Y., Stanič, S., Bergant, K., Gao, F., and Hua, D.: Properties of tropospheric aerosols observed over southwest Slovenia, J. Quant. Spectrosc. Ra., 217, 380–387, https://doi.org/10.1016/j.jqsrt.2018.06.009, 2018.

Highwood, E. J. and Kinnersley, R. P.: When smoke gets in our eyes: The multiple impacts of atmospheric black carbon on climate, air quality and health, Environ. Int., 32, 560–566, https://doi.org/10.1016/j.envint.2005.12.003, 2006.

Ivančič, M. and Vončina, R.: Modelling PM_{10} dispersion from road traffic and industry in Ljubljana Basin, in: zbornik HARMO'15 konference, Madrid, 2015.

Jacob, J., Prather, J., Rasch, J., Beagley, R., Bergmann, J., Blackshear, W. T., Chiba, M., Chipperfield, M. P., Dignon, E., Kasibhatla, S., Kritz, M. A., Penner, E., Ramonet, M., Reeves, C. E., Stockwell, Z., Velthoven, F. J. Van, Verver, G., and Yang, H.: Evaluation and intercomparison of global atmospheric transport models using ^{222}Rn and other short-lived tracer, J. Geophys. Res., 102, 5953–5970, 1997.

Jędruszkiewicz, J., Czernecki, B., and Marosz, M.: The variability of PM_{10} and $PM_{2.5}$ concentrations in selected Polish agglomerations: the role of meteorological conditions, 2006–2016, Int. J. Environ. Health Res., 27, 441–462, https://doi.org/10.1080/09603123.2017.1379055, 2017.

Kallos, G., Astitha, M., Katsafados, P., and Chris, S.: Long-range transport of anthropogenically and naturally produced particulate matter in the Mediterranean and North Atlantic: current state of knowledge, J. Appl. Meteorol. Climatol., 46, 1230–1251, https://doi.org/10.1175/JAM2530.1, 2006.

Karstens, U., Schwingshackl, C., Schmithüsen, D., and Levin, I.: A process-based ^{222}radon flux map for Europe and its comparison to long-term observations, Atmos. Chem. Phys., 15, 12845–12865, https://doi.org/10.5194/acp-15-12845-2015, 2015.

Kassomenos, P. A. and Koletsis, I. G.: Seasonal variation of the temperature inversions over Athens, Greece, Int. J. Climatol., 25, 1651–1663, https://doi.org/10.1002/joc.1188, 2005.

Kirichenko, L. V.: The vertical distribution of the products of decay of radon in the free atmosphere, in Problems of Nuclear Meteorology, edited by: Karol, I. L. and Malakhov, S. G., State Publishing House for Literature in the Field of Atomic Science and Engineering, Moscow, 99–124, 1962.

Kochowska, E., Kozak, K., Kozłowska, B., and Mazur, J.: Test measurements of thoron concentration using two ionization chambers AlphaGUARD vs. radon monitor RAD7, Nukleonika, 54, 189–192, 2009.

Kukkonen, J., Mia, P., Ranjeet, S. S., Lakhu, L., Nutthida, K., Lia, F., Minna, R., Erik, B., Viel, Ø., Leiv, H. S., Bruce, D., and Sandro, F.: Analysis and evaluation of selected local-scale PM_{10} air pollution episodes in four European cities: Helsinki, London, Milan and Oslo, Atmos. Environ., 39, 2759–2773, https://doi.org/10.1016/j.atmosenv.2004.09.090, 2005.

Langmann, B., Folch, A., Hensch, M., and Matthias, V.: Volcanic ash over Europe during the eruption of Eyjafjallajökull on Iceland, April–May 2010, Atmos. Environ., 48, 1–8, https://doi.org/10.1016/j.atmosenv.2011.03.054, 2012.

Lareau, N. P., Crosman, E., Whiteman, C. D., Horel, J. D., Hoch, S. W., Brown, W. O. J., and Horst, T. W.: The persis-

tent cold-air pool study, Bull. Am. Meteorol. Soc., 94, 51–63, https://doi.org/10.1175/BAMS-D-11-00255.1, 2013.

Largeron, Y. and Staquet, C.: Persistent inversion dynamics and wintertime PM_{10} air pollution in Alpine valleys, Atmos. Environ., 135, 92–108, https://doi.org/10.1016/j.atmosenv.2016.03.045, 2016a.

Largeron, Y. and Staquet, C.: The atmospheric boundary layer during wintertime persistent inversions in the Grenoble valleys, Front. Earth Sci., 4, 70, 2016b.

Lehner, M., Whiteman, C. D., Hoch, S. W., Jensen, D., Pardyjak, E. R., Leo, L. S., Di Sabatino, S., and Fernando, H. J. S.: A case study of the nocturnal boundary layer evolution on a slope at the foot of a desert mountain, J. Appl. Meteorol. Climatol., 54, 732–751, https://doi.org/10.1175/JAMC-D-14-0223.1, 2015.

Levin, I., Born, M., Cuntz, M., Langendörfer, U., Mantsch, S., Naegler, T., and Wagenbach, D.: Observations of atmospheric variability and soil exhalation rate of radon-222 at a Russian forest site. Technical approach and deployment for boundary layer studies, Tellus B, 54, 462–475, 2002.

Longlong, W., Stanič, S., Gregorič, A., Bergant, K., Mole, M., and Vučković, M.: Evolution of the planetary boundary layer in the presence of fog and plume, in: EGU General Assembly Conference Abstracts, 18, p. 15363, 2016.

Marcazzan, G. M., Vaccaro, S., Valli, G., and Vecchi, R.: Characterisation of PM_{10} and $PM_{2.5}$ particulate matter in the ambient air of Milan (Italy), Atmos. Environ., 35, 4639–4650, https://doi.org/10.1016/S1352-2310(01)00124-8, 2001.

Mazur, J. and Kozak, K.: Complementary system for long term measurements of radon exhalation rate from soil, Rev. Sci. Inst., 85, 022104, doi/abs/10.1063/1.4865156, 2014.

Miranda, A., Silveira, C., Ferreira, J., Monteiro, A., Lopes, D., Relvas, H., Borrego, C., and Roebeling, P.: Current air quality plans in Europe designed to support air quality management policies?, Atmos. Pollut. Res., 6, 434–443, https://doi.org/10.5094/APR.2015.048, 2015.

Moritz, S.: imputeTS: Time series missing value imputation in R, R Packag. version 2.5, available at: https://cran.r-project.org/package=imputeTS, last access: 11 August 2019, 2017.

Moses, H., Stehney, A. F., and Lucas Jr, H. F.: The effect of meteorological variables upon the vertical and temporal distributions of atmospheric radon, J. Geophys. Res., 65, 1223–1238, 1960.

Pak, M.: Ljubljana, in: Enciklopedija Slovenije, edited by: Javornik M., Mladinska knjiga, Ljubljana, 218–220, 1992.

Perrino, C., Pietrodangelo, A., and Febo, A.: An atmospheric stability index based on radon progeny measurements for the evaluation of primary urban pollution, Atmos. Environ., 35, 5235–5244, 2001.

Petkovšek, Z.: Dissipation of the upper layer of all-day radiation fog in basins, Zb. Meteor. Hidrol. Rad, 5, 71–74, 1974.

Petkovšek, Z.: Relief meteorologically relevant characteristics of basins (air land interactions in quasi-closed system), Z. Meteorol., 28, 333–340, 1978.

Petkovšek, Z.: The termination of air pollution periods in valley basins, Z. Meteorol., 35, 370–372, 1985.

Petkovšek, Z.: Turbulent dissipation of cold air lake in a basin, Meteorol. Atmos. Phys., 47, 237–245, https://doi.org/10.1007/BF01025620, 1992.

Pey, J., Querol, X., Alastuey, A., Forastiere, F., and Stafoggia, M.: African dust outbreaks over the Mediterranean Basin during 2001–2011: PM_{10} concentrations, phenomenology and trends, and its relation with synoptic and mesoscale meteorology, Atmos. Chem. Phys., 13, 1395–1410, https://doi.org/10.5194/acp-13-1395-2013, 2013.

Pitari, G., Coppari, E., De Luca, N., and Di Carlo, P.: Observations and box model analysis of radon-222 in the atmospheric surface layer at L'Aquila, Italy: March 2009 case study, Environ. Earth Sci., 71, 2353–2359, https://doi.org/10.1007/s12665-013-2635-1, 2014.

Poberžnik, M. and Štrumbelj, E.: The effects of air mass transport, seasonality, and meteorology on pollutant levels at the Iskrba regional background station (1996–2014), Atmos. Environ., 134, 138–146, https://doi.org/10.1016/j.atmosenv.2016.03.059, 2016.

Podstawczyńska, A. and Chambers, S. D.: Radon-based technique for the analysis of atmospheric stability – a case study from Central Poland, Nukleonika, 63, 47–54, https://doi.org/10.2478/nuka-2018-0006, 2018.

Pope, C. A. and Dockery, D. W.: Health effects of fine particulate air pollution: Lines that connect, J. Air Waste Manag. Assoc., 56, 709–742, https://doi.org/10.1080/10473289.2006.10464485, 2006.

R Development Core Team: R: A language and environment for statistical computing, R Found. Stat. Comput. Vienna Austria, https://doi.org/10.1038/sj.hdy.6800737, 2008.

Rakovec, J., Merše, J., Jernej, S., and Paradiž, B.: Turbulent dissipation of the cold-air pool in a basin: Comparison of observed and simulated development, Meteorol. Atmos. Phys., 79, 195–213, https://doi.org/10.1007/s007030200003, 2002.

Reddy, P. J., Barbarick, D. E., and Osterburg, R. D.: Development of a statistical model for forecasting episodes of visibility degradation in the Denver metropolitan area, J. Appl. Meteorol., 34, 616–625, 1995.

Šajn, R., Gosar, M., Bidovec, M., Pirc, S., and Alijagić, J.: Geochemical mapping of Ljubljana urban and suburban area, Slovenia, in: Mapping the Chemical Environment of Urban Areas, 375–392, 2011.

Salzano, R., Pasini, A., Casasanta, G., Cacciani, M., and Perrino, C.: Quantitative interpretation of air radon progeny fluctuations in terms of stability conditions in the atmospheric boundary layer, Bound.-Lay. Meteorol., 160, 529–550, https://doi.org/10.1007/s10546-016-0149-6, 2016.

Salzano, R., Pasini, A., Ianniello, A., Mazzola, M., Traversi, R., and Udisti, R.: High time-resolved radon progeny measurements in the Arctic region (Svalbard islands, Norway): results and potentialities, Atmos. Chem. Phys., 18, 6959–6969, https://doi.org/10.5194/acp-18-6959-2018, 2018.

Satterly, J.: I. On the amount of radium emanation in the lower regions of the atmosphere and its variation with the weather, London, Edinburgh, Dublin Philos. Mag. J. Sci., 20, 1–36, https://doi.org/10.1080/14786441008636877, 1910.

Schery, S. D. and Huang, S.: An estimate of the global distribution of radon emissions from the ocean, Geophys. Res. Lett., 31, L19104, https://doi.org/10.1029/2004GL021051, 2004.

Sesana, L., Caprioli, E., and Marcazzan, G. M.: Long period study of outdoor radon concentration in Milan and correlation between its temporal variations and dispersion properties of atmosphere, J. Environ. Radioact., 65, 147–160, https://doi.org/10.1016/S0265-931X(02)00093-0, 2003.

Silcox, G. D., Kelly, K. E., Crosman, E. T., Whiteman, C. D., and Allen, B. L.: Wintertime $PM_{2.5}$ concentrations during persistent, multi-day cold-air pools in a mountain valley, Atmos. Environ., 46, 17–24, https://doi.org/10.1016/j.atmosenv.2011.10.041, 2012.

Szegvary, T., Leuenberger, M. C., and Conen, F.: Predicting terrestrial ^{222}Rn flux using gamma dose rate as a proxy, Atmos. Chem. Phys., 7, 2789–2795, https://doi.org/10.5194/acp-7-2789-2007, 2007.

Szegvary, T., Conen, F., and Ciais, P.: European ^{222}Rn inventory for applied atmospheric studies, Atmos. Environ., 43, 1536–1539, https://doi.org/10.1016/j.atmosenv.2008.11.025, 2009.

Triantafyllou, A. G.: PM_{10} pollution episodes as a function of synoptic climatology in a mountainous industrial area, Enviro, Pollut., 112, 491–500, 2001.

Vardoulakis, S. and Kassomenos, P.: Sources and factors affecting PM_{10} levels in two European cities: Implications for local air quality management, Atmos. Environ., 42, 3949–3963, https://doi.org/10.1016/j.atmosenv.2006.12.021, 2008.

Vrhovec, T.: Analysis of mesometeorological temperature fields, Meteorol. Atmos. Phys., 43, 235–240, 1990.

Wang, F., Chambers, S. D., Zhang, Z., Williams, A. G., Deng, X., Zhang, H., Lonati, G., Crawford, J., Griffiths, A. D., Ianniello, A., and Allegrini, I.: Quantifying stability influences on air pollution in Lanzhou, China, using a radon-based "stability monitor": Seasonality and extreme events, Atmos. Environ., 145, 376–391, https://doi.org/10.1016/j.atmosenv.2016.11.003, 2016.

Whiteman, C. D., Eisenbach, S., Pospichal, B., and Steinacker, R.: Comparison of vertical soundings and sidewall air temperature measurements in a small Alpine Basin, J. Appl. Meteorol., 43, 1635–1647, https://doi.org/10.1175/JAM2168.1, 2004.

Whiteman, C. D., Hoch, S. W., Horel, J. D., and Charland, A.: Relationship between particulate air pollution and meteorological variables in Utah's Salt Lake Valley, Atmos. Environ., 94, 742–753, https://doi.org/10.1016/j.atmosenv.2014.06.012, 2014.

WHO: Ambient (outdoor) air quality and health, available at: http://www.who.int/mediacentre/factsheets/fs313/en/ (last access: 26 November 2015), 2014.

Wickham, H.: ggplot: Using the grammar of graphics with R, New York Springer, 2009.

Wigand, A. and Wenk, F.: Der gehalt der luft an Radium-emanation, nach messungen bei flugzeugaufstiegen, Ann. Phys., 391, 657–686, 1928.

Williams, A., Zahorowski, W., Chambers, S., and Griffiths, A.: The vertical distribution of radon in clear and cloudy daytime terrestrial boundary layers, J. Atmos. Sci., 68, 155–174, https://doi.org/10.1175/2010JAS3576.1, 2011.

Williams, A. G., Chambers, S., and Griffiths, A.: Bulk mixing and decoupling of the nocturnal stable boundary layer characterized using a ubiquitous natural tracer, Bound.-Lay. Meteorol., 149, 381–402, https://doi.org/10.1007/s10546-013-9849-3, 2013.

Williams, A. G., Chambers, S. D., Conen, F., Reimann, S., Hill, M., Griffiths, A. D., and Crawford, J.: Radon as a tracer of atmospheric influences on traffic-related air pollution in a small inland city, Tellus B, 68, 1–21, https://doi.org/10.3402/tellusb.v68.30967, 2016.

Wright, J. R. and Smith, O. F.: The variation with meteorological conditions of the amount of radium emanation in the atmosphere, in the soil gas, and in the air exhaled from the surface of the ground, at Manila, Phys. Rev., 5, 459–482, https://doi.org/10.1103/PhysRev.5.459, 1915.

Yao, W. and Zhong, S.: Nocturnal temperature inversions in a small, enclosed basin and their relationship to ambient atmospheric conditions, Meteorol. Atmos. Phys., 103, 195–210, https://doi.org/10.1007/s00703-008-0341-4, 2009.

Zhuo, W., Guo, Q., Chen, B., and Cheng, G.: Estimating the amount and distribution of radon flux density from the soil surface in China, J. Environ. Radioact., 99, 1143–1148, https://doi.org/10.1016/j.jenvrad.2008.01.011, 2008.

4.2 Comparison of Atmospheric Dispersion in Two Contrasting Topographic Regions using Radon-based Mixing Classification

The main aim of this study was to use the diurnal radon-based stability classification method in summer (under non-PTI conditions) to compare the atmospheric dispersion characteristics of two contrasting topographic regions: a basin environment (the Ljubljana Basin), and a valley (Vipava Valley).

Briefly, the method is developed in a few steps: (i) isolating mixing-related (diurnal) changes in near-surface radon concentrations at each site by estimating and removing air mass fetch effects, (ii) assigning stability thresholds at each site to mean values of radon accumulation within a defined nocturnal window (10-h), and (iii) quartiles of the nocturnal-mean mixing-related radon were used at each site to define four classes of nocturnal stability: near-neutral (#1), weakly stable (#2), moderately stable (#3), and most stable (#4). Corresponding daytime stability conditions were then inferred and atmospheric stability classes (#1 through #4) were assigned to whole 24-h periods.

A comparison of air pressure and rainfall between sites within each of the mixing classes indicated that atmospheric mixing conditions at both sites were controlled by the same synoptic processes. Wind speeds characteristic of the most stable nights were higher at Ljubljana (0.2–0.3 m s^{-1}) than at Ajdovščina (0–0.2 m s^{-1}). An analysis of wind direction indicated that stable conditions at Ljubljana are associated with drainage flow into the basin along the Sava River valley, whereas at Ajdovščina there is light katabatic flow from the flanks of the Trnovski gozd barrier on stable nights. These results are presented in the peer-reviewed article entitled "Radon-based atmospheric stability classification in contrasting sub-Alpine and sub-Mediterranean environments". Significantly, comparing **Figures 5c and 5d** of this manuscript to **Table 1.2** (above), the radon-based method is seen to provide more detail and better distinction between atmospheric stability categories than is possible with the PG technique.

In spite of the complex and contrasting topography between the two sites, the radon-based atmospheric stability classification method successfully demonstrated a clear and consistent variation of meteorological parameters within the assigned daily atmospheric mixing classes. The success of the diurnal radon-based method in characterizing meteorological conditions for different stability conditions suggest that it may also be a good tool for characterizing pollutant concentrations deriving from local surface-based sources, which stands to provide a better understanding of pollution movement and behavior in these complex environments. Based on the synoptic influences observed, class #1 and #2 days would be best suited for investigating pollution transport from remote sources to the sites, whereas class #3 and #4 days would provide the most representative information about local source contributions to air quality.

In this scientific article, the candidate developed the research question, performed data collection, curation and formal analysis. She performed all visualization of data, concepts, interpreted the results and wrote the complete original draft of the manuscript.

Journal of Environmental Radioactivity 203 (2019) 125–134

Contents lists available at ScienceDirect

Journal of Environmental Radioactivity

journal homepage: www.elsevier.com/locate/jenvrad

Radon-based atmospheric stability classification in contrasting sub-Alpine and sub-Mediterranean environments

Dafina Kikaj[a,*], Scott D. Chambers[b], Janja Vaupotič[c]

[a] Jožef Stefan International Postgraduate School, Jamova cesta 39, 1000, Ljubljana, Slovenia
[b] ANSTO, Environmental Research, Locked Bag 2001, Kirrawee DC, NSW, 2232, Australia
[c] Jožef Stefan Institute, Department of Environmental Sciences, Jamova cesta 39, 1000, Ljubljana, Slovenia

ARTICLE INFO

Keywords:
Radon
Atmospheric stability
Topography
Lithology
Sub-Alpine basin
Sub-Mediterranean valley

ABSTRACT

A recently-developed radon-based technique is used to investigate relative changes in summertime atmospheric stability at two sites in Slovenia with contrasting geographical settings. Although atmospheric stability for both sites (50 km apart) was shown to be governed by similar synoptic conditions, their contrasting settings caused differences in mixing conditions for each stability category. At the urban sub-Alpine site Ljubljana, situated within a topographic basin, wind speeds associated with the most stable conditions were 0.2–0.3 m s^{-1}. By comparison, corresponding wind speeds for the near-coastal sub-Mediterranean site Ajdovščina, located at the foothills of the Trnovski gozd barrier, were 0–0.2 m s^{-1}. The wind direction at Ljubljana under stable conditions (~80°) was consistent with drainage flow into the basin along the Sava River valley. The corresponding wind direction at Ajdovščina was 20–40°, consistent with gentle katabatic drainage from the flanks of the Trnovski gozd barrier. After removing fetch effects on radon variability at each site, a large contrast in local contributions to the radon signal was noted: the diurnal amplitude of the local radon signal increased from ~24 Bq m^{-3} at Ljubljana to ~47 Bq m^{-3} at Ajdovščina. This difference was attributed to a greater nocturnal radon accumulation rate at Ajdovščina (3.5 Bq m^{-3} h^{-1} vs 2.1 Bq m^{-3} h^{-1}) due to higher radon fluxes from flysch and carbonate rocks compared to the sea and lake sediments in the Ljubljana Basin. The ability of radon to consistently distinguish subtle changes in atmospheric mixing at sites with contrasting topographic settings indicates that it will be a powerful tool for characterising air quality in these complex environments. Specifically, diurnal radon cycles indicate that the capability of the atmosphere to dilute primary pollutants is considerably less in the basin environment.

1. Introduction

Understating relative changes in atmospheric stability is important when trying to characterise air pollution variability, which has become a major global environmental issue. Atmospheric stability is a term often used to describe the degree to which vertical mixing in the lower troposphere is suppressed or enhanced over a specific site under certain meteorological conditions.

Historically, atmospheric stability has usually been estimated using routine or specialised near-surface meteorological observations (e.g., Pasquill-Gifford schemes, Pasquill, 1961; Pasquill and Smith, 1983; Turner, 1964; Richardson Number approaches; or Monin-Obukhov similarity theory; Foken, 2006). Such methods vary widely in terms of their complexity, required instrument maintenance, accuracy, and cost (Bowen, 1994; Crawford et al., 2016; Gifford, 1976; Kahl and Chapman, 2018). A less conventional, yet comparatively economical, method of classifying atmospheric stability that has recently increased in popularity relies upon near-surface measurements of the atmospheric radon concentration. The radioactive gas radon (^{222}Rn, $t_{1/2}$ = 3.82 d) is a member of the uranium (^{238}U) decay chain. It is formed from the decay of radium (^{226}Ra, $t_{1/2}$ = 1600 years), which is ubiquitous throughout the Earth's crust. Consequently, the terrestrial radon flux is fairly uniformly distributed on local to regional scales (0.75–1.25 atom cm^{-2} s^{-1}; Jacob et al., 1997; Karstens et al., 2015). The radon source function, for unsaturated/unfrozen terrestrial surfaces, is around 2–3 orders of magnitude greater than that from the open ocean (Schery and Huang, 2004). Being an inert gas, radon does not chemically react with other atmospheric constituents and its low solubility makes it unlikely to be washed out by rainfall, so its main atmospheric sink is radioactive decay (Jacob and Prather, 1990; Li and Chang, 1996; Minato, 1983).

* Corresponding author.
E-mail address: dafina.kikaj@ijs.si (D. Kikaj).

https://doi.org/10.1016/j.jenvrad.2019.03.010
Received 17 December 2018; Received in revised form 8 March 2019; Accepted 8 March 2019
Available online 19 March 2019
0265-931X/ © 2019 Elsevier Ltd. All rights reserved.

Once emitted to the atmosphere radon is directly influenced by the meteorological processes that regulate turbulent mixing, namely, vertical and horizontal components of dispersion. Its half-life, conveniently between the timescales of diurnal and synoptic events, is ideal for characterising a wide range of meteorological events (Kikaj et al., 2019; Williams et al., 2013; Zahorowski et al., 2004). Combined, these characteristics make radon unique and powerful indicator of atmospheric stability.

Soon after its discovery in 1900, pioneering studies using radon as an atmospheric tracer began (e.g., Elster and Geitel, 1901; Satterly, 1910). Its popularity as a tool for indicating atmospheric stability increased markedly from the 1960s (Jacobi and André, 1963; Moses et al., 1960; Pearson and Jones, 1965; Turekian et al., 1977), and more recently it has become quite well-accepted by the scientific community generally as an atmospheric tracer (Balkanski et al., 1993; Desideri et al., 2006; Dueñas et al., 1996; Jacob et al., 1997; Szegvary et al., 2009; Williams et al., 2016, 2013; Zahorowski et al., 2005, 2004). In studies related to atmospheric stability, single-height radon measurements have mostly been used. Radon time series measurements are affected by a range of different atmospheric processes, from meso to synoptic scales (Chambers et al., 2015; Galmarini, 2006; Sesana et al., 2003), and represent a combination of local and non-local radon signals. Local radon contributions are controlled by the local (~20 km diameter) radon flux and daily changes in the atmospheric mixing depth. Non-local contributions are consequence of synoptic processes, which bring radon from other places into the measuring site. So far, the main obstacles to the wider use of radon as a quantitative indicator of atmospheric stability have been a lack of continuous radon gradient measurements, which are ideal for this purpose, or failure to properly calculate and remove the non-local radon contributions from single-height radon measurements. Some landmark studies in this field in recent decades include: the findings of Sesana et al. (2006, 2003) and Perrino et al. (2001), which clearly demonstrated good correlation between diurnal variations of radon concentrations with urban pollutants (accumulated at night and diluted during the day); direct measurements of radon concentration gradients and their relationship to near-surface atmospheric mixing by Butterweck et al. (1994), Chambers et al. (2011), Cohen et al. (1972), Moses et al. (1960) and Williams et al. (2013); and the technique of Chambers et al. (2015) to estimate and remove non-local contributions to observed radon time series. Together, the results of these studies helped lead to the development of a method that reliably provides a "relative measure" of near-surface mixing at a site (by way of classes of atmospheric stability) that is based on near-surface single-height radon measurements (Chambers et al., 2018, and references therein).

The radon-based stability classification approach introduced by Chambers et al. (2015) is a comparatively new method for characterising relative changes in atmospheric stability at a site for a range of scientific purposes. Williams et al. (2016) used four stability classes derived from radon observations 15 m above ground level (a.g.l.) to accurately characterise carbon monoxide and benzene concentrations across the diurnal cycle throughout all seasons in Bern, Switzerland. Pal et al. (2015) used the same method applied to radon concentrations recorded at 180 m a.g.l., to improve understanding of the daytime behaviour of trace gases in the lower atmosphere of rural site in France. Further, Chambers et al. (2016a) and Melintescu et al. (2018) used radon observations from 10 m a.g.l., to investigate the influence of atmospheric stability on anthropogenic and natural atmospheric radioisotopes in the vicinity of a decommissioned nuclear research reactor in Romania near Bucharest. The radon-based technique for stability classification was also applied to radon observations 2 m a.g.l., to assess urban heat island intensity in the relatively flat region of Łódź in central Poland (Chambers et al., 2016b, 2018; Podstawczyńska and Chambers, 2018), and to see the influence of atmospheric mixing on canopy-level climate between the urban centre Łódź and the surrounding agricultural land in Ciosny, Poland (Podstawczyńska, 2016).

While meteorological processes have the largest influence on atmospheric stability, geographic setting and local topography can also have an important influence on the atmospheric mixing state. Such influences can usually also be seen in the temporal variations of atmospheric radon concentration. For cases when the local topography is flat or relatively simple, radon concentration shows a typical diurnal variation; a minimum in the late afternoon followed by a maximum in the early hours of the next morning. This cycle reflects the diurnal concentrating and diluting effect of changes in mixing depth of the atmospheric boundary layer; which is closely related to atmospheric stability. At sites with more complex topography, however, such as sheltered basins or valleys surrounded by Alps, under certain synoptic conditions the atmospheric radon concentration can show little diurnal variation for days at a time, as observed in Ljubljana, Slovenia (Kikaj and Vaupotič, 2017; Kikaj et al., 2019), and in Milan, Italy (Allegrini et al., 1994). These extended periods of stagnation within basins or valleys, especially in wintertime, are often referred to as 'persistent temperature inversion' (PTI) events (Kikaj et al., 2019; Largeron and Staquet, 2016; Marcazzan et al., 2001; Petkovšek, 1985; Rakovec et al., 2002), during which radon and other pollutants can accumulate for many days. By contrast, areas located near high mountains are usually influenced diurnally by anabatic and katabatic ("upslope" and "downslope") flow regimes, due to heating and cooling of the flanks of the mountains, resulting in strong winds that cause high air dilution and thus larger variability in the near-surface atmospheric mixing state (Bajić, 1988, 1989; Belušić et al., 2007; Yoshino, 1976). Lastly, due to the contrast in radon flux between land and water, sites located near the coast can experience large fetch-related changes in radon concentration on sub-diurnal timescales that are unrelated to the atmospheric mixing state. There is currently a lack of ongoing radon measurements in such areas, which has led to inadequate interpretation of data.

In order to help reduce this knowledge gap, here we present summertime radon measurements in a sub-Mediterranean valley and a sub-Alpine basin, and demonstrate how they can be used to characterise the atmospheric stability of the respective environments. The summer season was selected for this initial evaluation to: (i) minimise the influence of soil saturation/freezing/snow cover on the regional radon flux; and (ii) exclude complications resulting from persistent temperature inversion (PTI) events, which cannot be suitably identified by existing radon-based stability classification methods. The synoptic stagnation conditions leading to the development of PTI events violate important assumptions of the radon-based stability classification method described by Chambers et al. (2018). Developing an appropriate radon-based method for the identification of PTI events is the subject of a separate investigation (Kikaj et al., 2019).

The main aims of our study are: (i) to use the paired summertime radon observations to assign nocturnal and daytime stability classes at both sites; (ii) to compare the atmospheric radon concentration between the two sites under contrasting atmospheric stability classifications; and (iii) to characterise and compare meteorological parameters (i.e., air pressure, air temperature, relative humidity, precipitation, wind speed and direction) between the sites within each of the atmospheric stability classes.

2. Methods

Hourly atmospheric radon concentrations and meteorological parameters have been monitored at a sub-Alpine basin site (**SA**; Ljubljana Bežigrad, 46.07° N, 14.52° E), and a sub-Mediterranean valley site (**SM**; Dolenje pri Ajdovščini, 45.86° N, 13.9° E), since December 2016, and are ongoing. Here we focus on only summer (June–August) observations in 2018.

All statistical analyses were conducted using the ggplot2 (Wickham, 2009) and ImputeTS (Moritz, 2017) packages under R 3.3.1 (R Development Core Team, 2008). All reported times are local (LT = UTC + 1 h).

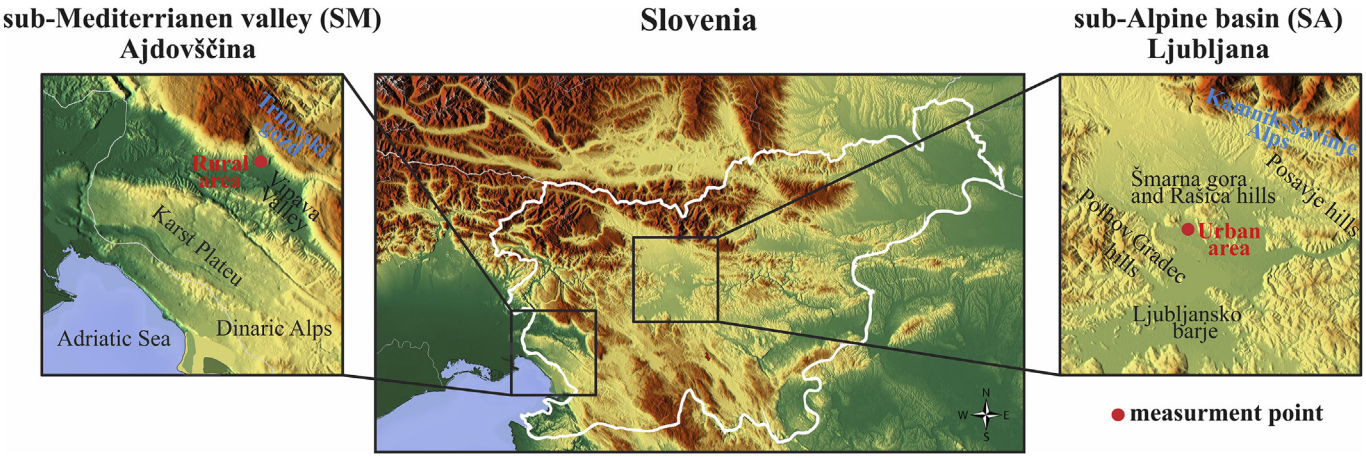


Fig. 1. (Color online) Topographic map of Slovenia with the locations of the sub-Mediterranean valley (SM) and sub-Alpine basin (SA) sites indicated.

2.1. Sites and surrounds

Ljubljana (299 m above sea level, a.s.l. ~280,000 inhabitants), is the capital city of Slovenia (Fig. 1). The SA site, at the northern edge of Ljubljana city, is located between the Julian, Kamnik-Savinje, and Dinaric Alps (Vrhovec, 1990) within a basin. The climate of this site, temperate and continental, is typical for sub-Alpine regions. A characteristic feature of the local climate is generally calm winds within the basin, which results in a high number of foggy days, with frequent persistent temperature inversion events (120 d y^{-1}), mostly restricted to the colder months (autumn, winter). Prevailing winds for the region are within the sector NNE to ENE (ARSO, 2017), and the mean wind speed changes only slightly from summer (1.4 m s^{-1}) to winter (1.3 m s^{-1}). The mean air temperature at the site reveals a distinct seasonal cycle, with the summer mean daily maximum reaching 22 °C and the winter mean daily minimum 0 °C. Rainfall distribution is irregular, 1400 mm y^{-1}, with a peak in the summer (ARSO, 2017).

Ajdovščina (98 m a.s.l. ~6800 inhabitants) is a small rural town in the Vipava Valley, Slovenia (Fig. 1). The terrain surrounding the SM site rises from southwest (the Adriatic coast, 0 m a.s.l.) to the northeast (Karst plateau, 500 m a.s.l), over a distance of less than 30 km. Continuing in this direction, the elevation then falls into the Vipava Valley (100 m a.s.l.) before rising again to the Trnovski gozd barrier (up to 1500 m a.s.l.). Due to the location and topography, strong surface winds (known as 'Bora' wind) can occur as a result of katabatic winds that flow down the mountains (Mole et al., 2017; Smith, 1985). Although the Bora wind can be observed year-round at night, it is most vigorous and frequent in the winter, when it can persist for several days, often reaching speeds of more than 28 m s^{-1} in gusts (Grisogono and Belušić, 2009). The prevailing wind directions at this site are: N-NE during Bora wind events, moderate (< 5 m s^{-1}) SW flow from the coast, or SE winds that usually follow Bora wind events (typically < 20 m s^{-1}). The climate of the SM site is sub-Mediterranean. The mean air temperature is 24 °C in summer, and 4 °C in winter. Annual rainfall in the valley is 1500 mm, peaking in autumn (ARSO, 2017).

The straight-line distance between SM and SA is about 50 km. In addition to the differences in topography and climate of the two sites, they also differ in lithology. The SA site is situated on sea and lake sediments, whereas SM is situated on flysch, with carbonates at a distance of less than a few km.

2.2. Atmospheric radon and meteorology observations

Hourly observations of meteorological parameters including air pressure (hPa), air temperature (°C), relative humidity (%), precipitation (mm h^{-1}), wind speed (m s^{-1}), and wind direction (°), recorded 2 m a.g.l., were provided by the National Meteorological Service at the Environmental Agency of the Republic of Slovenia (ARSO).

Atmospheric radon measurements are conducted using AlphaGUARD monitors (Bertin Instruments) operating in diffusion mode with a 1-h integration time (Kikaj and Vaupotič, 2017). The devices are mounted 1.5 m a.g.l., within Stevenson Screen instrument shelters. Both AlphaGUARD's have a lower limit of detection (LLD) of around 2 Bq m^{-3}. Only about 0.01% of atmospheric radon data at SM and 0.02% at SA, respectively, were estimated to fall below the LLD during the summer measurement period, which justifies the use of this kind of monitor in our study.

3. Results and discussion

3.1. Radon-based atmospheric stability classification

Typical diurnal cycles of summer radon concentration (based on hourly means) at SA and SM are shown in Fig. 2 (red lines). The diurnal cycles are characterised by a mid-afternoon minimum when the lower atmosphere is most deeply mixed, and a nocturnal maximum near dawn when the lower atmosphere is shallowest. The amplitude of these diurnal cycles (7–24 Bq m^{-3} at SA, and 8–32 Bq m^{-3} at SM) is primarily attributable to the mean day-night change in summertime atmospheric mixing depth (or "stability") due to factors such as local sun exposure, surface characteristics (roughness, albedo, etc.), and topography. A secondary influence on the mean amplitude of the diurnal cycles is the strength of the local radon source function (which, on synoptic timescales and above, depends primarily on the lithology of each site). By comparison, the magnitude of the afternoon minimum value of each diurnal cycle (7 Bq m^{-3} at SA and 8 Bq m^{-3} at SM), is more closely related to the mean summertime remote air mass fetch resulting from synoptic processes; which is expected to be quite similar for both sites, given that the distance between them is only 50 km.

The grey shaded areas in Fig. 2a and b (between 14:00–19:00 LT at SA and 12:00–17:00 LT at SM) represent the period of the diurnal cycle in which the minimum radon concentration was typically found each day. At this time, when the lower atmosphere is most deeply mixed, the ratio of remote-to-local source influences on measured radon concentrations is maximised. Pre-dawn, when the stable nocturnal inversion frequently isolates near-surface measurements from remote influences, the ratio of remote-to-local influences on measured radon concentrations is minimised. By linearly interpolating between consecutive daily minimum radon concentrations (from one afternoon to the next), it is possible to obtain an approximation of the non-local radon contributions; similar to that which might be measured by a second radon monitor sampling from a higher altitude (e.g., 250–500 m a.g.l.; above the nocturnal boundary layer). Calculating the difference between the measured radon concentrations and the interpolated non-

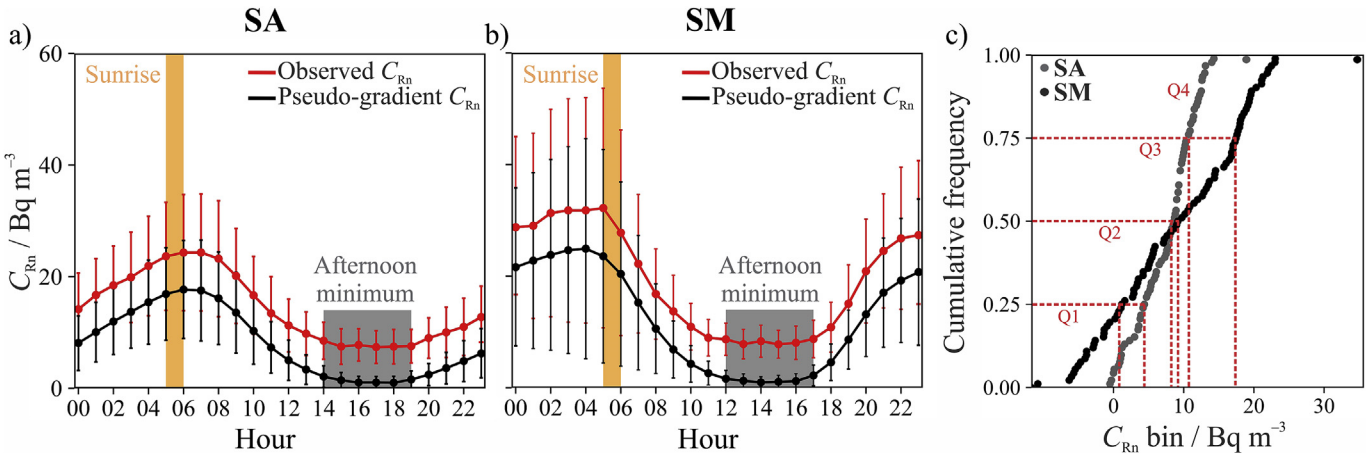


Fig. 2. (Color online) Summertime mean hourly diurnal composites of observed radon and the local contribution to radon (pseudo-gradient) at a) the sub-Alpine basin site (SA), b) sub-Mediterranean valley site (SM), whiskers represent ± σ; and c) cumulative distribution of the nocturnal mean of pseudo-gradient radon (19:00–05:00 LT) at the SA and SM, with quartiles ranges indicated.

local radon contributions is then analogous to calculating a radon gradient measurement. Consequently, the local radon contribution will henceforth be referred to as the "radon pseudo-gradient". Analysis of the radon pseudo-gradient can therefore be used as an economical, approximate alternative to vertical radon gradient measurements (Chambers et al., 2015).

Composite diurnal cycles of the radon pseudo-gradient at each site in summer are plotted in Fig. 2 (black lines). The amplitudes of these diurnal cycles (1–18 Bq m^{-3} at SA, and 1–25 Bq m^{-3} at SM), from which non-local contributions have been removed, are almost identical to those of the measured radon concentrations (7–24 Bq m^{-3} at SA, and 8–32 Bq m^{-3} at SM); proof that approximation and removal of the non-local radon effects within the radon measurements has not altered the local contribution to the observed radon signal.

After calculating the radon pseudo-gradient at each site for the entire dataset, the next step of the atmospheric stability classification process was to calculate the mean radon pseudo-gradient each night from shortly after sunset until around sunrise (19:00–05:00 LT) (e.g., Wang et al., 2016; Williams et al., 2016). A cumulative histogram of these nocturnal-mean radon pseudo-gradient values was then calculated for each site (Fig. 2c). In some cases, more often at SM which is closer to the coast, the nocturnal-mean pseudo-gradient becomes negative. This is a result of nocturnal radon concentrations occurring that are below "afternoon minimum" values, which usually indicates synoptic non-stationarity (e.g. a frontal system) or change in air mass fetch from land to recently oceanic.

Quartiles of the nocturnal-mean radon pseudo-gradient were used to denote threshold values for the four assigned relative atmospheric stability classes (Table 1): "near-neutral" (class #1), "weakly stable" (class #2), "moderately stable" (class #3) and "most stable" (class #4). Based on the three months of summer observations, there are $^{92}/_{4} = 23$ nights per class. As stated, these stability classes are related only to the respective night-time conditions. However, based on the assigned nocturnal classes, and an assumption of short-term synoptic atmospheric persistence, mixing classifications for the remaining daytime component of each 24-h period (defined afternoon-to-afternoon; 15:00–14:00 LT) were inferred (Table 1) (see also Chambers et al., 2018; Podstawczyńska and Chambers, 2018). In general, atmospheric conditions leading to the 'most stable' nights (clear sky-strong radiative cooling, low mechanical mixing) are the same conditions that result in the 'most unstable' days (clear sky-intensified thermal mixing). 'Near-neutral' nights (overcast, moderate to strong mechanical mixing), on the other hand, are usually followed by 'near neutral' daytime conditions (overcast, moderate to strong mechanical mixing).

Diurnal composite plots (based on hourly mean values) of the local radon contribution at each site in summer for each of the four designated stability classes are illustrated in Fig. 3a and b. The lowest nocturnal accumulation of locally-generated radon at each site was noted when conditions were 'near-neutral' (class #1), with the amplitude of diurnal radon cycle 6 Bq m^{-3} at SA and 14 Bq m^{-3} at SM, respectively (see Table 1 and Fig. 3a and b). It is worth noting that, in addition to the uniformly windiest nights, the 'near-neutral' class here also includes periods of synoptic non-stationarity and sudden large changes in air mass fetch, often accompanied by gusty winds and/or precipitation, which can affect the local radon exhalation rate. Changes of local radon source function under such conditions are mainly associated with water content of the soil (i.e., related to the frequency and amount of precipitation), and frontal situations with the fast changes of gradient air pressure (Mazur and Kozak, 2014). At SM in particular, fetch changes can incorporate quite recent oceanic air mass fetch, which is usually associated with large short-term changes in radon concentration. Consequently, the single-height radon-based atmospheric stability classification technique is least representative under class #1 conditions. The most noticeable daily variations of the local radon contribution were observed under class #4 conditions at each site. Therefore, from here on the relation between the radon accumulation and atmospheric stability is discussed only for the most stable conditions (class #4).

At SA on stable nights (class #4) the diurnal variability of the radon pseudo-gradient was only a half of that at SM. At SA radon concentrations reached their peak value (25 Bq m^{-3}) in the early morning (06:00 LT). Due to the nature of the topographic basin surrounding SA, katabatic winds mainly drain radon down into the basin, where it pools, with little opportunity to escape until sunrise. After sunrise (06:00 LT), convection begins and the mixing starts to reduce the near-surface radon concentration (Fig. 3a), as has also been found in other studies (Chambers et al., 2015; Perrino et al., 2001; Sesana et al., 2003; Wang et al., 2016; Williams et al., 2016).

By comparison, Fig. 3b shows that the local radon contribution at the rural SM site has a higher amplitude (47 Bq m^{-3}) on class #4 days. However, under such conditions the peak radon concentration (48 Bq m^{-3}) is reached much earlier, at about 03:00 LT in the morning (Fig. 3b), a phenomenon for this site reported here for the first time. When compared to the SA diurnal cycle, the time difference in peak concentration for class #4 days shown in Fig. 3a and b is most likely attributable to the contrasting topography (basin cf. open valley; see section 2.1). At the SM site a weak katabatic drainage flow (from the N-NE) was observed to start around 03:00 LT on class #4 days that drained radon away from the site towards the coast. Nearer the coast this flow may also combine with a land-breeze circulation. During the day at SM on class #4 days the low afternoon radon concentrations

Table 1
Quartile ranges of the mean local radon concentration (19:00–05:00 LT) for each site, sub-Alpine (SA) and sub-Mediterranean (SM), along with the assigned night-time and implied daytime stability classes, and expected meteorological conditions for each class. *The nocturnal mean concentrations are calculated from local radon contributions, see text in* section 3.1 *for details.*

Quartile (stability class)	Nocturnal mean of SA (Bq m^{-3})	Nocturnal mean of SM (Bq m^{-3})	Night-time (stability class)	Daytime (stability class)	Expected meteorological conditions
Q1 (#1)	< 4	< 1	near-neutral	near-neutral	Moderate to strong winds, often overcast, rainfall is common.
Q2 (#2)	4–9	1–9	weakly stable	weakly unstable	Light to moderate winds, cloudy or overcast, rainfall is common.
Q3 (#3)	9–11	9–18	moderately stable	moderately unstable	Light winds, scattered clouds, rainfall is uncommon.
Q4 (#4)	> 11	> 18	most stable	most unstable	Calm to light wind, clear sky, typically no rain.

observed (~3 Bq m^{-3}) were likely attributable to a combination of deep atmospheric mixing and the setup of a sea-breeze circulation in conjunction with local anabatic flow, based on the SW winds frequently observed at these times. The radon flux from sea water is typically 2–3 orders of magnitude lower than that from terrestrial surface (Schery and Huang, 2004; Zahorowski et al., 2013).

Lithology is also expected to have a large influence on the diurnal variability of the local radon contribution at the two sites. Across the study region, the highest radon exhalation rates are expected from flysch and carbonates, compared to other lithologies (e.g., sea and lake sediments) (Kardos et al., 2015). Since local radon contributions are directly related to the strength of local (radius ~10 km) radon source function, the larger diurnal amplitude at SM than SA on class #4 days indicates that the radon exhalation rate from the flysch (and carbonate rocks) in the vicinity of SM are larger than those from the sea and lake sediments at the SA site. To estimate the ratio of radon exhalation rates between sites, first we calculated the nocturnal radon accumulation rates at each site between 19:00–03:00 LT, which showed that the accumulation rate at SM was for a factor of 1.7 higher than at SA (SM 3.5 Bq m^{-3} h^{-1}, SA 2.1 Bq m^{-3} h^{-1}). Further assuming that both sites have similar height of nocturnal boundary layers (the radiative cooling rates were approximately the same, as later demonstrated in Section 3.1.2) and based on boundary layer box model (Fontan et al., 1979; Griffiths et al., 2013; Sesana et al., 2003), we can conclude that change in radon accumulation rate between sites are primary attributable to the change of their local radon source function. Compared to the SA site, the radon exhalation rate from carbonates in the vicinity of the SM site was a factor of 1.7 higher. In spite of the larger radon exhalation rate in the vicinity of SM, observed radon concentrations at this site are strongly correlated with wind direction (predominantly SW or NE) due to the proximity of the coast (20 km SW).

Significantly, comparing the relative reduction in peak magnitudes of the radon diurnal cycles for each stability class in Fig. 3a and b, it is clear that the ability of the atmosphere to dilute primary pollutants with surface-based sources (for which radon is a good proxy) is considerably less within the topographic basin setting of Ljubljana, than in the coastal setting of Ajdovščina.

3.2. Meteorological parameters within radon-based stability classes

The SA and SM sites differ in terms of their climate, lithology, topography and land type (rural and urban). Having classified the atmospheric stability for these contrasting regions (section 3.1), we sought to characterise the following meteorological parameters at each site: air pressure, air temperature, relative humidity, precipitation, wind speed and wind direction. Diurnal composite plots of these parameters (based on hourly means), corresponding to each of the radon-based atmospheric stability classes at SA and SM, are shown in Figs. 4 and 5.

3.2.1. Air pressure

The lowest amplitude diurnal cycles of pressure were observed under class #3 and #4 conditions, indicative of consistent synoptic conditions. Furthermore, the highest daily-mean pressures were also associated with these conditions, indicating that class #3 and #4 conditions were typically associated with anti-cyclonic conditions (Fig. 4a and b), which usually bring fair weather with light winds, few storms or precipitation, and nearly cloud-free skies. On the other hand, the largest diurnal amplitudes of pressure, and lowest daily-mean pressure values were associated with class #1 days. This is consistent with class #1 conditions being more frequently associated with either low-pressure systems, or rapidly changing (non-stationary) synoptic conditions. At these times the sky is more often covered by clouds, precipitation is more common, as are moderate to strong winds.

Synoptic weather systems typically have horizontal length scales of order ~1000 km, and timescales of days to weeks (Stull, 1988). If

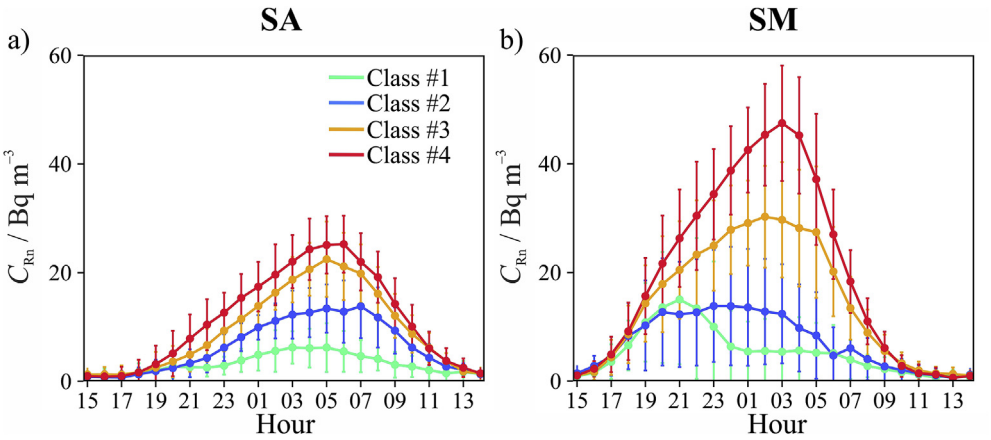


Fig. 3. (Color online) Mean hourly diurnal composites of the local radon concentration in summer season at a) the sub-Alpine basin site (SA), and b) the sub-Mediterranean valley site (SM), for each of the radon-based atmospheric stability classes; whiskers represent ± σ.

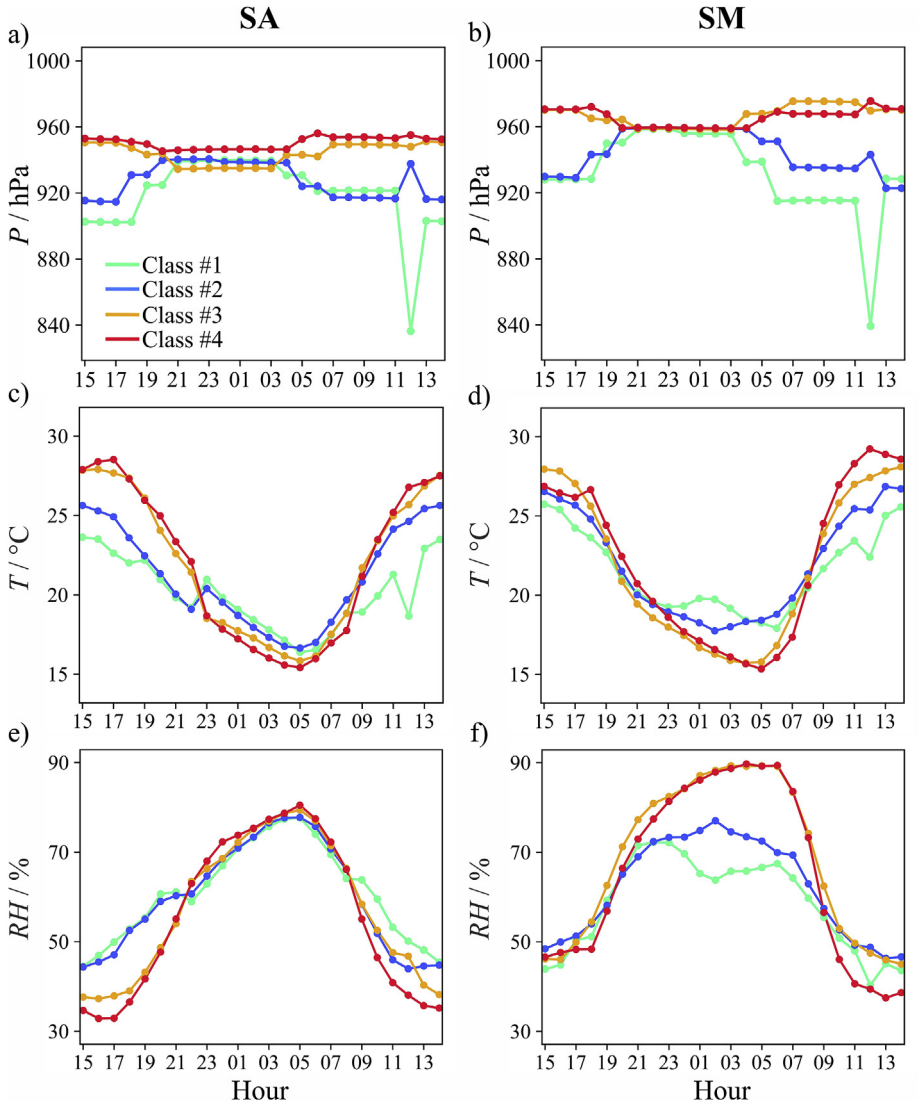


Fig. 4. (Color online) Mean hourly diurnal composite of air pressure (*P*), air temperature (*T*), and relative humidity (*RH*) at sub-Alpine basin (SA) (*left*) and sub-Mediterranean valley (SM) (*right*), in summer season for each of radon-based atmospheric stability classes.

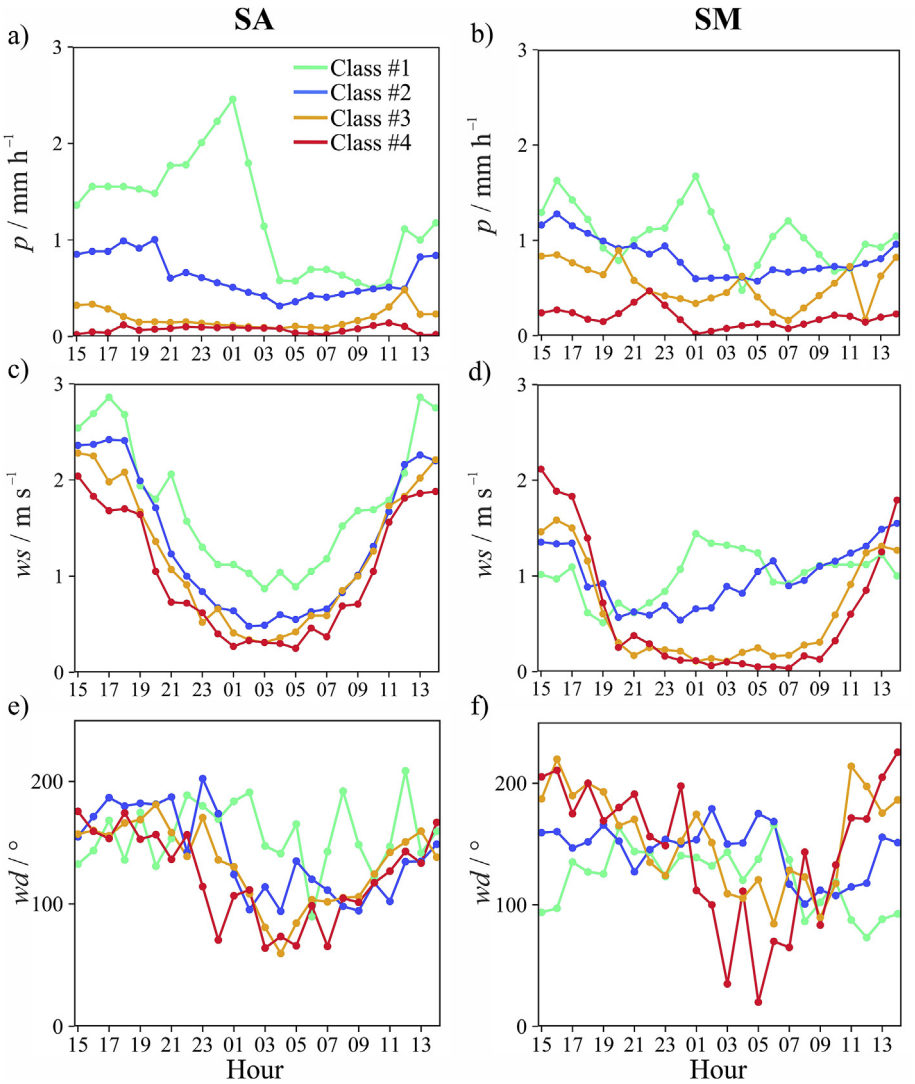


Fig. 5. (Color online) Mean hourly diurnal composite of precipitation (*p*), wind speed (*ws*), and wind direction (*wd*) at sub-Alpine basin (SA) (*left*) and sub-Mediterranean valley (SM) (*right*), in summer season for each of radon-based atmospheric stability classes.

radon-based stability classification and synoptic meteorology are related, a good correlation would be expected between the diurnal air pressure records of the two stations (which are only 50 km apart). The Pearson's linear correlation coefficient (*r*), showed a strong correlation within all atmospheric stability classes between the two sites ($r = 0.8$ for #1 and $r = 0.9$ for #2, #3 and #4 class), confirming a strong link between radon-based stability classification and synoptic processes.

3.2.2. Air temperature

The largest diurnal temperature amplitudes were observed on class #3 and #4 days (Fig. 4c and d). This situation typically occurs during anti-cyclonic conditions (regional subsidence), which result in clear sky conditions and low gradient winds. When there are clear skies this allows rapid radiative cooling of the surface (coldest nocturnal temperatures). Combined with low winds, this allows the formation of a strong nocturnal temperature inversion. Such nights are typically followed by clear sky days (most unstable conditions) with the most intense solar radiation and the highest daytime air temperature, due to the greatest rate of surface heating. Conversely, the lowest amplitude of diurnal air temperature was noticed within class #1 and #2 days (Fig. 4c and d). Here, the presence of significant amounts of clouds at night reduces the rate of radiative surface cooling, resulting in weakly stable to near-neutral conditions. Consequently, the nocturnal air temperature was typically higher on class #1 and #2 days than for class #3 and #4 days. Cloud cover also limits the amount of daytime heating on the weakly unstable and near-neutral days, resulting in the lowest observed daytime air temperatures.

The maximum air temperature within the radon-based stability classes is 0.2–2.1 °C higher at the sub-Mediterranean climate over rural area (SM) than in urban site with sub-Alpine (SA) climate (Fig. 4c and d). Variations in elevation (200 m change), proximity to the coast, terrain exposure to the sun, physical and vegetative elements of surface and generation of shadows from surrounding topography (Chambers et al., 2005, 2016b; Hoch and Whiteman, 2010) could all potentially play a role in higher maximum air temperature of SM site. Within all stability classes, the diurnal cycle of air temperatures at both sites reaches its minimum value before sunrise (05:00 LT) (Fig. 4c and d). On class #4 days, a time shift of the maximum temperature between sites was observed; at SA the maximum temperature was reached a few hours before sunset (16:00–17:00 LT) (Fig. 4c), whereas maximum temperatures at SM were reached during the mid-afternoon (12:00–14:00 LT) (Fig. 4d). The onset of a sea-breeze on class #4 days at SM might be responsible for the time shift in maximum air temperature. Accordingly, air temperature at SM has the largest amplitude under clear-sky conditions (class #4).

3.2.3. Relative humidity

Diurnal cycles of relative humidity within each stability class are shown in Fig. 4e and f. Higher daytime and lower nocturnal values were observed for classes #1 and #2. This situation is usually associated with increased low-level cloud cover, where air is more humid during the daytime. On weakly stable (class #2) and near-neutral nights (class #1) the clouds insulate the surface, keeping the air warmer, so the relative humidity was slightly lower compared to stable conditions (classes #3 and #4). Intense solar radiation during unstable days (classes #3 and #4) caused lower relative humidity, whereas rapid surface cooling on stable nights (classes #3 and #4) significantly increased relative humidity.

The largest difference in relative humidity between the two sites was observed on class #3 and #4 days. Presumably, the main reason for the ~12% lower relative humidity at SA is that it is an urban area. Relative humidity was found to be lower also in other urban areas, mostly due to the lack of evapotranspiration from vegetation (Fortuniak et al., 2006; Liu et al., 2015; Pal et al., 2012), which is typical for rural areas.

3.2.4. Precipitation

On average the synoptically-driven changes in stability revealed by the radon analysis were strongly related to precipitation events (Fig. 5a and b). Almost no precipitation occurred on class #3 and #4 days (anticyclonic conditions). On the other hand, low pressure episodes were often associated with clouds, often resulting in precipitation on class #1 and #2 days.

3.2.5. Wind speed and direction

The mean summer wind speed was different between sites (SA 1.4 $m\,s^{-1}$ and SM 0.9 $m\,s^{-1}$). Furthermore, looking at the diurnal cycles (Fig. 5c and d), differences in wind speed between the sites are more pronounced, and also change systematically, with atmospheric stability class.

At SA the diurnal amplitude of wind speed was similar for all four stability classes, but the nocturnal wind speeds were highest (~1 $m\,s^{-1}$) for class #1 and lowest (~0.5 $m\,s^{-1}$) for class #4. By contrast, at SM the diurnal amplitude of wind speed was much lower on class #1 and #2 days than was observed on class #3 and #4 days. On class #3 and #4, the nocturnal SM wind speed was very low (0–0.2 $m\,s^{-1}$), but daytime wind speed increased sharply (to 1.5–2.1 $m\,s^{-1}$), most likely attributable to a combination of convective mixing and the setup of a *sea-breeze* circulation ($180° \leq WD \leq 220°$; Fig. 5f). In the early mornings (03:00–05:00 LT) of class #4 days the wind direction of the light winds switches to NE-NNE, consistent with katabatic drainage, possibly in conjunction with a *land-breeze*. The large amplitude of wind speed and direction at SM on class #3 and #4 days was mainly the result of the differential heating over the area, due to mountains, valley and sea, when insolation is high (Grisogono and Belušić, 2009; Yoshino, 1976). On the other hand, when anticyclonic conditions dominate over the mountains surrounding SA, there are anabatic winds that blow *up* the slopes by day and katabatic winds that flow *down* the slopes at night (Fig. 5f). In general, mountains breezes are calm-to-weak winds with lowest diurnal variations, daytime (~0.5–1.8 $m\,s^{-1}$) and night-time (~0.3–0.5 $m\,s^{-1}$) (Fig. 5d).

The diurnal variability of wind speed and wind direction was typically lower on class #1 and #2 days (cyclonic conditions; Fig. 5c–f). Furthermore, the ESE/SSE wind direction within near-neutral conditions (class #1) was almost identical at both sites (Fig. 5e and f), confirming the simultaneous synoptic controls (in this case by cyclonic processes) on atmospheric stability at both sites. However, higher difference between the two sites was noticed in daytime wind speed under near-neutral conditions. The topographical setting in the SE direction of SA (Fig. 1) might influence that ESE/SSE wind to be channelled up the basin that SA site is in (Ivančič and Vončina, 2014; Scire et al., 2000). However, if wind approaches the SM site with the same direction, there are Dinaric Alps in its way, which block the winds.

4. Summary

In spite of the complex and contrasting topography between the two sites in this study, the radon-based atmospheric stability classification method successfully demonstrated a clear and consistent variation of meteorological parameters within the assigned daily atmospheric stability classes. These findings indicate that radon-based classification of the atmospheric mixing state (or stability) is versatile and reliable, and an important tool to improve understanding of meteorological changes and to assess the influence of atmospheric stability in regions of contrasting geographic setting and topography. The success of the radon-based method in characterising meteorological conditions for different stability conditions suggests that it may also be a good tool for characterising pollutant concentrations deriving from local surface-based sources, which stands to provide a better understanding of pollution movement and behaviour in these complex environments. Based on the synoptic influences observed, class #1 and #2 days would be best suited for investigating pollution transport from remote sources to the sites, whereas class #3 and #4 days would provide the most representative information about local source contributions to air quality. Given that radon has a well-distributed surface source, which is relatively constant in time, its diurnal patterns of accumulation are expected to be quite different to that of pollution generated from local sources, the strengths of which typically vary strongly in both space and time (Williams et al., 2016). However, the diurnal variability of the local contribution to observed radon concentration serves as a convenient proxy for the dilution effects of atmospheric mixing.

As previously noted, the reliability of the radon-based classification technique year-round at a given site depends strongly on two factors: (i) the ability to account for temporal (mainly seasonal) variation of the local radon exhalation rate due to long-term (greater than synoptic time-scale) changes in snow cover, soil freezing and soil moisture, and (ii) the ability to identify and exclude persistent temperature inversion events, which are not yet suitably identified by contemporary radon-based atmospheric stability classification techniques. Extending the radon-based classification of atmospheric stability at these sites to other seasons, and developing radon-based techniques to identify PTI events (e.g. Kikaj et al., 2019), will be the subject of our future work.

Lastly, for the purpose of atmospheric stability analysis it is important to select appropriate radon detectors on a case-by-case basis. The most reliable way to account for remote influences (fetch effects) on observed radon concentrations is by directly measuring near-surface radon gradients (e.g., Chambers et al., 2011). This approach, however, requires a pair of research-grade instruments such as the dual-flow-loop two-filter style of detector (Chambers et al., 2014; Griffiths et al., 2016; Williams et al., 2013) in order to consistently resolve daytime gradients that can be of order 0.1–0.2 Bq m^{-3}. The radon-based stability classification method used here uses only single-height radon measurements, but the approach depends on the ability to reliably identify the diurnal minimum radon concentration on a daily basis. It is important to select a radon detector with a lower limit of detection sufficient to resolve typical afternoon radon concentrations at the measurement site. For SA and SM, since afternoon minimum radon concentrations rarely dropped below 7 Bq m^{-3}, AlphaGUARD detectors (LLD ~2 Bq m^{-3}) were suitable. A discussion of problems that can arise when afternoon radon concentrations are often below the radon detector's LLD is provided in Chambers et al. (2018).

5. Conclusions

Continuous atmospheric radon concentrations and meteorological parameters from a sub-Alpine basin site (Ljubljana) and a sub-Mediterranean valley site (Ajdovščina) were analysed for the summer (June–August) of 2018.

Radon concentrations were used at each site to define four classes of nocturnal stability: near-neutral, weakly stable, moderately stable, and most stable. Corresponding daytime stability conditions were then inferred and atmospheric stability classes (#1 through #4) were assigned to whole 24-h periods. A comparison of air pressure and rainfall between sites within each of the stability classes indicated that atmospheric mixing conditions at both sites were controlled by the same synoptic processes. On class #4 days (with the most stable nocturnal conditions), the diurnal radon cycles were largest at both sites. Peak diurnal radon concentrations under these conditions were a factor of two higher at Ajdovščina due to greater rates of radon exhalation from flysch and carbonate rocks than from the sea and lake sediments characteristic of the Ljubljana basin region. Wind speeds characteristic of the most stable nights were higher at Ljubljana (0.2–0.3 m s^{-1}) than at Ajdovščina (0–0.2 m s^{-1}). An analysis of wind direction indicated that stable conditions at Ljubljana are associated with drainage flow into the basin along the Sava River valley, whereas at Ajdovščina there is light katabatic flow from the flanks of the Trnovski gozd barrier on stable nights.

The demonstrated ability of the radon-based technique to consistently distinguish between subtle changes in atmospheric mixing state at the two observation sites with strongly contrasting topographic settings indicates that it will be a powerful tool for characterising air quality in these complex environments. Specifically, the diurnal cycles of local radon contributions indicated that the capability of the atmosphere to dilute primary pollutants with surface sources (for which radon is a good proxy) is considerably less in the basin environment. The next stage of this research will involve expanding the radon-based atmospheric stability analysis to all seasons, which will rely heavily upon a separate radon-based technique being developed in parallel (Kikaj et al., 2019) to reliably identify persistent temperature inversion events in the Ljubljana Basin region in winter and autumn. The combined results of these studies promise to substantially improve understanding of air quality in Slovenia year round, and the techniques should be more broadly applicable to regions with similarly complex topography.

Acknowledgements

The authors acknowledge the financial support from the Slovenian Research Agency (research core funding No. P1-0143), Slovenian–Hungarian Scientific and Technological Cooperation (BI-HU/17-18-008) and from the Public Scholarship, Development, Disability and Maintenance Fund of the Republic of Slovenia (Contract no. 11011- 44/2016-18). The authors also gratefully acknowledge the Environment Agency of the Republic of Slovenia for the permission provided and the assistance by installing the weather instrument shelter for radon monitoring on their land and for providing the meteorological data.

Appendix A. Supplementary data

Supplementary data to this article can be found online at https://doi.org/10.1016/j.jenvrad.2019.03.010.

References

ARSO, Slovenian Environment Agency (Slovenian: Agencija Republike Slovenije za okolje), 2017. Climate Characteristics of Ljubljana - Wind Rose for the City of Ljubljana.

Allegrini, I., Febo, A., Pasini, A., Schiarini, S., 1994. Monitoring of the nocturnal mixed layer by means of particulate radon progeny measurement. J. Geophys. Res. 99, 18765–18777.

Bajić, A., 1989. Severe bora on the northern Adriatic Part I: statistical analysis. Hrvat. Meteorološki Časopis 6, 1–9.

Bajić, A., 1988. The strongest bora event during ALPEX-SOP. Hrvat. Meteorološki Časopis 23, 1–12.

Balkanski, Y.J., Jacob, D.J., Gardner, G.M., Graustein, W.C., Turekian, K.K., 1993. Transport and residence times of tropospheric aerosols inferred from a global three-dimensional simulation of ^{210}Pb. J. Geophys. Res. Atmos. 98, 20573–20586.

Belušić, D., Grisogono, B., Klaić, Z.B., 2007. Atmospheric origin of the devastating coupled air-sea event in the east Adriatic. J. Geophys. Res. Atmos. 112, 1–14. https://doi.org/10.1029/2006JD008204.

Bowen, B., 1994. Long-term tracer at Los Alamos, New Mexico. Part II: evaluation and comparison of several methods to determine dispersion coefficients. J. Appl. Meteorol. 33, 1236–1254.

Butterweck, G., Reineking, A., Kesten, J., Porstendörfer, J., 1994. The use of the natural radioactive noble gases radon and thoron as tracers for the study of turbulent exchange in the atmospheric boundary layer—case study in and above a wheat field. Atmos. Environ. 28, 1963–1969.

Chambers, S., Williams, A.G., Zahorowski, W., Griffiths, A., Crawford, J., 2011. Separating remote fetch and local mixing influences on vertical radon measurements in the lower atmosphere. Tellus Ser. B Chem. Phys. Meteorol. 63, 843–859. https://doi.org/10.1111/j.1600-0889.2011.00565.x.

Chambers, S.D., Beringer, J., Randerson, J.T., Chapin, I.S., 2005. Fire effects on net radiation and energy partitioning: contrasting responses of tundra and boreal forest ecosystems. J. Geophys. Res. D Atmos. 110, 1–9. https://doi.org/10.1029/2004JD005299.

Chambers, S.D., Galeriu, D., Williams, A.G., Melintescu, A., Griffiths, A.D., Crawford, J., Dyer, L., Duma, M., Zorila, B., 2016a. Atmospheric stability effects on potential radiological releases at a nuclear research facility in Romania: characterising the atmospheric mixing state. J. Environ. Radioact. 154, 68–82. https://doi.org/10.1016/j.jenvrad.2016.01.010.

Chambers, S.D., Hong, S.B., Williams, A.G., Crawford, J., Griffiths, A.D., Park, S.J., 2014. Characterising terrestrial influences on Antarctic air masses using Radon-222 measurements at King George Island. Atmos. Chem. Phys. 14, 9903–9916. https://doi.org/10.5194/acp-14-9903-2014.

Chambers, S.D., Podstawczyńska, A., Pawlak, W., Fortuniak, K., Williams, A., Griffiths, A., 2018. Characterizing the state of the urban surface layer using Radon-222. J. Geophys. Res. Atmos. 124, 770–788.

Chambers, S.D., Podstawczyńska, A., Williams, A.G., Pawlak, W., 2016b. Characterising the influence of atmospheric mixing state on urban heat island intensity using Radon-222. Atmos. Environ. 147, 355–368. https://doi.org/10.1016/j.atmosenv.2016.10.026.

Chambers, S.D., Williams, A.G., Crawford, J., Griffiths, A.D., 2015. On the use of radon for quantifying the effects of atmospheric stability on urban emissions. Atmos. Chem. Phys. 15, 1175–1190. https://doi.org/10.5194/acp-15-1175-2015.

Cohen, L.D., Barr, S., Krablin, R., Newstein, H., 1972. Steady-state vertical turbulent diffusion of radon. J. Geophys. Res. 77, 2654–2668.

Crawford, J., Chambers, S., Cohen, D., Williams, A., Griffiths, A., Stelcer, E., 2016. Assessing the impact of atmospheric stability on locally and remotely sourced aerosols at Richmond, Australia, using Radon-222. Atmos. Environ. 127, 107–117. https://doi.org/10.1016/j.atmosenv.2015.12.034.

Desideri, D., Roselli, C., Feduzi, L., Assunta Meli, M., 2006. Monitoring the atmospheric stability by using radon concentration measurements: a study in a Central Italy site. J. Radioanal. Nucl. Chem. 270, 523–530. https://doi.org/10.1007/s10967-006-0458-1.

Dueñas, C., Pérez, M., Fernández, M.C., Carretero, J., 1996. Radon concentrations in surface air and vertical atmospheric stability of the lower atmosphere. J. Environ. Radioact. 31, 87–102. https://doi.org/10.1016/0265-931X(95)00058-I.

Elster, J., Geitel, H., 1901. Über eine fernere Analogie in dem elektrischen Verhalten der natürlichen und der durch Becquerelstrahlen abnorm leitend gemachten Luft. Phys. Z. 2, 590–593.

Foken, T., 2006. 50 years of the Monin-Obukhov similarity theory. Boundary-Layer Meteorol. 119, 431–447. https://doi.org/10.1007/s10546-006-9048-6.

Fontan, J., Guedalia, D., Druilhet, A., Lopez, A., 1979. Une methode de mesure de la stabilite verticale de l'atmosphere pres du sol. Boundary-Layer Meteorol. 17, 3–14.

Fortuniak, K., Kłysik, K., Wibig, J., 2006. Urban–rural contrasts of meteorological parameters in Łódź. Theor. Appl. Climatol. 84, 91–101. https://doi.org/10.1007/s00704-005-0147-y.

Galmarini, S., 2006. One year of ^{222}Rn concentration in the atmospheric surface layer. Atmos. Chem. Phys. 6, 2865–2886. https://doi.org/10.5194/acp-6-2865-2006.

Gifford, F.A., 1976. Turbulent diffusion-typing schemes: a review. Nucl. Saf 17, 68–86.

Griffiths, A.D., Chambers, S.D., Williams, A.G., Werczynski, S., 2016. Increasing the accuracy and temporal resolution of two-filter radon-222 measurements by correcting for the instrument response. Atmos. Meas. Tech. 9, 2689–2707. https://doi.org/10.5194/amt-9-2689-2016.

Griffiths, A.D., Parkes, S.D., Chambers, S.D., McCabe, M.F., Williams, A.G., 2013. Improved mixing height monitoring through a combination of lidar and radon measurements. Atmos. Meas. Tech. 6, 207–218. https://doi.org/10.5194/amt-6-207-2013.

Grisogono, B., Belušić, D., 2009. A review of recent advances in understanding the meso- and microscale properties of the severe Bora wind. Tellus Ser. A Dyn. Meteorol. Oceanogr. 61 A, 1–16. https://doi.org/10.1111/j.1600-0870.2008.00369.x.

Hoch, S.W., Whiteman, C.D., 2010. Topographic effects on the surface radiation balance in and around Arizona's Meteor crater. J. Appl. Meteorol. Climatol. 49, 1114–1128. https://doi.org/10.1175/2010JAMC2353.1.

Ivančič, M., Vončina, R., 2014. Determinating the influence of different PM_{10} sources on air quality in Ljubljana basin with CALPUFF dispersion model. Int. J. Environ. Pollut. 54, 251. https://doi.org/10.1504/IJEP.2014.065126.

Jacob, D.J., Prather, M.J., 1990. Radon-222 as a test of convective transport in a general circulation model. Tellus B 42, 118–134. https://doi.org/10.1034/j.1600-0889.1990.00012.x.

Jacob, J., Prather, J., Rasch, J., Beagley, R., Bergmann, J., Blackshear, W.T., Chiba, M., Chipperfield, M.P., Dignon, E., Kasibhatla, S., Kritz, M.A., Penner, E., Ramonet, M.,

Reeves, C.E., Stockwell, Z., Velthoven, F.J. Van, Verver, G., Yang, H., 1997. Evaluation and intercomparison of global atmospheric transport models using ^{222}Rn and other short-lived tracer. J. Geophys. Res. 102, 5953–5970.
Jacobi, W., André, K., 1963. The vertical distribution of radon 222, radon 220 and their decay products in the atmosphere. J. Geophys. Res. 68, 3799–3814. https://doi.org/10.1029/JZ068i013p03799.
Kahl, J.D.W., Chapman, H.L., 2018. Atmospheric stability characterization using the Pasquill method: a critical evaluation. Atmos. Environ. 187, 196–209. https://doi.org/10.1016/j.atmosenv.2018.05.058.
Kardos, R., Gregorič, A., Jónás, J., Vaupotič, J., Kovács, T., Ishimori, Y., 2015. Dependence of radon emanation of soil on lithology. J. Radioanal. Nucl. Chem. 304, 1321–1327.
Karstens, U., Schwingshackl, C., Schmithüsen, D., Levin, I., 2015. A process-based ^{222}radon flux map for Europe and its comparison to long-term observations. Atmos. Chem. Phys. 15, 12845–12865. https://doi.org/10.5194/acp-15-12845-2015.
Kikaj, D., Vaupotič, J., 2017. Parameters influencing deviation of radon concentration from its typical diurnal pattern in the winter and summer seasons. Geol. Maced. 31, 157–170.
Kikaj, D., Vaupotič, J., Chambers, S.D., 2019. Identifying 'persistent temperature inversion' events in a Subalpine Basin using Radon-222. Atmos. Meas. Tech. Discuss. 1–32. https://doi.org/10.5194/amt-2018-405.
Largeron, Y., Staquet, C., 2016. Persistent inversion dynamics and wintertime PM_{10} air pollution in Alpine valleys. Atmos. Environ. 135, 92–108. https://doi.org/10.1016/j.atmosenv.2016.03.045.
Li, Y., Chang, J.S., 1996. A three-dimensional global episodic tracer transport model: 1. Evaluation of its transport processes by radon 222 simulations. J. Geophys. Res. Atmos. 101, 25931–25947.
Liu, H., Wanli, M., Junlong, Q., Juzhen, C., Xianman, Y., Jiahui, L., Xueyuan, W., 2015. Effect of urbanization on the urban meteorology and air pollution in Hangzhou. J. Meteorol. Res. 29, 950–965. https://doi.org/10.1007/s13351-015-5013-y.1.
Marcazzan, G.M., Vaccaro, S., Valli, G., Vecchi, R., 2001. Characterisation of PM_{10} and $PM_{2.5}$ particulate matter in the ambient air of Milan (Italy). Atmos. Environ. 35, 4639–4650. https://doi.org/10.1016/S1352-2310(01)00124-8.
Mazur, J., Kozak, K., 2014. Complementary system for long term measurements of radon exhalation rate from soil. Rev. Sci. Instrum. 85. https://doi.org/10.1063/1.4865156.
Melintescu, A., Chambers, S.D., Crawford, J., Williams, A.G., Zorila, B., Galeriu, D., 2018. Radon-222 related influence on ambient gamma dose. J. Environ. Radioact 189, 67–78.
Minato, S., 1983. Estimate of radon-222 concentrations in rainclouds from radioactivity of rainwater observed at ground level. J. Radioanal. Chem. 78, 199–207.
Mole, M., Wang, L., Stanič, S., Bergant, K., Eichinger, W.E., Ocaña, F., Strajnar, B., Škraba, P., Vučković, M., Willis, W.B., 2017. Lidar measurements of Bora wind effects on aerosol loading. J. Quant. Spectrosc. Radiat. Transf. 188, 39–45. https://doi.org/10.1016/j.jqsrt.2016.05.020.
Moritz, S., 2017. imputeTS: Time Series Missing Value Imputation in R. R Package. version 2.5.
Moses, H., Stehney, A.F., Lucas Jr., H.F., 1960. The effect of meteorological variables upon the vertical and temporal distributions of atmospheric radon. J. Geophys. Res. 65, 1223–1238.
Pal, S., Lopez, M., Schmidt, M., Ramonet, M., Gibert, F., Ciais, P., 2015. Investigation of the atmospheric boundary layer depth variability and its impact on the ^{222}Rn concentration at a rural site in France. J. Geophys. Res. Atmos. 120, 623–643. https://doi.org/10.1002/2014JD022322.
Pal, S., Xueref-Remy, I., Ammoura, L., Chazette, P., Gibert, F., Royer, P., Dieudonné, E., Dupont, J.C., Haeffelin, M., Lac, C., Lopez, M., Morille, Y., Ravetta, F., 2012. Spatio-temporal variability of the atmospheric boundary layer depth over the Paris agglomeration: an assessment of the impact of the urban heat island intensity. Atmos. Environ. 63, 261–275. https://doi.org/10.1016/j.atmosenv.2012.09.046.
Pasquill, F., 1961. The estimation of the dispersion of windborne material. Meteorol. Mag. 90, 33–49.
Pasquill, F., Smith, F.B., 1983. Atmospheric Diffusion: Study of the Dispersion of Windborne Material from Industrial and Other Sources, third ed. Ellis Horwood Ltd., Chichester.
Pearson, J.E., Jones, G.E., 1965. Emanation of radon 222 from soils and its use as a tracer. J. Geophys. Res. 70, 5279–5290.
Perrino, C., Pietrodangelo, A., Febo, A., 2001. An atmospheric stability index based on radon progeny measurements for the evaluation of primary urban pollution. Atmos. Environ. 35, 5235–5244.
Petkovšek, Z., 1985. The termination of air pollution periods in valley basins. Z. Meteorol. 35, 370–372.
Podstawczyńska, A., 2016. Differences of near-ground atmospheric Rn-222 concentration between urban and rural area with reference to microclimate diversity. Atmos. Environ. 126, 225–234. https://doi.org/10.1016/j.atmosenv.2015.11.037.
Podstawczyńska, A., Chambers, S.D., 2018. Radon-based technique for the analysis of atmospheric stability – a case study from Central Poland. Nukleonika 63, 47–54. https://doi.org/10.2478/nuka-2018-0006.
R Development Core Team, 2008. R: A Language and Environment for Statistical Computing. R Found. Stat. Comput. Vienna Austria 03-900051-07-0 {ISBN}. https://doi.org/10.1038/sj.hdy.6800737.
Rakovec, J., Merše, J., Jernej, S., Paradiž, B., 2002. Turbulent dissipation of the cold-air pool in a basin: comparison of observed and simulated development. Meteorol. Atmos. Phys. 79, 195–213. https://doi.org/10.1007/s007030200003.
Satterly, J., 1910. I. On the amount of radium emanation in the lower regions of the atmosphere and its variation with the weather. London, Edinburgh, Dublin Philos. Mag. J. Sci. 20, 1–36. https://doi.org/10.1080/14786441008636877.
Schery, S.D., Huang, S., 2004. An estimate of the global distribution of radon emissions from the ocean. Geophys. Res. Lett. 31, L19104. https://doi.org/10.1029/2004GL021051.
Scire, J.S., Strimaitis, D.G., Yamartino, R.J., 2000. A User's Guide for the CALPUFF Dispersion Model.
Sesana, L., Caprioli, E., Marcazzan, G.M., 2003. Long period study of outdoor radon concentration in Milan and correlation between its temporal variations and dispersion properties of atmosphere. J. Environ. Radioact. 65, 147–160. https://doi.org/10.1016/S0265-931X(02)00093-0.
Sesana, L., Ottobrini, B., Polla, G., Facchini, U., 2006. ^{222}Rn as indicator of atmospheric turbulence: measurements at Lake Maggiore and on the pre-Alps. J. Environ. Radioact. 86, 271–288. https://doi.org/10.1016/j.jenvrad.2005.09.005.
Smith, R., 1985. On severe downslope winds. J. Atmos. Sci. 42, 2597–2603.
Stull, R., 1988. An Introduction to Boundary Layer Meteorology. Kluwer Academic Publishers, Netherlands.
Szegvary, T., Conen, F., Ciais, P., 2009. European ^{222}Rn inventory for applied atmospheric studies. Atmos. Environ. 43, 1536–1539. https://doi.org/10.1016/j.atmosenv.2008.11.025.
Turekian, K.K., Nozaki, Y., Benninger, L.K., 1977. Geochemistry of atmospheric radon and radon products. Annu. Rev. Earth Planet Sci. 5, 227–255.
Turner, B., 1964. A diffusion model for an urban area. J. Appl. Meteorol. 3, 83–91.
Vrhovec, T., 1990. Analysis of mesometeorological temperature fields. Meteorol. Atmos. Phys. 43, 235–240.
Wang, F., Chambers, S.D., Zhang, Z., Williams, A.G., Deng, X., Zhang, H., Lonati, G., Crawford, J., Griffiths, A.D., Ianniello, A., Allegrini, I., 2016. Quantifying stability influences on air pollution in Lanzhou, China, using a radon-based "stability monitor": seasonality and extreme events. Atmos. Environ. 145, 376–391. https://doi.org/10.1016/j.atmosenv.2016.11.003.
Wickham, H., 2009. Ggplot: Using the Grammar of Graphics with R.
Williams, A.G., Chambers, S., Griffiths, A., 2013. Bulk mixing and decoupling of the nocturnal stable boundary layer characterized using a ubiquitous natural tracer. Boundary-Layer Meteorol. 149, 381–402. https://doi.org/10.1007/s10546-013-9849-3.
Williams, A.G., Chambers, S.D., Conen, F., Reimann, S., Hill, M., Griffiths, A.D., Crawford, J., 2016. Radon as a tracer of atmospheric influences on traffic-related air pollution in a small inland city. Tellus Ser. B Chem. Phys. Meteorol. 68, 1–21. https://doi.org/10.3402/tellusb.v68.30967.
Yoshino, M., 1976. Local Wind Bora. University of Tokyo Press, Tokyo.
Zahorowski, W., Chambers, S., Wang, T., Kang, C.H., Uno, I., Poon, S., Oh, S.N., Werczynski, S., Kim, J., Henderson-Sellers, A., 2005. Radon-222 in boundary layer and free tropospheric continental outflow events at three ACE-Asia sites. Tellus Ser. B Chem. Phys. Meteorol. 57, 124–140. https://doi.org/10.1111/j.1600-0889.2005.00133.x.
Zahorowski, W., Chambers, S.D., Henderson-Sellers, A., 2004. Ground based radon-222 observations and their application to atmospheric studies. J. Environ. Radioact. 76, 3–33. https://doi.org/10.1016/j.jenvrad.2004.03.033.
Zahorowski, W., Griffiths, A.D., Chambers, S.D., Williams, A.G., Law, R.M., Crawford, J., Werczynski, S., 2013. Constraining annual and seasonal radon-222 flux density from the Southern Ocean using radon-222 concentrations in the boundary layer at Cape Grim. Tellus Ser. B Chem. Phys. Meteorol. 65. https://doi.org/10.3402/tellusb.v65i0.19622.

4.3 Combining Diurnal and Synoptic Timescale Radon-based Mixing Classification Methods and Testing Their Applicability to Urban Pollution Studies

The main aims of this study were (i) to combine, for the first time, the existing diurnal radon-based atmospheric mixing classification method with a newly-developed radon-based tool for identification of synoptic timescale PTI events, in order to characterize urban pollution (CO, BC, NO_2, SO_2, PM_{10}, and O_3) variability in the city of Ljubljana; and (ii) to use the existing radon-based stability classification method to better constrain remote pollution transport into the Ljubljana Basin region.

Combination of the two radon-based methods resulted in five diurnal and one synoptic (PTI) mixing classes being defined. Furthermore, "strong" and "weak" categories of the PTI class were defined based on diurnal radon variability within that class.

In the first of two scientific articles addressing these aims, entitled "Characterizing atmospheric controls on winter urban pollution in a topographic basin setting using Radon-222", diurnal and synoptic timescale influences on the atmospheric mixing state were characterized for two consecutive winter periods of contrasting permanent snow cover. Key differences in urban pollutant concentrations observed between the two winters were attributed to a combination of changes in the atmospheric mixing state and changes in source strengths. The second scientific article, entitled "Radon-222: a year-round indicator of thermodynamic structure and air quality within a topographic basin" demonstrated a strong seasonality in primary pollutant (BC, NO_2, SO_2, CO, and PM_{10}) concentrations within the six radon-based mixing classes that, in this case, were characterized year-round (although no PTI events occurred in summer). For the first time in this region, a clear distinction was made between individual high-pollution events associated with passing high-pressure systems (on class #5 nights), and persistent high-pollution episodes associated with the lingering presence of the "Siberian High". In both cases the meteorological conditions associated with these episodes were characterized and compared over the whole diurnal cycle.

In the second article above we demonstrated (for the first time) the ability of the radon-based approach to group similar atmospheric conditions (class types) throughout the deeper atmosphere (i.e. beyond the SNBL where the technique was developed), through an analysis of winter radio-sonde profiles around dawn. Furthermore, as an example of additional validation of the combined diurnal and synoptic radon-based mixing methods in all seasons (Dec 2016–Nov 2017), composite vertical sonde profiles of air temperature and wind speed are presented in **Appendix B**. The sonde profiles, composited by radon-derived mixing class, clearly demonstrate that all six radon-derived mixing classes actually apply to at least the lower several kilometres of the troposphere. In the case of the PTI events, these composite sonde profiles help to clearly explain the regional meteorological conditions contributing to the highest pollution events. While near-surface radon observations are not predictive of the vertical atmospheric structure and cannot replace the detailed information provided by radio-sondes or laser/acoustic profilers, radon-based class typing is capable of grouping "similar" atmospheric conditions (i.e. with reduced variability) throughout the lower troposphere.

The combined diurnal and synoptic timescale radon-based mixing classification techniques described here are not specific to the Ljubljana Basin region. They are universally applicable to non-coastal urban centers in Europe (e.g. Poland: Chambers & Podstawczyńska, (2019)), as well as to other continental mid- to high-latitude regions (e.g. central North America). Combined radon-based atmospheric classes provide, for the first

time, a consistent and representative method by which to account for both diurnal and synoptic changes in the atmospheric mixing state in complex terrain.

In these two studies, the candidate developed the research question, performed data collection, curation and formal analysis. She performed all visualization of data, concepts, interpreted the results and wrote the complete original draft of the manuscript.

Atmospheric Research 237 (2020) 104838

Contents lists available at ScienceDirect

Atmospheric Research

journal homepage: www.elsevier.com/locate/atmosres

Characterizing atmospheric controls on winter urban pollution in a topographic basin setting using Radon-222

Dafina Kikaj[a,b], Scott D. Chambers[c], Matjaž Kobal[d], Jagoda Crawford[c], Janja Vaupotič[b,*]

[a] Jožef Stefan International Postgraduate School, Jamova cesta 39, 1000 Ljubljana, Slovenia
[b] Jožef Stefan Institute, Department of Environmental Sciences, Jamova cesta 39, 1000 Ljubljana, Slovenia
[c] ANSTO, Environmental Research, Locked Bag 2001, Kirrawee DC, NSW 2232, Australia
[d] Aerosol d.o.o. Kamniška ulica 39A, 1000 Ljubljana, Slovenia

ARTICLE INFO

Keywords:
Radon
Stability
Persistent temperature inversion
Complex topography
Urban pollution

ABSTRACT

Using hourly meteorological, air quality and radon observations over two winters (2016–2017 and 2017–2018), we combine diurnal and synoptic timescale radon-based mixing classification techniques, for the first time, to better understand air quality variability in the sub-Alpine city of Ljubljana. Of the two winters, only the second experienced significant snow cover (> 1 month). A total of six mixing classes were defined for each winter: 5 diurnal and 1 synoptic ("persistent temperature inversion", PTI); the latter being internally categorised as "strong" or "weak". Diurnal and synoptic changes in mixing state played an important role in air quality variability in both winters. Little diurnal accumulation of local pollutants (CO, NO_2, PM_{10} and BC) was observed for wind speeds ≥ 1.5 m s^{-1} (mixing classes #1 to #3). Under these windy conditions significant remote contributions to SO_2 and O_3 concentrations in Ljubljana were observed, primarily from the Po Valley region. The most stable conditions (class #5 and PTI days), characterized by nocturnal wind speeds ≤ 0.5 m s^{-1} or rates of 2 m air temperature change ≥ 1.5 °C h^{-1}, were associated with the worst air quality conditions. Only under class #5 and PTI conditions did daily-mean PM_{10} concentrations exceed both EU and WHO guideline values. The absence of snow cover in the first winter resulted in stronger thermodynamic stability and higher pollution concentrations. Other contributing factors included a 28% larger traffic source near the monitoring site and a 17% greater consumption of heating fuel that winter in Ljubljana.

1. Introduction

The rapid growth of urbanization, vehicle numbers, energy consumption, and industrialization throughout Europe has degraded urban air quality (Karanasiou and Mihalopoulos, 2013; EEA, 2018). Most pollutants are emitted directly into the atmospheric boundary layer (ABL) from surface-based sources, or formed there as a result of precursor reactions. Since commuters and urban buildings primarily inhabit the lower ~10% of the ABL, air pollution has become a major cause of diseases and premature deaths (Pope and Dockery, 2006; Goudie, 2014). Consequently, the World Health Organization (WHO) and European Union (EU) have recommended limits for "criteria pollutant" concentrations based on short-term (≤24-h) and long-term (annual) exposure periods. Despite recent improvements in some aspects of air quality (e.g. sulphur dioxide, SO_2, and carbon monoxide, CO, levels; EEA, 2016, 2017, 2018), non-compliance with air quality guidelines values for some species is still reported in many parts of Europe, especially in the Mediterranean Basin Region (MBR). In particular, target limits for nitrogen dioxide (NO_2), particulate matter (PM) and tropospheric ozone (O_3) are frequently exceeded in the MBR (EEA, 2017, 2018). However, the levels of some pollutants (e.g. black carbon; BC) are not yet regulated by the WHO or EU, despite exposure to even small concentrations of BC having been linked with cardiorespiratory diseases (Janssen et al., 2011; Dons et al., 2012).

Since urban pollution scales with population (Ayers et al., 1982), and the size and population of urban regions is continually increasing, it will be important to continually review target limits and assess the efficacy of mitigation measures. The ability to do so effectively will rely upon understanding controls on pollutant concentration variability near the surface in the "zone of habitation". In this regard, it is important to recognise that pollution concentrations vary according to both "controllable" and "uncontrollable" influences. The ability to distinguish between these influences will be crucial to more accurately assessing the efficacy of mitigation measures.

* Corresponding author.
E-mail address: janja.vaupotic@ijs.si (J. Vaupotič).

https://doi.org/10.1016/j.atmosres.2019.104838
Received 15 August 2019; Received in revised form 22 December 2019; Accepted 26 December 2019
Available online 27 December 2019
0169-8095/ © 2020 The Authors. Published by Elsevier B.V. This is an open access article under the CC BY-NC-ND license (http://creativecommons.org/licenses/BY-NC-ND/4.0/).

"Controllable" influences, the target of mitigation measures, relate to matters directly affecting pollution source strengths and their spatial and temporal variability. "Uncontrollable" influences, on the other hand, include: meteorology, geographic setting and topographic effects, and cross-boundary (remote) pollution transport. Diurnal timescale changes in the ABL mixing state ("stability"), associated with daytime convection and the formation of nocturnal inversion layers, are known to influence pollution concentrations (Chambers et al., 2015; Wang et al., 2016; Williams et al., 2016). Furthermore, in regions of complex topography such as basin or steep valley environments, longer timescale (e.g. synoptic) changes in the ABL mixing state can also occur. The most severe examples are persistent temperature inversions (PTIs) typically occur in winter months, when days are short and persistent snow-cover limits the extent of daytime convection, under regional subsidence (anticyclonic) conditions, which further retard dispersion and lead to pollution events of potentially life-threatening duration and intensity (Wang et al., 2019; Rakovec et al., 2002, 2015; Silcox et al., 2012; Whiteman et al., 2014; Largeron and Staquet, 2016; Baasandorj et al., 2017; Kikaj et al., 2019a). In Europe, where political boundaries can be very close, another form of synoptic-timescale variability of urban pollution arises through cross-boundary advection events from regions whose land-use practices and emissions policies are beyond the influence of local government mitigation efforts (Kallos et al., 2006; Poberžnik and Štrumbelj, 2016; Chambers et al., 2016a; Chambers et al., 2017; He et al., 2018).

It has been well-established that near-surface atmospheric radon (^{222}Rn or radon-progeny) measurements are a powerful indicator of diurnal mixing and synoptic-timescale transport in the ABL, largely attributable to radon's ubiquitous nature and unique combination of physical characteristics (Allegrini et al., 1994; Perrino et al., 2001; Sesana et al., 2003; Zahorowski et al., 2004; Williams et al., 2013; Kikaj et al., 2019a). Furthermore, in many situations radon-based atmospheric stability classification provides a simpler, more consistent and representative indication of the nocturnal or daytime mean atmospheric mixing state than conventional meteorological approaches (Bowen, 1994; Chambers et al., 2015, 2019a; Crawford et al., 2016; Kahl and Chapman, 2018).

Vertical radon gradients provide the most direct evidence of the integrated effects of diurnal timescale near-surface mixing processes since they automatically account for air mass fetch effects (Moses et al., 1960; Cohen et al., 1972; Porstendörfer et al., 1991; Chambers et al., 2011; Williams et al., 2011). Such measurements, however, have very stringent requirements on instrument performance. Single-height near-surface radon measurements, on the other hand, can be used to provide a good approximation of vertical radon gradient observations for diurnal timescale ABL mixing studies (Chambers et al., 2015; Williams et al., 2016), with more relaxed measurement requirements. In fact, at sites sufficiently removed from coastal influences (i.e. by at least 10–20 km), near-surface radon concentrations are often high enough to be measured with portable, inexpensive instruments (e.g. Chambers et al., 2016b). However, a fundamental assumption of both of these approaches is that changes in the atmospheric mixing state do not contribute to observed radon concentration variability on greater than diurnal timescales. In complex terrain under PTI conditions this assumption is clearly violated, since the basin atmosphere stagnates for several days, allowing radon to accumulate between the surface and synoptic inversion. Under these conditions a shallow stable nocturnal boundary layer may also develop, but it would be weaker than if the overlying persistent synoptic inversion was not present. When this surface inversion breaks down the following morning, it mixes with the already high-radon air beneath the persistent synoptic inversion. In these situations, if "fetch effects" are removed as described by Chambers et al. (2015), the multi-day accumulation of radon under the synoptic inversion is incorrectly removed as a "fetch effect", and the affected measurement days are incorrectly assigned to an intermediate stability class due to weaker surface inversion conditions. In regions prone to the development of PTI conditions it is therefore necessary to identify synoptic timescale PTI conditions separately to the classification of diurnal timescale changes in the atmospheric mixing state. To this end, several approaches for PTI identification have been discussed in the literature (Largeron and Staquet, 2016; Fiorella et al., 2018; Kikaj et al., 2019a).

The primary objective of this study is to combine, for the first time, new (Kikaj et al., 2019a) and existing (e.g. Chambers et al., 2019a, and references therein) radon-based methods of atmospheric stability classification to separately characterize local influences on urban pollution variability in the Ljubljana Basin region on diurnal and synoptic timescales, as well as remote contributions to pollution on synoptic timescales. The statistics based on each of the defined mixing states, with well-defined occurrence frequencies, are used to inform upon potential health effects within the Ljubljana Basin compared with existing WHO and EU guideline values. Robust pollution statistics derived for only the most stable nocturnal mixing conditions, when atmospheric mixing depths are most well-constrained, will provide a benchmark against which future values can be compared to test the efficacy of mitigation measures.

Our study focuses only on winter months (December–February), the time of most frequent pollution exceedance events, due to the typically high rates of energy consumption (Energy Balance of City of Ljubljana, Final Report, City of Ljubljana, 2018) and frequent occurrence of PTIs in the Ljubljana Basin (Petkovšek, 1985, 1992; Rakovec et al., 2002; Kikaj et al., 2019a). Two winter periods of contrasting permanent snow cover are compared. Our results will summarize progress on the following specific tasks: (i) estimating nocturnal and forecasting daytime stability classes for whole 24-h periods across two winters (2016–2017 and 2017–2018) (Section 2.3); (ii) identifying synoptic timescale persistent temperature inversion events to extend the daily stability classifications of (i) from 5 to 6 classes (Section 2.3); (iii) characterizing meteorological conditions across the diurnal cycle for each of the six 24-h atmospheric stability classes (Section 3.1); (iv) characterizing the concentration variability of selected urban pollutants across the diurnal cycle for each of the mixing classes (Section 3.3); (v) constraining remote contributions to pollution variability in the Ljubljana Basin under conditions of strong advection (Section 3.4); and (vi) comparing extremes of pollution variability to WHO and EU guideline values (Section 3.5).

2. Methods

Hourly air quality, meteorology and atmospheric radon concentration (^{222}Rn) were monitored during the winters of 2016–2017 ($W_{16–17}$) and 2017–2018 ($W_{17–18}$) at a sub-Alpine Basin site (SAB; Ljubljana Bežigrad; Fig. 1b), in the central part of Ljubljana city, considered to be an urban background site (Titos et al., 2015; Gjerek et al., 2016; Pucer and Štrumbelj, 2018).

2.1. Site and surrounds

Ljubljana (299 m above sea level, a.s.l.), the capital of Slovenia, is a city of modest size (~280,000 inhabitants) situated in a sub-Alpine basin. The SAB site is surrounded by peaks of the Julian, Kamnik-Savinje, and Dinaric Alps reaching elevations of ~1000 m (Vrhovec, 1990; Hitzenberger et al., 2006). The complexity of the topography surrounding the basin retards synoptic winds, resulting in mean winter wind speeds of 1.3 m s^{-1} with frequent periods of PTI (33% of the year; ARSO, 2017). The PTI periods are characterized by foggy days favouring the build-up of locally-sourced emissions (Kikaj et al., 2019a).

Air quality within Ljubljana Basin is influenced by a combination of local and remote sources, the relative contributions of which depend on the prevailing meteorology. Since there are no large industries in city, the dominant local source of pollution is traffic; as well as domestic heating in the colder months, which has increased by 17% in the last

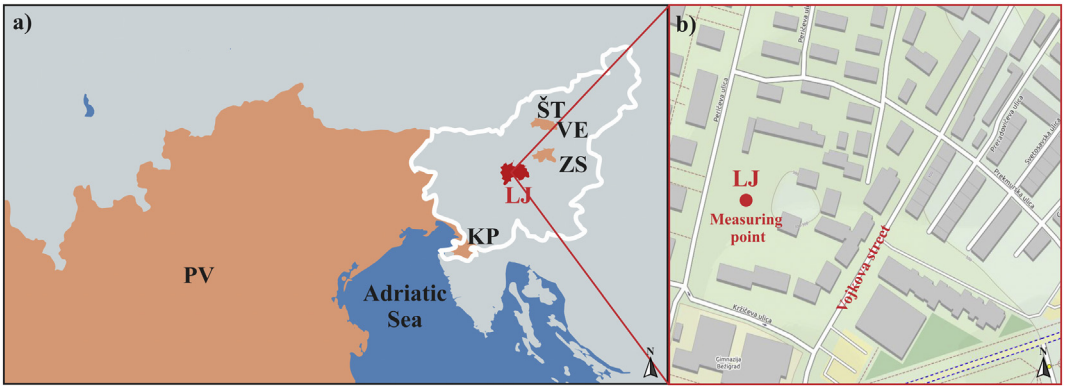


Fig. 1. a) Location of Ljubljana (LJ) within the most industrialized sites around (shaded area, Po Valley-PV, Port of Koper-KP, Zasavje-ZS, Šoštanj-ŠT and Velenje-VE), and b) close-up of Ljubljana city, showing the location of monitoring point (radon, meteorological and air quality data), the nearest street (Vojkova) with modest traffic. *Basemap source: © OpenStreetMap and mapchart.*

2 years (2016–2018) (Energy Balance of City of Ljubljana, Final Report, City of Ljubljana, 2018). For $W_{16–17}$ an overall higher consumption of fuels was noted, mostly due to the lower air temperatures during the heating season (Energy Balance of City of Ljubljana, Final Report, City of Ljubljana, 2018). In contrast to $W_{16–17}$, the next winter ($W_{17–18}$) was characterized by higher air temperatures and 31 days of snow cover. In the city, the Toplarna thermal power plant is located 3 km ESE of the SAB monitoring site. In Ljubljana, road maintenance and detours significantly reduced traffic flow in $W_{17–18}$ compared with $W_{16–17}$, including the number of vehicles passing through Vojkova Street (closest to the measuring point, Fig. 1b). On average, there were 8128 vehicles per day on Vojkova Street in $W_{16–17}$, compared with 6329 in $W_{17–18}$.

In terms of remote pollution sources, due its location the Ljubljana Basin serves as a “crossroads” for polluted air masses originating from: Africa (Kallos et al., 2006); across Europe from the North Atlantic Ocean and across Italy from the Mediterranean Sea (He et al., 2018); the northern Balkan Peninsula, and Eastern Europe (Poberžnik and Štrumbelj, 2016; He et al., 2018). Specifically, the heavily industrialized Po Valley region of Northern Italy (Bigi et al., 2017) and the shipping emissions (Slovenian seaport-Port of the Koper) lies 335 km and 60 km WSW, respectively, of Ljubljana city, while the Zasavje region with coal mines and various kinds of heavy industry (Lafarge Cement plant, Steklarna Hrastnik glass production, IGM Zagaroje building material company) lies 37 km to the NE, and Velenje town with Slovenia's largest lignite-thermal power plant-Šoštanj lies 56 km to the NE (see Fig. 1a) (Gjerek et al., 2016; Gjerek et al., 2017; He et al., 2018; Pucer and Štrumbelj, 2018).

2.2. Air quality and meteorology observations

Air quality parameters including particulate matter of median aerodynamic diameter ≤ 10 μm (PM_{10}), carbon monoxide (CO), nitrogen dioxide (NO_2), sulphur dioxide (SO_2), and ozone (O_3), were provided by the National Meteorological Service at the Slovenian Environmental Agency (ARSO). PM_{10} concentrations were measured with a continuous direct mass measurement for particulate matter utilizing a tapered element oscillating microbalance (TEOM). NO_2 was measured with chemiluminescence, SO_2 with ultraviolet fluorescence, and O_3 with ultraviolet photometry (Gjerek et al., 2017). In addition, black carbon (BC) was measured with a Magee Scientific Aethalometer AE-33 and the data were provided by Aerosol d.o.o., Ljubljana, Slovenia. The total concentration of BC is the result of traffic (BC_{tr}) and biomass burning (BC_{bb}) sources (Sandradewi et al., 2008). The Aethalometer was only installed at the end of November 2017, therefore BC data is not available for $W_{16–17}$.

Hourly observations of meteorological parameters including atmospheric pressure (hPa), global solar radiation (W m^{-2}), air temperature (°C), wind speed (m s^{-1}), wind direction (°), precipitation (mm h^{-1}) were provided by ARSO.

In addition to the measurements outlined above, total cloud cover (%) was obtained from the global data assimilation system (GDAS) model of NOAA/ARL (National Oceanic and Atmospheric Administration/Air Resources Laboratory).

2.3. ^{222}Rn observations and stability analysis

Atmospheric radon measurements were conducted using an AlphaGUARD PQ2000 PRO (Bertin Instruments) operating in diffusion mode with a 1-h integration time (Kikaj et al., 2019a; Kikaj and Vaupotič, 2017). The instrument was mounted 1.5 m a.g.l., within a Stevenson Screen instrument shelter. The AlphaGUARD has a lower limit of detection (LLD) of 2 Bq m^{-3}. Setup in this way it is expected that > 95% of the measured radon represents the isotope ^{222}Rn (Kochowska et al., 2009). Therefore, relative to the AlphaGUARD's measurement uncertainty for typical outdoor ambient radon monitoring conditions, contributions of isotopes ^{220}Rn (thoron) and ^{219}Rn (actinon) to the overall radon signal can be ignored.

Radon-based classification of diurnal timescale changes in stability ($^{222}Rn_{DS}$) have already been described by S. Chambers et al., 2019b; S. D. Chambers et al., 2019a and Kikaj et al. (2019b). Briefly, the approach involves isolating mixing-related (diurnal) changes in near-surface radon concentrations by estimating and removing air mass fetch effects, and then assigning stability thresholds to mean values of radon accumulation within a defined nocturnal window (10h). Corresponding daytime mixing states for each 24-h period are inferred from nocturnal conditions based on an assumption of short-term atmospheric persistence. The number of stability classes that can be distinguished in a statistically robust manner (typically 3 to 5) depends on the size of the available dataset.

Radon-based identification of synoptic timescale changes in the ABL mixing state ($^{222}Rn_{SS}$) (specifically PTI events), was first described by Kikaj et al. (2019a). Briefly, this method involves separating synoptic timescale variability in radon concentration from contributions occurring at other timescales, and then comparing the magnitudes of radon variability occurring at diurnal and synoptic timescales. When synoptic contributions to radon variability exceed the typical magnitude of diurnal ones for more than two consecutive days, a PTI event is considered to have occurred.

A summary of the six mixing classes (5 diurnal and 1 synoptic) for measurements at the SAB site that resulted from our combination of the above two classification techniques ($^{222}Rn_{DS}$ and $^{222}Rn_{SS}$) is presented in Table 1. The table also provides a relative breakdown of the number of events in each mixing class experienced in each winter period. Class #6 (PTI) days of each winter have been further subdivided into “strong”

Table 1
Summary and description of the 24-h radon-based atmospheric mixing classes assigned to SAB measurements for $W_{16–17}$ (December 2016–February 2017) and $W_{17–18}$ (December 2017–February 2018). Occurrence frequency (as a % of each 90-day winter period) of each stability class for both winters is also provided.

24-h mixing class	$W_{16–17}$ (%)	$W_{17–18}$ (%)	Night-time stability conditions	Daytime stability conditions	Expected meteorological conditions
#1	12	7	Mixed fetch or non-stationary	Mixed fetch or non-stationary	Moderate to strong gusty winds, often cloudy associated with passing strong synoptic systems or fronts, precipitation is common.
#2	20	15	Near-neutral	Near-neutral	Moderate to strong winds, often overcast, precipitation is common.
#3	19	19	Weakly stable	Weakly unstable	Light to moderate winds, broken cloud or overcast, possible precipitation.
#4	15	15	Moderately stable	Moderately unstable	Light winds, scattered clouds, precipitation is uncommon.
#5	14	14	Most stable	Most unstable	Calm to light wind, mostly clear sky, typically no precipitation.
#6	20	30	Persistent temperature inversion	Persistent temperature inversion	Calm gradient wind, foggy or low-level clouds, no precipitation.

Table 2
Quantile ranges of the amplitude of diurnal radon variability during persistent temperature inversion (PTI) events for $W_{16–17}$ (December 2016–February 2017) and $W_{17–18}$ (December 2017–February 2018).

Quantile ranges	$W_{16–17}$ (Bq m^{-3})	$W_{17–18}$ (Bq m^{-3})
10th	2	1
50th	7	4
90th	13	9

and “weak” categories based on the amplitude of diurnal radon variability. The selection threshold in this case was chosen to be the median (50th percentile) amplitude of diurnal radon variability during PTI events (Table 2). PTI days under the 50th percentile value are consider to be weak PTI events, and days that exceeded the 50th percentile value are consider to be strong PTI events.

3. Results and discussion

3.1. Meteorological characteristics of radon-based mixing classes

Two of the strongest meteorological indicators of the atmospheric mixing state are wind speed and the near-surface vertical temperature gradient. In the absence of vertical temperature gradient measurements at this site we found that the time rate of change in 2 m air temperature provided a better contrast between atmospheric mixing states than the observed hourly 2 m temperature record.

Class #1 days were characterized by strong and highly variable nocturnal wind speeds (Fig. 2a), consistent with non-stationary synoptic conditions (e.g. frontal passages), as described by Podstawczyńska and Chambers (2018). The non-stationary nature of these days violates important assumptions of the $^{222}Rn_{DS}$ method (Chambers et al., 2019b) and, as a result, complicates the interpretation of urban air quality statistics. Therefore, class #1 events (constituting only 7–12% of observations; Table 1) will be excluded from further discussion in this paper. Class #2 days had the highest nocturnal mean wind speeds (1.5–2 m s^{-1}), whereas the corresponding wind speed for class #5 days was much lower (0.2–0.5 m s^{-1}). The lowest of all nocturnal mean wind speeds were recorded on strong PTI days (consistently ~0.2 m s^{-1}). The wind directions under stable and PTI conditions were consistent with drainage flow (NE) into the basin along the Sava River valley (Kikaj et al., 2019b).

The windy (near-neutral) class #2 days were characterized by the lowest diurnal amplitudes of 2 m air temperature, as evidenced by average time rates of change in temperature of ≤0.2 °C h^{-1} over the diurnal cycle (Fig. 2b). By contrast, on class #5 days average 2 m temperature changes of ~1.5 °C h^{-1} were observed around sunset and sunrise. The highest rates of temperature change (≥2 °C h^{-1}) were observed on strong PTI days. It is of interest to note that nocturnal mean wind speeds of class #4 and #5 days are higher for $W_{16–17}$ than $W_{17–18}$. However, the thermodynamic stability on $W_{16–17}$ nights is stronger, which acts to suppress vertical mixing. This is a good example of the combined influences of these two parameters on the net effects of nocturnal near-surface mixing processes, and the consistency of the results is testimony to the ability of radon observations, alone, to distinguish between these mixing conditions.

Generally, from class #2 to #5 days the intensity of daytime solar radiation increased (Fig. 2c), indicating a reduction in average cloud cover (see also Table 3). It is the reduction in cloud cover, particularly at night, that enables the increased rates of surface cooling/heating after sunset and sunrise exhibited in Fig. 2b. PTI events are known to occur under persistent cold-season anticyclonic conditions (see also Table 3). Usually the anticyclonic regime persists for several days, leading to the development of synoptic subsidence inversion layer (or basin “capping inversion”). The height of this layer is usually coincides with the average elevation of the summits surrounding the basin (Whiteman, 1982; Largeron and Staquet, 2016), and persists for the whole anticyclonic period. The fact that strong PTI events of both winter periods (as selected only by radon) exhibit more intense solar radiation than the weak PTI events, indicates that strong PTI events occur closer to the centre of the anticyclonic systems, where regional scale subsidence is strongest and the air driest; a hypothesis that is supported by the atmospheric pressure observations in Table 3. On the other hand, lower intensity of solar radiation on weak PTI events indicate the low-level cloud cover or/and fog occurrence (VanReken et al., 2017). The snow cover in $W_{17–18}$ was the reason that PTI events of this winter lasted longer than those of $W_{16–17}$ (Tables 1, 20% in $W_{16–17}$ and 30% in $W_{17–18}$). Snow-covered ground is cold across the whole diurnal cycle, and its white colour reflects almost all incoming solar radiation. Combined with shorter winter day lengths, this is one of the main mechanisms leading to the development and long durations of these inversion conditions (Whiteman et al., 2004).

The final piece of evidence regarding the efficacy of the radon-based scheme to objectively and effectively separate atmospheric conditions on diurnal and synoptic timescales is in the progressive reduction in daily mean precipitation observed from class #2 to class #6 days (Fig. 2d). These observations are consistent with the cloud cover and atmospheric pressure summary of Table 3, and give credence to the ‘expected meteorological conditions’ summarized in Table 1.

3.2. Diurnal variability of radon concentrations within each mixing class

Diurnal radon concentrations corresponding to each of the six radon-based atmospheric mixing classes for the two winter seasons ($W_{16–17}$ and $W_{17–18}$) are shown in Fig. 3a. The lowest amplitude of diurnal radon concentrations was observed on the windy class #2 days for both winters. Since radon concentrations serve as a good proxy for the behavior of local primary pollutants with surface-based sources, this is an indication that little diurnal accumulation of urban pollution would be expected at this site for nocturnal wind speeds ≥1.5 m s^{-1}. A similar conclusion was drawn by Sesana et al. (2003, 2006). The amplitude of the diurnal radon cycle (via nocturnal accumulation)

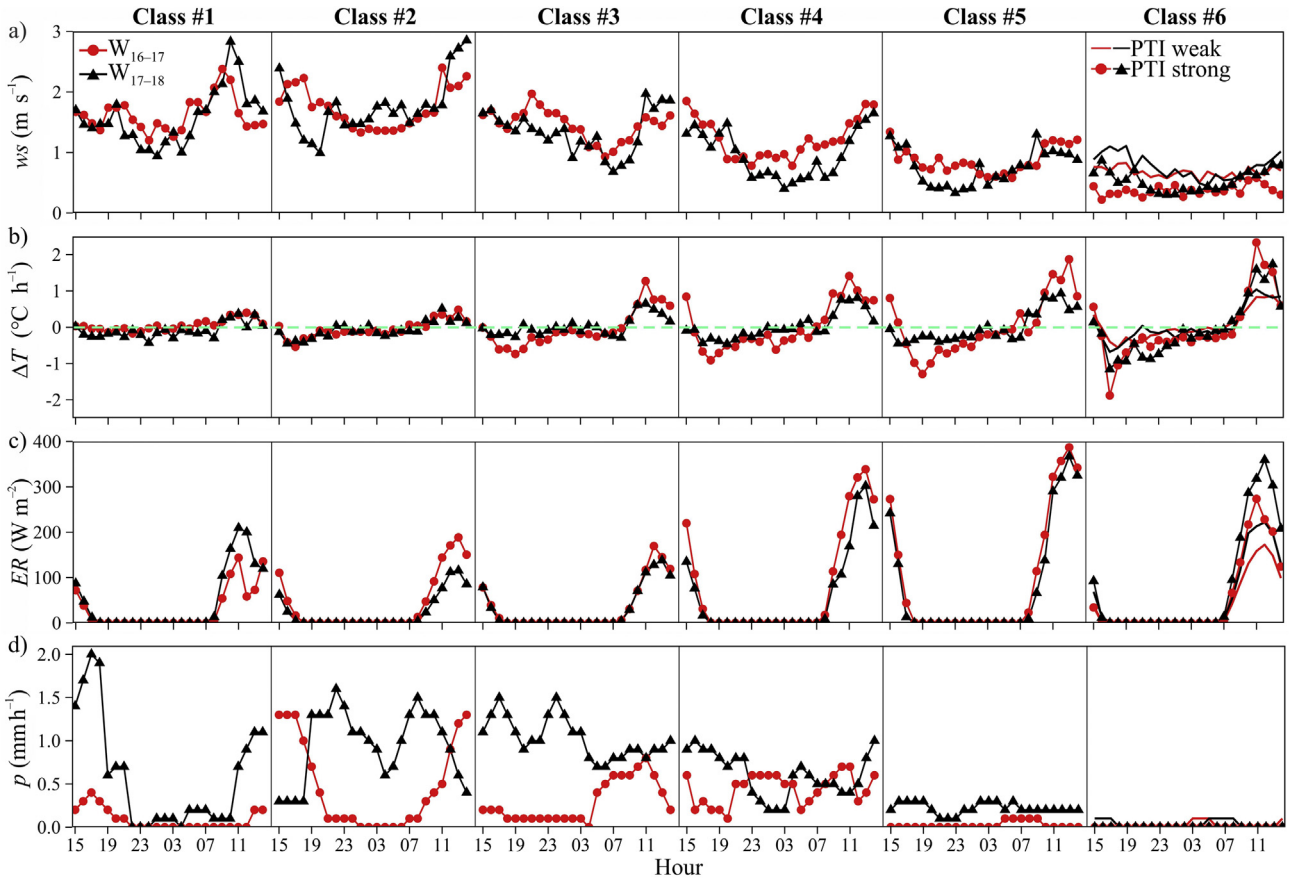


Fig. 2. Diurnal composite plots of hourly mean a) wind speed, b) time rate changes of air temperature, c) solar radiation, and d) precipitation for W_{16-17} (December 2016–February 2017) and W_{17-18} (December 2017–February 2018) and six radon-based atmospheric mixing classes.

Table 3
Daily mean atmospheric pressure and cloud cover (μ ± σ) for W_{16-17} (December 2016–February 2017) and W_{17-18} (December 2017–February 2018) and six radon-based atmospheric mixing classes.

24-h mixing class	W_{16-17}		W_{17-18}	
	P (hPa) μ ± σ	*CC* (%) μ ± σ	*P* (hPa) μ ± σ	*CC* (%) μ ± σ
#1	988 ± 11	51 ± 28	980 ± 5	76 ± 33
#2	985 ± 10	68 ± 35	979 ± 6	87 ± 18
#3	988 ± 8	55 ± 37	976 ± 9	87 ± 22
#4	989 ± 8	45 ± 36	978 ± 7	77 ± 26
#5	992 ± 8	33 ± 31	989 ± 7	44 ± 26
#6 (weak)	991 ± 6	55 ± 40	988 ± 7	57 ± 36
#6 (strong)	996 ± 6	16 ± 15	990 ± 6	33 ± 29

progressively increased from class #2 to class #5 conditions (Fig. 3a). In all mixing classes of W_{16-17}, the amplitude of the diurnal radon cycle was a factor of 2–3 higher than in W_{17-18} (Fig. 2a). This was largely attributable to a slight reduction of radon exhalation rate (Levin et al., 2002; Mazur and Kozak, 2014) in W_{17-18} due to the snow cover, higher ice content of the frozen soils and soil moisture. However, within each winter the radon source function was fairly consistent, enabling the increase of nocturnal radon concentrations from class #2 to #5 conditions to be interpreted as a decrease in mixing volume (formation of a progressively stronger and shallower stable nocturnal boundary layer, SNBL). This increase of radon concentration is consistent with the low wind speeds and increase thermodynamic stability of classes #4 and #5 as indicated in Fig. 2a and b.

Typically, the afternoons of classes #4 and #5 were characterized by low observed radon concentrations due to stronger convective mixing of the atmosphere (Fig. 3b). By contrast, during PTI events (class #6), the synoptic inversion layer and low wind speeds inhibit the vertical and horizontal dispersal of radon across the whole diurnal cycle, resulting in higher afternoon observed radon concentrations (Fig. 3b). Another contributing factor to the higher radon concentrations generally on PTI days is the extended air mass time over land resulting from the near-stagnant synoptic anticyclonic conditions.

As evident from Fig. 3a, the highest diurnal amplitude of local radon contribution was noted during strong PTI events, which cycle indicates the formation of a shallow (strong) SNBL within synoptic inversion layer around sunset that erodes after sunrise. The modest diurnal amplitude of local radon contribution of weak PTI events, on the other hand, indicated the presence of a deeper (weak) SNBL within the synoptic subsidence inversion layer.

3.3. Variability of pollutant concentration with atmospheric mixing class

The diurnal composites of air pollutants (BC_{tr}, NO_2, CO, BC_{bb}, PM_{10}, SO_2 and O_3) classified by the $^{222}Rn_{DS}$ and $^{222}Rn_{SS}$ for both winters, are shown in Fig. 4. The diurnal cycle of pollutants is mainly influenced by their source strengths and the diurnal and synoptic changes of atmospheric mixing. A clear distinction is evident between diurnal behavior of BC_{tr} (specifically related to vehicle emissions) on class #5 days and NO_2, CO, BC_{bb} and PM_{10} (related to either combustion, or a combination of traffic and combustion sources). Only BC_{tr} reflects a pronounced drop in source strength between 01:00–05:00 LT, when there are fewer vehicles on the roads, but some domestic heaters were still active. During classes #2 and #3 when diurnal variability of average temperature rate of change (Fig. 2b) was the lowest (overcast conditions) and the mean nocturnal wind speed was above 1 m s^{-1} (Fig. 2c) almost no accumulation of local (traffic related: BC_{tr}, NO_2, CO and domestic

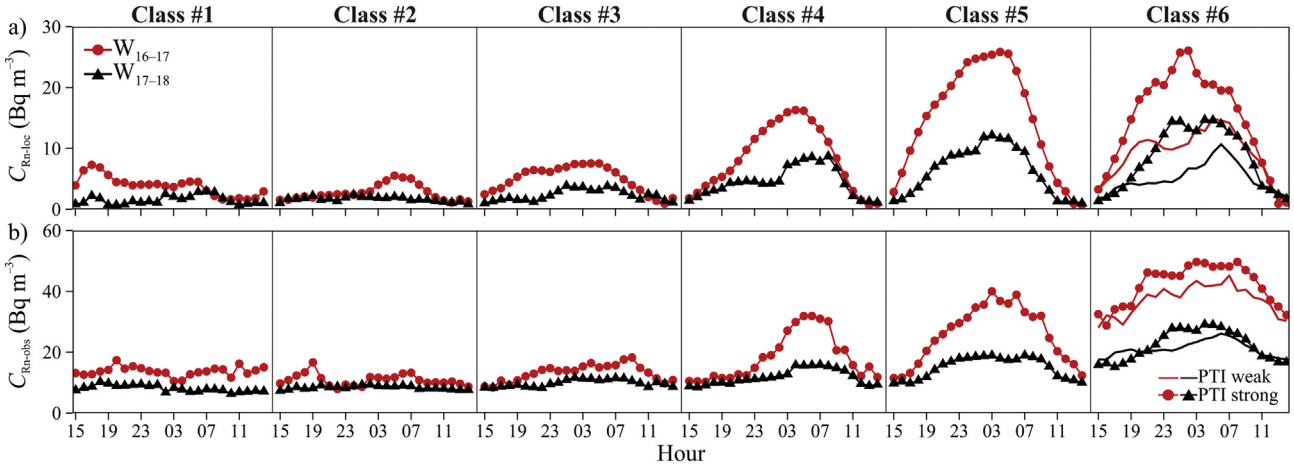


Fig. 3. Diurnal composite plots of hourly mean a) diurnal (local) radon contribution ($C_{Rn\text{-}loc}$), and b) observed radon concentration ($C_{Rn\text{-}obs}$) for W_{16-17} (December 2016–February 2017) and W_{17-18} (December 2017–February 2018) and six radon-based atmospheric mixing classes.

heating: CO, BC_{bb}, PM_{10}) pollution occurred (Fig. 4a–e). On class #4 and #5 days, the diurnal amplitude of locally-sourced pollutants increased (Fig. 4a–e), due to the near-calm wind conditions and strong thermal suppression (using average temperature rate of change as proxy) (Fig. 2c). Under such conditions (classes #4 and #5), BC_{tr} and NO_2 exhibited a bimodal diurnal distribution with one peak in morning (07:00–08:00 LT) and other in afternoon (17:00–19:00 LT) (Fig. 4a and b). These peaks are attributable to an overlap between "rush hour" vehicle emissions and a period of the day when the mixing depth is either low, or transitioning between day/night max/min values. On average, peak BC_{tr} and NO_2 concentrations on class #5 were a factor of 2–3 higher than for class #2 (Fig. 4a and b). The diurnal cycle of CO was more similar to those of combustion-dominated (BC_{bb} and PM_{10}) than traffic related pollutants. The pronounced diurnal peaks of CO, BC_{bb}, PM_{10} occurred between 21:00 LT and 23:00 LT (Fig. 4c–e), and concentrations remained high for few hours. During evening time, the traffic usually decreases, and residential heating increases as the air temperature drops.

Over the composites of classes #4 and #5, there were two periods when local pollutant concentrations reached minimum values: (i) in the morning (03:00–05:00 LT) when light katabatic drainage winds flush away some of the urban pollution, and (ii) in the afternoon (11:00–15:00 LT) when vertical mixing was the highest (deepest ABL) (Fig. 4a–e).

The amplitudes of diurnal cycles of traffic and domestic related pollutants on class #5 days were similar to those on class #6 days (PTI strong and weak). However, in an absolute sense a significant increase of pollutant concentrations was observed under PTI conditions due to the accumulation of pollutants either from upwind sources or under near-stagnant conditions, as evidenced by increased afternoon concentrations. The peak concentration of BC_{tr}, NO_2, CO, BC_{bb} and PM_{10} increased by a factor of 1.2–3 from most stable conditions (class #5) to PTI strong conditions (class #6) (Fig. 4a–e) as a consequence of an increase in source strength and decrease in SNBL under strong PTI conditions.

As evident from Fig. 4a–e, the diurnal cycle amplitudes of local pollutants (BC_{tr}, NO_2, CO, BC_{bb} and PM_{10}) under weak PTI conditions was lower than those observed under strong PTI conditions, when a stronger SNBL formed within the persistent synoptic subsidence inversion. For example, under strong PTI conditions, the diurnal PM_{10} amplitude was 52 μg m^{-3} (50–102 μg m^{-3}) in W_{16-17} and 20 μg m^{-3} (31–51 μg m^{-3}) in W_{17-18}. By comparison, during corresponding weak PTI events, the diurnal PM_{10} amplitude decreased from 27 μg m^{-3} (61–88 μg m^{-3}) in W_{16-17} to 11 μg m^{-3} (32–43 μg m^{-3}) in W_{17-18}. Although the concentrations typically trend downward from night to day, the daytime concentrations of pollutants under PTI conditions (weak and strong) did not reach the low daytime levels characteristic of class #5 conditions. The stagnant anticyclonic conditions inhibited the daytime mixing that usually disperses accumulated nocturnal pollution on class #5 days.

The key differences in local pollutant concentrations observed between the two winters were attributable to a combination of changes in stability and changes in source strength. In W_{16-17} there was a larger traffic source near the monitoring site (Section 2.1), the domestic heating source was also larger (due to lower air temperatures), and the lack of snow cover lead to increased nocturnal atmospheric stability. Combined, these factors lead to higher pollutant concentrations under class #5 and PTI conditions in W_{16-17} compared with W_{17-18}.

Within all mixing classes the diurnal cycles of SO_2 and O_3 were markedly different compared with those of locally-generated primary pollutants (Fig. 4f–g). In the case of SO_2, peak concentrations occurred after the breakdown of the nocturnal inversion, when the ABL was deeper and more well-mixed. By contrast, SO_2 concentrations reduced at night when the SNBL isolates the near-surface observations from more remote influences. Consequently, while local traffic and domestic heating are expected to contribute a little to SO_2 concentrations in Ljubljana, remote SO_2 sources dominated in the winters of this study. As an example, SO_2 concentrations were higher over the whole diurnal cycle under weak PTI conditions in W_{16-17} when wind speeds were slightly higher, than for the strong PTI conditions.

Compared with radon and locally-sourced pollutants, the atmospheric mixing state appeared to have the opposite effect on O_3 concentrations. This is largely due to the fact that O_3 is a highly reactive, photochemically-produced secondary pollutant. When trapped in a shallow inversion layer (e.g. classes #4, #5 and #6) O_3 either reacts with surface roughness elements (dry deposition), or gets titrated by NO emissions. Comparing night-time O_3 levels on strong and weak PTI events, the lowest values were found on strong PTI events due to the stronger SNBL formation, which traps NO. By comparison, on class #2 and #3 nights, with the increase of wind speeds, the highest nocturnal O_3 concentrations were found due to remotely-sourced O_3 being mixed down to the surface from the residual layer or troposphere (Querol et al., 2018). As nocturnal wind speeds decrease from class #3 to #4 conditions, a decrease of O_3 levels in the morning is noticed due to the titration by NO in the morning peak hour traffic. The highest overall O_3 concentrations were observed during the day under class #5 conditions, when skies were clear and solar radiation was most intense.

The combined radon-based atmospheric stability techniques performed in this study helps to separate "uncontrollable" (natural) influences from controllable influences on pollution variability.

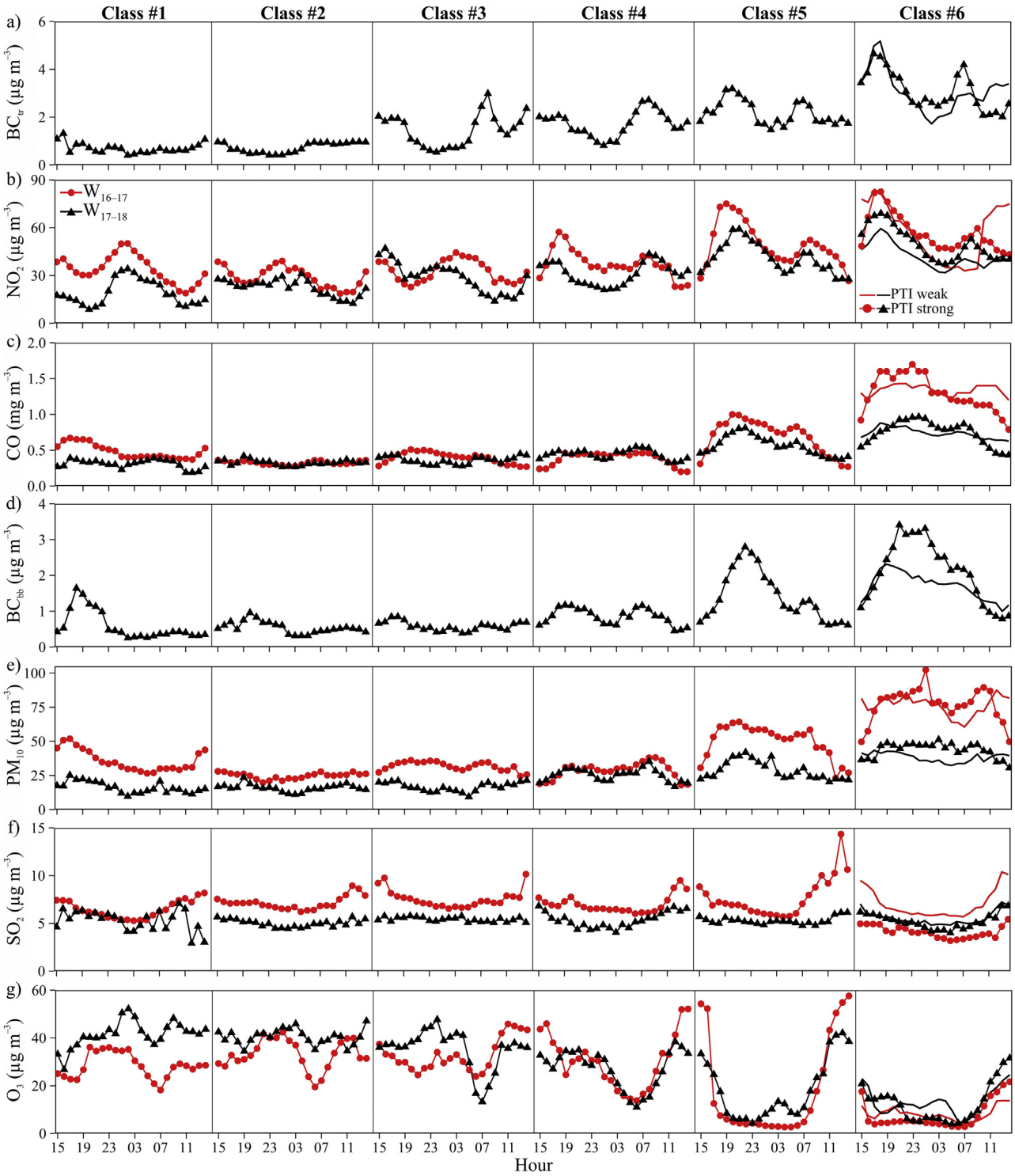


Fig. 4. Diurnal composite plots of hourly mean: a) BC_{tr}, b) NO_2, c) CO, d) BC_{bb}, e) PM_{10}, f) SO_2 and g) O_3 for $W_{16–17}$ (December 2016–February 2017) and $W_{17–18}$ (December 2017–February 2018) and six radon-based atmospheric mixing classes.

Consequently, the results summarized in Figs. 2, 3 and 4 also constitute a valuable benchmarking dataset that could be used in future evaluation studies of chemical transport model performance (e.g. Chambers et al., 2019b). Repeating this study in the future and comparing diurnal pollutant variability under well-constrained class #5 and PTI conditions would also provide valuable information regarding the efficacy of any imposed pollution mitigation measures.

3.4. Cross boundary pollution transport

In order to better distinguish distant pollution sources (e.g. industry, electricity production) from local Ljubljana emissions we investigated SO_2 and O_3 concentrations under only the more windy conditions (classes #1 to #3). Here we also considered class #1 days since strong frontal weather systems are also effective at transporting pollution. As an example of the contrasting airmass fetch characteristics between moderate-to-strong gradient wind conditions (classes #1 and #2) and

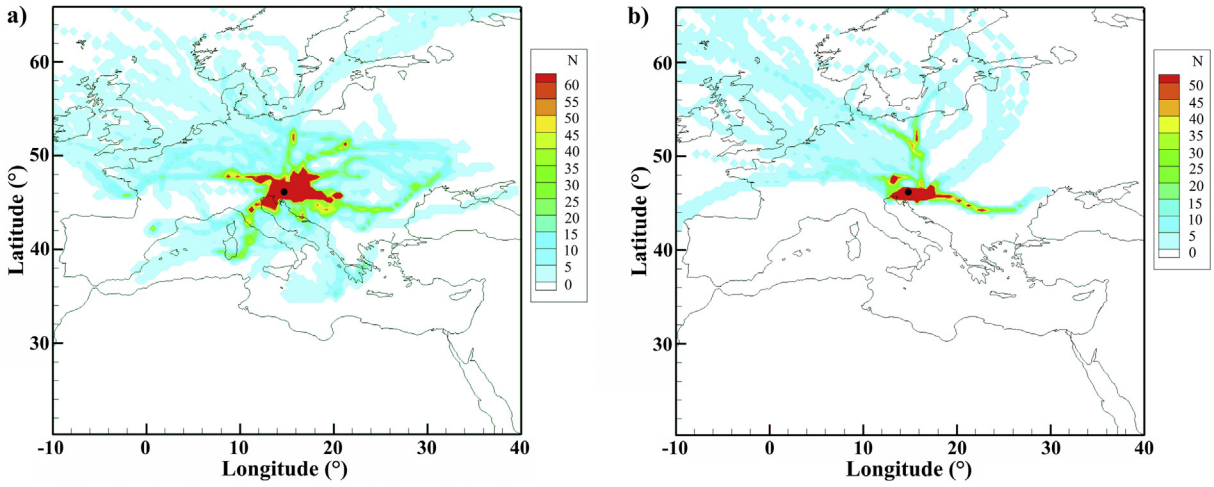


Fig. 5. Trajectory density plots of a) radon-based atmospheric mixing classes #1 and #2, and b) radon-based atmospheric mixing class #5 for $W_{16–17}$ (December 2016–February 2017) and $W_{17–18}$ (December 2017–February 2018). *N* represents the number of times a trajectory passes through a 0.5 × 0.5 grid cell. Ljubljana sub-Alpine Basin is indicated with a black circle.

weak gradient wind conditions (class #5), Fig. 5 compares density plots constructed from 4-day NOAA HYSPLIT v4.0 back trajectories with a starting height of 100 m a.g.l. Shading in these figures represents the different number of times that individual trajectories pass through a given grid cell. Based on the red through green shading on these plots, it is evident that the strong gradient wind conditions represent fetch regions in all directions surrounding Ljubljana, over a large portion of Europe (Fig. 5a). By contrast, airmass fetch for mixing class #5 days (with weak gradient winds), represents a much smaller area, predominantly to the east of Ljubljana, and completely excludes the Po Valley region (Fig. 5b). To minimise the chance of large local contributions to this signal we also employed a "diurnal sampling window" (between 11:00–15:00 LT), to best capture times when the near-surface pollutant observations were the most representative of the whole ABL. According to the GDAS mixing height information, this diurnal window represents the time of deepest, least variable mixing depth that would be representative of the largest fetch region. Further, to better identify the likely specific sources of remotely-generated pollution, we used the Conditional Probability Function technique (CPF) (Uria-Tellaetxe and Carslaw, 2014), which estimates the probability of pollutant concentrations (> 90th percentile) occurring as a function of wind direction. CPF plots of SO_2 and O_3 for the three $^{222}Rn_{DS}$ classes (#1, #2 and #3) of $W_{16–17}$ and $W_{17–18}$ based on data within the 11:00–15:00 LT sampling window are shown in Figs. 6 and 7.

On class #1, #2 and #3 days, the O_3 and SO_2 concentrations generally began to increase from background values as wind speeds increased beyond 2–3 m s^{-1} (Figs. 6 and 7). These results suggested that O_3 and SO_2 concentrations were dominated by remote sources under these conditions, since we have shown that little diurnal accumulation of local emissions is observed for wind speeds ≥1.5 m s^{-1}. Hourly SO_2 (> 90th percentile) ranged 12–32 μg m^{-3} (6.7–10.0 μg m^{-3}) in $W_{16–17}$ ($W_{17–18}$) (Figs. 6 and 7). While hourly O_3 concentrations (> 90th percentile) ranged 72–95 μg m^{-3} (65–100 μg m^{-3}) in $W_{16–17}$ ($W_{17–18}$) (Figs. 6 and 7). As evident from Figs. 6 and 7, in case of O_3, the highest probability (0.9–1.0) was found when the directions were SW (Po Valley/Port of Koper) or NE (Zasavje area). Probabilities were less consistent (0.6) in the easterly direction. The CPF plots clearly reveal four potential sources for SO_2 (NE-Zasavje/Šoštanj area, E-Toplarna power plant, and SW-Po Valley, shipping emissions-Port of Koper) with probability range from 0.04 to 1 (Figs. 6 and 7). Taking into consideration a conversion rate of 0.02 h^{-1} for $SO_2 \rightarrow SO_4^{2-}$ oxidation during the long-range transport (Seinfeld and Pandis, 2006), and assuming that pure SO_2 was emitted at the identified source regions, then SO_4^{2-}/SO_2 ratio would have become 0.6, 1.6, and 3.3 after 24 h, 48 h and 72 h of transport, respectively (typical transport times from Po Valley to Ljubljana indicated by HYSPLIT back trajectories under near-neutral conditions). Thus, SO_2 concentration becomes 61%, 38% and 23% of initial SO_2 after the 24 h, 48 h and 72 h of transport, respectively.

In addition to the prevailing meteorology, the ability to detect sources at specific receptor locations also depends on the terrain surrounding the observation site. Terrain influences for the SAB site are expected to influence that SW/SSW wind to be channeled up to the basin, therefore, the bivariate polar plot reveals exactly the identified pollution sources. The same, when winds approach from the NE/E directions, the dispersion of pollutants is almost in straight lines unaffected by hills going through the Sava Basin.

3.5. Health implications

Based on mean air quality data from Fig. 4, the worst potential public exposure in Ljubljana urban background site occurs during the most stable (nights of class #5) and strong PTI (class #6) conditions. Class #5 conditions comprise 14% and PTI conditions 20–30% of observations for winter season. Due to that we indicated the variability ($\mu \pm 1\sigma$) in air quality associated only with these two classes (Fig. 8). The $\mu \pm 1\sigma$ PM_{10} concentrations exceeded both EU and WHO values during the class #5 and strong PTI events (Fig. 8 and Table 4). The $\mu \pm 1\sigma$ concentrations of CO, NO_2, SO_2 and O_3 were well below hourly and daily maximum of EU and WHO guidelines values. By looking into the $\mu \pm 2\sigma$, which is a good indication of the absolute hourly peak values clearly NO_2 also sometimes exceeded both EU and WHO values during the class #5 and strong PTI events (Fig. 8 and Table 4). Due to their high number concentrations and small diameters BC have higher surface area per mass to absorb toxic materials than larger particles (Sun et al., 2019), however their concentration is not yet regulated by either EU or WHO. Peak BC_{tr} (BC_{bb}) concentrations during strong PTI events were 5 ± 16 μg m^{-3} (3 ± 5 μg m^{-3}). In an investigation of health effects of black carbon particles, Jannsen et al. (2011) concluded that daily mortality or hospital admissions were generally higher for increases in black carbon than for PM_{10} and $PM_{2.5}$.

4. Conclusions

The main aim of this study was to combine, for the first time, diurnal ($^{222}Rn_{DS}$) and synoptic ($^{222}Rn_{SS}$) timescale radon-based

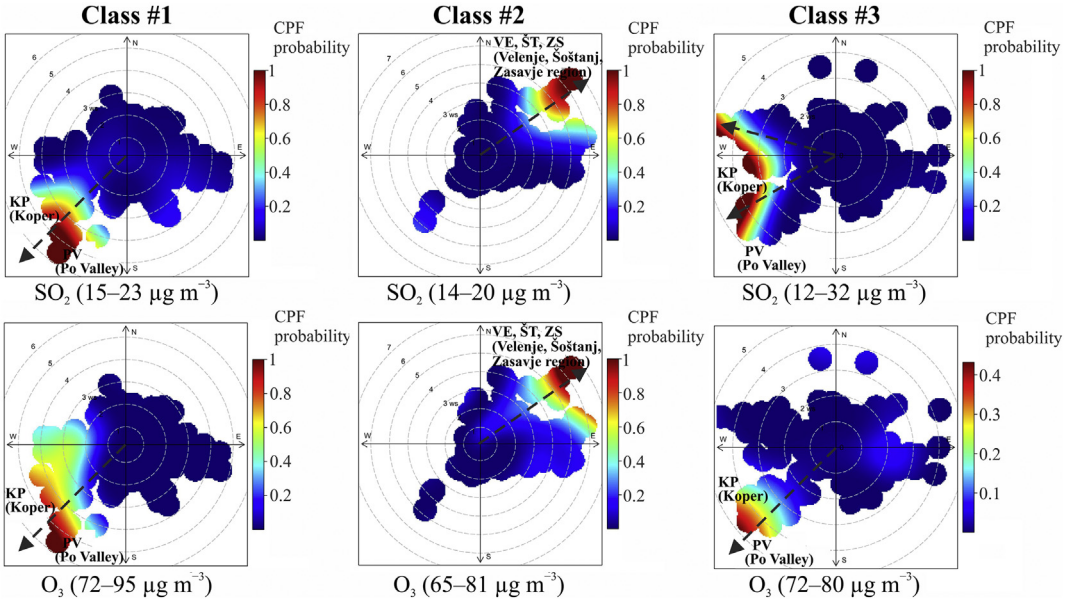


Fig. 6. The Conditional Probability Function (CPF) plots of SO_2 and O_3 for concentrations > 90th percentile during "diurnal sampling window" (11:00–15:00 LT) of for $W_{16–17}$ (December 2016–February 2017) for radon-based atmospheric mixing classes #1, #2 and #3. The dashed lines show the direction of potential known sources (see text for details).

atmospheric stability classification methods to improve understanding of urban pollution variability in the urban sub-Alpine site Ljubljana. For this purpose, hourly air quality, meteorology and atmospheric radon concentration were monitored during two winter periods of 2016–2017 ($W_{16–17}$) and 2017–2018 ($W_{17–18}$). The combination of the two methods ($^{222}Rn_{DS}$ and $^{222}Rn_{SS}$), resulted in 5 diurnal and 1 synoptic (persistent temperature inversion, PTI) mixing classes being defined. Furthermore, "strong" and "weak" categories of the PTI class were defined based on diurnal radon variability within that class.

Key differences in urban pollutant concentrations observed between the two winters were attributable to a combination of changes in stability and changes in source strengths. In $W_{16–17}$ there was a 28% larger traffic source near the monitoring site and the domestic heating source was also 17% larger (due to lower air temperatures). Based on the meteorological conditions for the 6 distinct mixing states, the thermodynamic stability on stable nights of $W_{16–17}$ was stronger, which acts to suppress vertical mixing. Combined, these factors lead to higher pollutant concentrations under stable (class #5) and PTI conditions in $W_{16–17}$ compared with $W_{17–18}$. Under the more windy conditions for both winters results suggested that SO_2 concentrations were dominated by remote sources (primarily from the Po Valley region). The diurnal characteristics of O_3 concentrations indicated both local and remote sources. Little diurnal accumulation of local pollutants (BC_{tr}, NO_2, CO, BC_{bb} and PM_{10}) was observed for wind speeds ≥ 1.5 m s^{-1}.

The combined radon-based atmospheric classification methods performed in this study help to separate "uncontrollable" (meteorology, geographic setting, topographic effects, and cross-boundary pollution) influences from controllable (source strength) influences on pollution

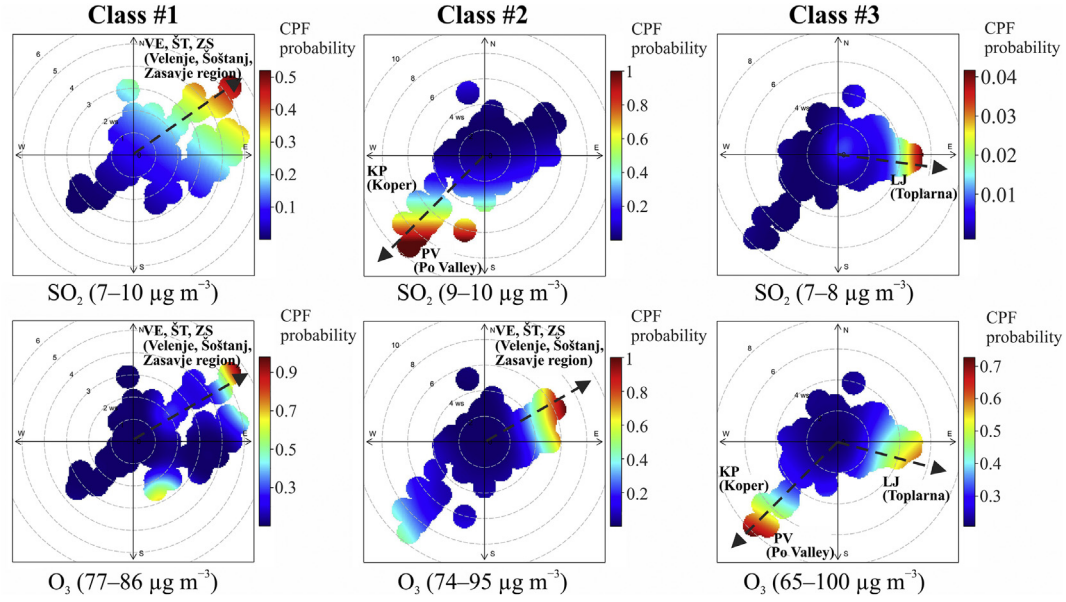


Fig. 7. The Conditional Probability Function (CPF) plots of SO_2 and O_3 for concentrations > 90th percentile during "diurnal sampling window" (11:00–15:00 LT) of for $W_{17–18}$ (December 2017–February 2018) for radon-based atmospheric mixing classes #1, #2 and #3. The dashed lines show the direction of potential known sources (see text for details).

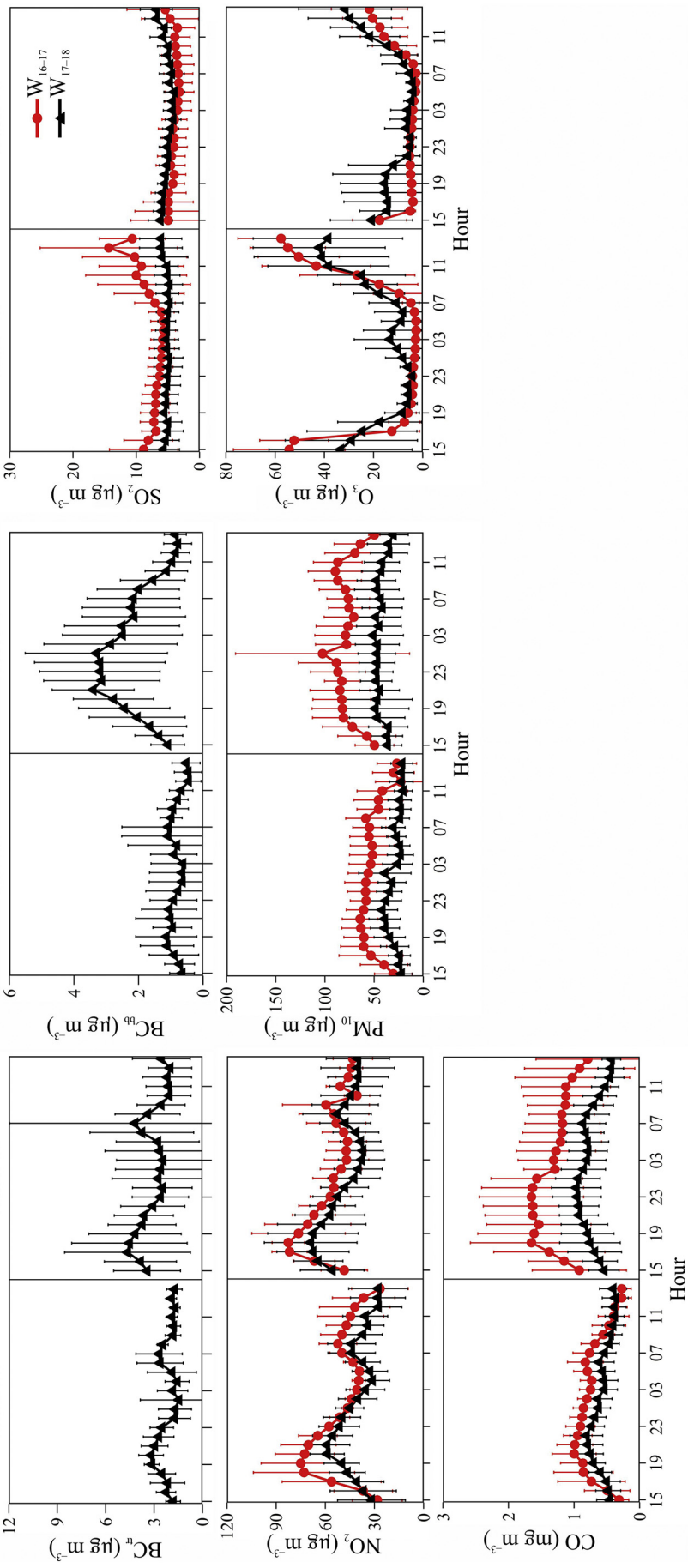


Fig. 8. Comparison of variability associated with the highest pollution (BC_{tr}, NO_2, CO, BC_{bb}, PM_{10}, SO_2 and O_3) concentration events during class #5 and class #6 (strong PTI) mixing conditions for W_{16-17} (December 2016–February 2017) and W_{17-18} (December 2017–February 2018). Whiskers represent ± σ.

Table 4
Air quality standards for the protection of health, given by the European Union (EU) and World Health Organization (WHO). Air quality standards in brackets represent those stipulated by the WHO (EEA, 2018).

	CO mg m^{-3}	NO_2 μg m^{-3}	PM_{10} μg m^{-3}	SO_2 μg m^{-3}	O_3 μg m^{-3}
Max daily			50 (50)	125 (20)	
Max daily 8-h mean	10 (10)				120 (100)
Max hourly	(30)	200		350	240 (200)

variability. Consequently, the results also constitute a valuable benchmarking dataset that could be used in future evaluation studies of chemical transport model performance. Repeating this study in the future and comparing diurnal pollutant variability under well-constrained most stable and PTI conditions would also provide valuable information regarding the efficacy of any imposed pollution mitigation measures. Based on the success of this winter study, the next step is to characterize diurnal and synoptic timescale influences on the atmospheric mixing state at this site year-round, and use this information in conjunction with detailed traffic density data to better relate specific source strengths to observed air quality variability in Ljubljana.

Author contribution statement

The investigation was jointly conceptualized by DK, SC, MK and JV. Radon monitoring instrumentation was deployed and managed by DK and JV, and black carbon data by MK. Data collection and curation was performed by DK. Formal data analysis was performed by DK. Acquisition of funding for the research was arranged by JV. The research methodology was jointly developed by DK and SC and investigation jointly conducted by DK and JV. The project was administered by JV, with JV and SC responsible for supervision. All visualization of data, concepts, and results was performed by DK, while the script written to acquire, separate and process the back trajectories for visualization was performed by JC. DK wrote the complete original draft of the paper, which was subsequently edited and reviewed jointly by DK, SC, MK, JC and JV.

Declaration of Competing Interest

The authors declare that they have no known competing financial interests or personal relationships that could have appeared to influence the work reported in this paper.

Acknowledgements

The authors acknowledge the financial support from the Slovenian Research Agency (research core funding No. P1-0143 and research project STRAP – Sources, TRAnsport and fate of persistent air Pollutants in the environment of Slovenia No. J1-1716) and from the Public Scholarship, Development, Disability and Maintenance Fund of the Republic of Slovenia (contract No. 11011-44/2016-18). The authors also gratefully acknowledge the Slovenian Environmental Agency for the permission provided and the assistance by installing the weather instrument shelter for radon monitoring on their land and for providing the meteorological and air quality data.

References

Allegrini, I., Febo, A., Pasini, A., Schiarini, S., 1994. Monitoring of the nocturnal mixed layer by means of particulate radon progeny measurement. J. Geophys. Res. 99, 18765–18777.
ARSO, Slovenian Environment Agency (Slovenian): Agencija Republike Slovenije za Okolje), 2017. Climate characteristics of Ljubljana - Wind Rose for the City of Ljubljana.
Ayers, G.P., Bigg, E.K., Turvey, D.E., Manton, M.J., 1982. Urban influence on condensation nuclei over a continent. Atmos. Environ. 16, 951–954.
Baasandorj, M., Hoch, S.W., Bares, R., Lin, J.C., Brown, S.S., Millet, D.B., Martin, R., Kelly, K., Zarzana, K.J., Whiteman, C.D., Dube, W.P., Tonnesen, G., Jaramillo, I.C., Sohl, J., 2017. Coupling between chemical and meteorological processes under persistent cold-air pool conditions: evolution of wintertime $PM_{2.5}$ pollution events and N_2O_5 observations in Utah's Salt Lake Valley. Environ. Sci. Technol. 51, 5941–5950. https://doi.org/10.1021/acs.est.6b06603.
Bigi, A., Bianchi, F., De Gennaro, G., Di Gilio, A., Fermo, P., Ghermandi, G., Prévôt, A.S.H., Urbani, M., Valli, G., Vecchi, R., Piazzalunga, A., 2017. Hourly composition of gas and particle phase pollutants at a central urban background site in Milan, Italy. Atmos. Res. 186, 83–94.
Bowen, B., 1994. Long-term tracer at Los Alamos, New Mexico. Part II: Evalution and comparison of several methods to determine dispersion coefficients. J. Appl. Meteorol. 33, 1236–1254.
Chambers, S., Williams, A.G., Zahorowski, W., Griffiths, A., Crawford, J., 2011. Separating remote fetch and local mixing influences on vertical radon measurements in the lower atmosphere. Tellus Ser. B Chem. Phys. Meteorol. 63, 843–859. https://doi.org/10.1111/j.1600-0889.2011.00565.x.
Chambers, S.D., Podstawczyńska, A., Pawlak, W., Fortuniak, K., Williams, A., Griffiths, A., 2019a. Characterising the state of the urban surface layer using Radon-222. J. Geophys. Res. Atmos. 124, 770–788.
Chambers, S.D., Williams, A.G., Crawford, J., Griffiths, A.D., 2015. On the use of radon for quantifying the effects of atmospheric stability on urban emissions. Atmos. Chem. Phys. 15, 1175–1190. https://doi.org/10.5194/acp-15-1175-2015.
Chambers, S.D., Galeriu, D., Williams, A.G., Melintescu, A., Griffiths, A.D., Crawford, J., Dyer, L., Duma, M., Zorila, B., 2016a. Atmospheric stability effects on potential radiological releases at a nuclear research facility in Romania: Characterising the atmospheric mixing state. J. Environ. Radioact. 154, 68–82. https://doi.org/10.1016/j.jenvrad.2016.01.010.
Chambers, S., Guérette, E.-A., Monk, K., Griffiths, A., Zhang, Y., Duc, H., Cope, M., Emmerson, K., Chang, L., Silver, J., Utembe, S., Crawford, J., Williams, A., Keywood, M., 2019b. Skill-testing chemical transport models across contrasting atmospheric mixing states using Radon-222. Atmosphere 10, 25. https://doi.org/10.3390/atmos10010025.
Chambers, S.D., Kang, C.-H., Williams, A.G., Crawford, J., Griffiths, A.D., Kim, K.-H., Kim, W.-H., 2016b. Improving the representation of cross-boundary transport of anthropogenic pollution in East Asia using Radon-222. Aerosol Air Qual. Res. 16, 958–976. https://doi.org/10.4209/aaqr.2015.08.0522.
Chambers, S.D., Kim, K.H., Kwon, E.E., Brown, R.J.C., Griffiths, A.D., Crawford, J., 2017. Statistical analysis of Seoul air quality to assess the efficacy of emission abatement strategies since 1987. Sci. Total Environ. 580, 105–116. https://doi.org/10.1016/j.scitotenv.2016.09.151.
Cohen, L.D., Barr, S., Krablin, R., Newstein, H., 1972. Steady-state vertical turbulent diffusion of radon. J. Geophys. Res. 77, 2654–2668.
Crawford, J., Chambers, S., Cohen, D., Williams, A., Griffiths, A., Stelcer, E., 2016. Assessing the impact of atmospheric stability on locally and remotely sourced aerosols at Richmond, Australia, using Radon-222. Atmos. Environ. 127, 107–117. https://doi.org/10.1016/j.atmosenv.2015.12.034.
Dons, E., Int Panis, L., Van Poppel, M., Theunis, J., Wets, G., 2012. Personal exposure to black carbon in transport microenvironments. Atmos. Environ. 55, 392–398. https://doi.org/10.1016/j.atmosenv.2012.03.020.
EEA: Air quality in Europe, 2016. 2016 Report.
EEA: Air quality in Europe, 2017. 2017 Report.
EEA: Air quality in Europe, 2018. 2018 Report.
Fiorella, R.P., Bares, R., Lin, J.C., Ehleringer, J.R., Bowen, G.J., 2018. Detection and variability of combustion-derived vapor in an urban basin. Atmos. Chem. Phys. 18, 8529–8547. https://doi.org/10.5194/acp-18-8529-2018.
Gjerek, M., Koleša, T., Logar, M., Matavž, L., Murovec, M., Paradiž, B., Rus, M., Žabkar, R., 2016. Kakovost zraka v Sloveniji v letu 2016. Tech. Rep. ARSO.
Gjerek, M., Koleša, T., Logar, M., Matavž, L., Murovec, M., Paradiž, B., Rus, M., Žabkar, R., 2017. Kakovost zraka v Sloveniji v letu 2017. Tech. Rep. ARSO.
Goudie, A.S., 2014. Desert dust and human health disorders. Environ. Int. 63, 101–113. https://doi.org/10.1016/j.envint.2013.10.011.
He, T., Chen, Y., Stanič, S., Bergant, K., Gao, F., Hua, D., 2018. Properties of tropospheric aerosols observed over Southwest Slovenia. J. Quant. Spectrosc. Radiat. Transf. 217, 380–387. https://doi.org/10.1016/j.jqsrt.2018.06.009.
Hitzenberger, R., Ctyroky, P., Berner, A., Turšič, J., Podkrajšek, B., Grgić, I., 2006. Size distribution of black (BC) and total carbon (TC) in Vienna and Ljubljana. Chemosphere 65, 2106–2113. https://doi.org/10.1016/j.chemosphere.2006.06.042.
Janssen, N.A.H., Hoek, G., Simic-lawson, M., Fischer, P., Van Bree, L., Brink, H., Keuken, M., Atkinson, R.W., Anderson, H.R., Brunekreef, B., Cassee, F.R., 2011. Black carbon and health effects of airborne particles compared with PM_{10} and $PM_{2.5}$. Environ. Health Perspect. 119, 1691–1699. https://doi.org/10.1289/ehp.1003369.
Kahl, J.D.W., Chapman, H.L., 2018. Atmospheric stability characterization using the Pasquill method: a critical evaluation. Atmos. Environ. 187, 196–209. https://doi.org/10.1016/j.atmosenv.2018.05.058.
Kallos, G., Astitha, M., Katsafados, P., Chris, S., 2006. Long-range transport of anthropogenically and naturally produced particulate matter in the Mediterranean and North Atlantic: current state of knowledge. J. Appl. Meteorol. Climatol. 46, 1230–1251. https://doi.org/10.1175/JAM2530.1.
Karanasiou, A., Mihalopoulos, N., 2013. Air Quality in Urban Environments in the Eastern Mediterranean. In: Viana, M. (Ed.), Urban Air Quality in Europe. Springer, pp. 219–238.
Kikaj, D., Vaupotič, J., 2017. Parameters influencing deviation of radon concentration from its typical diurnal pattern in the winter and summer seasons. Geol. Maced. 31, 157–170.

Kikaj, D., Vaupotič, J., Chambers, S.D., 2019a. Identifying persistent temperature inversion events in a subalpine basin using radon-222. Atmos. Meas. Tech. 12 (8), 4455–4477.
Kikaj, D., Chambers, S.D., Vaupotič, J., 2019b. Radon-based atmospheric stability classification in contrasting sub-Alpine and sub-Mediterranean environments. J. Environ. Radioact. 203, 125–134. https://doi.org/10.1016/j.jenvrad.2019.03.010.
Kochowska, E., Kozak, K., Kozłowska, B., Mazur, J., 2009. Test measurements of thoron concentration using two ionization chambers AlphaGUARD vs radon monitor RAD7. Nukleonika 54, 189–192.
Largeron, Y., Staquet, C., 2016. Persistent inversion dynamics and wintertime PM_{10} air pollution in Alpine valleys. Atmos. Environ. 135, 92–108. https://doi.org/10.1016/j.atmosenv.2016.03.045.
Levin, I., Born, M., Cuntz, M., Langendörfer, U., Mantsch, S., Naegler, T., Schmidt, M., Varlagin, A., Verclas, S., Wagenbach, D., 2002. Observations of atmospheric variability and soil exhalation rate of radon-222 at a Russian forest site: Technical approach and deployment for boundary layer studies. Tellus Ser. B Chem. Phys. Meteorol. 54, 462–475. https://doi.org/10.1034/j.1600-0889.2002.01346.x.
Mazur, J., Kozak, K., 2014. Complementary system for long term measurements of radon exhalation rate from soil. Rev. Sci. Instrum. 85. https://doi.org/10.1063/1.4865156.
Moses, H., Stehney, A.F., Lucas Jr., H.F., 1960. The effect of meteorological variables upon the vertical and temporal distributions of atmospheric radon. J. Geophys. Res. 65, 1223–1238.
Perrino, C., Pietrodangelo, A., Febo, A., 2001. An atmospheric stability index based on radon progeny measurements for the evaluation of primary urban pollution. Atmos. Environ. 35, 5235–5244.
Petkovšek, Z., 1985. The termination of air pollution periods in valley basins. Zeitschrift für Meteorol. 35, 370–372.
Petkovšek, Z., 1992. Turbulent dissipation of cold air lake in a basin. Meteorog. Atmos. Phys. 47, 237–245. https://doi.org/10.1007/BF01025620.
Poberžnik, M., Štrumbelj, E., 2016. The effects of air mass transport, seasonality, and meteorology on pollutant levels at the Iskrba regional background station (1996 – 2014). Atmos. Environ. 134, 138–146. https://doi.org/10.1016/j.atmosenv.2016.03.059.
Podstawczyńska, A., Chambers, S.D., 2018. Radon-based technique for the analysis of atmospheric stability – a case study from Central Poland. Nukleonika 63, 47–54. https://doi.org/10.2478/nuka-2018-0006.
Pope, C.A., Dockery, D.W., 2006. Health effects of fine particulate air pollution: Lines that connect. J. Air Waste Manag. Assoc. 56, 709–742. https://doi.org/10.1080/10473289.2006.10464485.
Porstendörfer, J., Butterweck, G., Reineking, A., 1991. Diurnal variation of the concentrations of radon and its short-lived daughters in the atmosphere near the ground. Atmos. Environ. Part A, Gen. Top. 25, 709–713. https://doi.org/10.1016/0960-1686(91)90069-J.
Pucer, J., Štrumbelj, E., 2018. Impact of changes in climate on air pollution in Slovenia between 2002 and 2017. Environ. Pollut. 242, 398–406. https://doi.org/10.1016/j.envpol.2018.06.084.
Querol, X., Alastuey, A., Gangoiti, G., Perez, N., Lee, H.K., Eun, H.R., Park, Y., Mantilla, E., Escudero, M., Titos, G., Alonso, L., Temime-Roussel, B., Marchand, N., Moreta, J.R., Revuelta, M.A., Salvador, P., Artíñano, B., Dos Santos, S.G., Anguas, M., Notario, A., Saiz-Lopez, A., Harrison, R.M., Millán, M., Ahn, K.H., 2018. Phenomenology of summer ozone episodes over the Madrid Metropolitan Area. central Spain. Atmos. Chem. Phys. 18, 6511–6533. https://doi.org/10.5194/acp-18-6511-2018.
Rakovec, J., Merše, J., Jernej, S., Paradiž, B., 2002. Turbulent dissipation of the cold-air pool in a basin: Comparison of observed and simulated development. Meteorog. Atmos. Phys. 79, 195–213. https://doi.org/10.1007/s007030200003.
Rakovec, J., Skok, G., Žabkar, R., Žagar, N., 2015. The influence of the depth of a very shallow cool-pool lake on nocturnal cooling. Agric. For. Meteorol. 203, 17–29.
Sandradewi, J., Prévôt, A.S.H., Weingartner, E., Schmidhauser, R., Gysel, M., Baltensperger, U., 2008. A study of wood burning and traffic aerosols in an Alpine valley using a multi-wavelength Aethalometer. Atmos. Environ. 42, 101–112. https://doi.org/10.1016/j.atmosenv.2007.09.034.
Seinfeld, J.H., Pandis, S.N., 2006. Atmospheric Chemistry and Physics: From Air Pollution to Climate Change. John Willey & Sons Inc., New York.
Sesana, L., Caprioli, E., Marcazzan, G.M., 2003. Long period study of outdoor radon concentration in Milan and correlation between its temporal variations and dispersion properties of atmosphere. J. Environ. Radioact. 65, 147–160. https://doi.org/10.1016/S0265-931X(02)00093-0.
Sesana, L., Ottobrini, B., Polla, G., Facchini, U., 2006. ^{222}Rn as indicator of atmospheric turbulence: Measurements at Lake Maggiore and on the pre-Alps. J. Environ. Radioact. 86 (2), 271–288. https://doi.org/10.1016/j.jenvrad.2005.09.005.
Silcox, G.D., Kelly, K.E., Crosman, E.T., Whiteman, C.D., Allen, B.L., 2012. Wintertime $PM_{2.5}$ concentrations during persistent, multi-day cold-air pools in a mountain valley. Atmos. Environ. 46, 17–24. https://doi.org/10.1016/j.atmosenv.2011.10.041.
Sun, J., Birmili, W., Hermann, M., Tuch, T., Weinhold, K., Spindler, G., Schladitz, A., Bastian, S., Löschau, G., Cyrys, J., Gu, J., 2019. Variability of black carbon mass concentrations, sub-micrometer particle number concentrations and size distributions: results of the German Ultrafine Aerosol Network ranging from city street to high Alpine locations. Atmos. Environ. 202, 256–268.
Titos, G., Lyamani, H., Drinovec, L., Olmo, F.J., Močnik, G., Alados-Arboledas, L., 2015. Evaluation of the impact of transportation changes on air quality. Atmos. Environ. 114, 19–31. https://doi.org/10.1016/j.atmosenv.2015.05.027.
Uria-Tellaetxe, I., Carslaw, D.C., 2014. Conditional bivariate probability function for source identification. Environ. Model. Softw. 59, 1–9. https://doi.org/10.1016/j.envsoft.2014.05.002.
VanReken, T.M., Dhammapala, R.S., Jobson, B.T., Bottenus, C.L., VanderSchelden, G.S., Kaspari, S.D., Gao, Z., Zhu, Q., Lamb, B.K., Liu, H., Johnston, J., 2017. Role of persistent low-level clouds in mitigating air quality impacts of wintertime cold pool conditions. Atmos. Environ. 154, 236–246. https://doi.org/10.1016/j.atmosenv.2017.01.043.
Vrhovec, T., 1990. Analysis of mesometeorological temperature fields. Meteorog. Atmos. Phys. 43, 235–240.
Wang, F., Chambers, S.D., Zhang, Z., Williams, A.G., Deng, X., Zhang, H., Lonati, G., Crawford, J., Griffiths, A.D., Ianniello, A., Allegrini, I., 2016. Quantifying stability influences on air pollution in Lanzhou, China, using a radon-based "stability monitor": Seasonality and extreme events. Atmos. Environ. 145, 376–391. https://doi.org/10.1016/j.atmosenv.2016.11.003.
Wang, L., Stanič, S., Eichinger, W., Močnik, G., Drinovec, L., Gregorič, A., et al., 2019. Investigation of Aerosol Properties and Structures in Two Representative Meteorological Situations over the Vipava Valley Using Polarization Raman LiDAR. Atmosphere 10 (3), 128–140. https://www.mdpi.com/2073-4433/10/3/128.
Whiteman, C.D., 1982. Breakup of temperature inversions in deep mountain valleys: Part I. observations. J. Appl. Meteorol. https://doi.org/10.1175/1520-0450(1983)022<1314:COOTII>2.0.CO;2.
Whiteman, C.D., Eisenbach, S., Pospichal, B., Steinacker, R., 2004. Comparison of vertical soundings and sidewall air temperature measurements in a small Alpine Basin. J. Appl. Meteorol. 43, 1635–1647. https://doi.org/10.1175/JAM2168.1.
Whiteman, C.D., Hoch, S.W., Horel, J.D., Charland, A., 2014. Relationship between particulate air pollution and meteorological variables in Utah's Salt Lake Valley. Atmos. Environ. 94, 742–753. https://doi.org/10.1016/j.atmosenv.2014.06.012.
Williams, A., Zahorowski, W., Chambers, S., Griffiths, A., 2011. The vertical distribution of radon in clear and cloudy daytime terrestrial boundary layers. J. Atmos. Sci. 68, 155–174. https://doi.org/10.1175/2010JAS3576.1.
Williams, A.G., Chambers, S., Griffiths, A., 2013. Bulk mixing and decoupling of the nocturnal stable boundary layer characterized using a ubiquitous natural tracer. Boundary-Layer Meteorol. 149, 381–402. https://doi.org/10.1007/s10546-013-9849-3.
Williams, A.G., Chambers, S.D., Conen, F., Reimann, S., Hill, M., Griffiths, A.D., Crawford, J., 2016. Radon as a tracer of atmospheric influences on traffic-related air pollution in a small inland city. Tellus, Ser. B Chem. Phys. Meteorol. 68, 1–21. https://doi.org/10.3402/tellusb.v68.30967.
Zahorowski, W., Chambers, S.D., Henderson-Sellers, A., 2004. Ground based radon-222 observations and their application to atmospheric studies. J. Environ. Radioact. 76, 3–33. https://doi.org/10.1016/j.jenvrad.2004.03.033.

Radon-222: a year-round indicator of thermodynamic structure and air quality within a topographic basin

Dafina Kikaj[1,2], Scott D. Chambers[3], Matjaž Kobal[4], Janja Vaupotič[2]

[1]Jožef Stefan International Postgraduate School, Jamova cesta 39, 1000 Ljubljana, Slovenia
[2]Jožef Stefan Institute, Department of Environmental Sciences, Jamova cesta 39, 1000 Ljubljana, Slovenia
[3]ANSTO, Environmental Research, Locked Bag 2001, Kirrawee DC, NSW 2232, Australia
[4]Aerosol d.o.o., Kamniška ulica 39A, 1000 Ljubljana, Slovenia

Correspondence to: Janja Vaupotič (janja.vaupotic@ijs.si)

Abstract. The efficacy of a new radon-based method for combined classification of diurnal and synoptic timescale changes in atmospheric stability is demonstrated using 1-year (Dec 2017–Nov 2018) of observations in Ljubljana (Slovenia). Five diurnal-timescale mixing classes (#1 to #5) were defined for each season. Due to the combined influences of complex topography and the pervasive cold-season "Siberian High", synoptic-timescale changes of the atmospheric mixing state were observed in winter and autumn, necessitating the definition of an additional mixing class (#6), representing "persistent temperature inversions" (PTI). Diurnal cycles of selected pollutants (BC, NO_2, CO, PM_{10}, SO_2 and O_3) exhibited substantial seasonality as a result of changing mixing conditions and source types and strengths. For the more well-mixed conditions (classes #1 to #3) wind speed was 3 times higher than during class #6 (PTI) conditions, resulting in a 3-fold reduction of primary pollutant accumulation. Daily-mean PM_{10} concentrations only exceeded EU and WHO guideline values in winter and autumn for two mixing classes: (i) class #5 (strongly stable surface conditions with a shallow stable nocturnal boundary layer, SNBL), and (ii) class #6 (PTI). Both mixing states were associated with low mean wind speeds (~0–0.7 m s^{-1}) and strong thermal stratification, as indicated both by pseudo-vertical temperature gradients ($\Delta T/\Delta z$) and radiosonde profiles. Diurnal $\Delta T/\Delta z$ values indicated limited opportunity for convective mixing of pollutants from the basin atmosphere under these conditions. Diurnal ozone (O_3) concentrations exhibited an inverse response to that of primary pollutants with changing mixing conditions. Clear-sky conditions (class #5) resulted in high daytime O_3, but low nocturnal values due to NO titration in the shallow SNBL. Overcast, windy conditions (class #2) resulted in low daytime O_3, but higher nocturnal values due to downward mixing of O_3 from the free troposphere. In summer and spring the 8-hour daytime mean O_3 concentrations exceeded EU and WHO guideline values 22 times for classes #3 to #5.

1 Introduction

Air pollution is recognised to be one of the most significant health-related problems of modern times (Griffin, 2005; Highwood and Kinnersley, 2006; Pope and Dockery, 2006; Goudie, 2014; EEA, 2018). Outdoor air pollution exceedance events are not simply related to emission sources and strengths, they arise through a complex interplay between numerous factors. As noted

in Chambers et al. (2019a), the challenge of air quality management is exacerbated by uncontrollable factors such as changes in the mixing state of the atmospheric boundary layer (ABL), often referred to as its stability. Diurnal and synoptic timescale changes in meteorology, along with topographic setting, are the main factors influencing atmospheric stability, which in turn affect the vertical and horizontal mixing of pollution at a wide range of temporal and spatial scales.

Numerous studies have been conducted to determine the relationship between atmospheric stability and air pollution variability on diurnal timescales (Triantafyllou, 2001; Klingner and Sahn, 2008; Vardoulakis and Kassomenos, 2008; Grundstrom et al., 2015; Jędruszkiewicz et al., 2017; Wang et al., 2019).

Among the atmospheric stability classification tools most readily available for routine use is the Pasquill-Gifford (PG) scheme (Pasquill, 1961; Turner, 1964; Pasquill and Smith, 1983). However, since topography can have a significant influence on the atmospheric mixing state, the PG turbulence scheme is often poorly applicable in basin/valley settings due to consistently low wind speeds (e.g., Chambers et al., 2015a; Wang et al., 2016). Air pollution events caused by emission and accumulation of pollutants under specific synoptic conditions (e.g., enduring cold-season anticyclones) can persist for days to weeks (Buchanan et al., 2002; Beaver et al., 2010) and can be misclassified or underestimated by using the PG atmospheric stability classification method (Chambers et al., 2015b; Kahl and Chapman, 2018).

Between the different synoptic situations that may occur, cyclonic conditions generally lead to the dispersion or venting of primary air pollutants from source regions, while enduring cold-season anticyclonic conditions (often resulting in persistent temperature inversion (PTI) conditions) lead to their accumulation, particularly in complex terrain e.g., in some parts of Western Europe and in the Mediterranean Basin Region (MBR). For example, in Grenoble, below the French Alps, Largeron and Staquet (2016) detected nine PM_{10} pollution events under PTI conditions from November 2006 to February 2007. In each of these events PM_{10} concentrations exceeded the EU air quality standards. A severe pollution event attributed to PTI conditions also took place in Valencia (Spain), where BC levels steadily increased from 3.2 μg m^{-3} to 4.9 μg m^{-3} (Segura et al., 2013). In Skopje valley (North Macedonia) extremely high pollutant concentrations were recorded during winter PTI events, with the highest hourly PM_{10} concentration 500 μg m^{-3} and corresponding NO_2 concentration 440 μg m^{-3} (Anttila et al., 2016). Likewise, in Ljubljana, PM_{10} and NO_2 guideline values were exceeded in winter during PTI conditions and fine-weather conditions (conducive to the formation of a strongly stable nocturnal boundary layer) (Kikaj et al., 2019c). In Zgierz (Poland) Chambers and Podstawczyńska (2019) reported that PM_{10} and SO_2 exceeded guideline values in non-summer months under PTI and fine weather nocturnal conditions, whereas, in Bern (Switzerland), situated in western foothills of the European Alps, diurnal maximum winter CO concentrations increased by a factor of 2 from windy to strongly stable conditions (Williams et al., 2016).

By contrast, in the warm season MBR countries are particularly susceptible to exceedances of the secondary pollutant O_3 target value, due to the influence of frequent clear-sky conditions that favor photochemical O_3 formation (EEA, 2018). In addition, its geographic location makes the basin a receptor of long-range pollution transport from Africa (Kallos et al., 2006), across Europe from the North Atlantic Ocean and across Italy from the Mediterranean Sea (He et al., 2018) and even from the North America (Lelieveld et al., 2002; Gerasopoulos et al., 2005). Long-range pollution transport events of both anthropogenic and

natural origin are often felt in many countries of the MBR region (Salvador et al., 2014), such as Portugal (Russo et al., 2014; Conceição et al., 2018), Spain (Diaz et al., 2014), Italy (Gobbi et al., 2019), Slovenia (Beeston et al., 2011), Croatia (Čanić et al., 2009), and Greece (Kaskaoutis et al., 2019a, 2019b).

To this end, it is very important to improve understanding of the influence of changing atmospheric mixing state on the temporal variability of air pollution on diurnal, synoptic and seasonal timescales. By consistently quantifying such effects in our study region we hope to contribute to the development of new control actions for air pollution prevention.

In atmospheric stability studies, near-surface radon (^{222}Rn) measurements have been shown to be a consistent indicator of diurnal and synoptic timescale mixing processes in the ABL, largely attributable to radon's ubiquitous nature and unique combination of physical characteristics (Moses et al., 1960; Cohen et al.,1972; Allegrini et al., 1994; Perrino et al., 2001; Sesana et al., 2003; Galmarini, 2006; Avino and Manigrasso, 2008; Chambers et al., 2011, 2019b; Williams et al., 2013; Pitari et al., 2014; Kikaj et al., 2019a). The present study demonstrates the efficacy of a new combined radon-based method for classification of diurnal and synoptic timescale changes in atmospheric stability in order to provide a better understanding of the seasonal variability of air pollution for one year in Ljubljana (Slovenia). Our results focus on the following specific tasks: (i) investigating changes in the atmospheric mixing state on seasonal, synoptic and diurnal timescales, including an analysis of the pseudo-vertical temperature gradient and wind speed over the basin environment; (ii) discussing of the implications of different aspects of the atmospheric mixing state on urban air pollutants (BC, NO_2, CO, PM_{10}, SO_2 and O_3); and (iii) relating extremes of air pollution to the World Health Organization (WHO) and the European Union (EU) guideline values in a statistically robust way that can be directly related to public exposure.

2 Methods

2.1 Site location and measurements

Continuous hourly radon (^{222}Rn) measurements started in Ljubljana in December 2016 and are ongoing, as are the monitoring of air quality parameters and standard meteorological observations. Detailed descriptions of the site and instrumentation have already been provided by Kikaj et al. (2019a, 2019b). Briefly, Ljubljana (capital of Slovenia; 299 m above sea level, a.s.l.), is situated in a subalpine basin surrounded by peaks of the Julian, Kamnik-Savinja, and Dinaric Alps reaching elevations of ~1000 m (Vrhovec, 1990; Hitzenberger et al., 2006). The climate is temperate and continental and is typical for subalpine regions. A characteristic feature is generally calm wind within the basin, which results in a high number of foggy days, with frequent PTI events (33% of the year), mostly restricted to the colder months (autumn, winter). Prevailing winds for the region are within the sector NNE to ENE (ARSO, 2017), and the mean wind speed changes only slightly from summer (1.4 m s^{-1}) to winter (1.3 m s^{-1}). The mean air temperature reveals a distinct seasonal cycle, with the summer mean daily maximum reaching 22 °C and the winter mean daily minimum 0 °C. Rainfall distribution is irregular, 1400 mm y^{-1}, with a peak in the summer (ARSO, 2017).

The Ljubljana Bežigrad (LjB) ground-based weather station (Figure 1) has a comprehensive suite of meteorological and air quality sensors, operated by the National Meteorological Service at the Slovenian Environment Agency (ARSO). The following parameters, aggregated to hourly temporal resolution, were used in this study: air temperature (°C), wind speed (m s^{-1}), particulate matter of median aerodynamic diameter ≤10 μm (PM_{10}), carbon monoxide (CO), nitrogen dioxide (NO_2), sulphur dioxide (SO_2), ozone (O_3), and black carbon (BC; data provided by Aerosol d.o.o., Ljubljana, Slovenia). The total concentration of BC is the result of traffic (BC_{tr}) and biomass burning (BC_{bb}) sources (Sandradewi et al., 2008).

Atmospheric ^{222}Rn measurements at LjB weather station are being conducted using an AlphaGUARD PQ2000 PRO monitor (Bertin Instruments). The device is mounted 1.5 m above ground level (a.g.l.), within a Stevenson Screen instrument shelter and operates continuously in diffusion mode with a 1-hour integration time. Over the whole period of measurements reported in this study, only about 3% of measured radon concentrations fell at or below 2 Bq m^{-3}, the lower limit of detection (LLD), indicating that the instrument is satisfactory for this kind of research (Kikaj and Vaupotič, 2017; Kikaj et al., 2019a). Further details regarding the calibration of the device and data quality assurance and control are provided by Kikaj et al. (2019b) and Murn and Stepišnik (2019).

In addition, air temperature observations were retrieved from seven ground-based weather stations on the sidewalls of the topographic basin at a range of elevations from 268 m to 1742 m. A full list of station names, abbreviations, and elevations is provided in Table 1, and their locations relative to LjB station are shown in Figure 1. The principle of the pseudo-vertical temperature gradient ($\Delta T/\Delta z$) calculation, detailed in Kikaj et al. (2019a) and Largeron and Staquet (2016), relies upon two key assumptions: (1) horizontal homogeneity of the air temperature between stations of similar elevations, and (2) the existence of significant vertical changes in air temperature between stations at different elevations (e.g., high–medium, high–low, or medium–low). To this end, the $\Delta T/\Delta z$ was derived from the average of the four station pairs $(\Delta T/\Delta z)_i$. The gradient pairs chosen were: (i) Li and K, $(\Delta T/\Delta z)_1$, 29 km apart, Δz=943 m; (ii) LjB and T, $(\Delta T/\Delta z)_2$, 19 km apart, Δz=396 m; (iii) LjB and PR, $(\Delta T/\Delta z)_3$, 35 km apart, Δz=720 m; (iv) LLj and Kr, $(\Delta T/\Delta z)_4$, 23 km apart, Δz=1378 m. In order to determine the atmospheric conditions under which the pseudo-vertical temperature gradients would provide the most useful proxy for the atmospheric mixing state, we also investigated vertical sounding data within the basin conducted daily between 4–6 a.m. local time by ARSO. However, the analysis of radiosonde data in this study is restricted to winter only, and a more detailed seasonal evaluation of this data will form the basis of a separate dedicated study. Furthermore, since radiosonde observations (to ~20 km a.g.l.) were only conducted in the mornings, evaluation of the pseudo-vertical temperature gradient technique is limited to this time of the day. For the purposes of this evaluation we will focus only on the profile information from the lower part of the troposphere (0–2 km a.s.l.).

The present study focuses on one full year of observations (December 2017–November 2018). All reported times are local (local time is UTC+1) and the Northern Hemisphere seasonal convention has been adopted (i.e., winter: December–February; spring: March–May; summer: June–August; autumn: September–November).

2.2 ^{222}Rn stability analysis

In studies where ^{222}Rn has been used to investigate the atmospheric mixing state, single-height radon measurements have mostly used (Perrino et al., 2001, 2006; Omori et al., 2009; Pal et al., 2015; Pitari et al., 2015; Podstawczyńska and Chambers, 2018), since vertical radon gradient measurements are challenging and expensive to make accurately (Chambers et al., 2011; Williams et al., 2013). The most successful attempts to consistently link single-height radon measurements to the atmospheric mixing state in a consistent quantitative way are attributable to researchers that have found ways to account for fetch effects (e.g., Fontan et al., 1979; Fujinami and Esaka, 1987; Perrino et al., 2001; Sesana et al. 2006; Chambers et al., 2015a; Kikaj et al., 2019a).

Considering that the mixing state of the Ljubljana basin ABL changes on diurnal and synoptic scales, we adapted the synoptic and diurnal radon-based classification scheme described in detail by Chambers et al. (2019a) and Kikaj et al. (2019a, 2019c). Briefly, the diurnal radon-based classification ($^{222}Rn_{DS}$) involves isolating mixing-related (diurnal) changes in near-surface radon concentrations by estimating and removing air mass fetch effects, and then assigning stability thresholds to mean values of radon accumulation within a defined 10-hour nocturnal window. Corresponding daytime mixing states for each 24-hour period are inferred from nocturnal conditions based on an assumption of short-term atmospheric persistence. The number of mixing classes that can be distinguished in a statistically robust manner (typically 3 to 5) depends on the size of the available dataset.

Radon-based identification of synoptic timescale changes in the ABL mixing state ($^{222}Rn_{SS}$) (specifically PTI events) involves separating synoptic timescale variability in radon concentration from contributions occurring at other timescales, and then comparing the magnitudes of radon variability occurring at diurnal and synoptic timescales. When synoptic contributions to radon variability exceed the typical magnitude of diurnal ones for more than two consecutive days, a PTI event is considered to have occurred.

In order to account for seasonality in the regional radon flux, both $^{222}Rn_{DS}$ and $^{222}Rn_{SS}$ methods need to be derived separately for each season.

A summary of the six mixing classes (5 diurnal and 1 synoptic) for the one year of measurements in Ljubljana Bežigrad that result from a combination of the above two classification techniques ($^{222}Rn_{DS}$ and $^{222}Rn_{SS}$), is presented in Table 2. The table also summarises the duration of conditions (%) for each mixing class in each of the four seasons. The mixed-fetch conditions (class #1) defined by $^{222}Rn_{DS}$ constituted the lowest number of observations (7–12%) in all seasons, and represent periods of pronounced synoptic non-stationarity (Podstawczyńska and Chambers, 2018; Kikaj et al., 2019c). These have been excluded from further analysis and discussion. The $^{222}Rn_{SS}$ detected no PTI conditions in spring and summer, while these conditions were experienced in winter and autumn for 30% and 20% of the time, respectively. Mixing classes #2 to #5, for which $^{222}Rn_{DS}$ is the best suited (Chambers et al., 2019a), constitute ~90% and ~70% in summer/spring and autumn/winter, respectively, of all observations.

3 Results and Discussion

3.1 Variability of radon concentrations within radon-based mixing classes

Diurnal composite plots of the mixing-related radon concentrations (i.e. fetch effects removed) for five of the six designated mixing classes in each season are illustrated in Figure 2. In general, relatively low nocturnal accumulation of radon was noted for class #2 days, while the most pronounced daily ^{222}Rn variation was observed in classes #4 and #5. These nights were characterized by weak katabatic winds and the formation of a strong nocturnal temperature inversion near the bottom of the basin.

For all mixing classes the shape and amplitude of the radon diurnal cycle changes substantially with season. For example, Figure 2 shows that diurnal radon concentrations have the largest amplitude for class #5 conditions (~24 Bq m^{-3} in summer, ~12 Bq m^{-3} in winter). Diurnal amplitudes of radon in spring and autumn (transitional months) were typically much more comparable. A similar seasonal trend of diurnal radon variability within radon-based mixing classes was found in Bern valley, Switzerland (Williams et al., 2016) and Ciosny, Poland (Chambers et al., 2016). In both studies, low winter radon values were attributable to a combination of significantly reduced winter radon exhalation rates due to the snow cover, high soil moisture or partially frozen surfaces, and a reduced diurnal change in mixing depth (shallower during the day and deeper at night). The same conclusion can be drawn for the Ljubljana observations (Figure 2). Based on the European radon flux map (Karstens et al., 2015), which includes modelled soil moisture effects, the radon exhalation rate in Ljubljana increases by a factor of 2 from winter to summer. Seasonal changes of thermodynamic stability (discussed in Section 3.2) are also expected to influence the nocturnal accumulation of radon between seasons. Certainly, a combination of these factors is well reflected in the composite plot of class #6 in Figure 2. Under PTI conditions, almost identical diurnal trend and peak average between autumn and winter radon concentration is observed. This fact points to the substantially reduced radon exhalation and intense thermodynamic stability in winter and vice versa in autumn (higher radon exhalation and weaker thermodynamic stability). It should be noted, however, during the synoptic timescale PTI conditions a secondary near-surface inversion layer (some 10s of meters thick) would often form within the overlying PTI inversion. The comparatively low diurnal amplitude of the mixing component of radon for class #6 conditions shown in Fig. 2 reflects the overnight accumulation of radon from a reduced wintertime source within this surface inversion. The higher afternoon "measured" radon concentrations compared with "mixing component" values shown in this figure is a result of synoptic timescale accumulation of radon within the deeper PTI inversion.

3.2 Variability of meteorological parameters within radon-based mixing classes

Diurnal composites of the pseudo-vertical temperature gradient ($\Delta T/\Delta z$) and wind speed for each season, each classified according to the radon-based mixing classes, are shown in Figure 3. We also grouped daily radiosonde data (air temperature and wind speed) according to the radon-based scheme, but here we will focus only on three of the mixing classes (#2, #5 and #6) in winter (Figure 4). Wind speed and $\Delta T/\Delta z$ are strongly linked with changes in atmospheric mixing state (e.g., Ivey et al. (2019) and references therein). Systematic changes in the diurnal cycles of $\Delta T/\Delta z$ and the 2 m LjB wind speed are noted across

the six radon-derived mixing classes as well as seasons. Vertical profiles of wind speed and temperature also changed systematically across the three radon mixing classes (Figure 4). For reference, the adiabatic lapse rate of the standard atmosphere (–6.5 °C km^{-1}) has been superimposed on the diurnal cycles of $\Delta T/\Delta z$ (Figure 3a) and the air temperature profiles (Figure 4). Temperature gradients more negative than adiabatic lapse rate (i.e. super-adiabatic lapse rates), are indicative of an unstable basin atmosphere, whereas gradients less negative than the adiabatic lapse rate (sub adiabatic) are indicative of an atmosphere that is stable, or tending toward stability.

In general, near-neutral (class #2) periods experience the highest mechanical air mixing with daily average near surface wind speeds ≥1 m s^{-1} (Figure 3b). Wind profiles (Figure 4a) indicated the presence of cyclonic conditions, with a wind speed maximum (18.2 m s^{-1}) at around 2030 m a.g.l. (2325 m a.s.l.), from the SE direction (not shown). During these conditions it is expected that basin air is mixed only by mechanical turbulence and that there should be little to no heating by the surface (i.e. $\Delta T/\Delta z \geq$ –6.5 °C km^{-1}). In winter, pseudo-vertical temperature gradient values were the lowest and quite consistent across the diurnal cycle, with a tendency to be slightly unstable ($\Delta T/\Delta z$~–8 °C km^{-1}) for about six hours near the middle of the day (Figure 3a). For the rest of the time $\Delta T/\Delta z$ was almost perfectly adiabatic in its behaviour. Similarly, morning vertical air temperature profiles for class #2 days had a lapse rate of –6.1 °C km^{-1} (Figure 4a), which was very close to the corresponding early morning winter $\Delta T/\Delta z$ value (04:00–06:00 LT; Figure 3a). In the other seasons under class #2 (well-mixed) conditions $\Delta T/\Delta z$ values indicated that the basin atmosphere tended to be unstable during the day, and tending toward stable at night.

By contrast, stable nights (classes #3 to #5) were associated with strong near surface nocturnal inversions ($\Delta T/\Delta z$ peaking at ~+2 K km^{-1} before sunrise; Figure 3a), and low wind speeds (on average 0–0.7 m s^{-1}; Figure 3b) typically from the NE between sunset and sunrise, consistent with katabatic drainage flow. Under these conditions vertical mixing from the basin was considerably suppressed. However, the temperature inversions on these nights (classes #3 to #5) vanished abruptly each morning shortly after the onset of convective mixing ($\Delta T/\Delta z \leq$ –6.5°C km^{-1}) as a result of intense sunlight on basin surfaces, promoting the ventilation of pollution from the basin despite low gradient wind speeds. In spring and summer mixing classes #3 to #5 exhibited the highest $\Delta T/\Delta z$ diurnal cycle amplitudes (12 K km^{-1}; Figure 3a) due to the longer duration and strongest intensity of solar radiation and clear sky conditions. In winter and autumn, the diurnal amplitude of $\Delta T/\Delta z$ decreased (6 K km^{-1}; Figure 3a) as a consequence of longer nights, wet/frozen surface, high albedo (snow cover), low solar radiation and more frequent cloud cover. Figure 4b also shows morning soundings for class #5 winter conditions. The sonde-derived morning lapse rate over the depth of the basin was sub-adiabatic (–2.6 °C km^{-1}) indicating that the deeper basin atmosphere was tending toward stability, but a shallow stable surface layer is also visible. The wind speed profile under class #5 conditions (Figure 4b) indicated speeds below 5 m s^{-1} to a height of 700 m a.s.l., with stronger winds aloft (~10 m s^{-1} at 1800 m a.s.l.).

In addition to the seasonal and diurnal changes the basin's diurnal ABL mixing described above, the combined radon-based mixing scheme also detected periods associated with mixing changes at synoptic timescales (so-called PTI events) in winter and autumn (Figures 3a and 4c, class #6). As discussed by Kikaj et al. (2019a, 2019c), PTI periods are controlled by a high-pressure ridge (originating east of Ljubljana) that leads to the development of basin capping inversion layer. These conditions

usually persist for few days to a week. At Ljubljana the winter snow cover led to an intensification and longer duration of PTI conditions (Table 2; 30% of winter observations), consistent with the findings of Whiteman et al. (2004). In both autumn and winter, however, the diurnal trends of $\Delta T/\Delta z$ were similar, although winter peak average $\Delta T/\Delta z$ was a factor of 2 higher than in autumn (Figure 3a, class #6), emphasizing that the strongest and most persistent thermodynamic stability conditions occurred on winter PTI days. Based on the vertical air temperature profile in Figure 4c the sonde-derived lapse rate over the depth of the basin (300 to 1200 m) under class #6 conditions was +1 °C km^{-1}, indicative of overall stability. Within the basin atmosphere, however, more structure is evident. On average a strong surface inversion (at ~20 m) is evident, with a second inversion around 700 m a.s.l., and from this point until around 1400 m a.s.l. the atmosphere is clearly tending toward stability (Figure 4c). The elevated inversions, which effectively decouple much of the basin atmosphere from the free troposphere above, are a result of the subsidence and low gradient winds associated with anticyclonic systems. Once decoupled from the free troposphere, the lower atmosphere of the basin is free to develop a local dynamic of its own (Largeron and Staquet, 2016b), including a thermal basin wind system involving katabatic winds from the NE-E (not shown). Winds of class #6 events within the northeast-east-oriented Ljubljana basin were found to be almost calm (Figures 3b and 4).

Our comparison of radiosonde temperature profiles with the pseudo-vertical temperature gradients showed that pseudo-vertical temperature gradient method was a good proxy at our site for the state of the basin atmosphere on winter mornings. If more frequent sonde releases were available, it would be good to evaluate the $\Delta T/\Delta z$ observations over more of the diurnal cycle.

The main advantages of the pseudo-vertical temperature gradient method over radiosondes is that measurements can be made easily, economically and continuously, 24-hours a day, while radiosondes are usually only launched between 1–4 times per day, depending on the site. Most importantly, however, atmospheric mixing classification based on single-height, near-surface radon measurements alone (i.e. independent of all meteorological measurements), has successfully formed self-consistent groups of both near-surface and vertical profile atmospheric characteristics.

3.3 Variability of pollution within radon-based mixing classes

Selected air pollutants (BC, NO_2, CO, PM_{10}, SO_2, O_3), classified within the six radon-based mixing classes in each season, are presented in Figure 5 according to their main sources: BC_{tr}, NO_2 (traffic; Figure 5a); CO, PM_{10} (combination of traffic, combustion and dust), BC_{bb} (combustion) (Figure 5b); and SO_2 and O_3 (industrial and electricity production and secondary pollutant) (Figure 5c). While near-surface radon concentrations are a good proxy for the behavior of primary pollutants with near-surface sources in the urban "zone of habitation" (lowest several meters of the urban atmosphere), it should be noted that the relative response (radon accumulation) magnitudes across the diurnal cycle can differ substantially with seasonal due to variability of the radon source function. The criteria for radon-based stability classification therefore need to be determined separately for each season.

At any given location the amplitude of pollutant diurnal cycles is mainly driven by the interaction between the spatial and temporal heterogeneity of sources and their strengths, and variability of the atmospheric mixing state on diurnal, synoptic and seasonal timescales. From Figures 5a and 5b it is clearly evident that radon-based mixing classes indicate a consistent, gradual

increase in BC_{tr}, NO_2, CO, PM_{10}, and BC_{bb} concentrations from near-neutral (class #2) to PTI (class #6) conditions. It should be noted that due to instrument malfunctions autumn BC and spring CO data are missing. SO_2 concentrations (Figure 5c) often decreased with increasing atmospheric stability, indicating that SO_2 mainly derives from sources remote from Ljubljana. However, a tendency for SO_2 to increase during the rush hour periods shows that there is a small local SO_2 contribution (e.g., diesel fuelled vehicles).

The most pronounced seasonal cycle of BC_{tr}, NO_2, CO, PM_{10}, BC_{bb}, and SO_2 is observed in mixing classes #4 and #5, with lower concentrations in summer/spring and higher in winter/autumn (Figures 5a, 5b and 5c). The fact that primary pollutant composites showed opposing seasonal trends of nocturnal accumulation to those of radon (discussed in Section 3.1; Figure 2) is attributable to opposing seasonality of source strengths (the radon source function reduces from summer to winter, whereas the opposite is true for the source strengths of many primary pollutants; especially those related to domestic heating and electricity production) (EEA, 2014).

Only during classes #4 and #5 conditions do the traffic related (BC_{tr}, NO_2, CO) pollutants show a consistent clear bimodal diurnal cycle with one peak in morning and other in afternoon hours (Ježek et al., 2018). As evident in Figures 5a and 5b (CO), there is a time lag of the pollution peak between seasons; in winter/autumn the morning peak appears later (~08:00 LT) than in summer/spring (~06:00 LT). In the afternoon, accumulation of near-surface emissions begins around 16:00 LT in autumn and winter, but not until 18:00 LT in summer and spring. These features are attributable to the combined influence of morning/evening 'rush hour' periods, and the seasonal change in sunlight hours, necessary for the breakup or formation of the nocturnal inversion ($\Delta T/\Delta z \leq -6.5$°C km^{-1}; Figure 3a). Among the traffic related pollutants, the winter diurnal cycle of CO (Figure 5b) is particularly interesting, showing more similarity with combustion dominated sources (BC_{bb} and PM_{10}) (Figure 5b), which suggests that a significant proportion of the observed CO at this time might be derived from additional non-traffic related sources (e.g., domestic heating). The pronounced winter/autumn diurnal peaks of CO, BC_{bb}, PM_{10} concentrations occur between 21:00 LT and 23:00 LT (Figure 5b), the time when more intensive residential heating is used, and remain higher for several hours. As expected, BC_{bb} (specifically related to biomass burning) was present in a very low concentration within all mixing classes in summer (average ~0.2 μg m^{-3}) and spring (average ~0.4 μg m^{-3}) (Figure 5b).

In classes #4 and #5, BC_{tr}, NO_2, CO, PM_{10}, BC_{bb} concentrations attain secondary minimum values in the early morning (03:00–05:00 LT; Figures 5a and 5b) when light katabatic drainage (NE) winds flush away some of the urban pollution. A similar nocturnal "flushing" of urban pollutants has been reported for Bern, Switzerland by Williams et al. (2016), for Grünloch basin in the eastern Austrian Alps by Lehner et al. (2017) and for Zgierz, Poland by Chambers and Podstawczyńska (2019).

Under class #6 (PTI) conditions, which appear only in autumn and winter, the diurnal cycles of primary pollutants are similar to those in classes #4 and #5 (Figures 5a, 5b and 5c) but with significantly elevated concentrations across the whole diurnal cycle. The daytime concentrations of pollutants under PTI conditions do not drop to the low daytime levels characteristic of class #5 attributable to reduced opportunity for convective mixing from the basin (Figure 3a). The stagnant anticyclonic class #6 conditions inhibit the daytime mixing that usually disperses accumulated nocturnal pollution on class #5 days. On PTI days concentrations of BC_{tr}, NO_2, CO, BC_{bb}, and PM_{10} are approximately 2-fold higher in winter than in autumn, which is in good

agreement with the 2-fold increased intensity of winter $\Delta T/\Delta z$ for similar conditions reported in Figure 3a. The SO_2 PTI diurnal cycle appears out of phase with other primary pollutant (Figure 5c), characterized by maximum values around noon (when light convection briefly reconnects the local basin atmosphere to the regional atmosphere; Fig 3a), and minimum values at night. The same diurnal trend of SO_2 was found also in other classes (#2 to #5). The lack of nocturnal SO_2 accumulation likely indicates a lack of substantial local SO_2 sources since the nocturnal inversion layer isolates surface measurements from distant sources. Consequently, while domestic heating and traffic are expected to contribute a little to SO_2 concentrations in Ljubljana during the cold days, remote SO_2 sources dominate in the winter; more detailed information on this matter is provided by Kikaj et al. (2019c).

In windy conditions (classes #2 to #3) primary pollutants of local origin are usually efficiently dispersed. On average, peak BC_{tr}, NO_2, CO, BC_{bb} concentrations in class #2 are a factor of 2–3 lower than in class #5 (Figures 5a and 5b). Whereas PM_{10} concentrations in classes #2 and #3 (peak average ~35 μg m^{-3}), particularly those of spring season, show to be the highest (Figure 5b). Gunderstrom et al. (2015) also reported enhanced PM_{10} concentrations under windy conditions in Gothenburg, Sweden, where strong winds can result in the resuspension of coarser particles such as dust from roads and other surfaces. However, increased PM_{10} concentrations on classes #2 and #3 days can also be associated with long-range transport (Pateraki et al., 2012). It is estimated that 80–120 Tg of Sahara dust flows into the MB annually (Kaskaoutis et al., 2019b; D'Almeida, 1986). The dust events exhibit a distinct seasonality maximizing in spring due to the intensification of westerlies wind and development of the Sharav cyclones (Kaskaoutis et al., 2019a, 2019b). Slovenia was covered by a higher amount of Sahara dust (ARSO, 2018) in April 2018 (Figure 5b). As already discussed in Section 3.2, atmospheric mixing classes #2 and #3 are characterized by higher wind speeds (90^{th} percentile value of 3.2 m s^{-1}) in all seasons, particularly during spring days when winds are the highest from the WSW and SW, ideal conditions to support long-range air mass transport from the Sahara Desert. This is further evidence of the efficacy of the radon-based mixing classification scheme to consistently and effectively allow separate investigation of local and remote contributions to urban air quality.

Compared with radon and locally-sourced pollutants, diurnal ozone concentrations exhibited an almost inverse response to the atmospheric mixing (Figure 5c). Local O_3 production and depletion through NO_x and VOC chemistry, downward mixing of O_3 from the free troposphere, surface O_3 dry deposition and, to some extent, horizontal transportation, all played important roles in its diurnal cycles for each mixing class. During the periods with high nocturnal wind speeds (classes #2 and #3) the highest nocturnal O_3 concentrations were found due to remotely-sourced O_3 being mixed down to the surface from the residual layer or troposphere, as discussed by Querol et al. (2018). By comparing the windy nights (classes #2 and #3) of autumn and winter seasons, the lowest nighttime O_3 values were found in autumn season. Since the average autumn wind speeds were lower, this confirms the importance of the wind speeds in O_3 mixing down from the free troposphere. The strong influence of sunlight and temperature on near-surface O_3 formation is clearly evident when comparing daytime concentrations between seasons and mixing classes (Figure 5c). The daytime of classes #4 and #5 is associated with the clear sky and most intense solar radiation (see Table 1 in Chambers and Podstawczyńska et al. (2019)), which conditions led to the highest overall O_3 concentrations, particularly in spring and summer.

Despite higher concentrations of precursor species in winter, lower temperatures and the reduction in sunlight result in lowest daytime ozone concentrations in winter/autumn (class #5: peak average 42 /77 μg m^{-3}) than spring/summer (class #5: peak average 106/118 μg m^{-3}). However, as nocturnal wind speeds decrease from class #3 to #5 a shallow inversion layer forms, a significant decrease of nocturnal O_3 concentrations is observed due to the NO titration. While, autumn and winter O_3 is completely titrated during PTI nights with a slightly increases during the daytime, this cycle indicates the formation of a shallow nocturnal inversion layer within basin inversion layer around sunset that erodes after sunrise.

3.4 Outdoor air pollution in Ljubljana and EU and WHO air quality guidelines

In Ljubljana, the concentrations of CO, NO_2, and SO_2 in the outdoor air were well below hourly and daily maximum values of EU and WHO guidelines for all mixing classes and in all seasons of the year 2018. As reported by Pucer et al. (2018), in the last years the trend of SO_2 and NO_2 concentrations has significantly decreased in Slovenia.

Concentrations of BC, PM_{10} and O_3, which tend to be increased or exceed limits of EU and WHO guidelines (WHO, 2000, 2006; EU, 2008), are presented as box and whiskers plots of the radon-based mixing classes for each season (Figures 6 and 7). Box and whiskers plots of the BC_{tt} and BC_{bb} concentrations are shown in Figures 6a and 6b (autumn data are missing). Based on the breadth of the boxplots distribution, BC concentrations from both sources showed to be significantly elevated in winter during the most stable (class #5) and PTI (class #6) conditions, with the highest median BC concentration encountered from the traffic (2.2 μg m^{-3}; Figure 6a). It has to be pointed that the levels of BC are not yet regulated by either EU or WHO. However, as reported, already short-term (2 hours) exposure to BC were associated with changes in lung functions and signs of arterial stiffness (Janssen et al., 2011; Dons et al., 2012; Sinharay et al., 2018).

PM_{10} concentrations, as seen in the box and whisker plots of Figure 7a, are under 50 μg m^{-3} (PM_{10} threshold value of EU and WHO guidelines) in the near-neutral (class #2) conditions of all seasons. It is clear, however, that the upper whiskers (90^{th} percentile) of the PM_{10} concentrations exceed both the EU and WHO threshold values (50 μg m^{-3}) in spring, autumn and winter in the other mixing classes (#3 to #6). In the winter PTI conditions, on the other hand, even the upper quartile excceds the threshould value and the 90^{th} percentile values reach concentrations of 100 μg m^{-3}. The variability of PM_{10} concentrations associated with classes (#5 and #6) for particular winter is discussed in more detail in Kikaj et al. (2019c).

In winter and autumn, none of the hourly values of O_3 exceed the EU and WHO guidelines values (Figure 7b) but this was not the case for summer and spring. For the all mixing conditions (classes #2 to #5) in spring and summer 90^{th} percentile O_3 concentrations exceed the guideline values of both EU and WHO (120 μg m^{-3} for EU; 100 μg m^{-3} for WHO). Based on the ARSO data for summer 2018, max daily 8-hour mean of O_3 concentration was exceeded in Ljubljana 22 times (http://www.arso.gov.si/en/air/data/).

A clear benefit of using the radon-based stability classification approach is that each mixing category represents a clearly defined fraction of time each year and season (Table 2), making results easily applicable to exposure studies. Furthermore, the ability to characterize meteorological quantities within mixing categories that result in pollution exceedance events is expected

to help with efforts to predict such events using other available tools (measurement networks or regional models). Diurnal composites of meteorological and air quality parameters formed within better constrained mixing conditions, as possible with the radon-based method, help to account for effects of sub-grid-scale source heterogeneity and are therefore also well-suited to evaluating the performance of urban air quality models (Chambers et al., 2019a); an essential task for improved urban planning.

4 Conclusions

The main aim of this study was to demonstrate the efficacy and efficiency of the new combined diurnal and synoptic timescale radon-based atmospheric stability classification scheme for assessing urban air quality year round. The classification scheme and results presented were based on one full year (Dec 2017–Nov 2018) of radon, meteorological and air quality observations in Ljubljana (Slovenia), located in a subalpine basin. Five radon-based mixing classes (#1 to #5) were defined for each of the four seasons, representing mixing conditions on diurnal timescales. In winter and autumn, an additional class (#6), devoted to the "persistent temperature inversions" (PTI, periods associated with changes at synoptic scale), was added. Due to the complex topography of Ljubljana, with generally calm wind and high number of foggy days, this additional class is crucial for more accurate assessment of persistent atmospheric pollution events.

The strong observed seasonality in primary pollutant (BC, NO_2, SO_2, CO, and PM_{10}) concentrations within the six radon-based mixing classes, characterized by a summer/spring minimum and winter/autumn maximum, is attributable to a combination of changing atmospheric state (on both diurnal and synoptic timescales), as well as additional cold-season combustion sources. Particularly in mixing classes #4 and #5, whose nights are characterized by weak katabatic winds and formation of nocturnal temperature inversion, substantial seasonal differences are noted, both in the time and duration of peak pollutant concentrations within the diurnal cycle. Within the composites of classes #4 and #5, there were two periods when primary pollutant concentrations reached minimum values: (i) in the morning (03:00–05:00 LT) when light katabatic drainage winds flush away some of the urban pollution, and (ii) in the afternoon (11:00–15:00 LT) when vertical mixing was the highest (deepest ABL). However, the pollutant concentrations remained constantly increased during the winter and autumn PTI conditions; their daytime concentrations did not decrease to the low daytime levels characteristic of class #5 conditions. Pseudo vertical temperature gradient measurements indicated very limited opportunity for convective mixing of pollutants from the basin atmosphere in winter and autumn under classes #5 and #6 conditions. Under the more windy conditions (classes #2 and #3) in spring season radon-based method clearly illustrates that PM_{10} concentrations were dominated by remote sources (primarily from the Sahara Desert dust). By contrast, the diurnal characteristics of SO_2 and O_3 concentrations indicated both local and remote sources. In general, a little diurnal accumulation of local pollutants (BC, NO_2, CO and PM_{10}) was observed at wind speeds ≥ 1.5 m s^{-1}.

Box and whiskers plots indicate that the upper whisker of PM_{10} concentrations exceeds both EU and WHO threshold values (50 μg m^{-3}) in spring, autumn and winter (mixing classes #3 to #6), and especially during the winter PTI conditions (class #6).

On other hand, the upper whisker of O_3 concentrations exceeds the guideline values of both EU and WHO guidelines in spring and summer (classes #2 to #5).

The demonstrated ability of the radon-based atmospheric stability classification to consistently distinguish between subtle changes in atmospheric mixing state at seasonal, synoptic and diurnal timescale indicates that it may be a powerful tool for the development of new control actions of air pollution prevention.

Acknowledgements

The authors acknowledge the financial support from the Slovenian Research Agency (research core funding No. P1-0143 and research project STRAP – Sources, TRAnsport and fate of persistent air Pollutants in the environment of Slovenia No. J1-1716) and from the Public Scholarship, Development, Disability and Maintenance Fund of the Republic of Slovenia (contract No. 11011- 44/2016-18). The authors also gratefully acknowledge the Slovenian Environment Agency for the permission provided and the assistance by installing the weather instrument shelter for radon monitoring on their land and for providing the meteorological and air quality data.

Code/Data availability

Meteorological and air quality data are collected and supplied by the National Meteorological Service at the Environmental Agency of the Republic of Slovenia (ARSO) (https://meteo. arso.gov.si/, last access: 22 April 2020). Atmospheric radon data will be made available on request.

Competing interests

The authors declare that they have no conflict of interest.

Author contribution

The investigation was jointly conceptualized by DK, SC, MK and JV. Radon monitoring instrumentation was deployed and managed by DK and JV, and black carbon data by MK. Data collection and curation was performed by DK. Formal data analysis was performed by DK and SC. Acquisition of funding for the research was arranged by JV. The research methodology was jointly developed by DK and SC and investigation jointly conducted by DK and JV. The project was administered by JV, with JV and SC responsible for supervision. All visualization of data, concepts, and results was performed by DK. DK wrote the complete original draft of the paper, which was subsequently edited and reviewed jointly by DK, SC, MK and JV.

Tables:

Table 1: Ground-based weather station name, abbreviation, position and elevation above the sea level (a.s.l.) (adapted from Kikaj et al. (2019a)).

Weather station name	Acronym	Latitude (º N)	Longitude (º E)	Elevation a.s.l. (m)
Litija	Li	46º06'	14º81'	268
Ljubljana-Bežigrad	LjB	46º07'	14º52'	299
Letališče Jožeta Pučnika Ljubljana	LLj	46º21'	14º47'	364
Topol	T	46º09'	14º37'	695
Pasja Ravan	PR	46º09'	14º22'	1019
Kum	K	46º08'	15º07'	1211
Krvavec	Kr	46º29'	14º53'	1742

Table 2: Summary of the 24-hour radon-based atmospheric mixing classes (#1 to #5 diurnal, #6 synoptic) assigned for one year of measurements in the Ljubljana basin, and duration of conditions (%) for each mixing class in each of the four seasons.

24-h mixing class	Night-time mixing conditions	Daytime mixing conditions	Winter %	Spring %	Summer %	Autumn %
#1	Mixed fetch	Mixed fetch	7	12	11	8
#2	Near-neutral	Near-neutral	15	27	24	12
#3	Weakly stable	Weakly unstable	19	20	26	22
#4	Moderately stable	Moderately unstable	15	22	22	23
#5	Strongly stable	Strongly unstable	14	19	17	15
#6	Persistent temperature inversion	Persistent temperature inversion	30	NA	NA	20

Figures:

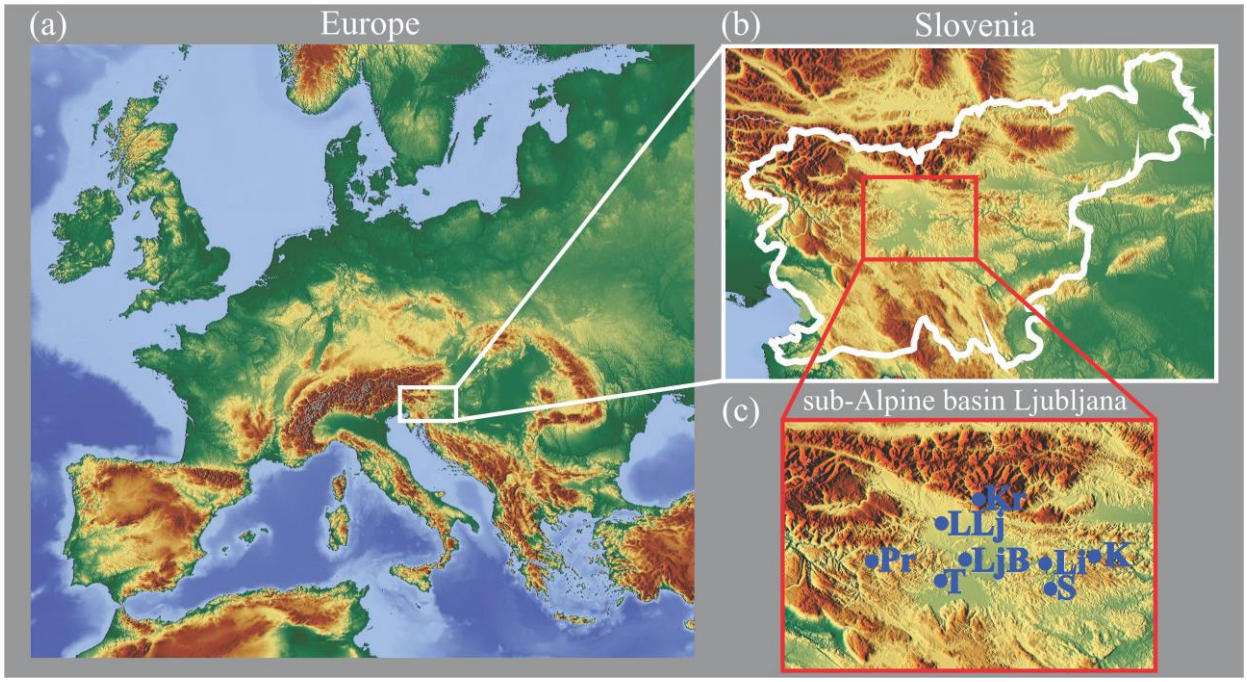


Figure 1: a) Location of Slovenia within Europe, b) topographic map of Slovenia with the location of Ljubljana indicated, and c) topographic map of the Ljubljana basin, with the locations of automatic weather stations indicated. ©OpenStreetMap contributors 2020. Distributed under a Creative Commons BY-SA License.

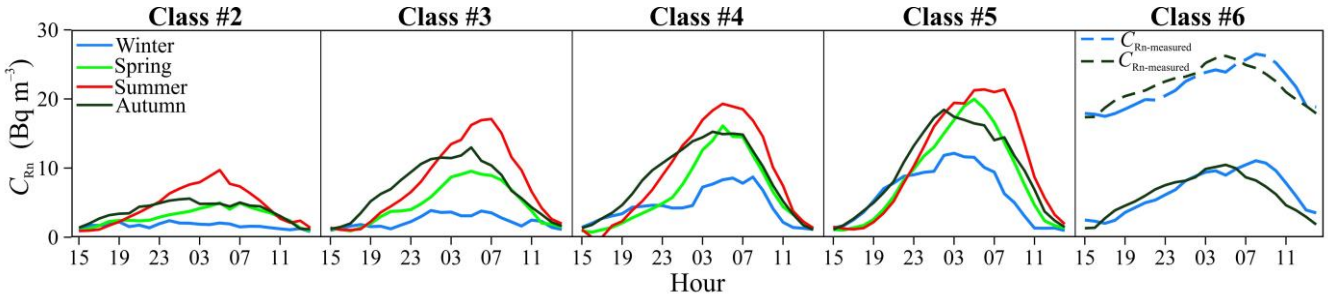


Figure 2: Diurnal composite plots of mixing-related radon concentration by season and radon-based atmospheric mixing classes.

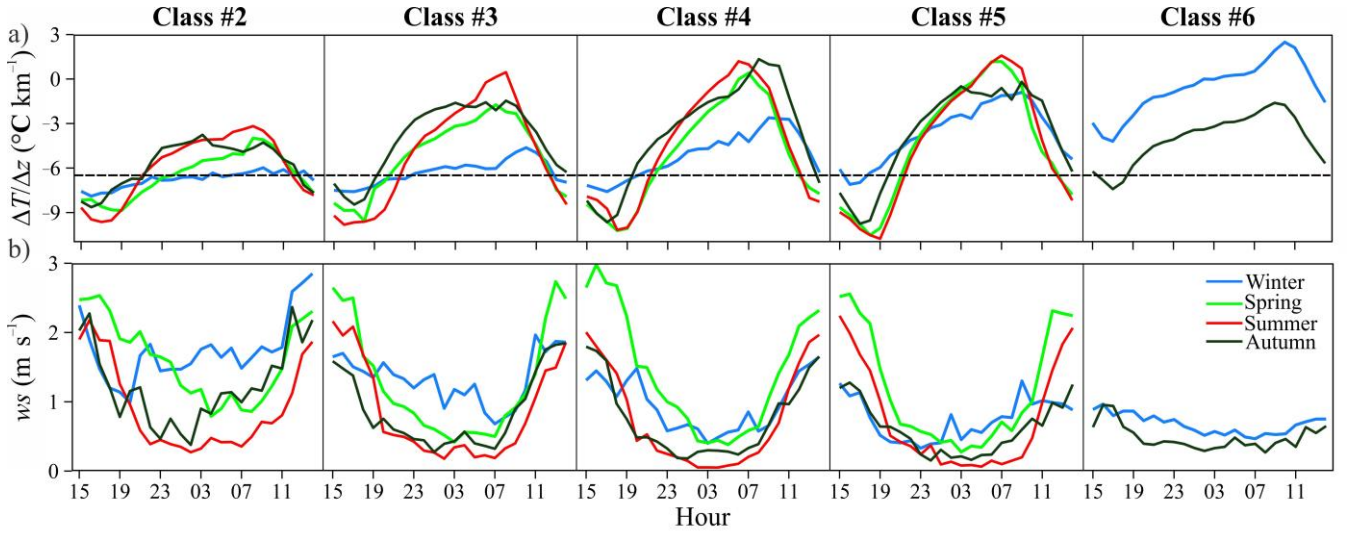


Figure 3: Diurnal composite plots of a) pseudo-vertical air temperature gradient, and b) wind speed by season and radon-based atmospheric mixing classes.

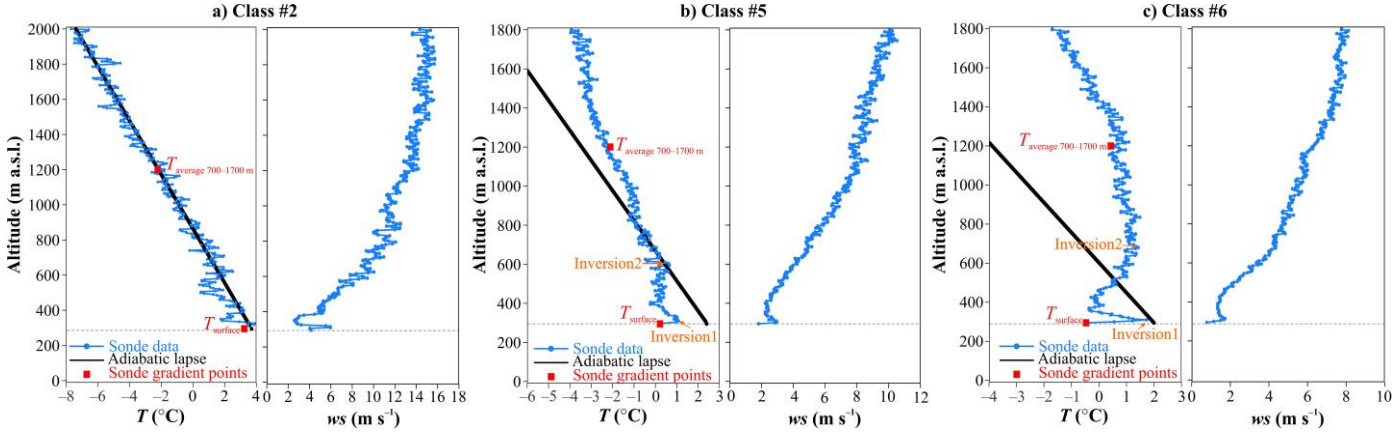


Figure 4: Morning vertical profile of air temperature and wind speed within three radon-based mixing classes in winter season: a) class #2 (near-neutral), b) class #5 (mostly stable), c) class #6 (persistent temperature inversion).

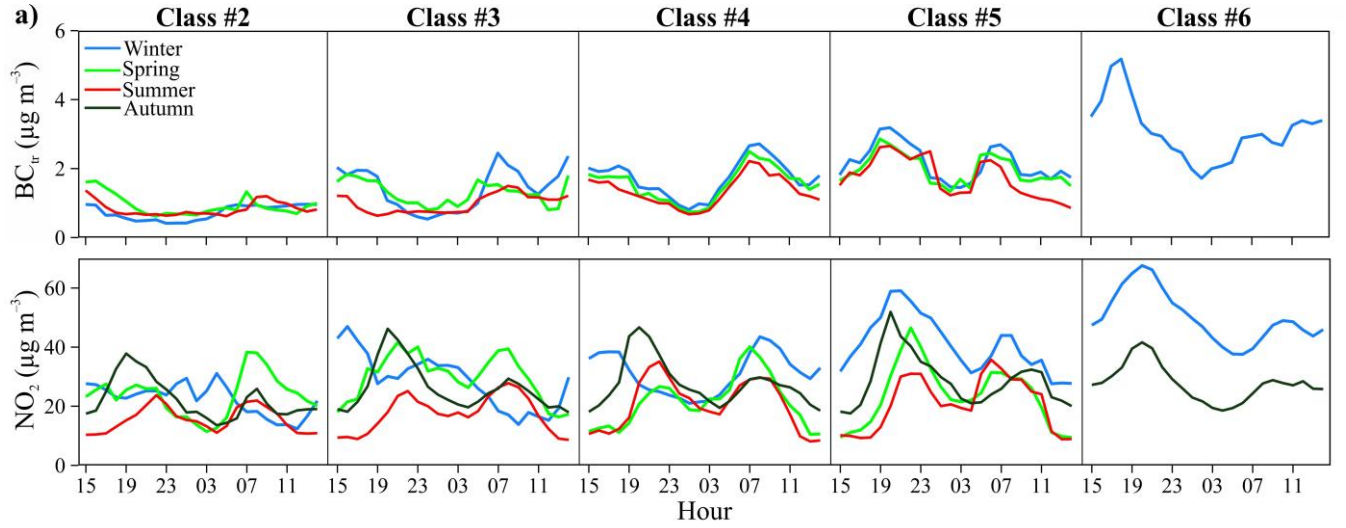


Figure 5a: Diurnal composite plots of BC_{tr}, and NO_2 (air pollutants related to traffic source) by season and radon-based atmospheric mixing classes.

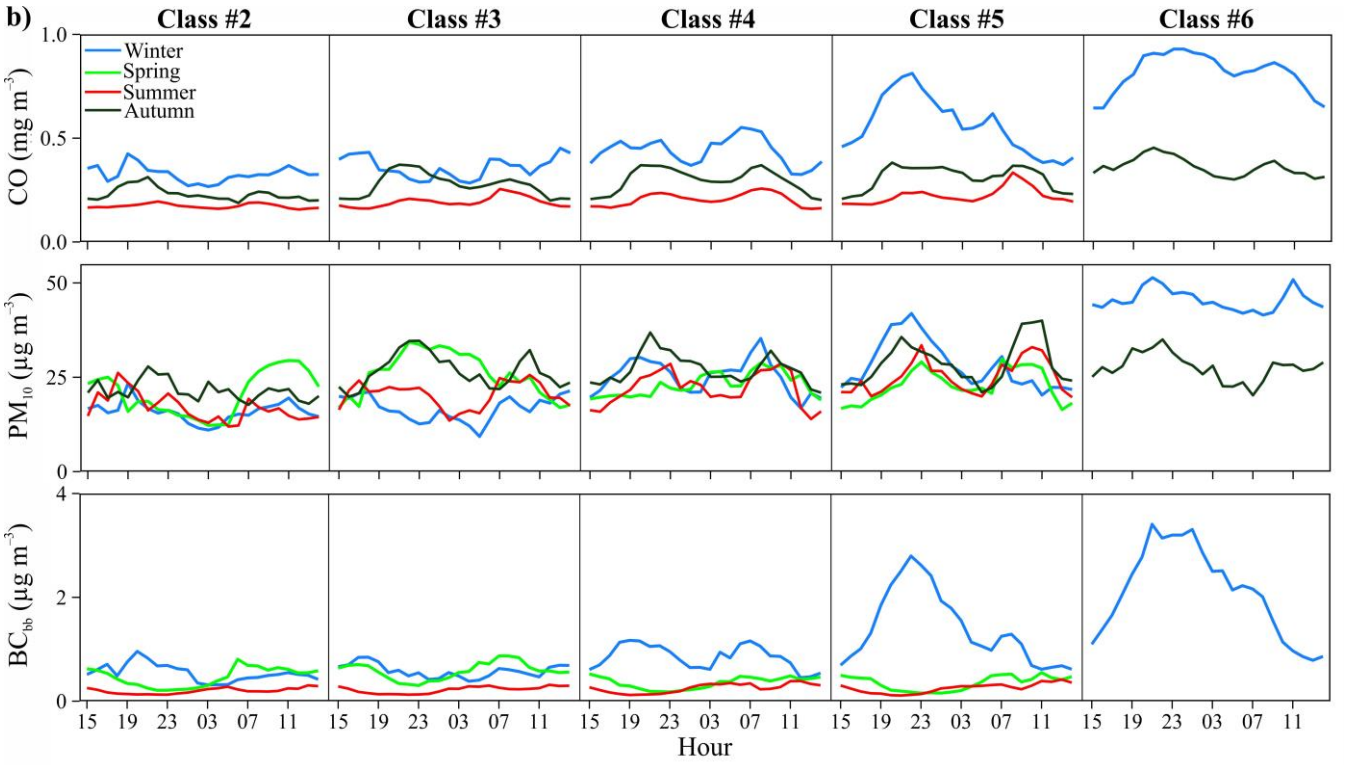


Figure 5b: Diurnal composite plots of CO, PM_{10} and BC_{bb} (air pollutants related to traffic and combustion sources) by season and radon-based atmospheric mixing classes.

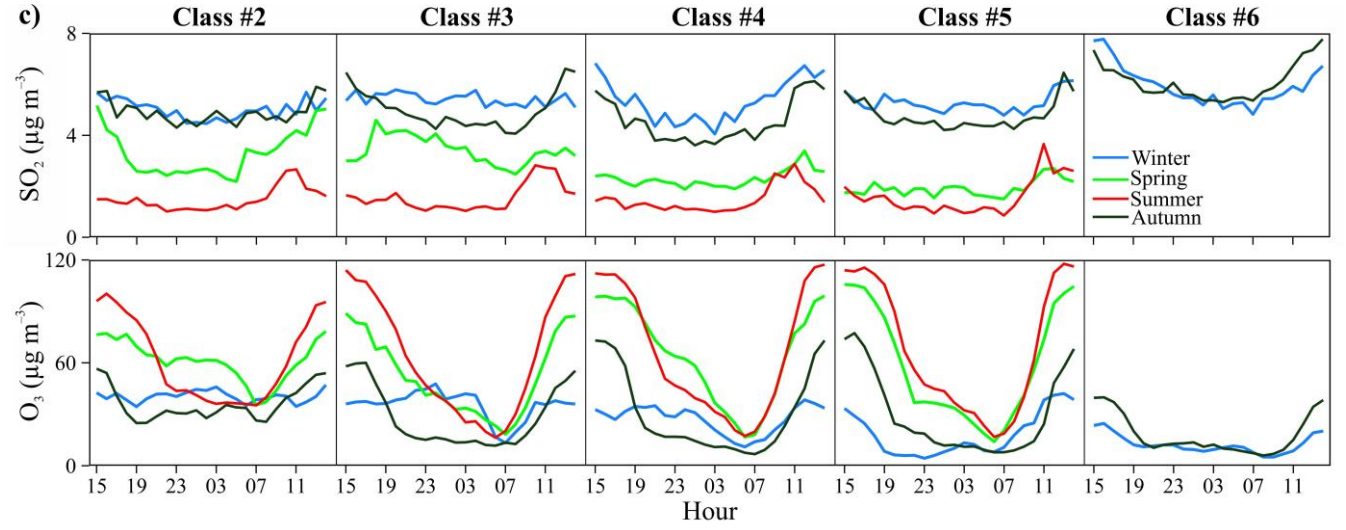


Figure 5c: Diurnal composite plots of SO_2 and O_3 (air pollutants related to industrial and electricity production sources) by season and six radon-based atmospheric mixing classes.

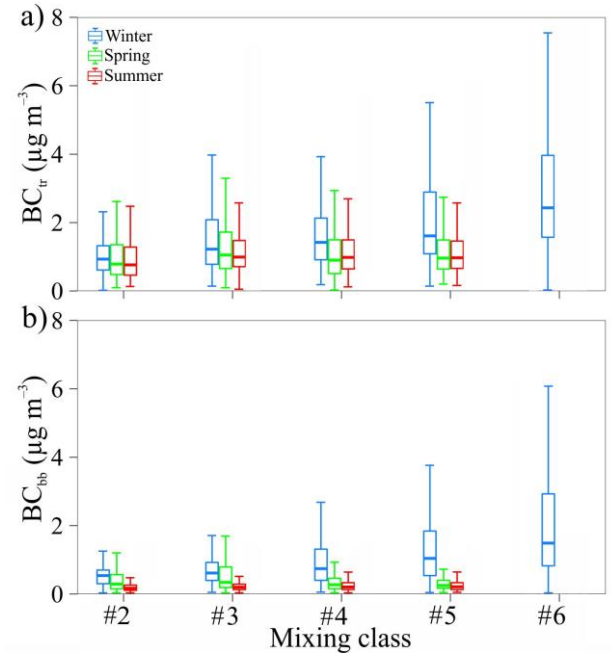


Figure 6: Box and whisker plots of: a) BC_{tr} and b) BC_{bb} grouped by each radon-based atmospheric mixing classes and season (horizontal line: median, boxes: the 25th–75th percentile, whiskers: 5th–90th percentile).

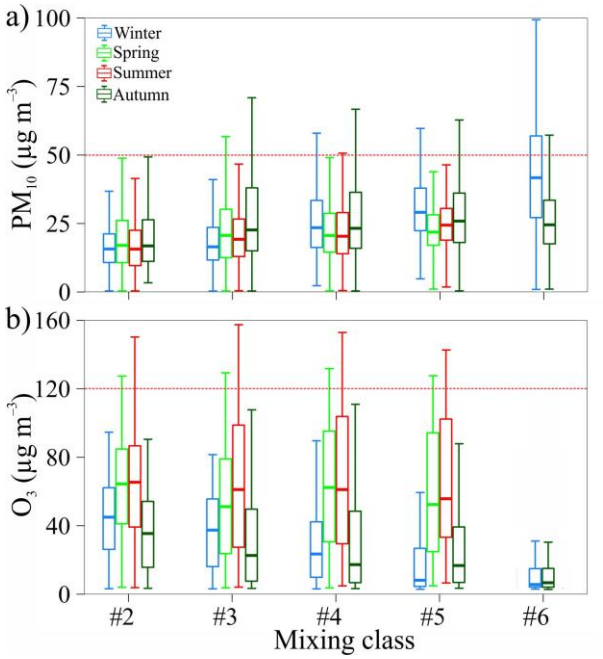


Figure 7: Box and whisker plots of: a) PM_{10} and b) O_3 grouped by each radon-based atmospheric mixing classes and season (horizontal line: median, boxes: the 25th–75th percentile, whiskers: 5th–90th percentile).

References

Allegrini, I., Febo, A., Pasini, A., Schiarini, S.: Monitoring of the nocturnal mixed layer by means of particulate radon progeny measurement, J. Geophys. Res. 99, 18765−18777, 1994.

Anttila, P., Stefanovska, A., Nestorovska-Krsteska, A., Grozdanovski, L., Atanasov, I., Golubov, N., Ristevski, P., Toceva, M., Lappi, S. and Walden, J.: Characterisation of extreme air pollution episodes in an urban valley in the Balkan Peninsula, Air Qual. Atmos. Heal., 9(2), 129–141, doi:10.1007/s11869-015-0326-7, 2016

ARSO: Slovenian Environment Agency (Slovenian: Agencija Republike Slovenije za Okolje): Climate characteristics of Ljubljana - Wind Rose for the City of Ljubljana, 2017.

Avino, P. and Manigrasso, M.: Ten-year measurements of gaseous pollutants in urban air by an open-path analyzer, Atmos. Environ., 42(18), 4138–4148, 2008.

Beaver, S., Palazoglu, A., Singh, A., Soong, S. T., and Tanrikulu, S.: Identification of weather patterns impacting 24-h average fine particulate matter pollution, Atmos. Environ., 44(14), 1761–1771, 2010.

Beeston, M., Grgić, I., Johannes, T. van E., Iskra, I., Kapun, G. and Močnik, G.: Chemical and morphological characterization of aerosol particles at Mt. Krvavec, Slovenia, during the Eyjafjallajökull Icelandic volcanic eruption, Environ. Sci. Pollut. Res., 19(1), 235–243, doi:10.1007/s11356-011-0563-8, 2011.

Buchanan, C. M., Beverland, I. J. and Heal, M. R.: The influence of weather-type and long-range transport on airborne particle concentraions in Edinburgh, UK, Atmos. Environ., 36(34), 5343–5354, 2002.

Chambers S. D., Guérette, E-A., Monk, K., Griffiths, A. D., Zhang Y, Duc, H., Cope, M., Emmerson, K. M., Chang, L.T., Silver, J.D., Utembe, S., Crawford, J., Williams, A. G. and Keywood, M.: Skill-testing chemical transport models across contrasting atmospheric mixing states using Radon-222, Atmosphere 10(1), 25, https://doi.org/10.3390/atmos10010025, 2019a.

Chambers, S. D. and Podstawczyńska, A.: Improved method for characterising temporal variability in urban air quality part II: Particulate matter and precursors in central Poland, Atmos. Environ., 219, 117040, doi:10.1016/j.atmosenv.2019.117040, 2019.

Chambers, S. D., Podstawczyńska, A., Pawlak, W., Fortuniak, K., Williams, A. and Griffiths, A.: Characterising the state of the urban surface layer using Radon-222, J. Geophys. Res. Atmos., 124(2), 770–788, 2019b.

Chambers, S. D., Podstawczyńska, A., Williams, A. G. and Pawlak, W.: Characterising the influence of atmospheric mixing state on urban heat island intensity using Radon-222, Atmos. Environ., 147, 355–368, doi:10.1016/j.atmosenv.2016.10.026, 2016.

Chambers, S.D., Wang, F., Williams, A.G., Deng, X., Zhang, H., Lonati, G., Crawford, J, Griffiths, A.D., Ianniello, A. and Allegrini, I.: Quantifying the influences of atmospheric stability on air pollution in Lanzhou, China, using a radon-based stability monitor, Atmos. Environ., 107, 233−243, 2015b.

Chambers, S.D., Williams, A.G., Crawford, J. and Griffiths, A.D.: On the use of radon for quantifying the effects of atmospheric stability on urban emissions, Atmos. Chem. Phys., 15, 1175−1190. https://doi.org/10.5194/acp-15-1175-2015, 2015.

Chambers, S., Williams, A.G., Zahorowski, W., Griffiths, A. and Crawford, J.: Separating remote fetch and local mixing influences on vertical radon measurements in the lower atmosphere, Tellus, Ser. B Chem. Phys. Meteorol., 63, 843−859. https://doi.org/10.1111/j.1600-0889.2011.00565.x, 2011.

Conceição, R., Silva, H. G., Mirão, J., Gostein, M., Fialho, L., Narvarte, L. and Collares-pereira, M.: Saharan dust transport to Europe and its impact on photovoltaic performance: A case study of soiling in Portugal, Sol. Energy, 160 (November 2017), 94–102, doi:10.1016/j.solener.2017.11.059, 2018.

Cohen, L.D., Barr, S., Krablin, R. and Newstein, H.: Steady-state vertical turbulent diffusion of radon, J. Geophys. Res., 77, 2654–2668, 1972.

Čanić, K. Š., Kavčič, I., and Klaić, Z. B.: An episode of Saharan dust over Croatia. Newsletter (European Association for the Science of Air Pollution. Online), 69, 2009.

D'Almeida, G.: A model for Saharan dust transport, J. Clim. Appl. Meteorol., 25(7), 903–916, 1986.

EEA: Air quality in Europe — 2018 report, 88 pp., 2018.

EEA: Air pollution fact sheet Slovenia — 2014 report, 20 pp., 2014.

EU: Directive2008/50/EC of the European Parliament and of the Council of 21 May 2008 on ambient air quality and cleaner air of Europe (Oj L152, 11.6.2008,) (https://eur-lex.europa.eu/eli/dir/2008/50/oj) accessed 22 December 2019, 44 pp., 2008.

Díaz, J., Linares, C., Carmona, R., Russo, A., Ortiz, C., Salvador, P., and Trigo, R. M.: Saharan dust intrusions in Spain: health impacts and associated synoptic conditions, Environ. Res., 156, 455–467, 2017.

Dons, E., Int Panis, L., Van Poppel, M., Theunis, J. and Wets, G.: Personal exposure to black carbon in transport microenvironments, Atmos. Environ., 55, 392–398. https://doi.org/10.1016/j.atmosenv.2012.03.020, 2012.

Fontan, J., Guedalia, D., Druilhet, A., and Lopez, A.: Une methode de mesure de la stabilite verticale de l'atmosphere pres du sol, Bound. Lay. Meteorol., 17(1), 3–14, 1979.

Fujinami, N., and Esaka, S.: Variations in radon 222 daughter concentrations in surface air with atmospheric stability, J. Geophys. Res. Atmos., 92(D1), 1041–1043, 1987.

Galmarini, S.: One year of ^{222}Rn concentration in the atmospheric surface laye,. Atmos. Chem. Phys., 6(10), 2865–2886, 2006.

Gerasopoulos, E., Kouvarakis, G., Vrekoussis, M., Kanakidou, M. and Mihalopoulos, N.: Ozone variability in the marine boundary layer of the eastern Mediterranean based on 7-year observations, J. Geophys. Res. Atmos., 110(D15), 1–12, 2005.

Gobbi, G. P., Barnaba, F., Liberto, L. Di, Bolignano, A., Lucarelli, F., Nava, S., Perrino, C., Pietrodangelo, A., Basart, S., Costabile, F., Dionisi, D., Rizza, U., Canepari, S. and Sozzi, R.: An inclusive view of Saharan dust advections to Italy and the Central Mediterranean, Atmos. Environ., 201(November 2018), 242–256, doi:10.1016/j.atmosenv.2019.01.002, 2019.

Goudie, A. S.: Desert dust and human health disorders, Environ. Int., 63, 101–113, doi:10.1016/j.envint.2013.10.011, 2014.

Griffin, D. W.: Atmospheric movement of microorganisms in clouds of desert dust and implications for human health, Clin. Microbiol. Rev., 20(3), 459−477, doi:10.1128/CMR.00039-06, 2005.

Grundström, M., Hak, C., Chen, D., Hallquist, M. and Pleijel, H.: Variation and co-variation of PM_{10}, particle number concentration, NO_x and NO_2 in the urban air – Relationships with wind speed, vertical temperature gradient and weather type, Atmos. Environ., 120, 317–327, 2015.

Ivey C. E., Balachandran, S., Colgan, S., Hu, Y. and Holmes H. A.: Investigating fine particulate matter sources in Salt Lake City during persistent cold air pool events, Atmos. Environ., 213, 568–578, 2019.

Ježek, I., Blond, N., Skupinski, G., and Močnik, G.: The traffic emission-dispersion model for a Central-European city agrees with measured black carbon apportioned to traffic, Atmos. Environ., 184, 177–190, 2018.

He, T., Chen, Y., Stanič, S., Bergant, K., Gao, F. and Hua, D.: Properties of tropospheric aerosols observed over southwest Slovenia, J. Quant. Spectrosc. Radiat. Transf., 217, 380–387, doi:10.1016/j.jqsrt.2018.06.009, 2018.

Highwood, E. J. and Kinnersley, R. P.: When smoke gets in our eyes: The multiple impacts of atmospheric black carbon on climate, air quality and health, Environ. Int., 32, 560−566, doi:10.1016/j.envint.2005.12.003, 2006.

Hitzenberger, R., Ctyroky, P., Berner, A., Turšič, J., Podkrajšek, B. and Grgić, I.: Size distribution of black (BC) and total carbon (TC) in Vienna and Ljubljana, Chemosphere, 65(11), 2106–2113, doi:10.1016/j.chemosphere.2006.06.042, 2006.

Janssen, N.A.H., Hoek, G., Simic-lawson, M., Fischer, P., Bree, L. Van, Brink, H., Keuken, M., Atkinson, R.W., Anderson, H.R., Brunekreef, B. and Cassee, F.R.: Black carbon and health effects of airborne particles compared with PM_{10} and $PM_{2.5}$, Environ. Health Perspect., 119, 1691–1699. https://doi.org/10.1289/ehp.1003369, 2011.

Jędruszkiewicz, J., Czernecki, B. and Marosz, M.: The variability of PM_{10} and $PM_{2.5}$ concentrations in selected Polish agglomerations: the role of meteorological conditions, 2006–2016, Int. J. Environ. Health Res., 27(6), 441–462, doi:10.1080/09603123.2017.1379055, 2017.

Kallos, G., Astitha, M., Katsafados, P. and Chris, S.: Long-range transport of anthropogenically and naturally produced particulate matter in the Mediterranean and North Atlantic: current state of knowledge, J. Appl. Meteorol. Climatol., 46, 1230−1251, doi:10.1175/JAM2530.1, 2006.

Kahl, J.D.W. and Chapman, H.L.: Atmospheric stability characterization using the Pasquill method: A critical evaluation, Atmos. Environ., 187, 196–209. https://doi.org/10.1016/j.atmosenv.2018.05.058, 2018.

Karstens, U., Schwingshackl, C., Schmithüsen, D. and Levin, I.: A process-based ^{222}radon flux map for Europe and its comparison to long-term observations, Atmos. Chem. Phys., 15(22), 12845−12865, doi:10.5194/acp-15-12845-2015, 2015.

Kaskaoutis, D. G., Dumka, U. C., Rashki, A., Psiloglou, B. E., Gavriil, A., Mo, A., Petrinoli, K., Karagiannis, D. and Kambezidis, H. D.: Analysis of intense dust storms over the eastern Mediterranean in March 2018 : Impact on radiative forcing and Athens air quality, Atmos. Environ., 209, 23–39, doi:10.1016/j.atmosenv.2019.04.025, 2019a.

Kaskaoutis, D. G., Rashki, A., Dumka, U. C., Mo, A., Kambezidis, H. D., Psiloglou, B. E., Karagiannis, D., Petrinoli, K. and Gavriil, A.: Atmospheric dynamics associated with exceptionally dusty conditions over the eastern Mediterranean and Greece in March 2018, Atmos. Res., 218, 269–284, doi:10.1016/j.atmosres.2018.12.009, 2019b.

Kikaj, D. and Vaupotič, J.: Parameters influencing deviation of radon concentration from its typical diurnal pattern in the winter and summer seasons, Geol. Maced., 31, 157–170, 2017.

Kikaj, D., Vaupotič, J. and Chambers, S. D.: Identifying persistent temperature inversion events in a subalpine basin using radon-222, Atmos. Meas. Tech., 12(8), 4455–4477, 2019a.

Kikaj, D., Chambers, S. D. and Vaupotič, J.: Radon-based atmospheric stability classification in contrasting sub-Alpine and sub-Mediterranean environments, J. Environ. Radioact., 203, 125–134, doi:10.1016/j.jenvrad.2019.03.010, 2019b.

Kikaj, D., Chambers, S. D., Kobal, M., Crawford, J. and Vaupotič, J.: Characterising atmospheric controls on winter urban pollution in a topographic basin setting using Radon-222, Atmos. Res., 237, 104838, https://doi.org/10.1016/j.atmosres.2019.104838, 2019c.

Largeron, Y. and Staquet, C.: Persistent inversion dynamics and wintertime PM_{10} air pollution in Alpine valleys, Atmos. Environ., 135, 92−108, doi:10.1016/j.atmosenv.2016.03.045, 2016.

Lehner, M., Whiteman, C. D., and Dorninger, M.: Inversion build-up and cold-air outflow in a small Alpine sinkhole, Bound. Lay. Meteorol., 163(3), 497−522, 2017.

Lelieveld, J., Berresheim, H., Borrmann, S., Crutzen, P. J., Dentener, F. J., Fischer, H., Feichter, J., Flatau, P. J., Heland, J., Holzinger, R., Korrmann, R., Lawrence, M. G., Levin, Z., Markowicz, K. M., Mihalopoulos, N., Minikin, A., Stephanou, E. G., Stier, P., Traub, M. and Warneke, C.: Global air pollution crossroads over the Mediterranean, Science, 298, 794–799, 2002.

Tanja Murn and Matjaž Stepišnik: Intercomparison measurements of Radon-222 concentrations at ICJT (in Slovenian), December 2019.

Moses, H., Stehney, A.F., Lucas Jr, H.F.: The effect of meteorological variables upon the vertical and temporal distributions of atmospheric radon, J. Geophys. Res., 65, 1223–1238, 1960.

Omori, Y., Tohbo, I., Nagahama, H., Ishikawa, Y., Takahashi, M., Sato, H., and Sekine, T.: Variation of atmospheric radon concentration with bimodal seasonality, Radiat. Meas., 44, 1045−1050, 2009.

Pal, S., Lopez, M., Schmidt, M., Ramonet, M., Gibert, F., Xueref-Remy, I., and Ciais, P.: Investigation of the atmospheric boundary layer depth variability and its impact on the ^{222}Rn concentration at a rural site in France, J. Geophys. Res. Atmos., 120(2), 623–643, 2015.

Pateraki, S., Asimakopoulos, D. N., Flocas, H. A., Maggos, T. and Vasilakos, C.: The role of meteorology on different sized aerosol fractions (PM_{10}, $PM_{2.5}$, $PM_{2.5–10}$), Sci. Total Environ., 419, 124–135, 2012.

Pasquill, F.: The estimation of the dispersion of windborne material, Meteorol. Mag., 90, 33–49, 1961.

Pasquill, F., and Smith, F. B.: Atmospheric diffusion: Study of the Dispersion of Windborne Material from Industrial and Other Sources, third ed. Ellis Horwood Ltd., Chichester, 1983.

Pitari, G., Coppari, E., De Luca, N., and Di Carlo, P.: Observations and box model analysis of radon-222 in the atmospheric surface layer at L'Aquila, Italy: March 2009 case study, Environ. Earth Sci., 71(5), 2353–2359, 2014.

Pitari, G., De Luca, N., Coppari, E., Di Carlo, P. and Di Genova, G.: Seasonal variation of night-time accumulated Rn-222 in central Italy, Environ. Earth Sci., 73(12), 8589–8597, 2015.

Perrino, C., Pietrodangelo, A. and Febo, A.: An atmospheric stability index based on radon progeny measurements for the evaluation of primary urban pollution. Atmos. Environ., 35, 5235−5244, 2001.

Perrino, C., Catrambone, M., and Pietrodangelo, A.: Influence of atmospheric stability on the mass concentration and chemical composition of atmospheric particles: a case study in Rome, Italy, Environ. Int., 34(5), 621−628, 2008.

Podstawczyńska, A. and Chambers, S.D.: Radon-based technique for the analysis of atmospheric stability – a case study from Central Poland, Nukleonika, 63, 47−54. https://doi.org/10.2478/nuka-2018-0006, 2018.

Pope, C. A. and Dockery, D. W.: Health effects of fine particulate air pollution: Lines that connect, J. Air Waste Manag. Assoc., 56(6), 709–742, doi:10.1080/10473289.2006.10464485, 2006.

Pucer, J. and Štrumbelj, E.: Impact of changes in climate on air pollution in Slovenia between 2002 and 2017, Environ. Pollut., 242, 398–406. https://doi.org/10.1016/j.envpol.2018.06.084, 2018.

Querol, X., Alastuey, A., Gangoiti, G., Perez, N., Lee, H.K., Eun, H.R., Park, Y., Mantilla, E., Escudero, M., Titos, G., Alonso, L., Temime-Roussel, B., Marchand, N., Moreta, J.R., Revuelta, M.A., Salvador, P., Artíñano, B., Dos Santos, S.G., Anguas, M., Notario, A., Saiz-Lopez, A., Harrison, R.M., Millán, M., Ahn and K.H.: Phenomenology of summer ozone episodes over the Madrid Metropolitan Area, central Spain, Atmos. Chem. Phys., 18, 6511–6533, 2018.

Russo, A., Trigo, R. M., Martins, H., and Mendes, M. T.: NO_2, PM_{10} and O_3 urban concentrations and its association with circulation weather types in Portugal, Atmos. Environ., 89, 768–785, 2014.

Salvador, P., Alonso-Pérez, S., Pey, J., Artíñano, B., De Bustos, J. J., Alastuey, A., and Querol, X.: African dust outbreaks over the western Mediterranean Basin: 11-year characterization of atmospheric circulation patterns and dust source areas, Atmos. Chem. Phys., 14(13), 6759–6775, 2014.

Sandradewi, J., Prévôt, A.S.H., Weingartner, E., Schmidhauser, R., Gysel and M., Baltensperger, U.: A study of wood burning and traffic aerosols in an Alpine valley using a multi-wavelength Aethalometer, Atmos. Environ., 42, 101–112. https://doi.org/10.1016/j.atmosenv.2007.09.034, 2008.

Segura, S., Estellés, V., Esteve, A. R., Utrillas, M. P., and Martínez-Lozano, J. A.: Analysis of a severe pollution episode in Valencia (Spain) and its effect on ground level particulate matter, J. Aerosol Sci., 56, 41–52, 2013.

Sesana, L., Caprioli, E. and Marcazzan, G.M.: Long period study of outdoor radon concentration in Milan and correlation between its temporal variations and dispersion properties of atmosphere, J. Environ. Radioact., 65, 147−160. https://doi.org/10.1016/S0265-931X(02)00093-0, 2003.

Sesana, L., Ottobrini, B., Polla, G. and Facchini, U.: ^{222}Rn as indicator of atmospheric turbulence: Measurements at Lake Maggiore and on the pre-Alps, J. Environ. Radioact., 86(2), 271–288, doi:10.1016/j.jenvrad.2005.09.005, 2006.

Sinharay, R., Gong, J., Barratt, B., Ohman-Strickland, P., Ernst, S., Kelly, F. J., Junfeng, Zh., Collins, P., Cullinan, P. and Chung, K. F.: Respiratory and cardiovascular responses to walking down a traffic-polluted road compared with walking in a traffic-free area in participants aged 60 years and older with chronic lung or heart disease and age-matched healthy controls: a randomised, crossover study, The Lancet, 391(10118), 339−349, 2018.

Triantafyllou, A. G.: PM_{10} pollution episodes as a function of synoptic climatology in a mountainous industrial area, Enviromental Pollut., 112, 491−500, 2001.

Turner, D. B.: A diffusion model for an urban area. J. Appl. Meteorol., 3(1), 83−91, 1964.

Vardoulakis, S. and Kassomenos, P.: Sources and factors affecting PM_{10} levels in two European cities: Implications for local air quality management, Atmos. Environ., 42, 3949–3963, doi:10.1016/j.atmosenv.2006.12.021, 2008.

Vrhovec, T.: Analysis of mesometeorological temperature fields, Meteorol. Atmos. Phys., 43(1−4), 235−240, 1990.

Wang, F., Chambers, S.D., Zhang, Z., Williams, A.G., Deng, X., Zhang, H., Lonati, G., Crawford, J., Griffiths, A.D., Ianniello, A. and Allegrini, I.: Quantifying stability influences on air pollution in Lanzhou, China, using a radon-based “stability monitor”: seasonality and extreme events, Atmos. Environ., 145, 376−391, http://doi.org/10.1016/j.atmosenv.2016.09.014, 2016.

Wang, L., Stanič, S., Bergant, K., Eichinger, W., Močnik, G., Drinovec, L., and Gregorič, A.: Retrieval of vertical mass concentration distributions—Vipava Valley case study, Remote Sens., 11(2), 106, 2019.

Whiteman, C.D., Eisenbach, S., Pospichal, B., Steinacker, R.: Comparison of vertical soundings and sidewall air temperature measurements in a small Alpine Basin, J. Appl. Meteorol., 43, 1635–1647. https://doi.org/10.1175/JAM2168.1, 2004.

Williams, A. G., Chambers, S. D., Conen, F., Reimann, S., Hill, M., Griffiths, A. D. and Crawford, J.: Radon as a tracer of atmospheric influences on traffic-related air pollution in a small inland city, Tellus, Ser. B Chem. Phys. Meteorol., 68(1), 1−21, doi:10.3402/tellusb.v68.30967, 2016.

Williams, A.G., Chambers, S., Griffiths, A.: Bulk mixing and decoupling of the nocturnal stable boundary layer characterized using a ubiquitous natural tracer, Bound. Lay. Meteorol., 149, 381−402. https://doi.org/10.1007/s10546-013-9849-3, 2013.

WHO: Air quality guidelines for Europe, World Health Organization, Regional Office for Europe, Copenhagen (http://www.euro.who.int/en/publications/abstracts/air-quality-guidelines-for-europe) accessed 22 December 2019, 252 pp., 2000.

WHO: Air quality guidelines: Global update 2005 — Particulate matter, ozone, nitrogen dioxide and sulphur dioxide, World Health Organization, Regional Office for Europe, Copenhagen (http://www.euro.who.int/en/health-topics/environment-and-health/air quality/publications/pre2009/air-quality-guidelines.-global-update-2005.-particulate-matter,-ozone,-nitrogen-dioxide-and-sulfur-dioxide) accessed 22 December 2019, 484 pp., 2006.

4.4 Influence of Meteorological Parameters on Radon Time Series

In the following peer-reviewed articles, entitled "Parameters influencing deviation of radon concentration from its typical diurnal pattern in the winter and summer seasons" and "Role of meteorology and lithology in the temporal variation of the outdoor radon level" a study of the temporal variations of radon concentration at two contrasting sites is presented.

Events with high or low radon concentration are selected in the winter and summer seasons using simple statistical analysis. These events are studied in detail by being related to changes of the following meteorological parameters: air temperature, wind speed and direction, atmospheric pressure, precipitation, cloud cover, air masses history (back trajectories) and mixing height. Clear sky conditions (no precipitation and calm winds, especially at night) were identified as the reason for the greatest accumulation of radon. Conversely, precipitation, high wind speeds and maritime air masses were found to be responsible for influencing the dilution of radon and reducing the radon exhalation rate (soil moisture/freezing). In addition, the diurnal radon cycle in different seasons and different atmospheric mixing conditions reflected influences of the lithology and the radon flux at each of the study sites. Peak diurnal radon concentrations were a factor of two higher at Ajdovščina due to greater rates of radon exhalation from flysch and carbonate rocks than from the sea and lake sediments characteristic of the Ljubljana Basin region.

The results have confirmed the sensitivity of the diurnal and seasonal radon concentration to the ABL mixing state caused by meteorological changes at the two selected complex topographies.

In these two studies, the candidate developed the research question, performed data collection, curation and formal analysis. She performed all visualization of data, concepts, interpreted the results and wrote the complete original draft of the manuscript.

330
GEOME 2
Manuscript received: December 4, 2017
Accepted: December 16, 2017

Geologica Macedonica, Vol**. 31**, No. 2, pp. 157–170 (2017)
In print: ISSN 0352 – 1206
On line: ISSN 1857 – 8586
UDC: 539.16:551.510.411]:546.296
Original scientific paper

PARAMETERS INFLUENCING DEVIATION OF RADON CONCENTRATION FROM ITS TYPICAL DIURNAL PATTERN IN THE WINTER AND SUMMER SEASONS

Dafina Kikaj[1], Janja Vaupotič[2]

[1]*Jožef Stefan International Postgraduate School, Jamova cesta 39, 1000 Ljubljana, Slovenia*
[2]*Jožef Stefan Institute, Department of Environmental Sciences, Jamova cesta 39, 1000 Ljubljana, Slovenia*
dafina.kikaj@ijs.si

A b s t r a c t: Radon (^{222}Rn) has been used as an atmospheric tracer for studying the vertical mixing processes in the planetary boundary layer (PBL). Therefore, the time series of hourly atmospheric radon concentration obtained in Ljubljana city were analyzed along with the meteorological data and back trajectory information from December 2016 to November 2017. Radon concentration exhibited the annual cycle with a higher mean in the winter (20.7 ± 15.5 Bq m^{-3}) and a lower mean in the summer (14.6 ± 9 Bq m^{-3}) reflecting the PBL evolution on a seasonal timescale. Most of the time, radon showed the typical diurnal variation following its related mean seasonal level attributed to the vertical mixing processes. Among this typical pattern, deviations of atmospheric radon concentration by more than $\pm\sigma$ from the related seasonal mean value have been detected in 9 events ($\pm\sigma$ E_i) in the winter and summer seasons using simple statistical analysis. The parameter persistent/nocturnal inversion has usually been the reason for $+\sigma$ E_i. While, the temporal variation of the exhalation rate, wind direction/speed and maritime air masses have been the responsible influencing parameter for $-\sigma$ E_i.

Key words: atmospheric radon; continuous measurement; deviations in concentration; planetary boundary layer; persistent inversion; air masses

1. INTRODUCTION

Radon (^{222}Rn) is a radioactive noble gas appearing naturally in the environment as a product of radioactive transformation of radium (^{226}Ra). Only a fraction of radon atoms is able to emanate from the mineral grains and enter into air-filled pore space, transport through these pore space by diffusion and, for a longer distance, by advection, dissolved either in water or in carrier gases (Nazaroff, 1992). Eventually, it exhales into the atmosphere where it is distributed by turbulent mixing. The exhalation of radon into the atmosphere depends on many parameters, including its source (^{226}Ra content in the soil), geology (lithology), physical characteristics of upper soil layer (mineral structure, porosity, water content) and the combination of meteorological parameters (mainly of soil moisture, atmospheric pressure gradient and temperature) (Etiope & Martinelli, 2002; Levin et al., 2002; Mazur & Kozak, 2014; Papachristodoulou et al., 2007).

Much of the early interest in radon monitoring was related to the recognition of radon as a health risk in dwellings and working environments (WHO, 2009). Atmospheric levels of radon are typically more than an order of magnitude lower than generally obtained in dwellings and the working environment (Burian & Otahal, 2009; Sesana et al., 2003; Vaupotič et al., 2010). The keen interest in atmospheric radon monitoring can be attributed to its unique characteristics as a tracer for atmospheric processes. As a gas, it is mobile and carries information over long distances across Earth's crust, oceans and atmosphere. Being noble, its mobility is not affected by chemical reactions with any medium it passes. Furthermore, since radon is relatively insoluble in water, it is not susceptible to dry or wet atmospheric removal processes. The half-life of radon (3.82 d) is comparable to the lifetimes of the short-lived atmospheric pollutants (e.g. NO_x, SO_2, CO, O_3) and atmospheric residence time of water

and aerosols. Since its half-life is much larger than turbulent timescales (< 1 h), it can be considered a fairly conservative tracer for convective boundary layer (CBL) and nocturnal boundary layer (NBL) mixing studies. With a few assumptions, it is possible to derive an "equivalent mixing height" from a time series of near ground radon concentration for a selected time period of the diurnal cycle. The equivalent mixing height is derived from a box model of the accumulation of radon at night and then its dilution the following morning (Fontan et al., 1979; Sesana et al., 2003, 2006; Griffiths et al., 2013). Since terrestrial radon exhalation is 2–3 orders of magnitude greater than its oceanic exhalation, there is a large contrast in continental and oceanic air masses radon concentration. Radon's only significant atmospheric sink is radioactive decay process.

The first atmospheric radon observations sought to characterize the vertical distribution of radon in the atmosphere (Butterweck et al., 1994; Cohen et al., 1972; Moses et al., 1960; Ussler et al., 1994). The application of radon observations from the network of available ground stations has increased substantially over the last two decades (Zahorowski et al., 2004). Nowadays, 41 stations worldwide are identified where atmospheric radon is measured regularly for periods longer than one year (Zhang et al., 2011).

Currently, there are four major applications of radon in climate, air quality and pollution studies: 1) Tracing of horizontal air mass transport (Chambers et al., 2013; Dörr et al., 1983; Zahorowski et al., 2005) (C5). 2) Investigating vertical mixing in the lower atmosphere (Chambers et al., 2014; Grossi et al., 2016; Vinuesa et al., 2007; Williams et al., 2011). 3) Assessing the surface emissions of major greenhouse gases, such as CO_2, N_2O and CH_4 (Levin et al., 1999; Van der Laan et al., 2014; Vogel et al., 2012; Wada et al., 2013); 4) Validating and, to a lesser extent, parameterising, transport and mixing schemes in climate/weather models (Jacob & Prather, 1990).

A typical pattern of atmospheric radon on the simplest of cases has been documented most of the time, such as reaching a minimum during the CBL (on cloud-free day) when the vertical dilution occurs by combined thermal circulations and mechanical mixing and a maximum concentration during the night (NBL in near-neutral to moderately stable conditions) due to the formation of a surface temperature inversion. In the very stable boundary layer (persistent and strong nocturnal inversion) and in coupled cloud layers, vertical mixing processes remain poorly understood (Chambers et al., 2011, 2015; Chen et al., 2016; Willimas et al., 2011).

Among the typical pattern of atmospheric radon on the diurnal timescale attributed to the vertical mixing processes, sudden changes (either increase or decrease from the related mean seasonal value, here in after referred to as "events") may be observed in the time series of atmospheric radon. The objective of our work was the identification of the events in the winter and summer seasons and their relation to the parameters influencing deviation of radon concentration (i) persistent and strong nocturnal inversion, (ii) temporal variability of exhalation rate, (iii) wind direction/speed and (iv) history of air masses.

2. SITE AND METHODS

2.1. *Site characteristics*

All the observations were made at the meteorological station Ljubljana Bežigrad (46°07' N, 14°52' E), situated in the central part of the city. The city of Ljubljana is located between the "Ljubljansko polje" (Ljubljana Basin) in the north, bounded by hills, north by Šmarna Gora and Rašica hills that connect Polhov Gradec hills in the west with Posavje hills in the east. To the south is "Ljubjansko barje" (Ljubljana moor, 162 km^2) (Šajn et al., 2011), a drained ancient moor that was frequently a lake during the ice ages (Pak, 1992). Ljubljana Basin lies in a very clear-cut valley basin with a relief energy of about 300 m.

Temperate and continental, the city's climate can be classified as being typical for south-Alpine regions. Characteristics features of the local climate are generally calm winds within the basin results in a high amount of foggy days, frequent persistent and strong nocturnal inversion at 350 m altitude (120 d y^{-1}), especially in the winter. The prevailing winds are NE, NNE and ENE (ARSO, 2017). The mean wind speed was 1.3 m s^{-1} during the winter and 1.4 m s^{-1} during the summer. The mean air temperature at the site reveals a distinct seasonal cycle, with the summer mean daily maximum reaching 22°C and the winter mean daily minimum 0°C. Rainfall distribution is irregular, with a peak in the summer (ARSO, 2017).

Ljubljana Basin is located in a shallow sedimentary basin filled with heterogeneous Quaternary deposits. The bedrock of the basin is built of Permian and Carboniferous clastic rocks (claystones, sandstones, conglomerates) and partly of Mesozoic carbonate rocks. It outcrops on the margins of the hills. Ljubljana Basin is covered by gravel deposits of the Sava river and by sea and lake sediments. On the gravelly Ljubljana Basin, most water goes underground (Gregorič et al., 2013).

2.2. *Measurements method*

Continuous radon monitoring has been conducted by an AlphaGuard monitor (Saphymo, Germany), ionisation chamber operating in diffusion mode with a 1-h integration time, with a lower limit of detection (LLD) ~ 2 Bq m^{-3}. The device was set up inside the weather instrument shelter (Figure 1), 1.5 m above the ground. In addition to the radon measurements, hourly values of air temperature, relative humidity, wind speed, wind direction, wind gust, atmospheric pressure, precipitation, cloud cover, solar energy radiation and diffusive energy radiation were obtained from the Office of Meteorology of the Environmental Agency of the Republic of Slovenia. Backward trajectory analysis has been performed by using HYSPLIT (Hybrid Single Particle Lagrangian Integrated Trajectory) model (Draxler and Rolph, 2011) supplied by NOAA/ARL (National Oceanic and Atmospheric Administration/Air Resources Laboratory).



Fig 1. The weather instrument shelter with the AlphaGuard monitor inside at the meteorological station Ljubljana Bežigrad located at the Environmental Agency of the Republic of Slovenia

The grid resolution has been set to 1°× 1°. Mixing layer heights were used to assist the interpretation of the atmospheric data generated by the global data assimilation system (GDAS) model from NOAA/ARL (National Oceanic and Atmospheric Administration/Air Resources Laboratory).

The statistical analyses were performed by the openair package (Carslaw & Ropkins, 2012) under R 3.3.1 (R Development Core Team, 2008).

All reported times are local times (LST = UTC + 1 h) and the northern hemisphere seasonal convection has been adapted (i.e. Winter: December–February; Spring: March–May; Summer: June –August; Autumn: September–November).

2.3. *Methodology of data analysis*

The time series of hourly mean concentrations of atmospheric radon obtained between December 2016 and November 2017 (Figure 2) was split into four seasons, as described hereinabove. For this study, the means of atmospheric radon concentration were calculated separately for the winter and summer seasons. Atmospheric radon events were first expressed as deviations in a radon concentration of more than ±σ from the mean seasonal value. Secondly, to improve the identification of events, we chose the periods when:

1. radon concentration deviates by more than +σ from the releated mean seasonal value for more than 24 hours; they are considered as events caused possibly by persistent inversion or history of air masses;
2. radon concentration deviates by more than –σ from the releated mean seasonal value for more than 24 hours; they are considered as events caused possibly by temporal variability of exhalation rate, wind direction/speed or history of air masses.

The 24 hour period has been selected to represent: (i) the synoptic timescales (days to weeks) (i)

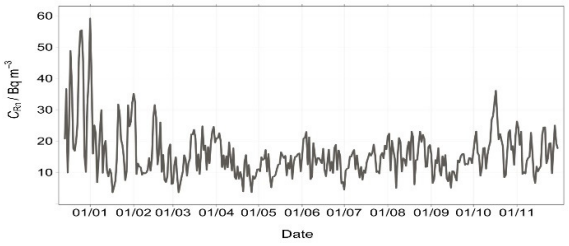


Fig. 2. Time series of daily mean atmospheric radon concentration in the period December 2016 – November 2017

persistent inversion which extends over few days and (iii) temporal variations of constant exhalation rate of radon associated mainly with water content of the soil (which implies the frequency and amount of precipitation). The frontal situations with the fast changes of gradient atmospheric pressure were not considered in this study.

To identify the strong nocturnal boundary layer (strong inversion), which breaks up near the afternoon, the condition when radon concentration deviates by more than +σ from the related seasonal value for more than 12 hours is considered as events possibly caused by strong nocturnal inversion.

3. RESULTS AND DISCUSSION

Hourly atmospheric radon concentration in the winter and summer as well as air temperature, solar energy radiation, diffusive energy radiation, atmospheric pressure, precipitation, mixing height are shown in Figures 3 and 4. Radon concentration exhibited the annual cycle with higher mean in the winter (20.7 ± 15.5 Bq m^{-3}) and lower mean in the summer (14.6 ± 9 Bq m^{-3}) reflecting the planetary boundary layer (PBL) evolution. During the winter, more cooling occurs during the long nights than heating during the short day, in the fair weather over land, reflecting the shrinking role of vertical mixing within PBL (Figure 3).

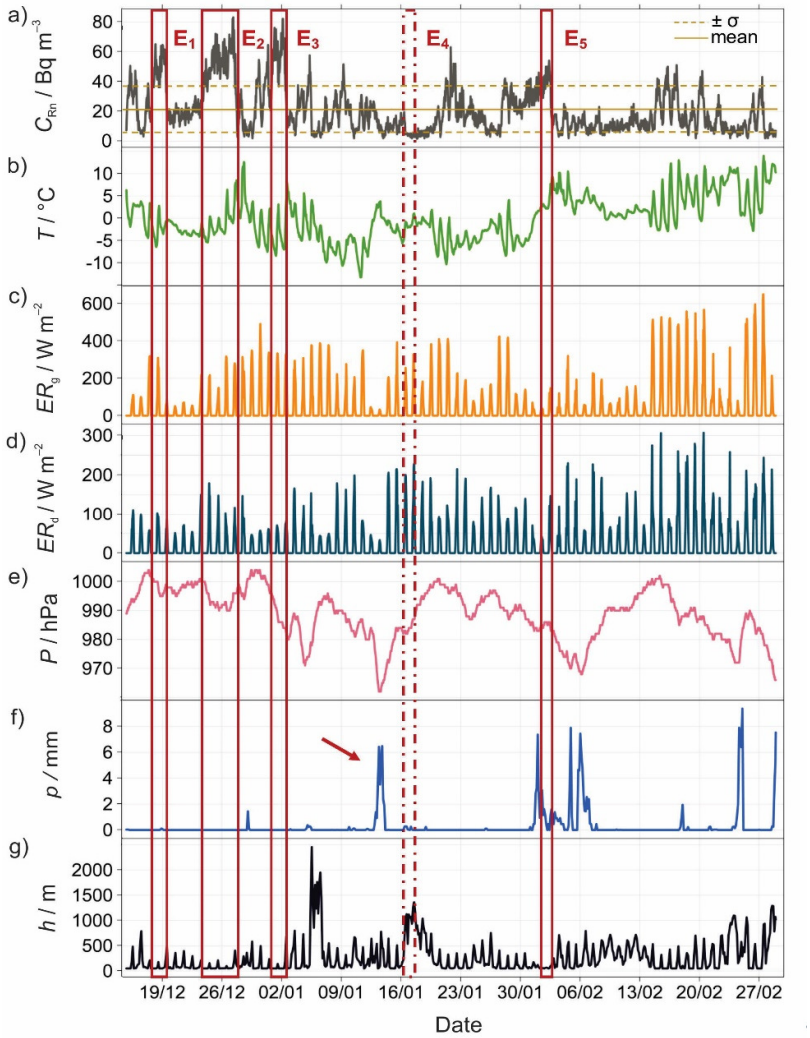


Fig. 3. Time series of a) atmospheric radon concentration (C_{Rn}), b) air temperature (T), c) global energy radiation (ER), d) diffusive energy radiation (ER), e) atmospheric pressure (P), f) precipitation (p) and g) mixing height (h) in the winter; open red boxes indicate events marked E_1, E_2, E_3, E_4 and E_5, discussed in section 3

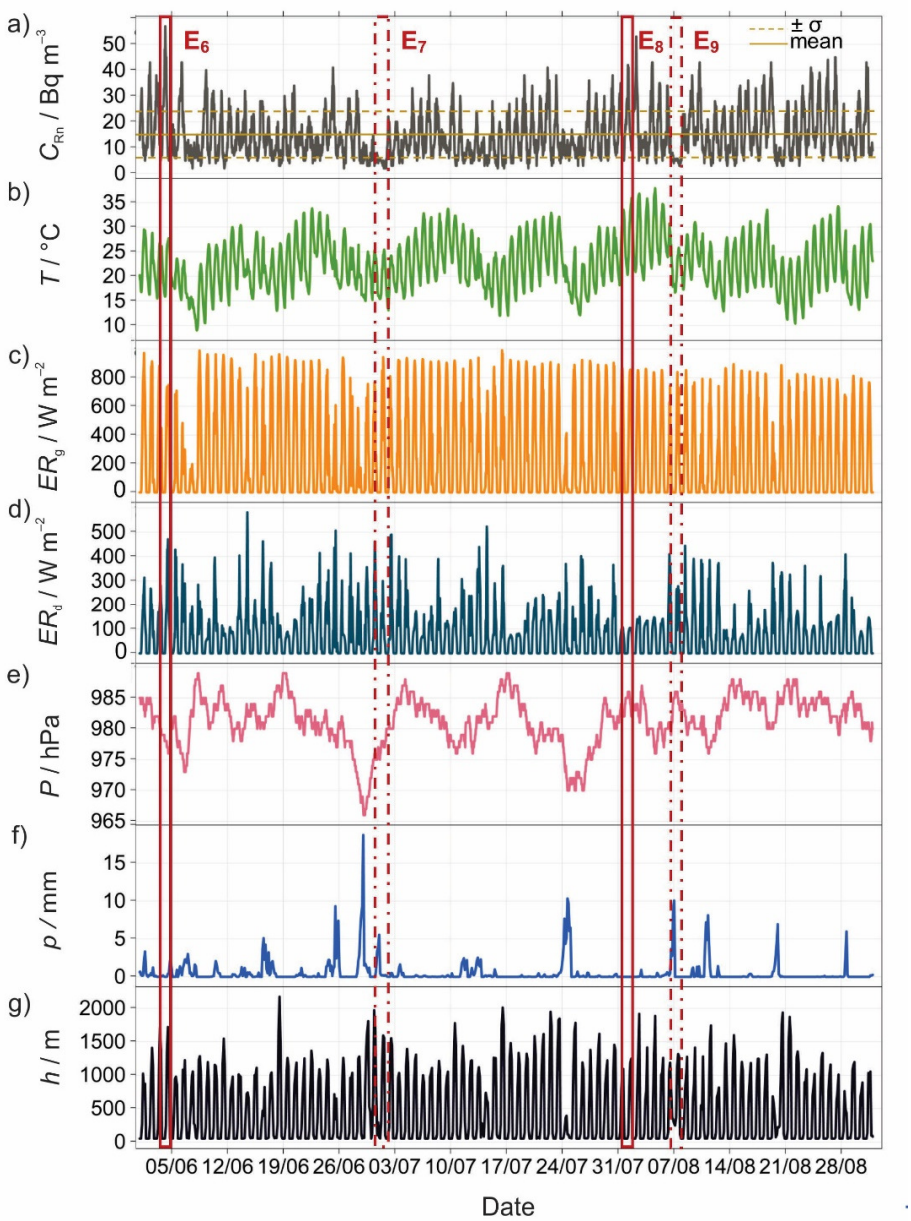


Fig. 4. Time series of a) atmospheric radon concentration (C_{Rn}), b) air temperature (T), c) global energy radiation (ER), d) diffusive energy radiation (ER), e) atmospheric pressure (P), f) precipitation (p) and g) mixing height (h) in the summer; open red boxes indicate events, marked E_6, E_7, E_8, and E_9, discussed in section 3

The growing of vertical mixing within PBL occurs during the summer, driven by the longer exposure of the land to sunlight as a result of days longer than nights (Figure 4) (Stull, 2011). Higher radon concentration in the winter and lower radon concentration in the summer was found by Pal et al., (2015) in central Europe, in southern Finland by Chen et al., (2016) and in Milan by Sesana et al., (2003).

The main distribution characteristics of atmospheric radon concentration, air temperature, relative humidity, wind speed and precipitation (mean, standard deviation, mean daily maximum and mean daily minimum) for the winter and summer seasons are shown in Table 1.

Vertical processes in very stable conditions, in mechanical turbulence (interaction of wind speed and surface roughness elements) and in cloudy days, horizontal processes and temporal variations in exhalation rate were assumed to affect the changes of radon concentration in the winter and summer for more than ±σ from the mean seasonal level for more than 24 hours. Concentrations outside of this region are considered as events and further evaluated.

Table 1

Basic statistics of radon concentration (C_{Rn}), air temperature (T), atmospheric pressure (P), relative humidity (RH), wind speed (ws) and precipitation (p) in the winter and summer seasons

	Winter December 2016–February 2017				Summer June–August 2017			
	AM	SD	AM max	AM min	AM	SD	AM max	AM min
C_{Rn} (Bq m^{-3})	20.7	15.5	35	9	14.6	9	29	5
T (°C)	–0.03	5	3	–3	22	5	29	16
P (hPa)	988	9	991	986	981	4	983	979
RH (%)	77	16	88	62	61	18	85	38
ws (m s^{-1})	1.3	1	2.6	0.4	1.5	1	3	0.2
p (mm)	0.3	1.1	1.1	0.05	0.5	1.5	2	0.03

AM – arithmetic mean, SD – standard deviation, AM max – mean daily maximum, AM min – mean daily minimum

A total of five events (hereinafter E_i) were detected in the winter 2016–17, their characteristics are reported in Table 2. Four of E_i were +σ (E_1, E_2, E_3 and E_5) and one –σ (E_4). E_5 has a short duration (14 hours) and is related to nocturnal inversion. E_1 and E_3 (duration 38 and 34 hours) are related with stable conditions (persistent inversion), and E_2 (with significantly longer duration of 75 hours) with very strong stable conditions (persistent inversion). All +σ E_i were compared with a bulk temperature gradient with a simple method for the detection of persistent inversions based on near ground temperature data on different altitudes as developed by Largeron and Staquet (2016) and a clear relation was confirmed.

Table 2

±σ E_i detected using criteria from section 2.3. The duration of each event and most responsible influencing parameter of the event.

Event	Duration	Influencing parameter
+σ E_1	18/12/2016 00:00 – 19/12/2016 10:00 (34 hours)	Persistent inversion
+σ E_2	24/12/2016 08:00 – 27/12/2016 12:00 (75 hours)	Persistent inversion
+σ E_3	31/12/2016 20:00 – 02/01/2017 10:00 (38 hours)	Nocturnal inversion
–σ E_4	16/01/2017 13:00 – 17/01/2017 23:00 (35 hours)	Katabatic wind and temporal variation of exhalation rate
+σ E_5	01/02/2017 23:00 – 02/02/2017 13:00 (14 hours)	Nocturnal inversion
+σ E_6	03/06/2017 21:00 – 04/06/2017 10:00 (13 hours)	Nocturnal inversion
–σ E_7	01/07/2017 00:00 – 02/07/2017 00:00 (24 hours)	Maritime air masses
+σ E_8	01/08/2017 22:00 – 02/08/2017 11:00 (13 hours)	Nocturnal inversion
–σ E_9	06/08/2017 23:00 – 07/08/2017 23:00 (24 hours)	Temporal variation of exhalation rate

The meteorological parameters, such as precipitation few days before (Figure 3f) and katabatic (downslope) wind with moderate speed revealed the reasons for –σ E_4.

In summer 2017, four E_i were detected. The main characteristics of each E_i in summer are presented in Table 2. Two +σ E_i (E_6 and E_8) were related to the nocturnal inversion (duration 13 hours), broke-up within 5–6 hours after sunrise. The very low level of radon concentration in the air during –σ E_7 was the result of the horizontal processes, connected to the maritime air masses, coming from the Adriatic Sea accompanied by southwestern winds.

While $-\sigma$ E_9 is explained with moderate wind speed during night and day and effect of the soil moisture on the exhalation rate of radon concentration.

The following four events, marked as E_3, E_4, E_6 and E_7, are explained in more details in the following sub chapters.

3.1. *The response of the atmospheric radon concentration to the nocturnal/persistent inversion (E_3 and E_6)*

High atmospheric pressure (> 985 hPa) under generally clear sky conditions (Figures 3e and 5f) occurred before and during E_3 (31/12/2016 20:00 – 2/01/2017 10:00). Wind speed remained below 0.5 m s^{-1}, air temperature and relative humidity showed a clear diurnal variation pattern (Figures 5b, 5d and 5e), typical for such conditions (Schnelle & Brown, 2002; Whiteman et al., 1999). There was no rainfall throughout the period.

The diurnal variation of atmospheric radon concentration with a maximum (~ 80 Bq m^{-3}) early in the morning and minimum (~ 40 Bq m^{-3}) in the afternoon was linked to the vertical mixing in the atmosphere; the mixing height was less than 300 m above ground level (a.g.l.) during daytime and as low as 50 m a.g.l. at night (Figure 3g). The mixing height evenly matched with the inversion in the basin which often fills the whole mixing layer from the ground to an inversion top which usually coincides with an average elevation of the peak surrounding the basin. In our case, this average elevation is about 695 m.

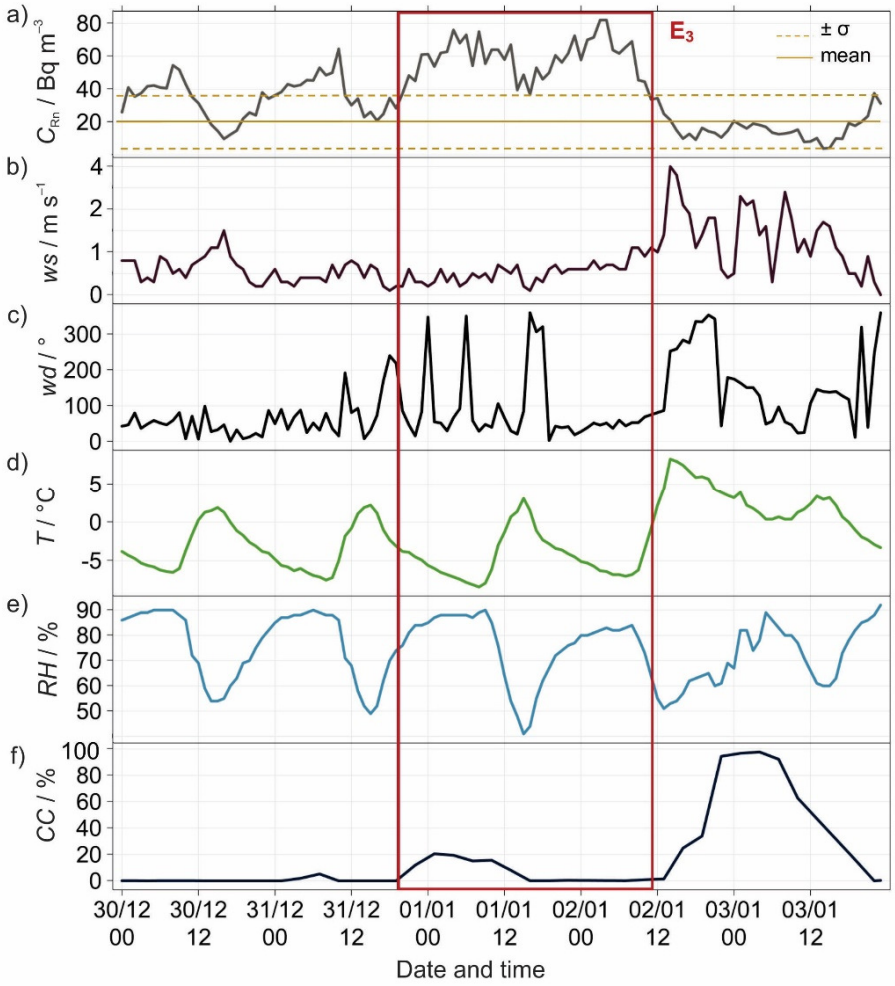


Fig. 5. Time series of a) atmospheric radon concentration (C_{Rn}), b) wind speed (*ws*), c) wind direction (*wd*), d) air temperature (*T*), e) relative humidity (*RH*) and f) cloud cover (*CC*) during the period before and after +σ E_3 (31/12/2016 20:00 – 02/01/2017 10:00)

The persistent inversion broke up within 3 hours after sunrise on 2 January (Figure 5a). The end of E_3 was with a low-pressure (< 980 hPa), enhanced wind speed (Figures 3e and 5b), which might be channelled in the basin and destroyed the persistent inversion (Whiteman et al., 2004). Radon concentration decreased rapidly achieving the typical mean level (Figure 5a).

Beginning on the morning of 3 June (E_6), the sky was clear with maximum air temperature 25°C and maximum wind speed ~ 4 m s^{-1} (Figures 6b, 6d and 6f). The atmospheric radon showed a typical diurnal variation with a minimum (7 Bq m^{-3}) in the afternoon (Figure 6a). After the sunset, the gradually built-up of radon concentration occurred with a maximum (55 Bq m^{-3}) by diverting the mean seasonal level, under the very calm wind speed conditions (Figures 6a and 6b). This substantial increased of radon concentration was clearly linked to the strong nocturnal inversion. Radon concentration in the morning did not show any changes with the sunrise, the decreasing of radon occurred after 10:00 with the dissipation of the nocturnal inversion. The mixing height during the night-time was less than 50 m a.g.l. and after broke up of the inversion reached the height 1430 m a.g.l. (Figure 4g).

In the summer months, compared with other seasons, the nocturnal inversions are rapidly dissolved because of the intense solar radiation (Kassomenos & Koletsis, 2005). In this case, the nocturnal inversion was broke-up within 5 hours after sunrise because of the latent heat flow, days before the high frequency of the precipitation occurred and the ground remained wet, a distinct part is converted into latent heat flow, due to evaporation, instead of sensible heat flow (Wezel & Chang, 1988). The daytime was followed with precipitation and radon concentration decreased on the typical mean level (Figures 4a and 4f).

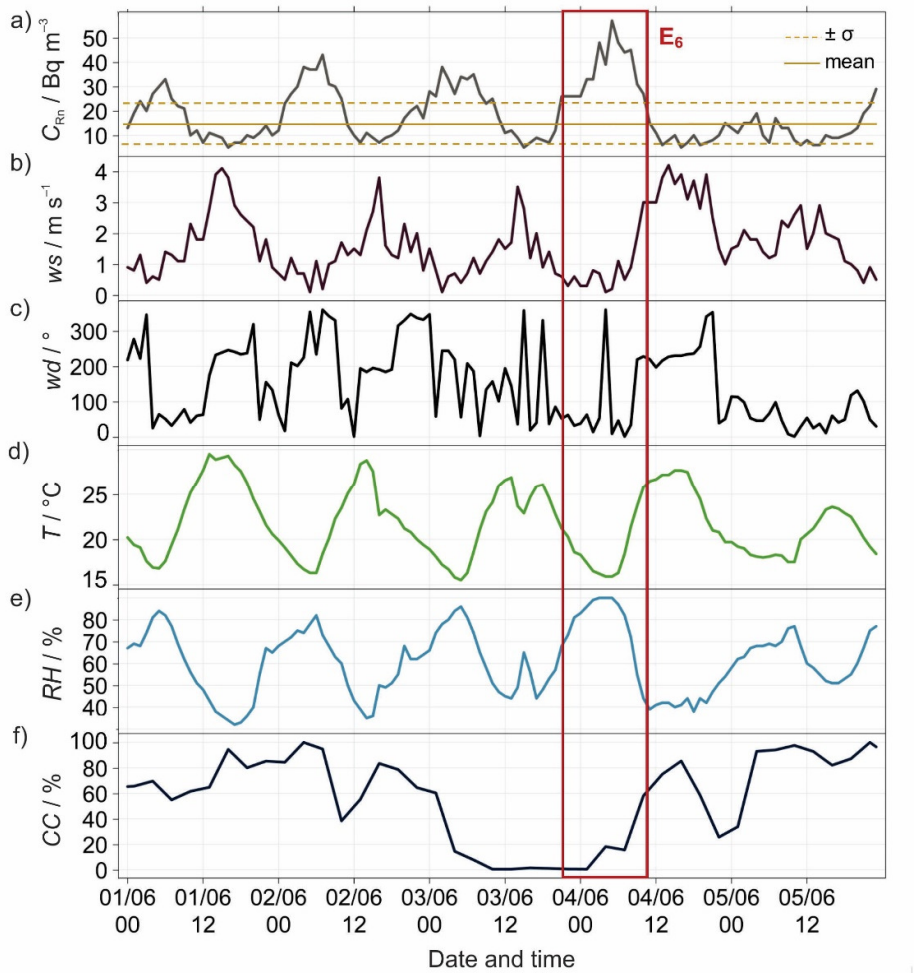


Fig. 6. Time series of a) atmospheric radon concentration (C_{Rn}), b) wind speed (*ws*), c) wind direction (*wd*), d) air temperature (*T*), e) relative humidity (*RH*) and f) cloud cover (*CC*) during the period before and after +σ E_6 (03/06/2017 21:00 – 04/06/2017 10:00).

3.2. *Changes on atmospheric radon as a function of the temporal variation of exhalation rate and wind direction/speed (E_4)*

Overcast conditions with a precipitation (~ 6 mm) occurred several days before the E_4 (Figures 3f and 7f). On 16 January after 12:00 the radon concentration decreased and did not show the variation for next 35 hours (Figure 7a). Since Ljubljana Basin has a lot of underground waters, the level of them might be increased because of the precipitation and affecting the exhalation rate. The soil moisture significantly reduces the diffusion and exhalation of radon from the soil (Nazaroff, 1992; Mattsson, 1970). By not neglecting the fact that air temperature before and during E_4 was under 0°C (Figure 7d), which could lead to the conclusion that the soil has been frozen and affected the total reduction of exhalation rate (Feichter & Crutzen, 1990; Jacob & Prather, 1990).

The decrease of the radon concentration during E_4 in Figure 7a was related to the change of the wind speed and direction (Figures 7b and 7c). The eastern katabatic wind coming from the Posavje hills (the highest peak 1219 m a.s.l.) with enhanced wind speed (Figure 8). Generally, the katabatic wind is nocturnal wind but it can also be formed in the daytime over snow- or ice-covered slopes (Figure 8) (Stull, 2011). Katabatic winds might lead to the formation of fog (Stull, 2011) in the Ljubljana Basin (Figure 7f).

Well-mixed conditions have occurred during the E_4 with mixing height more than 1000 m a.g.l. during daytime and as low as 500 m a.g.l. at night (Figure 3g).

3.3. *The effect of origin of air masses on atmospheric radon (E_7)*

Temporal variation of atmospheric radon, wind speed and direction, air temperature, relative humidity and cloud cover during the period before and after E_7 is shown in Figure 9 and the 4 days backward trajectories of air masses passing the measurement location in Ljubljana Basin are shown in Figure 10. A decreased of radon concentration after midnight on 7 June (Figure 9a) revealed the influence of maritime air masses originating over the Adriatic Sea and travelling with the southwestern moderate wind (Figure 11). After the E_7 the air masses were continental (Figure 10) and an increase of the radon concentration was observed on the typical mean level for the subsequent days (Figure 9a).

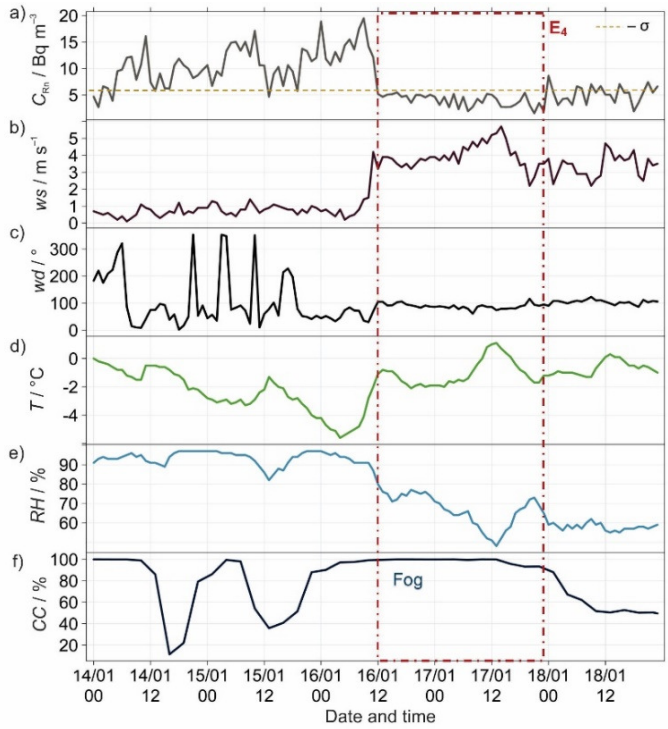


Fig. 7. Time series of a) atmospheric radon concentration (C_{Rn}), b) wind speed (*ws*), c) wind direction (*wd*), d) air temperature (*T*), e) relative humidity (*RH*) and f) cloud cover (*CC*) during the period before and after $-\sigma$ E_4 (16/01/2017 13:00 – 17/01/2017 23:00)

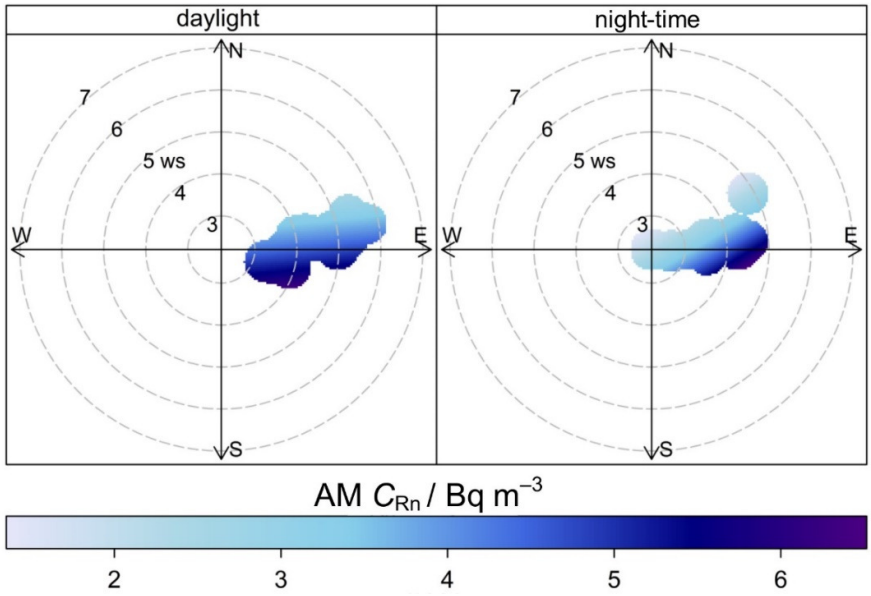


Fig. 8. The bivariate polar plot of mean atmospheric radon concentration on the day and night-time jointly with eastern (katabatic) wind during the $-\sigma$ E_4 (16.01.2017 13:00 – 17.01.2017 23:00).

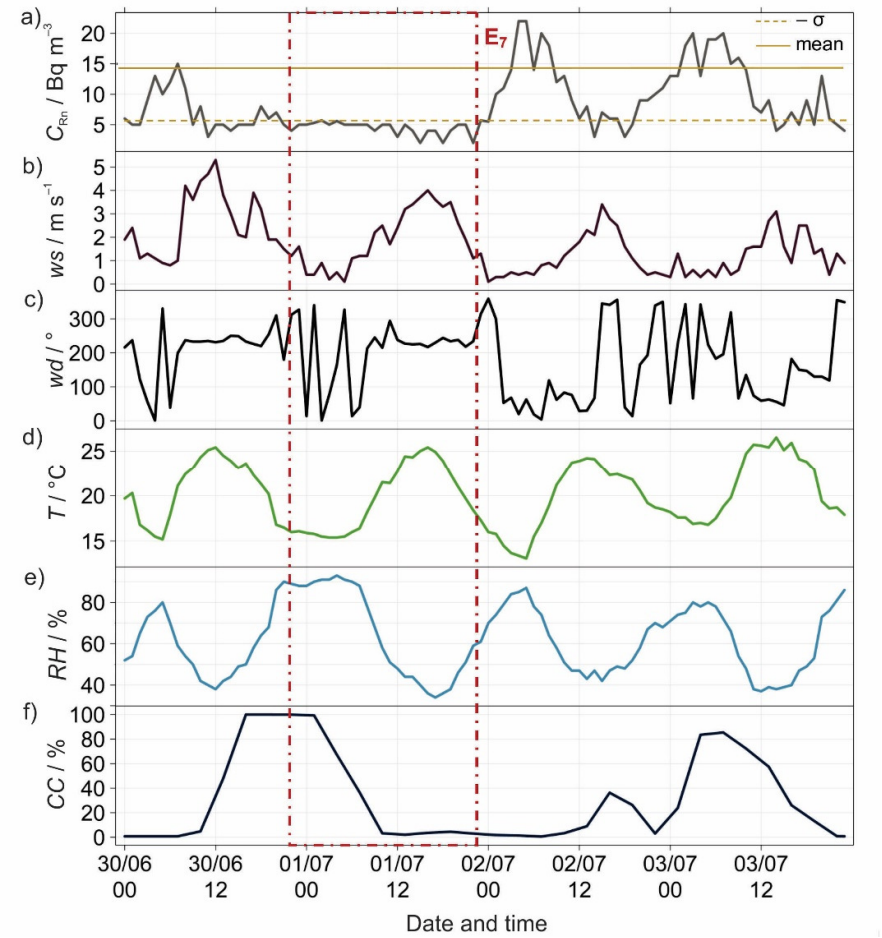


Fig. 9. Time series of a) atmospheric radon concentration (C_{Rn}), b) wind speed (*ws*), c) wind direction (*wd*), d) air temperature (*T*), e) relative humidity (*RH*) and f) cloud cover (*CC*) during the period before and after $-\sigma$ E_7 (01/07/2017 00:00 – 02/07/2017 00:00)

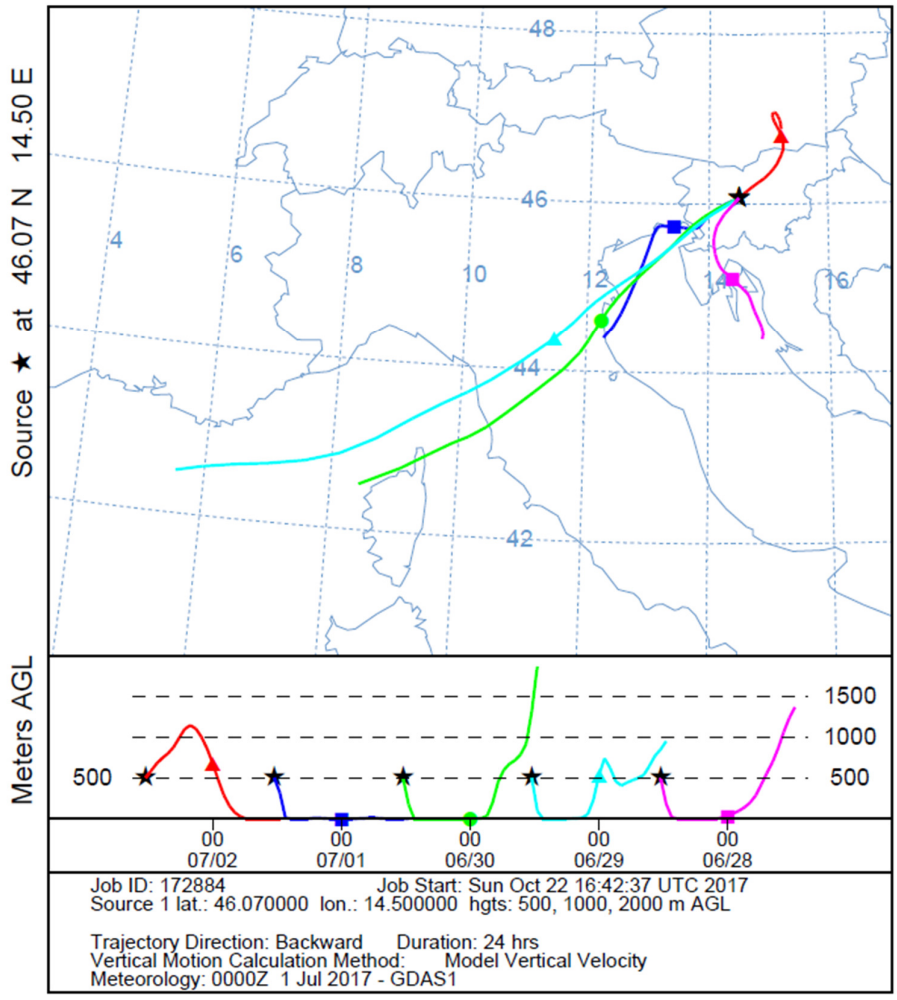


Figure 10. Four days HYSPLIT back trajectories centred on meteorological station Ljubljana Bežigrad for –σ E_7 (01/07/2017 00:00 – 02/07/2017 00:00), shown grouped for each day (every 24 hours new trajectory) and coloured accordingly

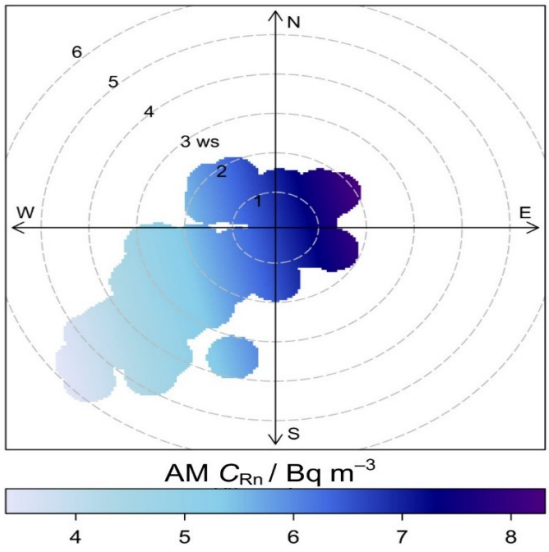


Figure 11. The bivariate polar plot of mean atmospheric radon concentration jointly with the southwestern wind during the *–σ E_7* (01/07/2017 00:00 – 02/07/2017 00:00)

4. CONCLUSIONS

The one year data series of atmospheric radon, obtained at the Ljubljana Bežigrad meteorological station during December 2016 – November 2017, was analyzed along with the meteorological data and back trajectory information.

Radon concentration exhibited the annual cycle with a higher mean in the winter (20.7 ± 15.5 Bq m^{-3}) and a lower mean in the summer (14.6 ± 9 Bq m^{-3}) reflecting the PBL evolution on a seasonal timescale. Most of the time, radon showed the typical diurnal variation following the related mean seasonal level attributed to the vertical mixing processes. Among this typical pattern, we were able to detect with a simple statistical analysis based on $\pm\sigma$ deviations of the atmospheric radon concentration from the seasonal mean value nine events (E_i). The parameter persistent/nocturnal inversion was the main reason for $+\sigma$ E_i. The temporal variation of the exhalation rate, wind direction/speed and maritime air masses have been recognized as responsible influencing parameter for $-\sigma$ E_i.

The obtained results imply that atmospheric radon is a suitable tool for studying the building and breaking up of the persistent/nocturnal inversion in the basin. The determining of the equivalent mixing height based on the radon box model is much simpler because there is no need to take into account the horizontal advection transport and residual radon concentration from a previous, deeper, mixed layer during the inversion periods. Radon proved to be a good indicator of the wind direction and influence of the origin of air masses.

The temporal variability of the exhalation rate of radon, which was mainly due to soil moisture, seems to influence the variation of the atmospheric radon. Therefore, the long-term experimental data of radon exhalation on the Ljubljana Basin would improve the usage of radon as an atmospheric tracer.

Acknowledgements: The authors acknowledge the financial support from the Slovenian Research Agency (research core funding No. P1-0143) and from the Public Scholarship, Development, Disability and Maintenance Fund of the Republic of Slovenia (Contract no. 11011-44/2016-18). The authors also gratefully acknowledge the Environmental Agency of the Republic of Slovenia for the permission provided to install the weather instrument shelter for radon monitoring on their land and for providing the meteorological data, NOAA Air Resources Laboratory (ARL) the using of the HYSPLIT transport and dispersion model, and the READY website (http.//www.arl.noaa.gov/ready.php).

REFERENCES

ARSO, Slovenian Environment Agency (Slovenian: Agencija Republike Slovenije za okolje): Climate characteristics of Ljubljana - Wind Rose for the City of Ljubljana (2017). http://meteo.arso.gov.si/uploads/probase/www/climate/table/sl/by_variable/wind/Ljubljana.html.

Burian I., & Otahal P. (2009): Radon and its decay products in outdoor air. *Applied Radiation and Isotopes*, **67** (5), 881–883.

Butterweck G., Reineking A., Kesten J., & Porstendörfer J. (1994): The use of the natural radioactive noble gases radon and thoron as tracers for the study of turbulent exchange in the atmospheric boundary layer—case study in and above a wheat field. *Atmospheric Environment*, **28** (12), 1963–1969.

Carslaw D. C., & Ropkins K. (2012): Openair – an R package for air quality data analysis. *Environmental Modelling & Software*, **27**, 52–61.

Chambers S. D., Williams A. G., Crawford J., & Griffiths A. D. (2015): On the use of radon for quantifying the effects of atmospheric stability on urban emissions. *Atmospheric Chemistry and Physics*, **15** (3), 1175–1190.

Chambers S., Williams A. G., Zahorowski W., Griffiths A., & Crawford J. (2011): Separating remote fetch and local mixing influences on vertical radon measurements in the lower atmosphere. *Tellus B*, **63** (5), 843–859.

Chambers S. D., Zahorowski W., Williams A. G., Crawford J., & Griffiths A. D. (2011): Identifying tropospheric baseline air masses at Mauna Loa Observatory between 2004 and 2010 using Radon-222 and back trajectories. *Journal of Geophysical Research: Atmospheres*, **118** (2), 992–1004.

Chen X., Paatero J., Kerminen V.-M., Riuttanen L., Hatakka J., Hiltunen V., Paasonen P., Hirsikko A., Franchin A., Manninen H. E., Petaja T., Viisanen Y., & Kulmala M. (2016): Responses of the atmospheric concentration of radon-222 to the vertical mixing and spatial transportation. *Boreal Environment Research,* **21**(3–4), 299–318.

Cohen L. D., Barr S., Krablin R., & Newstein H. (1972): Steady-state vertical turbulent diffusion of radon. *Journal of Geophysical Research*, **77**(15), 2654–2668.

Dörr H., Kromer B., Levin I., Münnich K. O., & Volpp H. J. (1983): CO_2 and Radon-222 as tracers for atmospheric transport. *Journal of Geophysical Research: Oceans*, **88** (C2), 1309–1313.

Etiope G., & Martinelli G. (2002): Migration of carrier and trace gases in the geosphere: an overview. *Physics of the Earth and Planetary Interiors*, **129** (3), 185–204.

Feichter J., & Crutzen P. J. (1990): Parameterization of vertical tracer transport due to deep cumulus convection in a global transport model and its evaluation with ^{222}Radon measurements. *Tellus B*, **42** (1), 100–117.

Fontan J., Guedalia D., Druilhet A., & Lopez A. (1979): Une methode de mesure de la stabilite verticale de l'atmosphere pres du sol. *Boundary-Layer Meteorology,* **17**, 3–14 (in French, with English abstract).

Gregorič A., Vaupotič J., Kardos R., Horváth M., Bujtor T., & Kovács T. (2013): Radon emanation of soils from different lithological units. *Carpathian Journal of Earth and Environmental Sciences*, **8** (2), 185–190.

Griffiths A. D., Parkes S. D., Chambers S. D., McCabe M. F., & Williams A. G. (2013): Improved mixing height monitoring through a combination of lidar and radon measurements. *Atmospheric Measurement Techniques*, **6** (2), 207–218.

Grossi C., Àgueda A., Vogel F. R., Vargas A., Zimnoch M., Wach P., Martín J. E., López-Coto I., Bolívar J. P., Morguí J. A., & Rodó X. (2016): Analysis of ground- based ^{222}Rn measurements over Spain: Filling the gap in southwestern Europe. *Journal of Geophysical Research: Atmospheres*, **121** (18) 11021–11037.

Jacob D. J., & Prather M. J. (1990): Radon-222 as a test of convective transport in a general circulation model. *Tellus B*, **42** (1), 118–134.

Kassomenos P. A., & Koletsis I. G. (2005): Seasonal variation of the temperature inversions over Athens, Greece. *International Journal of Climatology*, **25** (12), 1651–1663.

Largeron Y., & Staquet C. (2016): Persistent inversion dynamics and wintertime PM_{10} air pollution in Alpine valleys. *Atmospheric Environment*, **135**, 92–108.

Levin I., Born M., Cuntz M., Langendörfer U., Mantsch S., Naegler T., Schimdt M., Varlagin A., Verclas S., & Wagenbach D. (2002): Observations of atmospheric variability and soil exhalation rate of radon-222 at a Russian forest site. Technical approach and deployment for boundary layer studies. *Tellus B*, **54** (5), 462–475.

Levin I., Glatzel-Mattheier H., Marik T., Cuntz M., Schmidt M., & Worthy D. E. (1999): Verification of German methane emission inventories and their recent changes based on atmospheric observations. *Journal of Geophysical Research: Atmospheres*, **104** (D3), 3447–3456.

Mattsson R. (1970): Seasonal variation of short-lived radon progeny, Pb^{210} and Po^{210}, in ground level air in Finland. *Journal of Geophysical Research*, **75** (9), 1741–1744.

Mazur J., & Kozak K. (2014): Complementary system for long term measurements of radon exhalation rate from soil. *Review of Scientific Instruments*, **85** (2), 022104.

Moses H., Stehney, A. F. & Lucas H. F. (1960): The effect of meteorological variables upon the vertical and temporal distributions of atmospheric radon. *Journal of Geophysical Research*, **65** (4), 1223–1238.

Nazaroff W. W. (1992): Radon transport from soil to air. *Reviews of Geophysics*, **30** (2), 137–160.

Pak M. (1992): Ljubljana. In: Javornik M. (ed.), *Enciklopedija Slovenije 6*, 218–220. Mladinska knjiga, Ljubljana.

Pal S., Lopez M., Schmidt M., Ramonet M., Gibert F., Xueref-Remy I., & Ciais P. (2015): Investigation of the atmospheric boundary layer depth variability and its impact on the ^{222}Rn concentration at a rural site in France. *Journal of Geophysical Research: Atmospherees*, **120** (2), 623–643.

Papachristodoulou C., Ioannides K., & Spathis S. (2007): The effect of moisture content on radon diffusion through soil: assessment in laboratory and field experiments. *Health Physics*, **92** (3), 257–264.

R Core Team (2013): *R: A Language and Environment for Statistical Computing*. R Foundation for Statistical Computing, Vienna, Austria. http://www.R-project.org/.

Sesana L., Caprioli E., & Marcazzan G. M. (2003): Long period study of outdoor radon concentration in Milan and correlation between its temporal variations and dispersion properties of atmosphere. *Journal of Environmental Radioactivity*, **65** (2), 147–160.

Schnelle K. B., & Brown C. A. (2002): *The Air Pollution Control Technology Handbook*. CRC Press.

Stull R. (2011): *Meteorology for Scientists & Engineers,* 3rd Edition. University of British Columbia.

Šajn R., Gosar M., Bidovec M., Pirc S., & Alijagić J. (2011): Geochemical mapping of Ljubljana urban and suburban area, Slovenia. In: *Mapping the Chemical Environment of Urban Areas*, 375–392. John Wiley & Sons, New York.

Ussler W., Chanton J. P., Kelley C. A., & Martens C. S. (1994): Radon-222 tracing of soil and forest canopy trace gas exchange in an open canopy boreal forest. *Journal of Geophysical Research: Atmospheres*, **99** (D1), 1953–1963.

Van der Laan S., Van der Laan-Luijkx I. T., Zimmermann L., Conen F., & Leuenberger M. (2014): Net CO_2 surface emissions at Bern, Switzerland inferred from ambient observations of CO_2, $\delta(O_2/N_2)$, and ^{222}Rn using a customized radon tracer inversion. *Journal of Geophysical Research: Atmospheres*, **119** (3), 1580–1591.

Vaupotič J., Kobal I., & Križman M. J. (2010): Background outdoor radon levels in Slovenia. *Nukleonika*, **55**, 579–582.

Vinuesa J. F., Basu S., & Galmarini S. (2007): The diurnal evolution of ^{222}Rn and its progeny in the atmospheric boundary layer during the Wangara experiment. *Atmospheric Chemistry and Physics Discussions*, **7** (3), 8895–8931.

Vogel F. R., Ishizawa M., Chan E., Chan D., Hammer S., Levin I., & Worthy D. E. J. (2012): Regional non-CO_2 greenhouse gas fluxes inferred from atmospheric measurements in Ontario, Canada. *Journal of Integrative Environmental Sciences*, **9** (sup1), 41–55.

Wada A., Matsueda H., Murayama S., Taguchi S., Hirao S., Yamazawa H., Moriizumi J., Tsuboi K., Niwa Y, & Sawa Y. (2013): Quantification of emission estimates of CO_2, CH_4 and CO for East Asia derived from atmospheric radon-222 measurements over the western North Pacific. *Tellus B: Chemical and Physical Meteorology*, **65** (1), 1803–7.

Wetzel P. J., & Chang J. T. (1988): Evapotranspiration from nonuniform surfaces: A first approach for short-term numerical weather prediction. *Monthly Weather Review*, **116** (3), 600–621.

Whiteman C. D., Bian X., & Zhong S. (1999): Wintertime evolution of the temperature inversion in the Colorado Plateau Basin. *Journal of Applied Meteorology*, **38** (8), 1103–1117.

Whiteman C. D., Pospichal B., Eisenbach S., Weihs P., Clements C. B., Steinacker R., Mursch-Radlgruber E., & Dorninger M. (2004): Inversion breakup in small Rocky Mountain and Alpine basins. *Journal of Applied Meteorology*, **43** (8), 1069–1082.

Williams A. G., Zahorowski W., Chambers S., Griffiths A., Hacker J. M., Element A., & Werczynski S. (2011): The vertical distribution of radon in clear and cloudy daytime terrestrial boundary layers. *Journal of the Atmospheric Sciences*, **68** (1), 155–174.

World Health Organization: *WHO Handbook on Indoor Radon: A Public Health Perspective*. Geneva: World Health Organization, 2009.

Zahorowski W., Chambers S. D., & Henderson-Sellers A. (2004): Ground based radon-222 observations and their application to atmospheric studies. *Journal of Environmental Radioactivity*, **76** (1), 3–33.

Zahorowski W., Chambers S., Wang T., Kang C. H., Uno I., Poon S., Oh S. N., Werczynski S., Kim J., & Henderson-Sellers A. (2005): Radon-222 in boundary layer and free tropospheric continental outflow events at three ACE-Asia sites. *Tellus B*, **57** (2), 124–140.

Zhang K., Feichter J., Kazil J., Wan H., Zhuo W., Griffiths A. D., Sartorius H., Zahorowski W., Ramonet M., Schmidt M., Yver C., Neubert R. E. M., & Brunke E. G. (2011): Radon activity in the lower troposphere and its impact on ionization rate: a global estimate using different radon emissions. *Atmospheric Chemistry and Physics*, **11** (15), 7817–7838.

Р е з и м е

ПАРАМЕТРИ КОИ ВЛИЈААТ ВРЗ ОТСТАПУВАЊЕТО НА КОНЦЕНТРАЦИЈАТА НА РАДОН ОД НЕГОВАТА ТИПИЧНА ДНЕВНА ШЕМА ВО ЗИМСКА И ЛЕТНА СЕЗОНА

Дафина Кикај[1], Јања Ваупотич[2]

[1]Училиште за постдипломски студии Јожеф Штефан,
Јамова цеста 39, 1000 Љубљана, Словенија
[2]Институт Јожеф Штефан, Оддел за науки на животната средина,
Јамова цеста 39, 1000 Љубљана, Словенија
dafina.kikaj@ijs.si

Клучни зборови: атмосферски радон; континуирано мерење; девијации во концентрацијата; слој на планетарна граница; постојана инверзија; воздушни маси

Радонот (^{222}Rn) се користи како атмосферски трејсер за проучување на вертикалните процеси на мешање во рамките на планетарните слоеви (PBL). Поради тоа, временската серија часовни атмосферски концентрации на радон добиена во Љубљана беше анализирана заедно со метеоролошките податоци и информациите за соодветните траектории од декември 2016 до ноември 2017 година. Концентрацијата на радон покажала годишен циклус со највисока средна вредност во зима (20.7 ± 15.5 Bq m^{-3}) и најниска средна вредност во лето (14.6 ± 9 Bq m^{-3}) одразувајќи ја еволуцијата на PBL на ниво на сезонска временска скала. Во најголем дел од времето, радонот покажал карактеристични дневни варијации следејќи ги поврзаните средни сезонски нивоа, а што може да биде припишано на процесите на вертикално мешање. Меѓу овие типични шеми, девијациите на концентрацијата на атмосферскиот радон за повеќе од ±σ од соодветната сезонска средна вредност биле откриени во 9 случаи (±σ E_i) во зимска и летна сезона користејќи едноставна статистичка анализа. Параметарот перзистентна/ноќна инверзија обично е причина за +σ E_i, додека временската варијација на стапката на испарување, насоката на ветерот/брзината на ветерот и поморските воздушни маси се параметрите одговорни за –σ E_i.

Radiation Protection Dosimetry (2019), pp. 1–5 doi:10.1093/rpd/ncz079

ROLE OF METEOROLOGY AND LITHOLOGY IN THE TEMPORAL VARIATION OF THE OUTDOOR RADON LEVEL

D. Kikaj[1,2,*], T. Kovács[3,4] and J. Vaupotič[2]
[1]Jožef Stefan International Postgraduate School, Jamova cesta 39, 1000 Ljubljana, Slovenia
[2]Department of Environmental Sciences, Jožef Stefan Institute, Jamova cesta 39, 1000 Ljubljana, Slovenia
[3]Social Organization for Radioecological Cleanliness, Egyetem 10, 8200 Veszprém, Hungary
[4]Institute of Radiochemistry and Radioecology, University of Pannonia, Egyetem 10, 8200 Veszprém, Hungary

*Corresponding author: dafina.kikaj@ijs.si

The outdoor radon concentration was monitored together with the meteorological parameters at two contrasting complex topographies: sub-Alpine basin (SA) and sub-Mediterranean valley (SM) in winter (December 2017–February 2018) and summer (June–August 2018). The time series for each site and each season are evaluated in three different ways: (i) clear-sky and cloudy condition together, (ii) clear-sky conditions only (cloud cover <20%) and (iii) cloudy condition only (cloud cover >20%), and compared to the expected atmospheric boundary layer (ABL) 'mixing volume' caused by meteorological changes. The results have confirmed the sensitivity of diurnal and seasonal radon concentration to the expected ABL 'mixing volume' at the two selected sites. The relationship is more pronounced in calm clear-sky conditions. Cloudy conditions are associated with fast weather changes, when the ABL is well mixed and hourly mean radon concentrations do not follow the typical diurnal trend.

INTRODUCTION

The radioactive noble gas radon (^{222}Rn) is the product of α-radioactive transformation of radium (^{226}Ra) in the uranium (^{238}U) chain. From its origin in the Earth's crust, it migrates towards the surface and exhales eventually into the lower atmosphere—the so-called atmospheric boundary layer (ABL). Its activity concentration is mainly governed by the ABL volume into which it is mixed. The 'mixing volume' of the ABL derives by the combination of thermal and mechanical atmospheric processes, which cause diurnal and seasonal changes of ABL. The formation of thermal stratification during the night-time causes the suppression of ABL (≤0.1 km) and consequently to an increase of radon concentration, while the occurrence of thermal circulation and mechanical mixing during the daytime results in deeper ABL (≥1 km) and the dilution of radon[1]. Furthermore, the seasonal pattern of radon concentration is also affected by ABL[2–4]. In general, a lower mean radon concentration is found in the summer due to the highest mixing volume of the ABL, which is driven by the longer exposure of the land to sunlight, as a result of days that are longer than nights. During the winter, the lowest mixing volume of ABL reflects in the higher mean radon concentration, as a consequence of more cooling during the long nights than heating during the short days.

Radon does not chemically react and is poorly soluble. In particular, it is important that it just has an appropriate half-life ($t_{1/2}$ = 3.82 d) compared with the characteristic time of meteorological events. Therefore, temporal variations of outdoor radon concentration may give immediate information about current ABL conditions and its changes[2–6].

Numerous studies have already demonstrated the usefulness of radon as an atmospheric tool to determine the influence of atmospheric processes on ABL changes over flat land[5–6]. On the other hand, over the complex topographies, the atmospheric processes are still poorly understood[1] and, here, due to a lack of ongoing radon measurements, its applicability is not completely elucidated. The additional radon data can contribute to a better understanding of the influence of meteorological conditions on the 'mixing volume' of ABL.

Slovenia offers many possibilities for studying outdoor radon over the complex topographies. In this study, two contrasting terrains, a sub-Alpine basin and a sub-Mediterranean valley, are presented, where the diurnal (on clear-sky and cloudy conditions) and seasonal (winter and summer) variations of outdoor radon concentration have been related to the expected ABL 'mixing volume'.

SITES AND METHODS

The hourly outdoor radon activity concentration has been monitored, together with the meteorological parameters during the winter (December 2017–February 2018) and summer (June–August 2018) at

© The Author(s) 2019. Published by Oxford University Press. All rights reserved. For Permissions, please email: journals.permissions@oup.com

Downloaded from https://academic.oup.com/rpd/advance-article-abstract/doi/10.1093/rpd/ncz079/5499286 by Jozef Stefan Institute user on 23 July 2019

two different sites: in the Ljubljana sub-Alpine basin (SA) and Vipava sub-Mediterranean valley (SM).

The SA site is located between the Julian, Kamnik-Savinje and Dinaric Alps, within basin. The geographic setting of SA provides ideal conditions for near-calm periods, resulting in calm winds (1.3 m s^{-1}), frequent foggy days and temperature inversions in the wintertime. The rainfall distribution is irregular, with its peak in the summer. The SM site is at a distance of 30 km from the north Adriatic coast, situated between the Trnovski gozd barrier (1500 m above sea level, a.s.l.) and the Karst plateau (500 m a.s.l.) and is characterised by strong surface 'Bora' wind, which is more vigorous and frequent in the wintertime when it may persist for several days, often reaching speeds of more than 28 m s^{-1} in gusts[7]. The highest rainfall amount in the valley occurs in the autumn.

The air distance between SA and SM is about 50 km. The sites differ not only in the complex topography and climate but also in lithology; SA is situated on sea and lake sediments, whereas SM is situated on flysch with carbonates in the vicinity of few km.

Radon measurements have been conducted using AlphaGUARDPQ2000 PRO monitors (Bertin Instruments) operating in diffusion mode (1-h integration time) with a lower limit of detection (LLD) of about 2 Bq m^{-3}. The devices have been mounted 1.5 m above ground level (a.g.l.), within Stevenson Screen instrument shelters. About 0.01% of data at SM and 0.02% at SA, respectively, are detected to fall below LLD.

The hourly observations of air temperature (°C), relative air humidity (%), barometric pressure (hPa), precipitation (mm h^{-1}) and wind speed (m s^{-1}), recorded at 2 m a.g.l., were provided by the National Meteorological Service at the Environmental Agency of the Republic of Slovenia (ARSO). The total cloud cover (%) was obtained from the global data assimilation system (GDAS) model of NOAA/ARL (National Oceanic and Atmospheric Administration/ Air Resources Laboratory).

The time series of hourly mean outdoor radon concentrations are evaluated in three different ways, based on selected threshold of meteorological conditions, for each day in two seasons (winter and summer) and for each site (SA and SM). First, whole dataset is analysed together, then only parts of the data are extracted from the whole dataset, as follows:

(i) **Clear-sky and cloudy conditions**—whole dataset.
(ii) **Clear-sky conditions**—cloud cover <20%, wind speed <2 m s^{-1}, precipitation <1 mm h^{-1}; the periods with light winds, lack of storms and precipitations, nearly cloud-free sky (more intense solar radiation); in winter 90% at SA, 60% at SM, in summer 60% at SA, 80% at SM, respectively, of the total time;
(iii) **Cloudy conditions**—cloud cover >20%, wind speed >2 m s^{-1}, precipitation >1 mm h^{-1}; the periods with moderate to strong winds, overcast sky with precipitation; in winter 10% at SA, 40% at SM, in summer 40% at SA, 20% at SM, respectively, of the total time.

The ABL mixing volume was roughly estimated from the meteorological situation.

RESULTS AND DISCUSSION

Clear-sky and cloudy conditions

The diurnal radon activity concentrations, averaged for each hour of the day of whole winter and summer seasons under clear-sky and cloudy conditions, are presented in Figure 1. Regardless season, the diurnal radon activity concentrations are characterised by a mid-afternoon minimum values (~10 Bq m^{-3}) and a nocturnal maximum values near dawn (~25 Bq m^{-3}) at both sites[2–6]. However, the mean radon concentration and amplitude of radon diurnal cycle varied significantly with the season and the site.

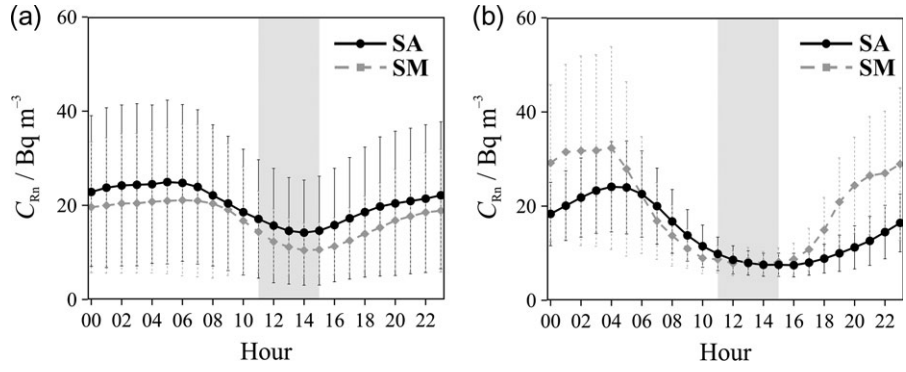


Figure 1. Diurnal variation of the hourly mean radon concentration at SA and SM sites in (**a**) winter and (**b**) summer (the highest thermal air mixing is shaded).

Downloaded from https://academic.oup.com/rpd/advance-article-abstract/doi/10.1093/rpd/ncz079/5499286 by Jozef Stefan Institute user on 23 July 2019

The winter mean radon concentrations are similar, 20.1 Bq m^{-3} at SA and 19.5 Bq m^{-3} at SM, with the low amplitude in diurnal cycle (Figure 1a). While the most pronounced difference between sites are observed in the minimum values of diurnal radon concentrations (afternoon) between 11:00 and 15:00 LT (shaded area, Figure 1a), when it is expected the highest ABL volume due to the thermal air mixing. On average, the afternoon radon concentration is at SM for a factor 1.4 lower than at SA. This is most likely due to the Bora wind occurrence at SM, which also causes the intensive mechanical mixing of ABL volume and dilution of radon. Contrarily, the calm conditions at SA, due to the frequent temperature inversion, certainly causes lower ABL mixing volume and higher concentrations of afternoon radon.

In the summer, approximately 15% higher mean radon concentration is found at SM, with largest radon amplitude, from 8 Bq m^{-3} to 32 Bq m^{-3} (Figure 1b). It is assumed that the increase in mean radon concentration at SM is a result of higher soil gas radon concentration and higher exhalation rate from flysch and carbonate rocks[8]. In addition, there is less precipitation during warm days at SM (average 0.3 mm h^{-1}) than at SA (average 0.7 mm h^{-1}) and, therefore, the radon flux is less affected. Due to the non-appearance of Bora wind (SM) and persistent temperature inversion (SA) in summer days, the mean ABL volume is expected to be about the same over both sites, which is best reflected in the same afternoon radon concentrations (shaded area, Figure 1b).

In order to analyse the influence of the estimated ABL mixing volume on radon concentrations at both sites and in both seasons more specifically, the two weather conditions are further discussed: clear-sky (intense insolation) and cloudy (precipitation and windy), based on selected threshold of meteorological conditions, as described in the previous section.

Clear-sky conditions

In clear-sky conditions, a notable difference between seasons and sites appears (Figure 2).

During the nights with a clear sky, the rapid radiative cooling of the surface occurs. When combined with calm wind and an absence of precipitation, it enables the formation of a strong thermal stratification. Under such conditions, the ABL volume is the lowest and the accumulation of radon is the highest. As evident in Figure 2, the nocturnal concentrations of radon are different at each site and in each season.

During *winter nights*, the calm katabatic (downslope) wind carries cold air from the mountains and 'pool' it in the basin (SA), thus contributing in additional reduction of the ABL volume[9]. On the other hand, the katabatic drainage in the open valley (SM) drains the air from the site towards the Adriatic Sea[7]. This difference between sites was confirmed by the 38% higher accumulation of radon during night hours at SA than at SM (Figure 2a). In contrast, during *summer nights*, the highest accumulation of radon occurs at SM site (Figure 2b). Due to the lack of precipitation, the soil is dry, and its permeability is enhanced. It is evident that under such conditions the permeability of flysch and carbonates (SM) is higher than of sea and lake sediments (SA).

On *winter days* in the SA basin, which is surrounded by mountains, the winter temperature inversion layer, formed during the night, may persist also in the daytime[9]. In the SM valley, on the other hand, the proximity of the Adriatic Sea and terrain exposure to the sun cause stronger convection and, therefore, in the morning hours the nocturnal layer is usually destroyed. In addition, in such conditions, the radon concentration is well correlated to the assumed ABL volume at both sites. Namely, at SA radon concentration is for a factor 1.6 higher than at SM, where well-mixed ABL is expected (Figure 2a).

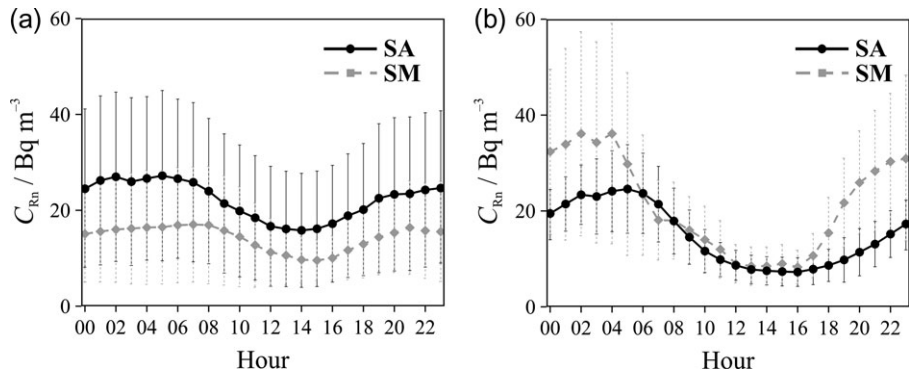


Figure 2. Diurnal variation of hourly mean radon concentration in clear-sky condition at SA and SM in (**a**) winter and (**b**) summer.

Downloaded from https://academic.oup.com/rpd/advance-article-abstract/doi/10.1093/rpd/ncz079/5499286 by Jozef Stefan Institute user on 23 July 2019

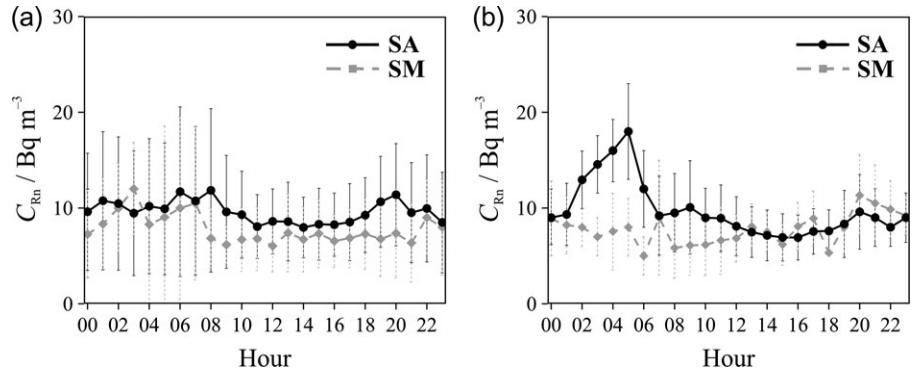


Figure 3. Diurnal variation of the hourly mean radon concentration in cloudy condition at SA and SM in (**a**) winter and (**b**) summer.

During *summer days,* the Earth's surface receives the highest rate of solar radiation. Therefore, the temperature inversion forms during nights, is broken up in the morning by strong convection also in the SA basin and not only in the SM valley, as is the case on winter days. Thermal mixing enables the dilution of radon at both sites to approximately the same concentration ~9 Bq m^{-3} (Figure 2b).

Cloudy conditions

The presence of a high amount of precipitation and moderate to strong wind cause a well-mixed ABL volume during the cloudy conditions. Therefore, compared to the clear-sky conditions, a decrease in the mean radon activity concentration for a factor 2 was found at both sites and in both seasons (Figures 2 and 3).

At SM, about 40% of wintertime was selected to have cloudy conditions, where the prevailing meteorological factor was 'Bora' wind. While, in SA basin, only 10% of the wintertime was classified to be under cloudy conditions with higher wind speed accompanied with precipitation. A clear difference in radon concentration between the two sites was noticed, with a factor 1.3 higher concentration at SA (Figure 3a).

The SA basin, closed almost from all sides with hills and mountains, does not frequently allow the occurrence of strong winds in the summertime, while the high mountain and proximity of the Adriatic Sea in the SM valley affect the presence of up-and-down winds and sea-and-land breezes (lower intensity then Bora wind)[7]. Mostly due to the topographic difference of the SA basin and the SM valley, a difference in summer radon concentration is found between the two sites, with higher values at SA and lower at SM, respectively (Figure 3b).

It is evident that cloudy conditions require a more detailed study, especially to explain some sharp changes of the trend in hourly mean radon concentrations, in which the important factors are wind direction and topography. It is also much more difficult to estimate the ABL changes.

The variability of radon concentration besides the ABL mixing volume strongly depends also on radon source function. Under the cloudy conditions, changes of radon source function are mainly associated with water content of the soil (related to the frequency and amount of precipitation) and frontal situations with the fast changes of gradient atmospheric pressure[10].

CONCLUSIONS

The hourly outdoor radon activity concentration has been monitored, together with meteorological parameters, during the winter and summer periods in the sub-Alpine basin (SA) and sub-Mediterranean valley (SM).

In clear-sky and cloudy conditions, mean radon concentrations are higher in winter months (for ~20 Bq m^{-3}) and during the night-time (for ~25 Bq m^{-3}) at both sites. The radon concentrations match with seasonal and diurnal variation of the assumed atmospheric boundary layer (ABL) volume; ABL is lower in the wintertime and in the night-time.

In clear-sky conditions (calm winds and no precipitation) during the winter season a strong temperature inversion is formed when the accumulation of radon is higher. At the SA, surrounded by mountains, radon reach air is 'pooled' into the basin for whole diurnal cycle. While, at the SM, weak downslope wind in the valley in the morning hours, drained radon away from the site toward the coast and, therefore, the mean diurnal radon concentration is for a factor of 1.2 lower than at SA. Contrarily, in the summer months when the influence of soil moisture on radon source function is reduced, a higher mean radon concentration was

Downloaded from https://academic.oup.com/rpd/advance-article-abstract/doi/10.1093/rpd/ncz079/5499286 by Jozef Stefan Institute user on 23 July 2019

found at the SM site, attributed to the higher radon exhalation rate from flysch and carbonate rocks.

In cloudy conditions (strong winds and precipitation), the mean radon activity concentration is for a factor of about 2 lower at both sites and in both seasons compared to clear-sky conditions. In the winter, a lower radon concentration is found at SM due to the strong surface 'Bora' wind. Cloudy conditions represent 40% of wintertime at SM valley, and 10% at SA basin, respectively.

The results have confirmed the sensitivity of the diurnal and seasonal radon concentration to the ABL 'mixing volume' caused by meteorological changes at the two selected complex topographies. However, this relationship is more pronounced in calm clear-sky conditions. Cloudy conditions are associated with fast weather changes when the ABL is well-mixed and the hourly mean radon concentrations do not follow the typical diurnal trend.

FUNDING

The authors acknowledge the financial support from the Slovenian Research Agency (research core funding no. P1-0143), the Public Scholarship, Development, Disability and Maintenance Fund of the Republic of Slovenia (contract no. 11011-44/2016-18), the Slovenian–Hungarian Scientific and Technological Cooperation (project no. BI-HU/17-18-008), and the meteorological data provided by the Environmental Agency of the Republic of Slovenia.

REFERENCES

1. Kallos, G., Astitha, M., Katsafados, P. and Spyrou, C. *Long-range transport of anthropogenically and naturally produced particulate matter in the Mediterranean and North Atlantic: current state of knowledge*. J. Appl. Meteorol. Climatol. **46**(8), 1230–1251 (2007).
2. Sesana, L., Caprioli, E. and Marcazzan, G. M. *Long period study of outdoor radon concentration in Milan and correlation between its temporal variations and dispersion properties of atmosphere*. J. Environ. Radioact. **65**(2), 147–160 (2003).
3. Kikaj, D. and Vaupotič, J. *Parameters influencing deviation of radon concentration from its typical diurnal pattern in the winter and summer seasons*. Geol. Maced. **170**, 157–170 (2017).
4. Chambers, S., Williams, A. G., Zahorowski, W., Griffiths, A. and Crawford, J. *Separating remote fetch and local mixing influences on vertical radon measurements in the lower atmosphere*. Tellus Ser. B: Chem. Phys. Meteorol. **63**(5), 843–859 (2016).
5. Chambers, S. D., Williams, A. G., Crawford, J. and Griffiths, A. D. *On the use of radon for quantifying the effects of atmospheric stability on urban emissions*. Atmos. Chem. Phys. **15**, 1175–1190 (2015).
6. Podstawczyńska, A. and Chambers, S. D. *Radon-based technique for the analysis of atmospheric stability – a case study from Central Poland*. Nukleonika **63**, 47–54 (2018).
7. Grisogono, B. and Belušić, D. *A review of recent advances in understanding the meso- and microscale properties of the severe Bora wind*. Tellus Ser. A: Dyn. Meteorol. Oceanogr. **61 A**, 1–16 (2009).
8. Kardos, R., Gregorič, A., Jónás, J., Vaupotič, J., Kovács, T. and Ishimori, Y. *Dependence of radon emanation of soil on lithology*. J Radioanal. Nucl. Chem. **304**(3), 1321–1327 (2015).
9. Rakovec, J., Merše, J., Jernej, S. and Paradiž, B. *Turbulent dissipation of the cold-air pool in a basin: comparison of observed and simulated development*. Meteorol. Atmos. Phys. **79**(3–4), 195–213 (2002).
10. Mazur, J. and Kozak, K. *Complementary system for long term measurements of radon exhalation rate from soil*. Rev. Sci. Instrum. **85**(2), 022104 (2014).

Downloaded from https://academic.oup.com/rpd/advance-article-abstract/doi/10.1093/rpd/ncz079/5499286 by Jozef Stefan Institute user on 23 July 2019

4.5 Radon Effective Doses at a Mediterranean Site

At a sub-Mediterranean valley site with moderate to high radon fluxes, changes in the atmospheric mixing state can increase outdoor environmental radon concentrations in the "zone of habitation" (≤2 m a.g.l.) by two orders of magnitude. In the summer months, when the influence of soil moisture on radon source function is reduced and the SNBL often forms at night, a higher mean radon concentration was found at the sub-Mediterranean site. This elevation of radon concentration in summer was the main reason of the dose calculation, results of which are presented in the scientific article entitled "Effective doses due to outdoor and indoor radon at a Mediterranean site".

Doses have been calculated for different exposure times, and thus for different averages of radon activity concentrations: (i) annual effective dose, (ii) summer effective dose, and (iii) realistic' summer effective dose – windows kept open.

The annual effective dose was 1.83 mSv, with 1.66 mSv from indoor and 0.17 mSv (9%) from outdoor radon. Although radon concentration often exceeded 50 Bq m^{-3}, the outdoor radon contribution did not contribute significantly to the total annual effective dose. Under such conditions, opening windows overnight to reduce radon levels significantly is not effective.

In this study, the candidate performed data collection and curation. She performed all visualization of data and interpreted the results and wrote the complete original draft of the manuscript.

Radiation Protection Dosimetry (2019), pp. 1–5 doi:10.1093/rpd/ncz155

EFFECTIVE DOSES DUE TO OUTDOOR AND INDOOR RADON AT A MEDITERRANEAN SITE

Dafina Kikaj[1,2] and Janja Vaupotič[2,*]
[1]Jožef Stefan International Postgraduate School, Jamova cesta 39, SI-1000 Ljubljana, Slovenia
[2]Jožef Stefan Institute, Jamova cesta 39, SI-1000 Ljubljana, Slovenia

*Corresponding author: janja.vaupotic@ijs.si

Received 6 February 2019; revised 5 May 2019; editorial decision 10 May 2019; accepted 27 May 2019

A year-long continuous measurement of the radon activity concentration in the outdoor air at a Mediterranean site has shown a range of 2–144 Bq m^{-3} and annual mean of 18 ± 14 Bq m^{-3}. Seasonal means were: 15 ± 10 Bq m^{-3} in winter, 15 ± 12 Bq m^{-3} in spring, 22 ± 19 Bq m^{-3} in summer and 17 ± 12 Bq m^{-3} in autumn. In summer, the average radon activity concentration in the daytime (6–22 h) was 15.2 Bq m^{-3} and in the night-time (22–6 h) 33.4 Bq m^{-3}. The annual effective dose was 1.83 mSv, with 1.66 mSv from indoor and 0.17 mSv (9%) from outdoor radon. The related doses for the summertime were (mSv): 0.29, 0.24 and 0.05 (18%).

INTRODUCTION

The noble gas radon (^{222}Rn, half-life, $t_{1/2}$ = 3.82 days) is created by the α-transformation of ^{226}Ra in the ^{238}U radioactive chain[1]. Like uranium, radon is also ubiquitously spread throughout the environment, being present at various levels in the soil, water and air. Breathing air with radon and its accompanying radioactive short-lived products (^{218}Po, ^{214}Pb, ^{214}Bi and ^{214}Po) contributes about half the effective dose a member of the general public receives from all natural radioactivity[2]. Likewise, ^{222}Rn is reported to cause about 8% of all lung cancers[3] second only to cigarette smoking. Therefore, in the last few decades, many countries have conducted extensive and systematic surveys of ^{222}Rn in the air of dwellings and public buildings[2]. Exposure of the population to ^{222}Rn and its short-lived products has been assessed, and, when necessary, mitigation measures have been undertaken in order to reduce the lung cancer risk.

In contrast to indoor radon, outdoor radon has been generally ignored in these national radon surveys and has been limited mostly to the vicinity of uranium mining and milling facilities[4–7]. There are fewer reports of systematic nationwide surveys of outdoor radon than for indoor radon. The results of 17 works were recently reported and summarised by Chen and Harley[8]. There are reports of other surveys. For example the outdoor radon activity concentration in Poland ranged from 3 Bq m^{-3} to 43 Bq m^{-3}, with average values of 5 ± 2 Bq m^{-3} in Łódź, 6 ± 4 Bq m^{-3} in Ciosny, and 10 ± 5 Bq m^{-3} in Kraków[9]. In Germany[10], the average concentration of ^{222}Rn reported for 173 locations throughout the country was 9 ± 1 Bq m^{-3}, with a maximum of 31 Bq m^{-3}. The trend in the ^{222}Rn concentration increases towards the south, which is further away from the seashore where the ^{222}Rn concentration is low. A similar trend between the shore and inland has also been observed at 18 points in Ireland[11], with an average value of 5.6 ± 0.7 Bq m^{-3}. In Slovenia[12], radon activity concentration in outdoor air at 60 points varied from 3.7 Bq m^{-3} to 41 Bq m^{-3}, with an average value of 14 ± 4 Bq m^{-3}. Accurate assessment of the concentration of radon outdoors is important in identifying dwellings where the indoor concentration of ^{222}Rn exceeds national limits[13].

Outdoor ^{222}Rn has been used for a long time as an indicator of volcanic[14] and seismic activity[15], and recently as a convenient tool to assess the stability of the atmosphere[16]. The latter topic has been the focus in one of our recent studies[17, 18] in which the ^{222}Rn and meteorological parameters in outdoor air have been monitored for more than a year. The two monitoring sites have different geology, topography and climate. One of the sites is located in a basin in the central part of the country whereas the other site is in a valley in the west. This paper will report elevated outdoor ^{222}Rn levels and effective doses for this valley location.

EXPERIMENTAL

The 30 km long Vipava valley runs SE−NW, at a distance of 20–30 km from the Trieste Bay, parallel to the coast. The valley is surrounded by 1000–1500 m high mountains on north and east, and by 300–500 m hills toward the sea side. On NW, the valley opens into the plane at the North Adriatic coast. The climate in the valley is sub-Mediterranean and is dominated by conditions related to the sea with mild winters and moderately hot summers (annual

© The Author(s) 2019. Published by Oxford University Press. All rights reserved. For Permissions, please email: journals.permissions@oup.com

Downloaded from https://academic.oup.com/rpd/advance-article-abstract/doi/10.1093/rpd/ncz155/5511484 by guest on 24 October 2019

average air temperature of 14 ± 9°C, ranging from −8°C to 36°C) and annual rainfall height of 600 mm. The site is known for a strong and gusty NE downhill wind 'bora', which is more vigorous and frequent in wintertime persisting for several days, often reaching momentary speeds of more than 30 m s^{-1}. The lithological basis of the measurement site is flysch with carbonates at a distance of less than a few km.

The concentration of ^{222}Rn has been monitored at the meteorological station (45.86° N, 13.9° E) in Dolenje pri Ajdovščini. An AlphaGuard PQ2000 PRO device (Bertin Instruments) was setup inside a Stevenson Screen instrument shelter at 1.5 m above ground, running in the diffusion mode continuously (1 h intervals), with a lower detection limit of about 2 Bq m^{-3}. Annually only 0.7% of radon concentrations were at or below this limit. All measurements fell into the operation range of the instrument reported by the producer (T: −10°C to +50°C, RH: 0–95%, P: 70 kPa to 110 kPa)[19]. The instrument is checked in the laboratory intercomparison test ones per year, using a reference AlphaGuard calibrated in the IFJ-KR-600 Radon Chamber of the Laboratory of Radiometric Expertise, Henryk Niewodniczański Institute of Nuclear Physics, Polish Academy of Sciences, Krakow, Poland[20].

RESULTS AND DISSCUSION

Radon levels

Figure 1 is a box and whisker plot showing results of hourly outdoor ^{222}Rn concentrations arranged by month. Results range from 2 Bq m^{-3} to 144 Bq m^{-3} with lower values of 15 ± 10 Bq m^{-3} observed in winter (21 December–20 March), 15 ± 12 Bq m^{-3} in spring (21 March–20 June), and 17 ± 12 Bq m^{-3} in autumn (23 September–20 December). Higher outdoor ^{222}Rn concentrations, 22 ± 19 Bq m^{-3}, were observed in the summer (21 June–22 September). The similar trend was found also in Ciosny, Łódź and Kraków in Poland[9]. In contrast, observations in Kowary in SW Poland, where magnetite and uranium were exploited, have demonstrated higher outdoor ^{222}Rn values for spring and winter[6], while observations in coastal area in Chiba, Japan only for winter[21].

The annual arithmetic mean of 18 ± 14 Bq m^{-3} at our valley location is higher than the world average of 10 Bq m^{-3}[2] and higher than the Slovenia's average of 14 ± 4 Bq m^{-3}[12]. It is also higher than that obtained at our second location of continuous ^{222}Rn measurements in the central part sub-Alpine basin[17, 18], of 11 ± 9 Bq m^{-3}, although the opposite was expected because the valley is close to the sea, while the basin is inland, more than 80 km away[9, 11].

The seasonal means of daily variation in the outdoor ^{222}Rn concentration for 2018 are presented in Figure 2. The daytime high turbulence in the air mixing layer results in decreasing, and the night-time formation of a surface thermal inversion, in increasing of ^{222}Rn concentration. The period of the highest radon concentration is at night between 22 h and 6 h. The similar observation has been reported by others[7, 9, 15].

Effective doses

The main reason for dose calculation was the elevated ^{222}Rn concentration in summer (Figure 2). Except ^{222}Rn concentration, information on other dosimetry-related parameters were not available, therefore the uncertainty of the estimated doses may be high. However, more than the effective dose itself, the outdoor ^{222}Rn contribution to the total effective dose is emphasised, particularly for summer.

The effective doses E have been calculated applying the UNSCEAR[2] recommendation:

$$E = C_{\mathrm{Rn}} \cdot F \cdot t \cdot f_{\mathrm{DC}},$$

with t—exposure time (h), C_{Rn}—average radon activity concentration (Bq m^{-3}) for period t, F—degree of secular equilibrium between radon and its short-lived products: 0.40 for indoors and 0.60 for outdoors, and f_{DC}—dose conversion factor: 9 nSv h^{-1} (Bq m^{-3})$^{-1}$. Although F values for both outdoors[8, 10] and indoors[8] may differ markedly from place to place, in our calculation, the values recommended by UNSCEAR[2] were taken due to the lack of measured data at our site. The only measured equilibrium factor (F = 0.38) in a house in the valley for the period April–October 2012 did not differ significantly from the above literature value used. The total effective dose (E_{t}) is a sum of the dose due to radon in indoor air (E_{in}) and outdoor air (E_{out}), i.e. $E_{\mathrm{t}} = E_{\mathrm{in}} + E_{\mathrm{out}}$.

Doses have been calculated for different exposure times, and thus for different averages of radon activity concentrations, as follows.

Annual effective dose

For this dose, the above annual arithmetic mean of 18 Bq m^{-3} and exposure time of 1760 h (occupancy factor 0.20) were taken for outdoors, and 66 Bq m^{-3} (as the annual average value in the dwellings in this valley[22]) and 7000 h for indoors (occupancy factor 0.80). The result is:

$$E_{\mathrm{t}} = E_{\mathrm{in}} + E_{\mathrm{out}} = 1.66\ \mathrm{mSv} + 0.17\ \mathrm{mSv} = 1.83\ \mathrm{mSv}.$$

Considering $E_{\mathrm{out}}/E_{\mathrm{t}}$ = 0.09 result, outdoor radon does not contribute significantly in this area. The

Downloaded from https://academic.oup.com/rpd/advance-article-abstract/doi/10.1093/rpd/ncz155/5511484 by guest on 24 October 2019

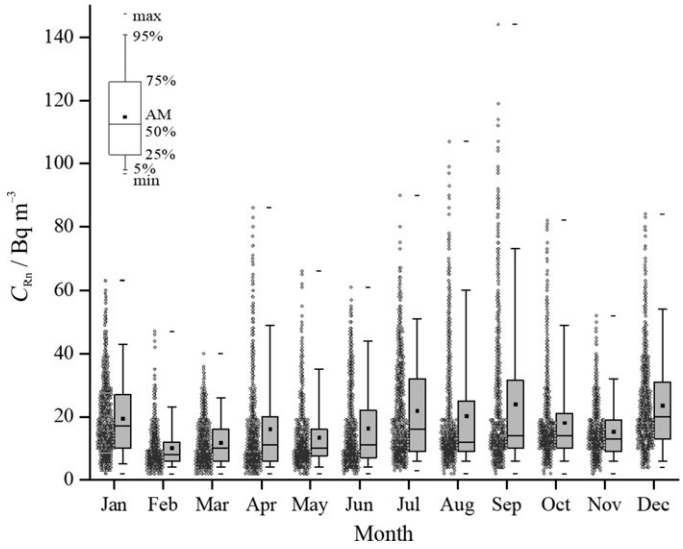


Figure 1. Box and whiskers diagram of hourly radon activity concentrations (C_{Rn}).

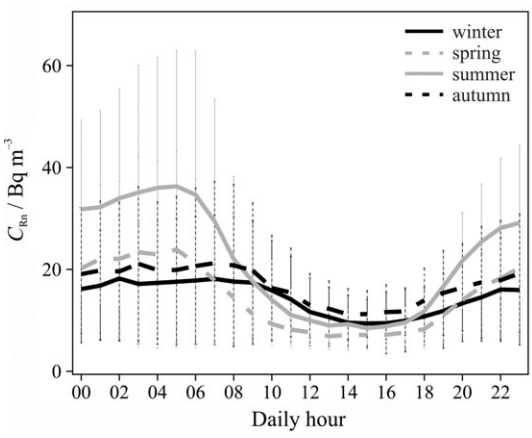


Figure 2. Pattern of seasonal mean outdoor radon concentration (C_{Rn}) in 2018.

annual effective dose E_t in this valley is lower than the Slovenian average E_{in} in homes, 2.2 mSv[23].

Summer effective dose

When the summer average of indoor air radon activity concentration of 37 Bq m^{-3}[20] and outdoor air of 22 Bq m^{-3} were considered (t equals 1765 h and 443 h, respectively), the summer effective dose is obtained: E_s = 0.29 mSv, composed of E_{in} = 0.24 mSv and E_{out} = 0.05 mSv (E_{out}/E_t = 0.18).

'Realistic' summer effective dose – windows kept open

In the Vipava valley, a specific situation could also be considered because in summertime (average air temperature of 23 ± 5°C, ranging from 13 to 36°C), residents keep their windows open day-and-night, except during heavy storms. Hence, radon activity concentration indoors may be equated to its outdoor concentration, with diurnal variation shown by the 'summer' curve in Figure 2. Daily averages of radon activity concentration, separately for daytime (6–22 h) and night-time (22–6 h), are shown in Figure 3. Time of 1765 h spent indoors (F = 0.40) is divided into 736 h spent in night-time (with average concentration of 33.4 Bq m^{-3}) and 1029 h in daytime (with average concentration of 15.2 Bq m^{-3}). For outdoor radon activity concentration 15.2 Bq m^{-3} (F = 0.60) and for t = 443 h have been considered. Taking this into account, the calculation gives: E_s = 0.18 mSv, with E_{in} = 0.14 mSv and E_{out} = 0.04 mSv (E_{out}/E_t = 0.22). These doses are more realistic than those in *'Summer effective dose*' above. Nonetheless, the question rises of whether taking F = 0.40 for 'outdoor' radon in the indoor environment is justified.

Effective dose based on the overall average of radon activity concentration in *'Summer effective dose*' sub-section appears to be about two times higher than that based on the daytime and night-time averages in *''Realistic' summer effective dose – windows kept open*' sub-section. Thus, the former approach is not only simpler than the latter one, but is also conservative, rather overestimating than underestimating doses.

Downloaded from https://academic.oup.com/rpd/advance-article-abstract/doi/10.1093/rpd/ncz155/5511484 by guest on 24 October 2019

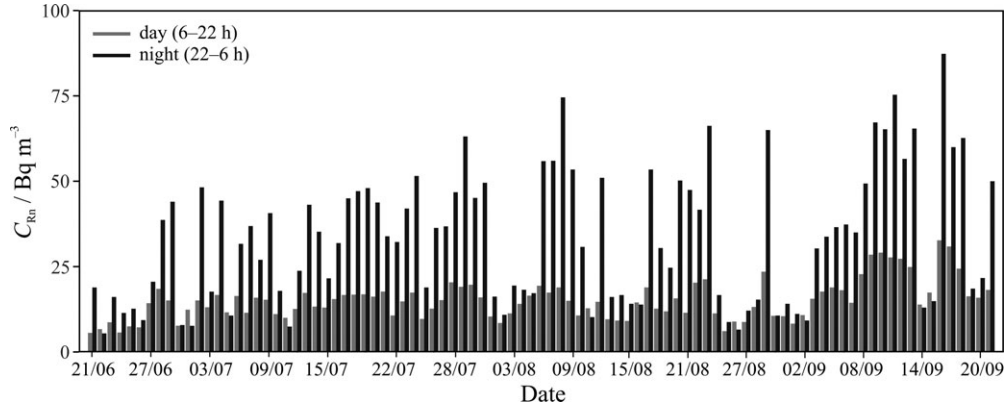


Figure 3. Averages of daytime and night-time radon activity concentration (C_{Rn}) in summer (21 June–22 September 2018).

The summer outdoor effective dose is relatively low and does not increase the total effective dose significantly. However, opening windows overnight to reduce exposure to radon, cannot be effective and, therefore, may not be advised to residents. This caution is particularly necessary because the night-time average radon activity concentration often exceeds 50 Bq m^{-3} (Figure 3) and some hourly spikes may reach over 100 Bq m^{-3} (Figure 1).

CONCLUSION

A year-long monitoring of radon in outdoor air in a valley with a sub-Mediterranean climate has shown the highest outdoor radon activity concentration in summer (22 ± 19 Bq m^{-3}) and the lowest in spring and winter (both 15 ± 12 Bq m^{-3}). In annual effective dose of 1.83 mSv, outdoor radon contributes 9%, and in summer effective dose of 0.29 mSv, it contributes 18%. Although radon concentration often exceeded 50 Bq m^{-3}, the outdoor radon contribution did not contribute significantly to the total annual effective dose. Under such conditions, opening windows overnight to reduce radon levels significantly is not effective.

When the measurements in the valley and in the inland basin have been finished, time series of radon and meteorological parameters will be thoroughly analysed and factors (lithology, meteorology) influencing radon levels and their variations evaluated.

ACKNOWLEDGEMENTS

The authors acknowledge the financial support from the Slovenian Research Agency (research core funding No. P1-0143) and from the Public Scholarship, Development, Disability and Maintenance Fund of the Republic of Slovenia (Contract no. 11011-44/2016-18). They wish to thank to the residents of the Vipava valley for exposure of radon detectors in their houses.

REFERENCES

1. Nero, A. V. *Radon and its decay products in indoor air*. In: Radon and Its Decay Products in Indoor Air. Nazaroff, W. W. and Nero, A. V., Jr, Eds (New York, NY (USA): John Wiley & Sons, Publishers, Inc.) pp. 1–53 (1988).
2. United Nations Scientific Committee on the Effects of Atomic Radiation. Sources, Effects and Risks of Ionizing Radiation. UNSCEAR 2016 Report. Report to the General Assembly, with scientific annexes. United Nations sales publication Sales No. E.17.IX.1. United Nations, New York, (2017).
3. Darby, S. *et al. Radon in homes and risk of lung cancer: collaborative analysis of individual data from 13 European case-control studies*. BMJ **330**, 223 (2005).
4. Kümmel, M., Dushe, C., Müller, S. and Gehrcke, K. *Outdoor ^{222}Rn-concentrations in Germany – part 2 – former mining areas*. J. Environ. Radioact. **132**, 131–137 (2014).
5. Xie, D., Wang, H., Kearfott, K. J., Liu, Z. and Mo, S. *Radon dispersion modeling and dose assessment for uranium mine ventilation shaft exhausts under neutral atmospheric stability*. J. Environ. Radioact. **129**, 57–62 (2014).
6. Tchorz-Trzeciakiewicz, D. E. and Kłos, M. *Factors affecting atmospheric radon concentration, human health*. Sci. Total Environ. **584**, 911–920 (2017).
7. Thinova, L., Bican, R., Fronka, A., Johnova, K., Solc, J. and Vosahlik, J. *Radon concentration in the area of waste rock dumps, Brod, CR–case study*. Radiat. Prot. Dosimetry **177**, 149–154 (2017).
8. Chen, J. and Harley, N. H. *A review of indoor and outdoor radon equilibrium factors–part I: ^{222}Rn*. Health Phys. **115**, 490–499 (2018).
9. Podstawczyńska, A., Kozak, K., Pawlak, W. and Mazur, J. *Seasonal and diurnal variation of outdoor radon (^{222}Rn) concentrations in urban and rural area*

Downloaded from https://academic.oup.com/rpd/advance-article-abstract/doi/10.1093/rpd/ncz155/5511484 by guest on 24 October 2019

with reference to meteorological conditions. Nukleonika **55**, 543–547 (2010).
10. Kümmel, M., Dushe, C., Müller, S. and Gehrcke, K. *Outdoor ^{222}Rn-concentrations in Germany – part 1 – natural background*. J. Environ. Radioact. **132**, 123–130 (2014).
11. Gunning, G. A., Pollard, D. and Finch, E. C. *An outdoor radon survey and minimizing the uncertainties in low level measurements using CR-39 detectors*. J. Radiol. Prot. **34**, 457–467 (2014).
12. Vaupotič, J., Kobal, I. and Križman, M. *Background outdoor radon levels in Slovenia*. Nukleonika **55**, 579–582 (2010).
13. Antignani, S., Venoso, G., Carpentieri, C. and Bochicchio, F. *Analytical method for evaluating (and correcting) the impact of outdoor radon concentration on the estimates of percentage of dwellings exceeding reference levels*. J. Environ. Radioact. **196**, 264–267 (2019).
14. Vaupotič, J., Žvab Rožič, P. and Giammanco, S. *Radon in outdoor air in the Mt. Etna area, Italy*. Nukleonika **55**, 573–577 (2010).
15. Kobayashi, Y. *et al*. *Annual variation in the atmospheric radon concentration in Japan*. J. Environ. Radioact. **146**, 110–118 (2015).
16. Chambers, S. D., Williams, A. G., Crawford, J. and Griffiths, A. D. *On the use of radon for quantifying the effects of atmospheric stability on urban emissions*. Atmos. Chem. Phys. **15**, 1175–1190 (2015).
17. Kikaj, D. and Vaupotič, J. *Parameters influencing deviation of radon concentration from its typical diurnal pattern in the winter and summer seasons*. Geol. Macedonica **31**, 157–170 (2017).
18. Kikaj, D., Chambers, S. D. and Vaupotič, J. *Radon-based atmospheric stability classification in contrasting sub-Alpine and sub-Mediterranean environments*. J. Environ. Radioact. **203**, 125–134 (2019).
19. AlphaGUARD, Portable Radon Monitor, User Manual 08/2012, Saphymo GmbH, Germany, (2012).
20. Kozak, K., Mazur, J., Vaupotič, J., Kobal, I., Janik, M. and Kochowska, E.: Calibration of the IJS-CRn and IFJ-PAN radon measuring devices in the IFJ-KR-600 radon chamber, Jožef Stefan Institute Report IJS-DP-10103, Ljubljana, (2009).
21. Janik, M. and Bossew, P. *Analysis of simultaneous time series of indoor, outdoor and soil air radon concentrations, meteorological and seismic data*. Nukleonika **61**, 295–302 (2016).
22. Vaupotič *et al*. *Radon survey within a regular grid in homes in Slovenia*. In: VII. Hungarian Radon Forum and Radon and Environment Satellite Workshop: Veszprém, Hungary, 2013. Kovács T., Ed. (Veszprém: Pannonian University Press) pp. 195–200 (2013).
23. Žunić, Z. S. *et al*. *Effective doses estimated from the results of direct radon and thoron progeny sensors (DRPS/DTPS), exposed in selected regions of Balkans*. Radiat. Prot. Dosimetry (2019). doi: 10.1093/rpd/ncz025.

Downloaded from https://academic.oup.com/rpd/advance-article-abstract/doi/10.1093/rpd/ncz155/5511484 by guest on 24 October 2019

Chapter 5

Conclusions

This study exploits the unique physical properties of the naturally occurring radioactive gas radon that make it a convenient and reliable indicator of the atmospheric mixing state (or "atmospheric stability") of the boundary layer. Atmospheric processes that influence the variability of pollutant concentration in urban settings are not completely understood, particularly in regions of complex topography (e.g. the Mediterranean Basin Region; MBR). Poor air quality in such complex environments can also be exacerbated by synoptic timescale persistent temperature inversion (PTI) conditions, which can lead to pollution events of potentially life-threatening duration and intensity. Consequently, the emphasis of this research was placed on characterizing and contrasting the atmospheric mixing state of two complex terrain environments (Ljubljana, an urban subalpine basin and Ajdovščina, a sub-Mediterranean town within Vipava Valley) on diurnal, synoptic, and seasonal timescales.

The scientific contributions of this study include seven peer-reviewed scientific papers. The main conclusions drawn from the present research, which consisted of three main aims that roughly follow the order of the scientific articles presented in this dissertation, can be summarised as follows:

1. The first investigation dealt with devising a reliable and seasonally independent radon-based method to identify synoptic timescale PTI events in topographic basin environments, and the following conclusions were derived:
    - radon-based identification of PTI events is more reliable than the conventional pseudo-vertical temperature gradient method;
    - the radon-based method enables superior characterization of relative changes in meteorology and air quality across the diurnal cycle during PTI events;
    - composite radiosonde profiles clearly explained the regional meteorological conditions contributing to the highest pollution episodes during PTI events detected by the radon-based method;
    - the PTI conditions identified can be separately grouped as a new atmospheric mixing class of the contemporary diurnal radon-based stability classification method.
2. The second investigation dealt with the use of a diurnal radon-based stability classification method in summer (under non-PTI conditions) to compare the atmospheric dispersion characteristics of two contrasting topographic regions: a basin environment (Ljubljana), and a valley region (Ajdovščina), from which the following conclusions were derived:
    - the ability of the diurnal radon-based method to consistently distinguish between subtle changes in the atmospheric mixing state at sites with contrasting topographic settings demonstrates that it is a powerful tool for characterising air quality variability in these contrasting environments;
    - diurnal radon cycles indicated that the capability of the atmosphere to dilute primary pollutants is considerably less in topographic basin environments.

3. The third investigation combined, for the first-time, an existing diurnal radon-based atmospheric mixing classification method with a novel radon-based tool (developed as part of this thesis) for the identification of synoptic timescale PTI events, from which the following conclusions were derived:
    - the variability of urban pollutant (CO, BC, NO_2, SO_2, PM_{10}, and O_3) concentrations within the Ljubljana Basin were characterised across the diurnal cycle each season with unprecedented detail;
    - for the first time in this region, a clear distinction was made between individual high-pollution events associated with passing high-pressure systems (on class #5 nights), and persistent high-pollution episodes associated with the lingering presence of the "Siberian High";
    - the ability of the radon-based approach to group similar atmospheric conditions (class types) throughout the deeper atmosphere (i.e. beyond the SNBL where the technique was developed) was demonstrated, through an analysis of one year (Dec 2016–Nov 2017) of radiosonde profiles around dawn each day.

The combined diurnal and synoptic timescale radon-based mixing classification techniques described here help to separate "uncontrollable" influences on air quality variability (e.g. meteorology, geographic setting, topographic effects, and cross boundary pollution), from controllable influences (e.g. source strengths and distribution). This is a crucial step toward being able to make a quantitative evaluation of pollution mitigation measures. The techniques described in this study are not specific to the Ljubljana Basin region. They are universally applicable to non-coastal urban centers in Europe as well as to other continental mid- to high-latitude regions (e.g. central North America).

The results of this Ph.D. project have demonstrated that radon-based methods of classifying the atmospheric mixing state in urban regions (in simple or complex topographic settings) is simpler and more effective than meteorological approaches. For the first time it has also been shown that radon-based classification methods can provide a consistent and representative tool by which to account for both diurnal and synoptic timescale changes in the atmospheric mixing state of complex terrain environments. While it was also shown that radon-based class typing is capable of grouping "similar" atmospheric conditions (i.e. with reduced variability) throughout the lower troposphere (0–2 km a.s.l.), near-surface radon observations are not predictive of the vertical atmospheric structure and cannot replace the detailed information provided by radiosondes or laser/acoustic profilers.

The results of the presented Ph.D. thesis are also important from a socioeconomic aspect. Based on the consistency and accuracy of radon-based atmospheric classification methods, and the fact that routine radon monitoring will become more common from a radiological public health perspective, it is expected that the method derived here will be a powerful tool in urban centers for air quality management and assessing public health risks.

Appendix A

Radon Data and Stability Analysis

A.1 Ljubljana Basin

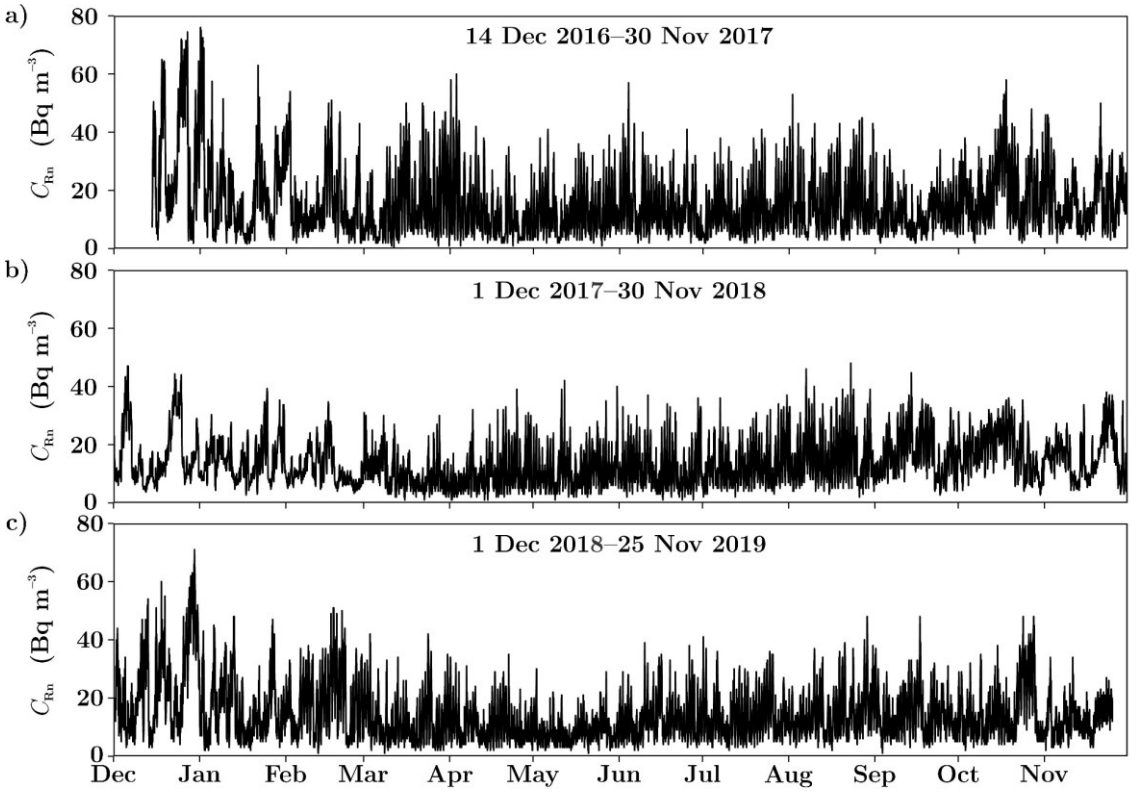


Figure A1.1: Time series of hourly radon concentration observations for three years: a) 14 Dec 2016–30 Nov 2017, b) 1 Dec 2017–30 Nov 2018, and c) 1 Dec 2018–25 Nov 2019.

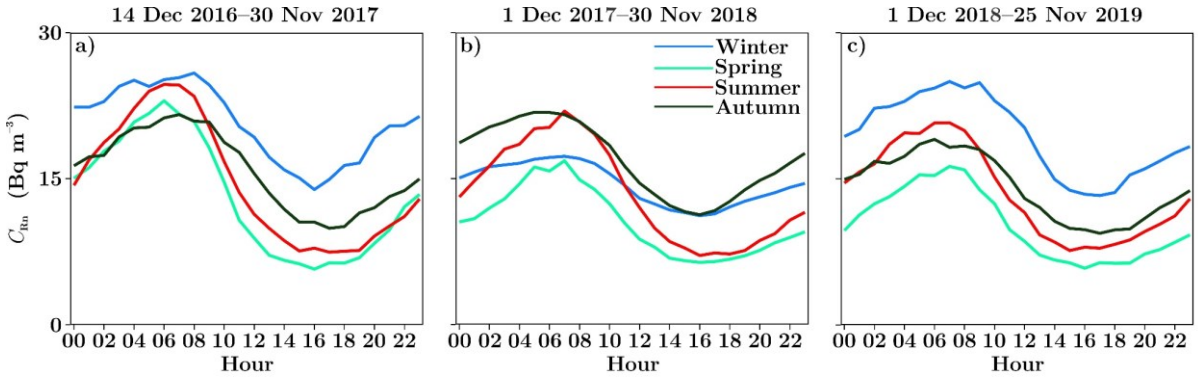


Figure A1.2: Diurnal composite plots of observed radon concentrations by season for three years: a) 14 Dec 2016–30 Nov 2017, b) 1 Dec 2017–30 Nov 2018, and c) 1 Dec 2018–25 Nov 2019.

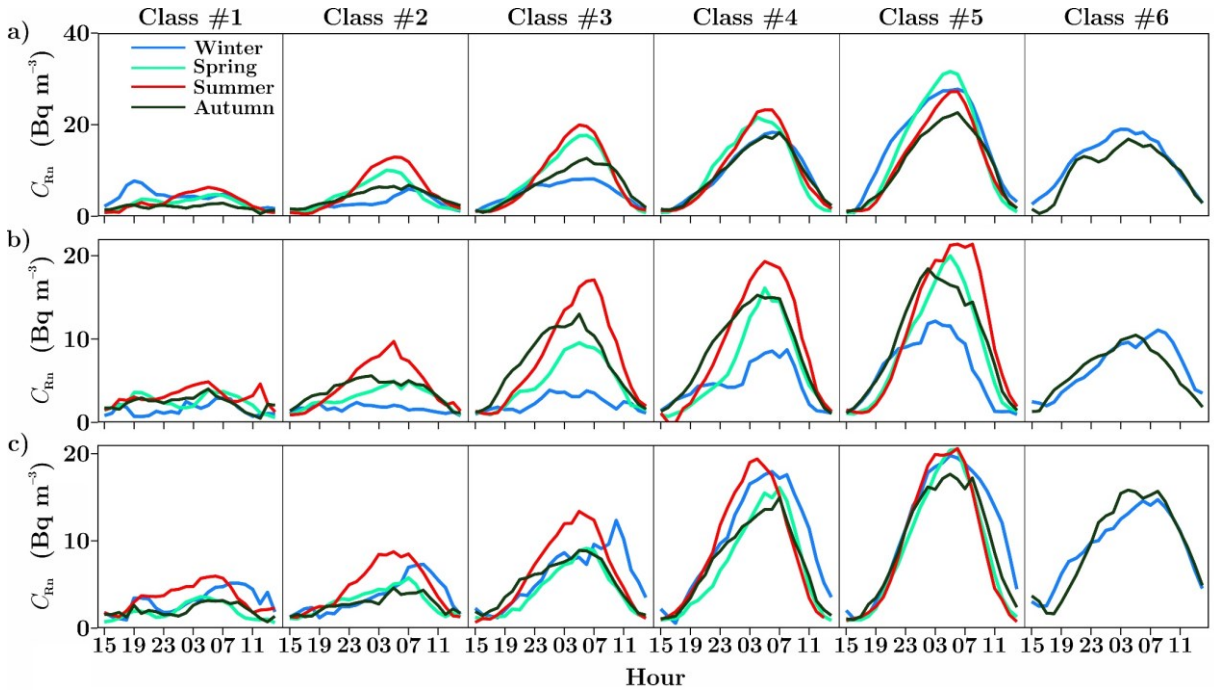


Figure A1.3: Diurnal composite plots of mixing-related radon concentrations by season and radon-based atmospheric mixing classes for three years: a) 14 Dec 2016–30 Nov 2017, b) 1 Dec 2017–30 Nov 2018, and c) 1 Dec 2018–25 Nov 2019.

Composite plots of hourly time rate of change of radon concentration (ΔC_{Rn}) within six mixing classes (#1 to #5 and weak/strong #6) as a evidence of weaker SNBL under the class #6 (PTI) conditions in comparison to class #5 (strongly stable) conditions.

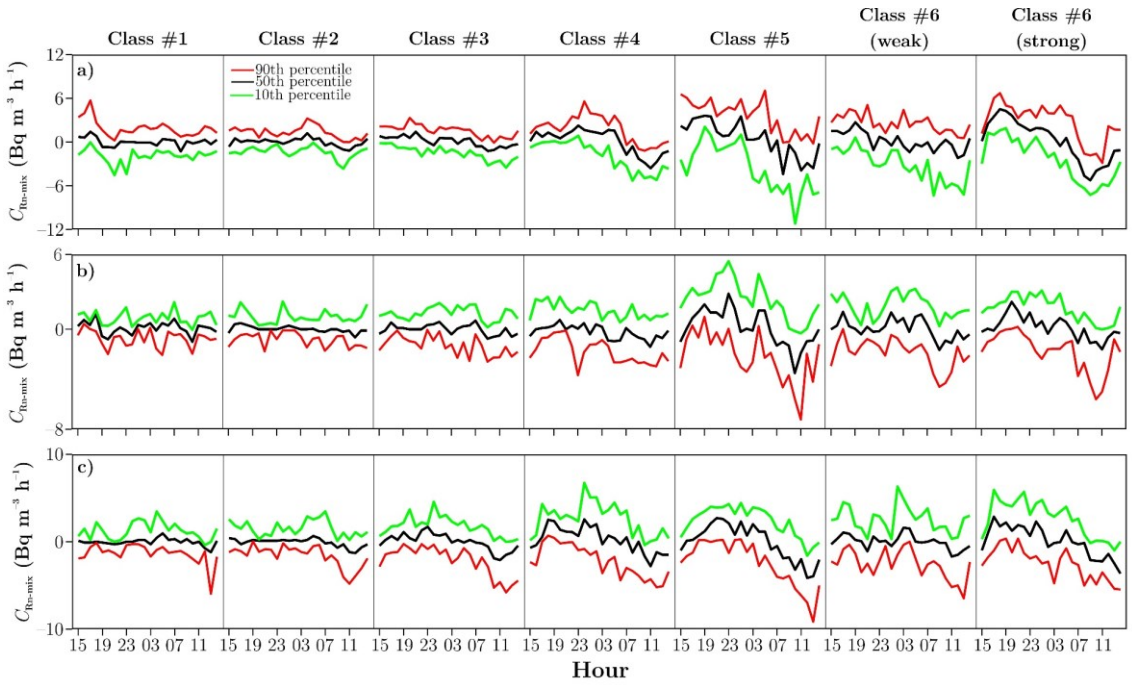


Figure A1.4: Composite plots of the hourly time rate of change of radon concentration within six radon-based atmospheric mixing classes (#1 to #5 and weak/strong #6) for three winters: a) 14 Dec 2016–28 Feb 2017, b) 1 Dec 2017–28 Feb 2018, and c) 1 Dec 2018–28 Feb 2019.

Table A1.1: Daily mean observed radon concentrations within each of the radon-based atmospheric mixing classes by season over the three years of measurements (Dec 2016–Nov 2019) in Ljubljana Basin.

	Winter (Dec 2016–Feb 2017)	**Spring (Mar 2017–May 2017)**	**Summer (Jun 2017–Aug 2017)**	**Autumn (Sep 2017–Nov 2017)**
Class	*Daily mean radon concentration (Bq m^{-3})*	*Daily mean radon concentration (Bq m^{-3})*	*Daily mean radon concentration (Bq m^{-3})*	*Daily mean radon concentration (Bq m^{-3})*
#1	13.8	7.3	8.4	8.4
#2	8.8	8.7	11.5	15.1
#3	12.4	11.0	14.7	13.8
#4	13.5	14.4	15.9	15.7
#5	29.0	21.4	20	20.9
#6	38.0	/	/	28.2
	Winter (Dec 2017–Feb 2018)	**Spring (Mar 2018–May 2018)**	**Summer (Jun 2018–Aug 2018)**	**Autumn (Sep 2018–Nov 2018)**
Class	*Daily mean radon concentration (Bq m^{-3})*	*Daily mean radon concentration (Bq m^{-3})*	*Daily mean radon concentration (Bq m^{-3})*	*Daily mean radon concentration (Bq m^{-3})*
#1	9.1	9.9	9.6	8.0
#2	8.6	8.9	9.1	11.3
#3	10.8	9.4	12.9	13.2
#4	10.9	11.7	15.4	15.3
#5	14.1	13.9	18.9	21.6
#6	22.3	/	/	22.8
	Winter (Dec 2018–Feb 2019)	**Spring (Mar 2019–May 2019)**	**Summer (Jun 2019–Aug 2019)**	**Autumn (Sep 2019–Nov 2019)**
Class	*Daily mean radon concentration (Bq m^{-3})*	*Daily mean radon concentration (Bq m^{-3})*	*Daily mean radon concentration (Bq m^{-3})*	*Daily mean radon concentration (Bq m^{-3})*
#1	8.5	6.5	10.3	13.8
#2	10.7	8.5	10.6	9.4
#3	15.7	8.4	11.5	11.9
#4	16.1	11.5	14.5	11.6
#5	20.9	15.6	16.8	19.5
#6	30.9	/	/	22.6

Table. A1.2: Seasonal threshold values used to define six radon-based atmospheric mixing classes during the three years of measurements (Dec 2016–Nov 2019) in Ljubljana Basin. Occurrence frequency (as a % of each 90-day) of each mixing class for all seasons of each year is also provided.

	Winter (Dec 2016–Feb 2017)		**Spring (Mar 2017–May 2017)**		**Summer (Jun 2017–Aug 2017)**		**Autumn (Sep 2017–Nov 2017)**	
Class	*Radon Concentration* ($Bq\ m^{-3}$)	*Duration* (%)	*Radon Concentration* ($Bq\ m^{-3}$)	*Duration* (%)	*Radon Concentration* ($Bq\ m^{-3}$)	*Duration* (%)	*Radon Concentration* ($Bq\ m^{-3}$)	*Duration* (%)
#1	$C_{\mathrm{Rn-noc}} < -0.1$	12	$C_{\mathrm{Rn-noc}} < 2.6$	20	$C_{\mathrm{Rn-noc}} < 3.8$	21	$C_{\mathrm{Rn-noc}} < 1.3$	13
#2	$-0.1 \leq C_{\mathrm{Rn-noc}} < 1.7$	20	$2.6 \leq C_{\mathrm{Rn-noc}} < 5.6$	19	$3.8 \leq C_{\mathrm{Rn-noc}} < 7.5$	19	$1.3 \leq C_{\mathrm{Rn-noc}} < 3.3$	23
#3	$1.7 \leq C_{\mathrm{Rn-noc}} < 4.8$	19	$5.6 \leq C_{\mathrm{Rn-noc}} < 8.9$	20	$7.5 \leq C_{\mathrm{Rn-noc}} < 9.3$	19	$3.3 \leq C_{\mathrm{Rn-noc}} < 6.1$	22
#4	$4.8 \leq C_{\mathrm{Rn-noc}} < 8.7$	15	$8.9 \leq C_{\mathrm{Rn-noc}} < 12.1$	20	$9.3 \leq C_{\mathrm{Rn-noc}} < 11.2$	19	$6.1 \leq C_{\mathrm{Rn-noc}} < 7.9$	21
#5	$C_{\mathrm{Rn-noc}} \geq 8.7$	14	$C_{\mathrm{Rn-noc}} \geq 12.1$	21	$C_{\mathrm{Rn-noc}} \geq 11.2$	21	$C_{\mathrm{Rn-noc}} \geq 7.9$	15
#6	$C_{\mathrm{Rn-syn}} > 6.8\ (sd\ C_{\mathrm{Rn-mix}}) \geq 48$ h	20	$C_{\mathrm{Rn-syn}} > 8.7\ (sd\ C_{\mathrm{Rn-mix}}) \geq 48$ h	0	$C_{\mathrm{Rn-syn}} > 7.9\ (sd\ C_{\mathrm{Rn-mix}}) \geq 48$ h	0	$C_{\mathrm{Rn-syn}} > 6.8\ (sd\ C_{\mathrm{Rn-mix}}) \geq 48$ h	6
	Winter (Dec 2017–Feb 2018)		**Spring (Mar 2018–May 2018)**		**Summer (Jun 2018–Aug 2018)**		**Autumn (Sep 2018–Nov 2018)**	
Class	*Radon Concentration* ($Bq\ m^{-3}$)	*Duration* (%)	*Radon Concentration* ($Bq\ m^{-3}$)	*Duration* (%)	*Radon Concentration* ($Bq\ m^{-3}$)	*Duration* (%)	*Radon Concentration* ($Bq\ m^{-3}$)	*Duration* (%)
#1	$C_{\mathrm{Rn-noc}} < -0.2$	7	$C_{\mathrm{Rn-noc}} < 0.6$	12	$C_{\mathrm{Rn-noc}} < 1.3$	11	$C_{\mathrm{Rn-noc}} < 0.6$	8
#2	$-0.2 \leq C_{\mathrm{Rn-noc}} < 0.7$	15	$0.6 \leq C_{\mathrm{Rn-noc}} < 2.8$	27	$1.3 \leq C_{\mathrm{Rn-noc}} < 6.2$	24	$0.6 \leq C_{\mathrm{Rn-noc}} < 3.5$	12
#3	$0.7 \leq C_{\mathrm{Rn-noc}} < 1.4$	19	$2.8 \leq C_{\mathrm{Rn-noc}} < 5$	20	$6.2 \leq C_{\mathrm{Rn-noc}} < 8.5$	26	$3.5 \leq C_{\mathrm{Rn-noc}} < 5.2$	22
#4	$1.4 \leq C_{\mathrm{Rn-noc}} < 3.5$	15	$5 \leq C_{\mathrm{Rn-noc}} < 7.1$	22	$8.5 \leq C_{\mathrm{Rn-noc}} < 10.4$	22	$5.2 \leq C_{\mathrm{Rn-noc}} < 7.3$	23
#5	$C_{\mathrm{Rn-noc}} \geq 3.5$	14	$C_{\mathrm{Rn-noc}} \geq 7.1$	19	$C_{\mathrm{Rn-noc}} \geq 10.4$	17	$C_{\mathrm{Rn-noc}} \geq 7.3$	15
#6	$C_{\mathrm{Rn-syn}} > 5\ (sd\ C_{\mathrm{Rn-mix}}) \geq 48$ h	30	$C_{\mathrm{Rn-syn}} > 5.3\ (sd\ C_{\mathrm{Rn-mix}}) \geq 48$ h	0	$C_{\mathrm{Rn-syn}} > 6.6\ (sd\ C_{\mathrm{Rn-mix}}) \geq 48$ h	0	$C_{\mathrm{Rn-syn}} > 6.1\ (sd\ C_{\mathrm{Rn-mix}}) \geq 48$ h	20
	Winter (Dec 2018–Feb 2019)		**Spring (Mar 2019–May 2019)**		**Summer (Jun 2019–Aug 2019)**		**Autumn (Sep 2019–Nov 2019)**	
Class	*Radon Concentration* ($Bq\ m^{-3}$)	*Duration* (%)	*Radon Concentration* ($Bq\ m^{-3}$)	*Duration* (%)	*Radon Concentration* ($Bq\ m^{-3}$)	*Duration* (%)	*Radon Concentration* ($Bq\ m^{-3}$)	*Duration* (%)
#1	$C_{\mathrm{Rn-noc}} < 0.3$	10	$C_{\mathrm{Rn-noc}} < 1.2$	14	$C_{\mathrm{Rn-noc}} < 2.3$	13	$C_{\mathrm{Rn-noc}} < 0.7$	9
#2	$0.3 \leq C_{\mathrm{Rn-noc}} < 2.3$	17	$1.2 \leq C_{\mathrm{Rn-noc}} < 2.5$	23	$2.3 \leq C_{\mathrm{Rn-noc}} < 5.2$	21	$0.7 \leq C_{\mathrm{Rn-noc}} < 2.5$	23
#3	$2.3 \leq C_{\mathrm{Rn-noc}} < 4.9$	16	$2.5 \leq C_{\mathrm{Rn-noc}} < 4.7$	23	$5.2 \leq C_{\mathrm{Rn-noc}} < 7.2$	24	$2.5 \leq C_{\mathrm{Rn-noc}} < 4.3$	21
#4	$4.9 \leq C_{\mathrm{Rn-noc}} < 8.6$	16	$4.7 \leq C_{\mathrm{Rn-noc}} < 7.2$	22	$7.2 \leq C_{\mathrm{Rn-noc}} < 8.8$	24	$4.3 \leq C_{\mathrm{Rn-noc}} < 7.3$	19
#5	$C_{\mathrm{Rn-noc}} \geq 8.6$	17	$C_{\mathrm{Rn-noc}} \geq 7.2$	18	$C_{\mathrm{Rn-noc}} \geq 8.8$	18	$C_{\mathrm{Rn-noc}} \geq 7.3$	17
#6	$C_{\mathrm{Rn-syn}} > 7.6\ (sd\ C_{\mathrm{Rn-mix}}) \geq 48$ h	24	$C_{\mathrm{Rn-syn}} > 5.5\ (+\sigma\ C_{\mathrm{Rn-mix}}) \geq 48$ h	0	$C_{\mathrm{Rn-syn}} > 6.2\ (sd\ C_{\mathrm{Rn-mix}}) \geq 48$ h	0	$C_{\mathrm{Rn-syn}} > 6\ (sd\ C_{\mathrm{Rn-mix}}) \geq 48$ h	11

*$C_{\mathrm{Rn-mix}}$ – mixing-related radon concentration;
*$C_{\mathrm{Rn-noc}}$ – nocturnal-mean diurnal radon;
*$C_{\mathrm{Rn-syn}}$ – synoptic radon concentration.

A.2 Vipava Valley

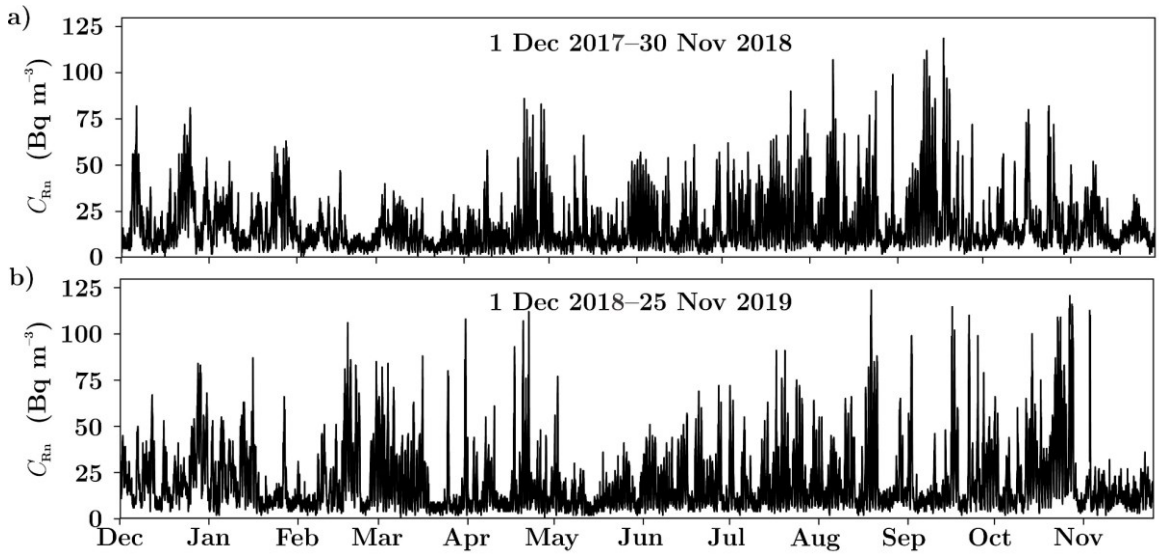


Figure A2.1: Time series of hourly radon concentration observations for two years: a) 1 Dec 2017–30 Nov 2018, and b) 1 Dec 2018–25 Nov 2019.

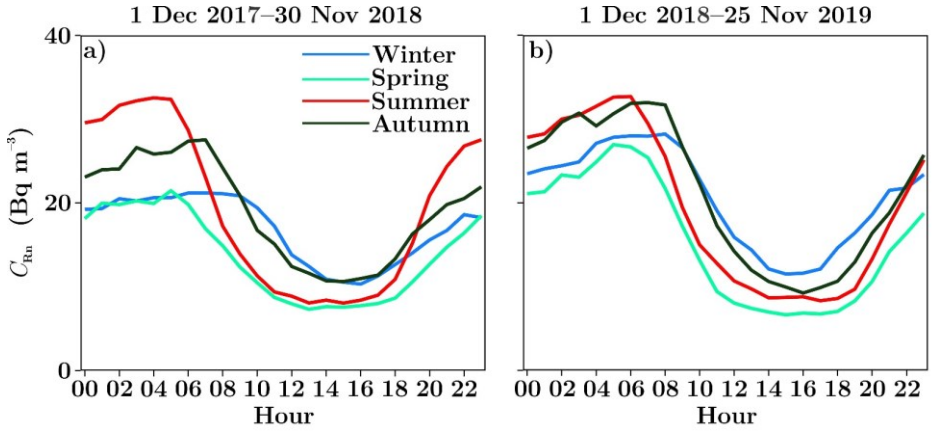


Figure A2.2: Diurnal composite plots of observed radon concentrations by season for two years: a) 1 Dec 2017–30 Nov 2018, and b) 1 Dec 2018–25 Nov 2019.

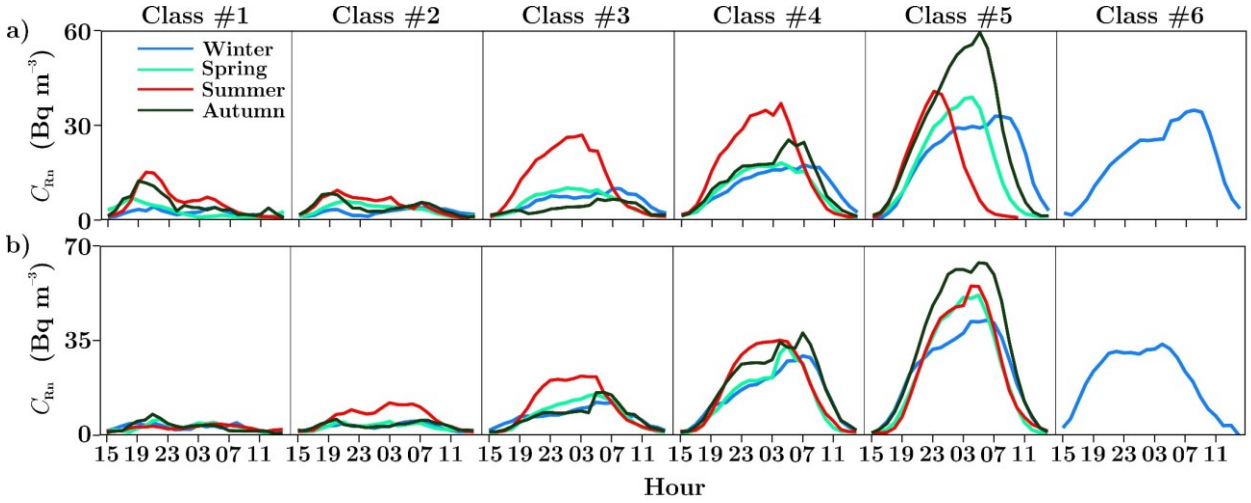


Figure A2.3: Diurnal composite plots of mixing-related radon concentrations by season and radon-based atmospheric mixing classes for two years: a) 1 Dec 2017–30 Nov 2018, and b) 1 Dec 2018–25 Nov 2019.

Table. A2.1: Daily mean measured radon concentrations within each radon-based atmospheric mixing class by season over the two and a half years of measurements (Sep 2017–Nov 2019) in Ajdovščina.

	Winter (Dec 2016–Feb 2017)	**Spring (Mar 2017–May 2017)**	**Summer (Jun 2017–Aug 2017)**	**Autumn (Sep 2017–Nov 2017)**
Class	*Daily mean radon concentration (Bq m^{-3})*	*Daily mean radon concentration (Bq m^{-3})*	*Daily mean radon concentration (Bq m^{-3})*	*Daily mean radon concentration (Bq m^{-3})*
#1				10.5
#2				9.2
#3				15.7
#4				28.4
#5				48.5
#6				/
	Winter (Dec 2017–Feb 2018)	**Spring (Mar 2018–May 2018)**	**Summer (Jun 2018–Aug 2018)**	**Autumn (Sep 2018–Nov 2018)**
Class	*Daily mean radon concentration (Bq m^{-3})*	*Daily mean radon concentration (Bq m^{-3})*	*Daily mean radon concentration (Bq m^{-3})*	*Daily mean radon concentration (Bq m^{-3})*
#1	7.2	8.8	12.1	13.6
#2	9.0	8.0	8.8	10.2
#3	13.6	10.4	17.5	14.4
#4	24.3	19.4	21.2	17.7
#5	39.4	24.1	28.6	38.4
#6	42.3	/	/	/
	Winter (Dec 2018–Feb 2019)	**Spring (Mar 2019–May 2019)**	**Summer (Jun 2019–Aug 2019)**	**Autumn (Sep 2019–Nov 2019)**
Class	*Daily mean radon concentration (Bq m^{-3})*	*Daily mean radon concentration (Bq m^{-3})*	*Daily mean radon concentration (Bq m^{-3})*	*Daily mean radon concentration (Bq m^{-3})*
#1	9.1	7.4	10.6	9.9
#2	9.5	7.5	13.8	11.8
#3	15.0	13.3	14.8	14.0
#4	20.5	16.4	23.5	22.4
#5	37.6	32.0	31.9	49.0
#6	41.9	/	/	/

Table. A2.2: Seasonal threshold values used to define the six radon-based atmospheric mixing classes during the two and a half years of measurements (Sep 2017–Nov 2019) in Ajdovščina. Occurrence frequency (as a % of each 90-day) of each mixing class for all seasons of each year is also provided.

	Winter (Dec 2016–Feb 2017)		**Spring (Mar 2017–May 2017)**		**Summer (Jun 2017–Aug 2017)**		**Autumn (Sep 2017–Nov 2017)**	
Class	*Radon Concentration* ($Bq\ m^{-3}$)	*Duration* (%)	*Radon Concentration* ($Bq\ m^{-3}$)	*Duration* (%)	*Radon Concentration* ($Bq\ m^{-3}$)	*Duration* (%)	*Radon Concentration* ($Bq\ m^{-3}$)	*Duration* (%)
#1							$C_{\mathrm{Rn-noc}} < 0$	16
#2							$0 \leq C_{\mathrm{Rn-noc}} < 2.7$	26
#3							$2.7 \leq C_{\mathrm{Rn-noc}} < 10.8$	24
#4							$10.8 \leq C_{\mathrm{Rn-noc}} < 17.3$	22
#5							$C_{\mathrm{Rn-noc}} \geq 17.3$	16
#6							$C_{\mathrm{Rn-syn}} > 14\ (sd\ C_{\mathrm{Rn-mix}}) \geq 48$ h	0
	Winter (Dec 2017–Feb 2018)		**Spring (Mar 2018–May 2018)**		**Summer (Jun 2018–Aug 2018)**		**Autumn (Sep 2018–Nov 2018)**	
Class	*Radon Concentration* ($Bq\ m^{-3}$)	*Duration* (%)	*Radon Concentration* ($Bq\ m^{-3}$)	*Duration* (%)	*Radon Concentration* ($Bq\ m^{-3}$)	*Duration* (%)	*Radon Concentration* ($Bq\ m^{-3}$)	*Duration* (%)
#1	$C_{\mathrm{Rn-noc}} < -0.4$	13	$C_{\mathrm{Rn-noc}} < -1.1$	12	$C_{\mathrm{Rn-noc}} < -3.5$	12	$C_{\mathrm{Rn-noc}} < -2.3$	8
#2	$-0.4 \leq C_{\mathrm{Rn-noc}} < 2.0$	23	$-1.1 \leq C_{\mathrm{Rn-noc}} < 2.5$	27	$-3.5 \leq C_{\mathrm{Rn-noc}} < 6.4$	24	$-2.3 \leq C_{\mathrm{Rn-noc}} < 0$	28
#3	$2.0 \leq C_{\mathrm{Rn-noc}} < 4.9$	26	$2.5 \leq C_{\mathrm{Rn-noc}} < 7.7$	20	$6.4 \leq C_{\mathrm{Rn-noc}} < 14.5$	26	$0 \leq C_{\mathrm{Rn-noc}} < 4.9$	27
#4	$4.9 \leq C_{\mathrm{Rn-noc}} < 11.7$	20	$7.7 \leq C_{\mathrm{Rn-noc}} < 13.7$	22	$14.5 \leq C_{\mathrm{Rn-noc}} < 22.8$	21	$4.9 \leq C_{\mathrm{Rn-noc}} < 17.6$	22
#5	$C_{\mathrm{Rn-noc}} \geq 11.7$	12	$C_{\mathrm{Rn-noc}} \geq 13.7$	19	$C_{\mathrm{Rn-noc}} \geq 22.8$	17	$C_{\mathrm{Rn-noc}} \geq 17.6$	15
#6	$C_{\mathrm{Rn-syn}} > 10\ (sd\ C_{\mathrm{Rn-mix}}) \geq 48$ h	6	$C_{\mathrm{Rn-syn}} > 10\ (sd\ C_{\mathrm{Rn-mix}}) \geq 48$ h	0	$C_{\mathrm{Rn-syn}} > 15\ (sd\ C_{\mathrm{Rn-mix}}) \geq 48$ h	0	$C_{\mathrm{Rn-syn}} > 15\ (sd\ C_{\mathrm{Rn-mix}}) \geq 48$ h	0
	Winter (Dec 2018–Feb 2019)		**Spring (Mar 2019–May 2019)**		**Summer (Jun 2019–Aug 2019)**		**Autumn (Sep 2019–Nov 2019)**	
Class	*Radon Concentration* ($Bq\ m^{-3}$)	*Duration* (%)	*Radon Concentration* ($Bq\ m^{-3}$)	*Duration* (%)	*Radon Concentration* ($Bq\ m^{-3}$)	*Duration* (%)	*Radon Concentration* ($Bq\ m^{-3}$)	*Duration* (%)
#1	$C_{\mathrm{Rn-noc}} < -1$	10	$C_{\mathrm{Rn-noc}} < -0.2$	11	$C_{\mathrm{Rn-noc}} < 0.4$	14	$C_{\mathrm{Rn-noc}} < -0.7$	11
#2	$-1 \leq C_{\mathrm{Rn-noc}} < 0.7$	23	$-0.2 \leq C_{\mathrm{Rn-noc}} < 4.3$	25	$0.4 \leq C_{\mathrm{Rn-noc}} < 7.9$	22	$-0.7 \leq C_{\mathrm{Rn-noc}} < 1.5$	25
#3	$0.7 \leq C_{\mathrm{Rn-noc}} < 5.1$	26	$4.3 \leq C_{\mathrm{Rn-noc}} < 10.4$	27	$7.9 \leq C_{\mathrm{Rn-noc}} < 21.2$	25	$1.5 \leq C_{\mathrm{Rn-noc}} < 10$	27
#4	$5.1 \leq C_{\mathrm{Rn-noc}} < 13$	18	$10.4 \leq C_{\mathrm{Rn-noc}} < 18.6$	22	$21.2 \leq C_{\mathrm{Rn-noc}} < 29.1$	24	$10 \leq C_{\mathrm{Rn-noc}} < 23.7$	21
#5	$C_{\mathrm{Rn-noc}} \geq 13$	18	$C_{\mathrm{Rn-noc}} \geq 18.6$	15	$C_{\mathrm{Rn-noc}} \geq 29.1$	15	$C_{\mathrm{Rn-noc}} \geq 23.7$	16
#6	$C_{\mathrm{Rn-syn}} > 14\ (sd\ C_{\mathrm{Rn-mix}}) \geq 48$ h	5	$C_{\mathrm{Rn-syn}} > 13\ (sd\ C_{\mathrm{Rn-mix}}) \geq 48$ h	0	$C_{\mathrm{Rn-syn}} > 16\ (sd\ C_{\mathrm{Rn-mix}}) \geq 48$ h	0	$C_{\mathrm{Rn-syn}} > 20\ (sd\ C_{\mathrm{Rn-mix}}) \geq 48$ h	0

*$C_{\mathrm{Rn-mix}}$ – mixing-related radon concentration;
*$C_{\mathrm{Rn-noc}}$ – nocturnal-mean diurnal radon;
*$C_{\mathrm{Rn-syn}}$ – synoptic radon concentration.

Appendix B

Radiosonde Vertical Profiles within Radon Atmospheric Mixing Classes

Morning radiosonde data (air temperature and wind speed) for each season (Winter: Dec 2016–Feb 2017; Spring: Mar 2017–May 2017; Summer: Jun 2017–Aug 2017; Autumn: Sep 2017–Nov 2017) are classified according to the radon-based atmospheric mixing classes derived near the surface within the SNBL (**Figures B1, B2, B3 and B4**).

In general, mixing classes #1, #2, and #3 experience the highest mechanical air mixing with daily average near surface wind speeds ≥ 1 m s^{-1} (**Figures B1 a-c, B2 a-c, B3 a-c, B4 a-c**). Wind profiles indicated the presence of cyclonic conditions, with a wind speed of maximum (in winter and autumn 10–14 m s^{-1}, see **Figures B1 a-c, B4 a-c**; in spring and summer 6–12 m s^{-1}, see **Figures B2 a-c, B2 a-c**), at around 1800 m a.g.l. During these conditions it is expected that basin air is mixed well and only by mechanical turbulence and that there should be little to no heating by the surface (i.e. $\Delta T/\Delta z \cong$ –6.5 °C km^{-1}). This was confirmed by morning vertical air temperature profiles for class #1, #2, and #3 days. These mixing classes had a lapse rate of ~ –6.5 °C km^{-1}, which corresponds to adiabatic lapse rate of the standard ("average") atmosphere.

By contrast, stable nights (classes #4 and #5) were associated with strong near surface nocturnal inversions. The sonde-derived morning lapse rate over the depth of the basin was sub-adiabatic (i.e. $\Delta T/\Delta z \geq$ –6.5 °C km^{-1}) indicating that the deeper basin atmosphere was tending toward stability. The wind speed profile under class #5 conditions indicated speeds below 5 m s^{-1} to a height of 600 m a.g.l., for winter and autumn (**Figures B1e, B4e**) and to a height of 1000 m a.g.l. for spring and summer (**Figures B2d, B3d**). In all seasons, stronger winds aloft were presented for class #5 (**Figures B1e, B2d, B3d, B4e**).

The combined radon-based mixing scheme also detected periods associated with mixing changes at synoptic timescales (class #6) in winter and autumn in Ljubljana Basin (**Figures B1f and B4f**). The sonde-derived lapse rate over the depth of the basin (300 to 1200 m) under class #6 conditions indicated of overall stability. Within the basin atmosphere, however, more structure was evident. On average a strong surface inversion (at ~20 m in winter and ~50 m in autumn) was evident, with a second inversion around 1000 m a.g.l.

B.1 Winter Season

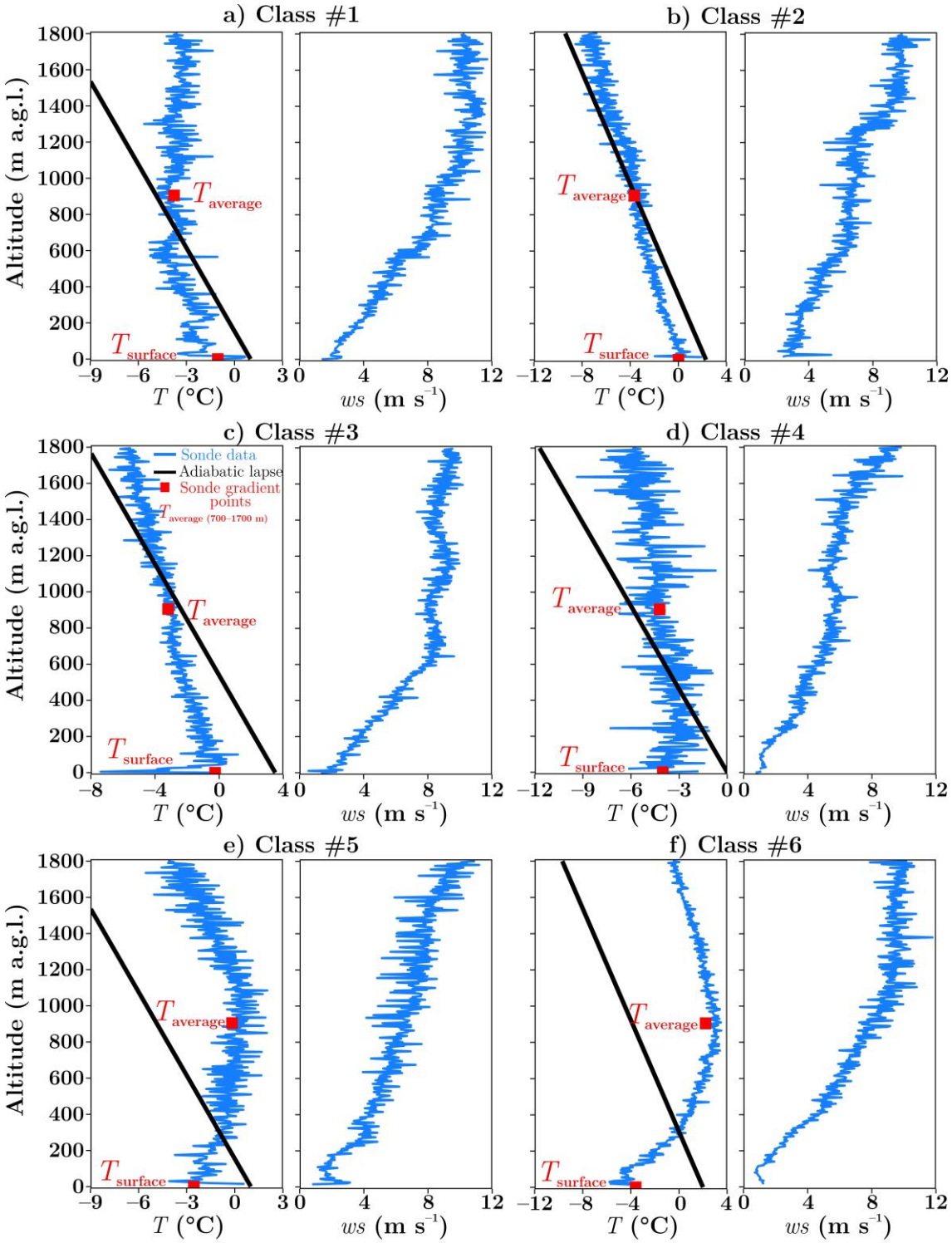


Figure B1: Morning vertical profile of air temperature and wind speed within six radon-based mixing classes in winter season: a) class #1 (mixed-fetch), b) class #2 (near-neutral), c) class #5 (weakly stable), d) class #5 (moderately stable), e) class #5 (mostly stable), and f) class #6 (persistent temperature inversion).

B.2 Spring Season

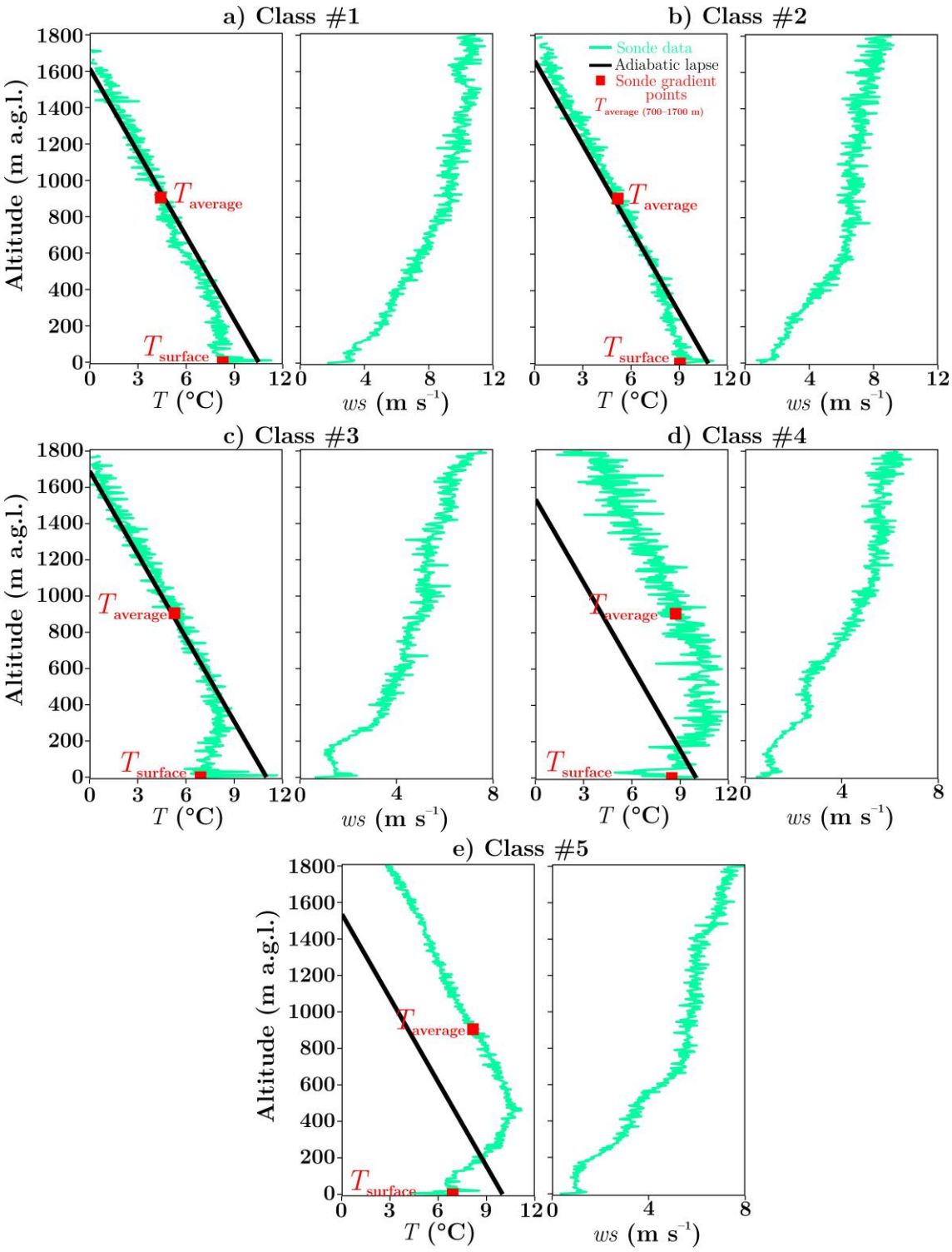


Figure B2: Morning vertical profile of air temperature and wind speed within five radon-based mixing classes in spring season: a) class #1 (mixed-fetch), b) class #2 (near-neutral), c) class #5 (weakly stable), d) class #5 (moderately stable), and e) class #5 (mostly stable).

B.3 Summer Season

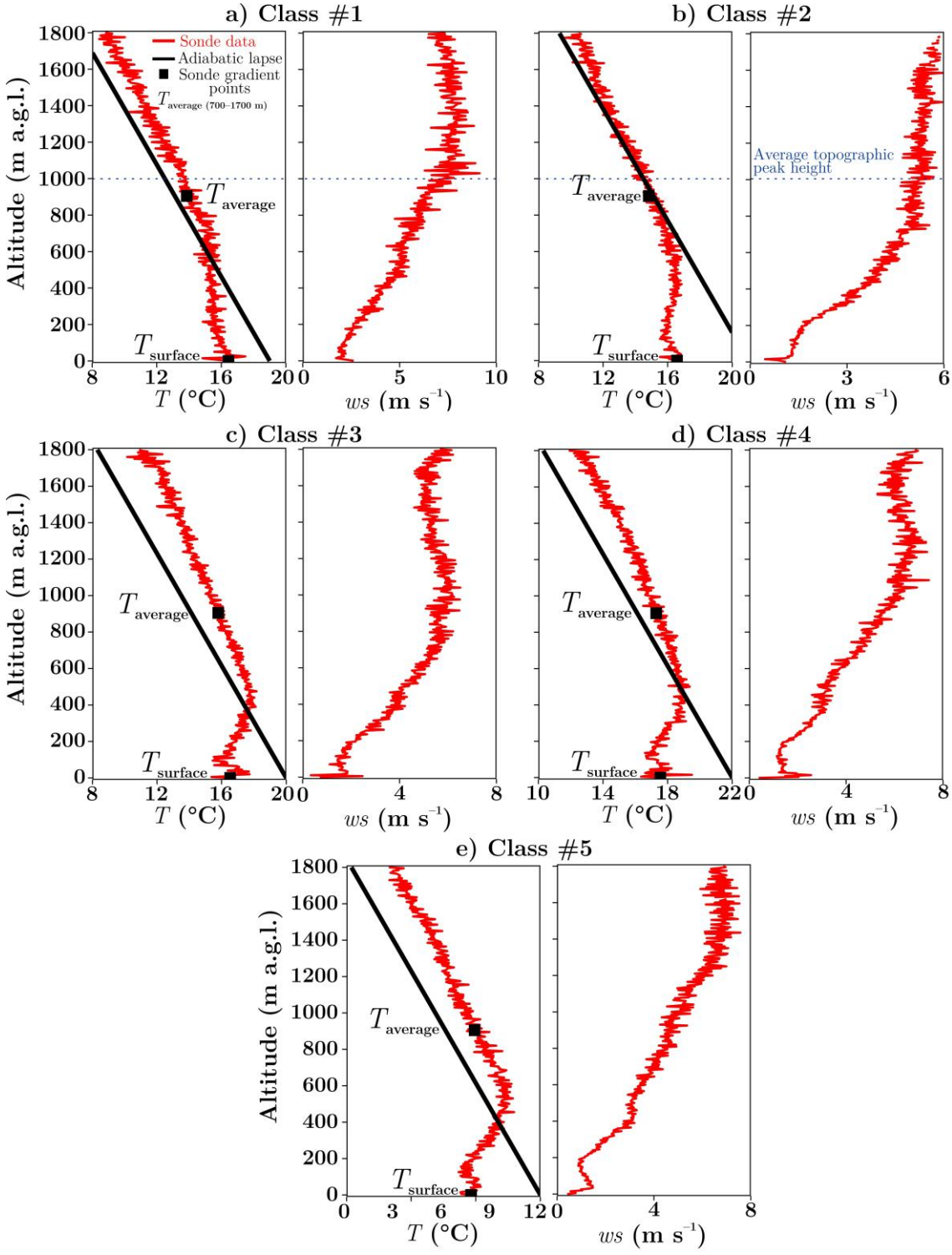


Figure B3: Morning vertical profile of air temperature and wind speed within five radon-based mixing classes in summer season: a) class #1 (mixed-fetch), b) class #2 (near-neutral), c) class #5 (weakly stable), d) class #5 (moderately stable), and e) class #5 (mostly stable).

B.4 Autumn Season

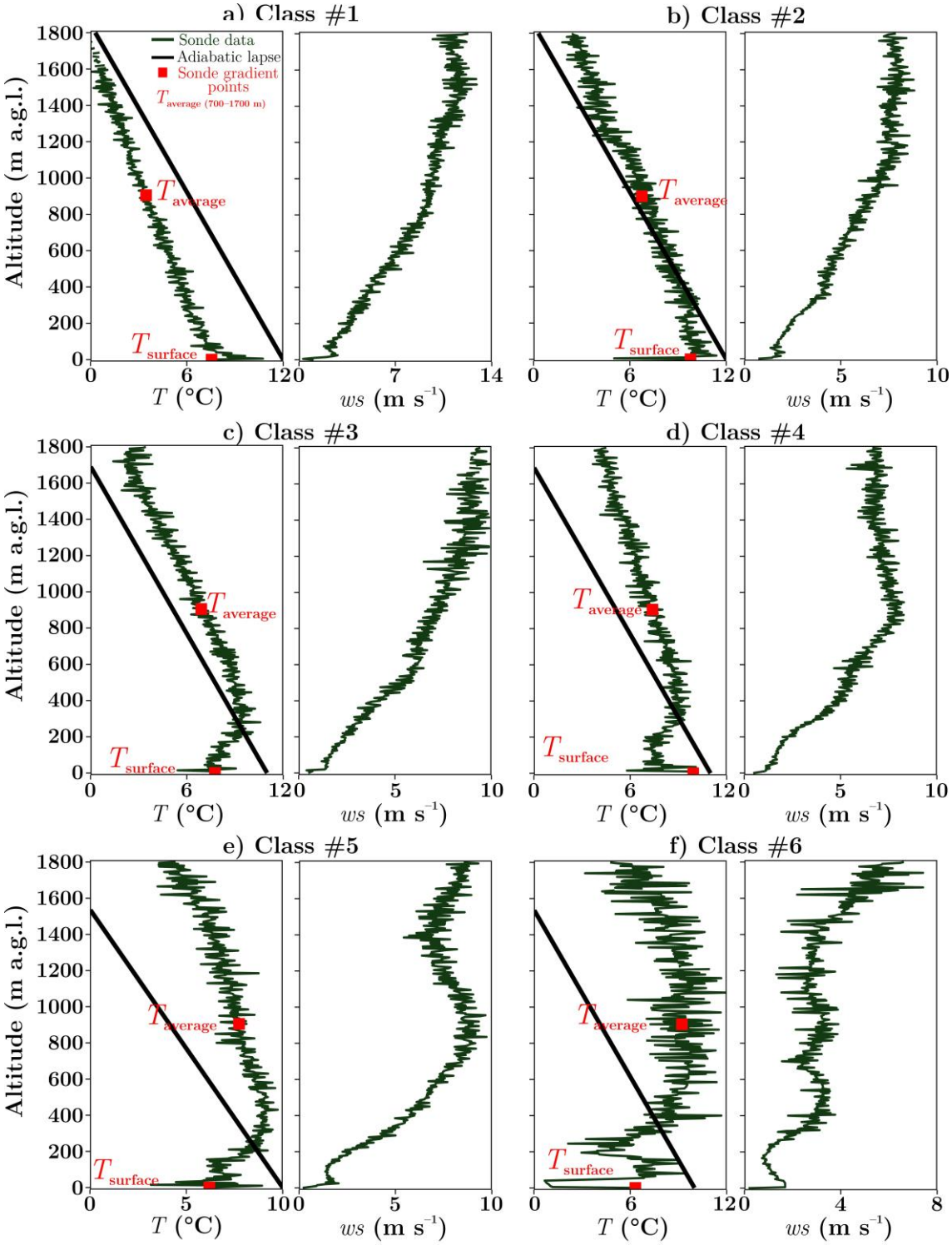


Figure B4: Morning vertical profile of air temperature and wind speed within six radon-based mixing classes in autumn season: a) class #1 (mixed-fetch), b) class #2 (near-neutral), c) class #5 (weakly stable), d) class #5 (moderately stable), e) class #5 (mostly stable), and f) class #6 (persistent temperature inversion).

References

Abumurad, K. M., & Al-Tamimi, M. (2001). Emanation power of radon and its concentration in soil and rocks. *Radiation Measurements*, *34*(1–6), 423–426.

Akber, R., & Holdsworth, S. (2004). Diffusion length and emanation coefficient of ^{220}Rn for zircon and monazite sample. *Radiation Protection in Australasia*, *21*(1), 7–13.

Anenberg, S. C., Schwartz, J., Shindell, D., Amann, M., Faluvegi, G., Klimont, Z., Janssens-maenhout, G., Pozzoli, L., Dingenen, R. Van, Vignati, E., & Emberson, L. (2012). Global air quality and health co-benefits of mitigating near-term climate change through methane and black carbon emission controls. *Environmental Health Perspectives*, *120*(6), 831–839.

Anenberg, S. C., Talgo, K., Arunachalam, S., Dolwick, P., & Jang, C. (2011). Impacts of global, regional, and sectoral black carbon emission reductions on surface air quality and human mortality. *Atmospheric Chemistry and Physics*, *11*, 10653–10691.

Anenberg, S. C., Talgo, K., Arunachalam, S., Dolwick, P., Jang, C., & West, J. J. (2011). Impacts of global, regional, and sectoral black carbon emission reductions on surface air quality and human mortality. *Atmospheric Chemistry and Physics*, *11*, 7253–7267.

Anisimov, S. V., Galichenko, S. V., Aphinogenov, K. V., Makrushin, A. P., & Shikhova, N. M. (2017) Radon volumetric acitivity and ion production in the undisturbed lower atmosphere. *Physics of the Solid Earth*, *53*(1), 147–161.

Atkinson, R. W., Carey, I. M., Kent, A. J., Staa, T. P. Van, Anderson, H. R., & Cook, D. G. (2013). Long-term exposure to outdoor air pollution and incidence of cardiovascular diseases. *Epidemiology*, *24*, 44–53.

ARSO, Slovenian Environment Agency (Slovenian: Agencija Republike Slovenije za okolje): Climate characteristics of Ljubljana - Wind Rose for the City of Ljubljana (2017). http://meteo.arso.gov.si/uploads/probase/www/climate/table/sl/by_variable/wind/Ljubljana.html.

Baasandorj, M., Hoch, S. W., Bares, R., Lin, J. C., Brown, S. S., Millet, D. B., Martin, R., Kelly, K., Zarzana, K. J., Whiteman, C. D., Dube, W. P., Tonnesen, G., Jaramillo, I. C., & Sohl, J. (2017). Coupling between chemical and meteorological processes under persistent cold-air pool conditions: evolution of wintertime $PM_{2.5}$ pollution events and N_2O_5 observations in Utah's Salt Lake Valley. *Environmental Science & Technology*, *51*, 5941–5950.

Badr, O., & Probert, S. D. (1994). Sources of atmospheric carbon monoxide. *Applied Energy*, *49*, 145–195.

Balkanski, Y. J., Jacob, D. J., Gardner, G. M., Graustein, W. C., & Turekian, K. K. (1993). Transport and residence times of tropospheric aerosols inferred from a global three-dimensional simulation of ^{210}Pb. *Journal of Geophysical Research: Atmospheres*, *98*(D11), 20573–20586.

Beeston, M., Grgić, I., Johannes, T. van E., Iskra, I., Kapun, G., & Močnik, G. (2011). Chemical and morphological characterization of aerosol particles at Mt. Krvavec, Slovenia, during the Eyjafjallajökull Icelandic volcanic eruption. *Environmental Science and Pollution Research*, *19*(1), 235–243.

Bolay, J. (2020). *Urban Planning Against Poverty*. Springer.

Bond, T. C. (2007). *Testimony for the Hearing on Black Carbon and Climate Change House Committee on Oversight and Government Reform United States House of Representatives the Honorable Henry A. Waxman, Chair October 18, 2007.*

Bond, T. C., Doherty, S. J., Fahey, D. W., Forster, P. M., Berntsen, T., Deangelo, B. J., Flanner, M. G., Ghan, S., Kärcher, B., Koch, D., Kinne, S., Kondo, Y., & Quinn, P. K. (2013). Bounding the role of black carbon in the climate system: A scientific assessment. *Journal of Geophysical Research: Atmospheres*, *118*, 5380–5552.

Bossew, P. (2003). The radon emanation power of building materials, soils and rocks. *Applied Radiation and Isotopes*, *59*(5–6), 389–392.

Bowen, B. (1994). Long-term tracer at Los Alamos, New Mexico. Part II: evaluation and comparison of several methods to determine dispersion coefficients. *Journal of Applied Meteorology and Climatology, 33*, 1236–1254.

Brauer, M., Amann, M., Burnett, R. T., Cohen, A., Dentener, F., Ezzati, M., Henderson, S. B., Krzyzanowski, M., Martin, R. V, Dingenen, R. Van, Donkelaar, A. Van, & Thurston, G. D. (2011). Exposure assessment for estimation of the global burden ofdisease attributable to outdoor air pollution. *Environmental Science & Technology*, *46*, 652–660.

Breitner, D., Arvela, H., Hellmuth, K. H., & Renvall, T. (2010). Effect of moisture content on emanation at different grain size fractions - A pilot study on granitic esker sand sample. *Journal of Environmental Radioactivity*, *101*(11), 1002–1006.

Butterweck, G., Reineking, A., Kesten, J., & Porstendörfer, J. (1994). The use of the natural radioactive noble gases radon and thoron as tracers for the study of turbulent exchange in the atmospheric boundary layer–case study in and above a wheat field. *Atmospheric Environment*, *28*(12), 1963–1969.

Carn, S. A., Yang, K., Prata, A. J., & Krotkov, N. A. (2015). Extending the long-term record of volcanic SO_2 emissions with the Ozone Mapping and Profiler Suite (OMPS) nadir mapper. *Geophysical Research Letters*, *42*, 925–932.

Carvalho, F. (1995). Origins and concentrations of ^{222}Rn, ^{210}Pb, ^{210}Bi and ^{210}Po in the surface air at Lisbon, Portugal, at the Atlantic edge of the European continental landmass. *Atmospheric Environment*, *29*(15), 1809–1819.

Chambers, S. D., Williams, A. G., Crawford, J., & Griffiths, A. D. (2015). On the use of radon for quantifying the effects of atmospheric stability on urban emissions. *Atmospheric Chemistry and Physics*, *15*(3), 1175–1190.

Chambers, S. D., Williams, A. G., Zahorowski, W., Griffiths, A., & Crawford, J. (2011). Separating remote fetch and local mixing influences on vertical radon measurements in the lower atmosphere. *Tellus, Series B: Chemical and Physical Meteorology*, *63*(5), 843–859.

Chambers, S. D., Galeriu, D., Williams, A. G., Melintescu, A., Griffiths, A. D., Crawford, J., Dyer, L., Duma, M., & Zorila, B. (2016b). Atmospheric stability effects on potential radiological releases at a nuclear research facility in Romania: Characterising the atmospheric mixing state. *Journal of Environmental Radioactivity*, *154*, 68–82.

Chambers, S. D., Podstawczyńska, A., Williams, A. G., & Pawlak, W. (2016c). Characterising the influence of atmospheric mixing state on urban heat island intensity using Radon-222. *Atmospheric Environment*, *147*, 355–368.

Chambers, S. D., Williams, A. G., Conen, F., Griffiths, A. D., Reimann, S., Steinbacher, M., Krummel, P. B., Steele, L. P., van der Schoot, M. V., Galbally, I. E., Molloy, S. B., & Barnes, J. E. (2016a). Towards a universal "Baseline" characterisation of air masses for high- and low-altitude observing stations using radon-222. *Aerosol and Air Quality Research*, *16*(3), 885–899.

Chambers, S. D, & Podstawczyńska, A. (2019). Improved method for characterising temporal variability in urban air quality part II: Particulate matter and precursors in central Poland. *Atmospheric Environment*, 117040.

Chambers, S. D, Preunkert, S., Weller, R., Hong, S., Humphries, R. S., Tositti, L., Angot, H., Legrand, M., Williams, A. G., Griffiths, A. D., Crawford, J., Simmons, J., Choi, T. J., Krummel, P. B., Molloy, S., Loh, Z., Galbally, I., Wilson, S., Magand, O., Sprovieri, F., Pirrone, N., & Dommergue, A. (2018). Characterizing atmospheric transport pathways to Antarctica and the remote Southern Ocean using Radon-222. *Frontiers in Earth Science*, *6*, 1–28.

Chambers, S. D., Podstawczyńska, A., Pawlak, W., Fortuniak, K., Williams, A., & Griffiths, A. (2019). Characterising the state of the urban surface layer using Radon-222. *Journal of Geophysical Research: Atmospheres*, *124*(2), 770–788.

Chambers, S. D., , Zahorowski, W., Matsumoto, K., & Uematsu, M. (2009). Seasonal variability of radon-derived fetch regions for Sado Island, Japan, based on 3 years of observations: 2002–2004. *Atmospheric Environment*, *43*(2), 271–279.

Chemel, C., Arduini, G., Staquet, C., Largeron, Y., Legain, D., Tzanos, D., & Paci, A. (2016). Valley heat deficit as a bulk measure of wintertime particulate air pollution in the Arve River Valley. *Atmospheric Environment*, *128*, 208–215.

Chen, R., Huang, W., Wong, C., Wang, Z., & Quoc, T. (2012). Short-term exposure to sulfur dioxide and daily mortality in 17 Chinese cities: The China air pollution and health effects study (CAPES). *Environmental Research*, *118*, 101–106.

Chen, T.-M., Gokhale, J., Shofer, S., & Kuschner, W. G. (2007). Outdoor air pollution: nitrogen dioxide, sulfur dioxide, and carbon monoxide health effects. *The American Journal of the Medical Sciences*, *333*(4), 249–256.

Clements, C. B., Whiteman, C. D., & Horel, J. D. (2003). Cold-air-pool structure and evolution in a mountain basin: Peter Sinks, Utah. *Journal of Applied Meteorology*, *42*, 752–768.

Cleugh, H., & Grimmond, S. (2012). Urban climates and global climate change. In K. Henderson-Sellers, A., McGuffie (Eds.), *The Future of the World's Climate* (pp. 47–76). Elsevier B.V.

Cohen, A. J., Anderson, H. R., Ostro, B., Dev, K., Krzyzanowski, M., Künzli, N., Gutschmidt, K., Pope, A., Romieu, I., & Samet, J. M. (2005). The global burden of disease due to outdoor air pollution. *Journal of Toxicology and Environmental Health*, *68*(13–14), 1301–1307.

Cohen, L. D., Barr, S., Krablin, R., & Newstein, H. (1972). Steady-state vertical turbulent diffusion of radon. *Journal of Geophysical Research*, *77*(15), 2654–2668.

Conceição, R., Silva, H. G., Mirão, J., Gostein, M., Fialho, L., Narvarte, L., & Collares-pereira, M. (2018). Saharan dust transport to Europe and its impact on photovoltaic performance: A case study of soiling in Portugal. *Solar Energy*, *160*, 94–102.

Crawford, J., Chambers, S., Cohen, D., Williams, A., Griffiths, A., & Stelcer, E. (2016). Assessing the impact of atmospheric stability on locally and remotely sourced aerosols at Richmond, Australia, using Radon-222. *Atmospheric Environment*, *127*, 107–117.

Davis, D., Grodzinsky, G., Kasibhatla, P., Crawford, J., Chen, G., Liu, S., Bandy, A., Thornton, D., Guan, H., & Sandholm, S. (2001). Impact of ship emissions on marine boundary layer NO_x and SO_2 distributions over the Pacific Basin. *Geophysical Research Letters*, *28*(2), 235–238.

Desideri, D., Roselli, C., Feduzi, L., & Assunta Meli, M. (2006). Monitoring the atmospheric stability by using radon concentration measurements: A study in a Central Italy site. *Journal of Radioanalytical and Nuclear Chemistry*, *270*(3), 523–530.

Dessler, A. E. (2000). *The Chemistry and Physics of Stratospheric Ozone*. Elsevier.

Díaz, J., Linares, C., Carmona, R., Russo, A., Ortiz, C., Salvador, P., & Machado, R. (2017). Saharan dust intrusions in Spain: Health impacts and associated synoptic conditions. *Environmental Research*, *156*, 455–467.

Dons, E., Int Panis, L., Van Poppel, M., Theunis, J., & Wets, G. (2012). Personal exposure to black carbon in transport microenvironments. *Atmospheric Environment*, *55*, 392–398.

Dorninger, M., Whiteman, C. D., Bica, B., Eisenbach, S., Pospichal, B., & Steinacker, R. (2011). Meteorological events affecting cold-air pools in a small basin. *Journal of Applied Meteorology and Climatology*, *50*(11), 2223–2234.

Dueñas, C., Pérez, M., Fernández, M. C., & Carretero, J. (1996). Radon concentrations in surface air and vertical atmospheric stability of the lower atmosphere. *Journal of Environmental Radioactivity*, *31*(1), 87–102.

Draxler, R. R. (2011). Hysplit (Hybrid single-particle lagrangian integrated trajectory) model access via NOAA ARL ready website. *http://ready. arl. noaa. gov/HYSPLIT. php*.

European Environment Agency (EEA). (2018). *Air quality in Europe – 2018 report*. EEA Technical Report (Issue 12/2018).

European Environment Agency (EEA). (2019). *Air quality in Europe – 2019 report*. EEA Technical Report (Issue 10/2019).

Elster, J., & Geitel, H. (1901). Über eine fernere analogie in dem elektrischen verhalten der natürlichen und der durch becquerelstrahlen abnorm leitend gemachten luft. *Physikalische Zeitschrift*, *2*, 590–593.

Etiope, G., & Martinelli, G. (2002). Migration of carrier and trace gases in the geosphere: An overview. *Physics of the Earth and Planetary Interiors*, *129*(3–4), 185–204.

Fioletov, V. E., Mclinden, C. A., Krotkov, N., Li, C., Joiner, J., Theys, N., Carn, S., & Moran, M. D. (2016). A global catalogue of large SO_2 sources and emissions derived from the Ozone Monitoring Instrument. *Atmospheric Chemistry and Physics*, *16*, 11497–11519.

Fiorella, R. P., Bares, R., Lin, J. C., Ehleringer, J. R., & Bowen, G. J. (2018). Detection and variability of combustion-derived vapor in an urban basin. *Atmospheric Chemistry and Physics*, *18*(12), 8529–8547.

Foken, T. (2006). 50 years of the Monin–Obukhov similarity theory. *Boundary-Layer Meteorology*, *119*(3), 431–447.

Galperin, B., Sukoriansky, S., & Anderson, P. S. (2007). On the critical Richardson number in stably stratified turbulence. *Atmospheric Science Letters*, *8*(3), 65–69.

Galmarini, S. (2006). One year of ^{222}Rn concentration in the atmospheric surface layer. *Atmospheric Chemistry and Physics*, *6*(10), 2865–2886.

Garg, A., Shukla, P. R., Bhattacharya, S., & Dadhwal, V. K. (2001). Sub-region (district) and sector level SO and NO emissions for India: assessment of inventories and mitigation flexibility. *Atmospheric Environment*, *35*, 703–713.

Ge, C., Wang, J., Carn, S., Yang, K., Ginoux, P., & Krotkov, N. (2016). Satellite-based global volcanic SO_2 emissions and sulfate direct radiative forcing during 2005–2012. *Journal of Geophysical Research: Atmospheres*, *121*, 3446–3464.

Gifford, F. A. (1976). Turbulent diffusion-typing schemes: A review. *Nuclear Safety, 17*, 25–43.

Gjerek, M., Koleša, T., Logar, M., Matavž, L., Murovec, M., Paradiž, B., Rus, M., & Žabkar, R. (2017). *Kakovost zraka v Sloveniji v letu 2017*. Technical Report ARSO.

Gjerek, M., Koleša, T., Logar, M., Matavž, L., Murovec, M., Rus, M., & Žabkar, R. (2018). *Kakovost zraka v Sloveniji v letu 2018*. Technical Report ARSO.

Gjerek, M., Koleša, T., Logar, M., Matavž, L., Murovec, M., Rus, M., & Žabkar, R. (2019). *Kakovost zraka v Sloveniji v letu 2019*. Technical Report ARSO.

Glojek, K., Gregorič, A., & Ogrin, M. (2018). Onesnaženost zraka s črnim ogljikom-študija primera iz Loškega Potoka. *Dela*, *50,* 5–23.

Gobbi, G. P., Barnaba, F., Liberto, L. Di, Bolignano, A., Lucarelli, F., Nava, S., Perrino, C., Pietrodangelo, A., Basart, S., Costabile, F., Dionisi, D., Rizza, U., Canepari, S., & Sozzi, R. (2019). An inclusive view of Saharan dust advections to Italy and the Central Mediterranean. *Atmospheric Environment*, *201*, 242–256.

Goudie, A. S. (2014). Desert dust and human health disorders. *Environment International*, *63*, 101–113.

Greeman, D. J., & Rose, A. W. (1996). Factors controlling the emanation of radon and thoron in soils of the eastern U.S.A. *Chemical Geology*, *129*(1–2), 1–14.

Gregorič, A., Vaupotič, J., Kardos, R., Horváth, M., Bujtor, T., & Kovács, T. (2013). Radon emanation of soils from different lithological units. *Carpathian Journal of Earth and Environmental Sciences*, *8*(2), 185–190.

Griffin, D. W. (2005). Atmospheric movement of microorganisms in clouds of desert dust and implications for human health. *Clinical Microbiology Reviews*, *20*(3), 459–477.

Grisogono, B., & Belušić, D. (2009). A review of recent advances in understanding the meso- and microscale properties of the severe Bora wind. *Tellus, Series A: Dynamic Meteorology and Oceanography*, *61A*(1), 1–16.

He, T., Chen, Y., Stanič, S., Bergant, K., Gao, F., & Hua, D. (2018). Properties of tropospheric aerosols observed over southwest Slovenia. *Journal of Quantitative Spectroscopy and Radiative Transfer*, *217*, 380–387.

Hasse, L., & H. Weber (1985). On the conversion of Pasquill categories for use over sea. *Boundary-Layer Meteorology, 31*, 177–185.

Hsu, J., & Prather, M. J. (2009). Stratospheric variability and tropospheric ozone. *Journal of Geophysical Research*, *114*, D06102.

Ielsch, G., Thieblemont, D., Labed, V., Richon, P., Tymen, G., Ferry, C., Robé, M. C., Baubron, J. C. & Bechennec, F. (2001). Radon (^{222}Rn) level variations on a regional scale: influence of the basement trace element (U, Th) geochemistry on radon exhalation rates. *Journal of Environmental Radioactivity*, *53*(1), 75–90.

The Intergovernmental Panel on Climate Change (IPCC). (2007). *The Physical Science Basis. Contribution of Working Group I to the Fourth Assessment Report of the Intergovernmental Panel on Climate Change*.

Iskandar, D., Yamazawa, H., & Iida, T. (2004). Quantification of the dependency of radon emanation power on soil temperature. *Applied Radiation and Isotopes*, *60*(6), 971–973.

Ivey, C. E., Balachandran, S., Colgan, S., Hu, Y., & Holmes, H. A. (2019). Investigating fine particulate matter sources in Salt Lake City during persistent cold air pool events. *Atmospheric Environment*, *213*, 568–578.

Jacob, J., Prather, J., Rasch, J., Beagley, R., Bergmann, J., Blackshear, W. T., Chiba, M., Chipperfield, M. P., Dignon, E., Kasibhatla, S., Kritz, M. A., Penner, E., Ramonet, M., Reeves, C. E., Stockwell, Z., Velthoven, F. J. Van, Verver, G., & Yang, H. (1997). Evaluation and intercomparison of global atmospheric transport models using ^{222}Rn and other short-lived tracer. *Journal of Geophysical Research*, *102*, 5953–5970.

Jacobi, W., & André, K. (1963). The vertical distribution of radon-222, radon-220 and their decay products in the atmosphere. *Journal of Geophysical Research*, *68*(13), 3799–3814.

Jacobson, M. Z. (2002). *Atmospheric Pollution - Histroy, Science, and Regulation*. Cambridge University Press.

Janssen, N. A. H., Hoek, G., Simic-Lawson, M., Fischer, P., Bree, L. Van, Brink, H., Keuken, M., Atkinson, R. W., Anderson, H. R., Brunekreef, B., & Cassee, F. R. (2011). Black Carbon as an additional indicator of the adverse health effects of airborne particles compared with PM_{10} and $PM_{2.5}$. *Environmental Health Perspectives*, *119*(12), 1691–1699.

Jobbágy, V., Somlai, J., Kovács, J., Szeiler, G., & Kovács, T. (2009). Dependence of radon emanation of red mud bauxite processing wastes on heat treatment. *Journal of Hazardous Materials*, *172*(2), 1258–1263.

Jurčec, B. V. (1981). On Mesoscale characteristics of Bora conditions in Yugoslavia. In *Weather and Weather Maps* (pp. 640–657).

Kahl, J. D. W., & Chapman, H. L. (2018). Atmospheric stability characterization using the Pasquill method: A critical evaluation. *Atmospheric Environment*, *187*, 196–209.

Kallos, G., Astitha, M., Katsafados, P., & Chris, S. (2006). Long-range transport of anthropogenically and naturally produced particulate matter in the Mediterranean and North Atlantic: current state of knowledge. *Journal of Applied Meteorology and Climatology*, *46*, 1230–1251.

Karanasiou, A., & Mihalopoulos, N. (2013). Air Quality in Urban Environments in the Eastern Mediterranean. In *Urban Air Quality in Europe* (pp. 219–238). Springer.

Kardos, R., Gregorič, A., Jónás, J., Vaupotič, J., Kovács, T., & Ishimori, Y. (2015). Dependence of radon emanation of soil on lithology. *Journal of Radioanalytical and Nuclear Chemistry*, *304*(3), 1321–1327.

Karstens, U., Schwingshackl, C., Schmithüsen, D., & Levin, I. (2015). A process-based ^{222}radon flux map for Europe and its comparison to long-term observations. *Atmospheric Chemistry and Physics*, *15*(22), 12845–12865.

Kaskaoutis, D. G., Dumka, U. C., Rashki, A., Psiloglou, B. E., Gavriil, A., Mo, A., Petrinoli, K., Karagiannis, D., & Kambezidis, H. D. (2019). Analysis of intense dust storms over the eastern Mediterranean in March 2018: Impact on radiative forcing and Athens air quality. *Atmospheric Environment*, *209*, 23–39.

Kaskaoutis, D. G., Rashki, A., Dumka, U. C., Mo, A., Kambezidis, H. . D., Psiloglou, B. E., Karagiannis, D., Petrinoli, K., & Gavriil, A. (2019). Atmospheric dynamics associated with exceptionally dusty conditions over the eastern Mediterranean and Greece in March 2018. *Atmospheric Research*, *218*, 269–284.

Knox, J. A. & Ackerman, S. (2010). *Meteorology: Understanding the Atmosphere*. Cengage Learning.

Kochowska, E., Kozak, K., Kozłowska, B., & Mazur, J. (2009). Test measurements of thoron concentration using two ionization chambers AlphaGUARD vs. radon monitor RAD7. *Nukleonika*, *54*(3), 189–192.

Kovács, T., Szeiler, G., Fábián, F., Kardos, R., Gregorič, A., & Vaupotič, J. (2013). Systematic survey of natural radioactivity of soil in Slovenia. *Journal of Environmental Radioactivity*, *122*, 70–78.

Kumar, P., Morawska, L., Birmili, W., Paasonen, P., Hu, M., Kulmala, M., Harrison, R. M., Norford, L., & Britter, R. (2014). Ultrafine particles in cities. *Environment International*, *66*, 1–10.

Lambert, G., Polian, G., & Taupin, D. (1970). Existence of periodicity in radon concentrations and in the large-scale circulation at lower altitudes between 40° and 70° south. *Journal of Geophysical Research*, *75*(12), 2341–2345.

Lareau, N. P., Crosman, E., Whiteman, C. D., Horel, J. D., Hoch, S. W., Brown, W. O. J., & Horst, T. W. (2013). The persistent cold-air pool study. *Bulletin of the American Meteorological Society*, *94*(1), 51–63.

Largeron, Y., & Staquet, C. (2016a). Persistent inversion dynamics and wintertime PM_{10} air pollution in Alpine valleys. *Atmospheric Environment*, *135*, 92–108.

Largeron, Y., & Staquet, C. (2016b). The Atmospheric Boundary Layer during Wintertime Persistent Inversions in the Grenoble Valleys. *Frontiers in Earth Science*, *4*(70), 1–19.

Lee, K. Y., Cho, S. Y., Yoon, Y. Y., & Jang, Y. N. (2012). Determination of the radon emanation fraction from phosphogypsum using LSC. *Journal of Radioanalytical and Nuclear Chemistry*, *291*(1), 197–200.

Lehner, M., Whiteman, C. D., Hoch, S. W., Jensen, D., Pardyjak, E. R., Leo, L. S., Di Sabatino, S., & Fernando, H. J. S. (2015). A case study of the nocturnal boundary layer evolution on a slope at the foot of a desert mountain. *Journal of Applied Meteorology and Climatology*, *54*(4), 732–751.

Lelieveld, J., Evans, J. S., Fnais, M., Giannadaki, D., & Pozzer, A. (2015). The contribution of outdoor air pollution sources to premature mortality on a global scale. *Nature Communications*, *525*(7569), 367–371.

Levin, I., Born, M., Cuntz, M., Langendörfer, U., Mantsch, S., Naegler, T., Schmidt, M., Varlagin, A., Verclas, S., & Wagenbach, D. (2002). Observations of atmospheric variability and soil exhalation rate of radon-222 at a Russian forest site: Technical approach and deployment for boundary layer studies. *Tellus, Series B: Chemical and Physical Meteorology*, *54*(5), 462–475.

Li, C., Zhang, Q., Krotkov, N. A., Streets, D. G., He, K., Tsay, S. C., & Gleason, J. F. (2010). Recent large reduction in sulfur dioxide emissions from Chinese power plants observed by the Ozone Monitoring Instrument. *Geophysical Research Letters*, *37*, L08807.

Lim, S. S., Vos, T., Flaxman, A. D., Danaei, G., Shibuya, K., Adair-rohani, H., Almazroa, M. A., Amann, M., Barker-collo, S., Baxter, A., Bell, M. L., Blore, J. D., Blyth, F., Bonner, C., Borges, G., Bourne, R., Boussinesq, M., Brauer, M., Brooks, P., … & Ezzati, M. (2012). A comparative risk assessment of burden of disease and injury attributable to 67 risk factors and risk factor clusters in 21 regions, 1990–2010: a systematic analysis for the Global Burden of Disease Study 2010. *The Lancet*, *380*, 2224–2260.

Luna, R. E., & H. W. Church. (1972). A comparison of turbulence intensity and stability ratio measurements to Pasquill stability classes. *Journal of Applied Meteorology, 11*, 663–669.

Madrigano, J., Kloog, I., Goldberg, R., Coull, B. A., & Mittleman, M. A. (2013). Long-term exposure to $PM_{2.5}$ and incidence of acute myocardial infarction. *Environmental Health Perspectives*, *192*(2), 192–196.

Mazur, J., & Kozak, K. (2014). Complementary system for long term measurements of radon exhalation rate from soil. *Review of Scientific Instruments*, *85*(2), 022104.

Melintescu, A., Chambers, S. D., Crawford, J., Williams, A. G., Zorila, B., & Galeriu, D. (2018). Radon-222 related influence on ambient gamma dose. *Journal of Environmental Radioactivity*, *189*, 67–78.

Middleton, N., Yiallouros, P., Kleanthous, S., Kolokotroni, O., Schwartz, J., Dockery, D. W., Demokritou, P., & Koutrakis, P. (2008). A 10-year time-series analysis of respiratory and cardiovascular morbidity in Nicosia, Cyprus: the effect of short-term changes in air pollution and dust storms. *Environmental Health*, *16*, 1–16.

Millán, M., Salvador, R., Mantilla, E., & Kallos, G. (1997). Photooxidant dynamics in the Mediterranean basin in summer: Results from European research projects. *Journal of Geophysical Research*, *102*(D7), 8811–8824.

Mills, G., Cleugh, H., Emmanuel, R., Endlicher, W., Erell, E., Mcgranahan, G., Ng, E., Nickson, A., Rosenthal, J., & Steemer, K. (2010). Climate information for improved planning and management of mega cities (Needs Perspective). *Procedia Environmental Sciences*, *1*, 228–246.

Mohan, S. M. (2016). An overview of particulate dry deposition: measuring methods, deposition velocity and controlling factors. *International Journal of Environmental Science and Technology*, *13*(1), 387–402.

Mole, M., Wang, L., Stanič, S., Bergant, K., Eichinger, W. E., Ocaña, F., Strajnar, B., Škraba, P., Vučković, M., & Willis, W. B. (2017). Lidar measurements of Bora wind effects on aerosol loading. *Journal of Quantitative Spectroscopy and Radiative Transfer*, *188*, 39–45.

Monks, P. S., Archibald, A. T., Colette, A., Cooper, O., Coyle, M., Derwent, R., Fowler, D., Granier, C., Law, K. S., Mills, G. E., Stevenson, D. S., Tarasova, O., Thouret, V., Von Schneidemesser, E., Sommariva, R., Wild, O., & Williams, M. L. (2015). Tropospheric ozone and its precursors from the urban to the global scale from air quality to short-lived climate forcer. *Atmospheric Chemistry and Physics*, *15*(15), 8889–8973.

Moses, H., Lucas, H. F., & Zerbe, G. A. (1963). The effect of meteorological variables upon radon concentration three feet above the ground. *Journal of the Air Pollution Control Association*, *13*(1), 12–19.

Murn, T., & Stepišnik, M. (2019). *Intercomparison measurements of Radon-222 concentrations at ICJT* (in Slovenian).

Nazaroff, W. W. (1992). Radon transport from soil to air. *Reviews of Geophysics*, *30*(2), 137–160.

Nazaroff, W. W., & Nero, A. V. (1988). *Radon and Its Decay Products in Indoor Air*. John Wiley and Sons Inc., New York, NY (USA).

Nieuwstadt, Frans T. M. (1984). The turbulent structure of the stable, nocturnal boundary layer. *Journal of the Atmospheric Sciences, 41*(14), 2202–2216.

Oberdörster, G., Oberdörster, E., & Oberdörster, J. (2005). Nanotoxicology: An emerging discipline evolving from studies of ultrafine particles. *Environmental Health Perspectives*, *113*(7), 823–839.

Oke, T. R., Mills, G., Christen, A., & Voogt, J. A. (2017). *Urban Climates*. Cambridge University Press.

Pak, M. (1992). Ljubljana. In M. Javornik (Ed.), *Enciklopedija Slovenije* (pp. 218–220).

Pal, S., Lopez, M., Schmidt, M., Ramonet, M., Gibert, F., & Ciais, P. (2015). Investigation of the atmospheric boundary layer depth variability and its impact on the ^{222}Rn concentration at a rural site in France. *Journal of Geophysical Research: Atmospheres*, *120*, 623–643.

Pandey, P., Kumar, D., Prakash, A., Masih, J., Singh, M., Kumar, S., Jain, V. K., & Kumar, K. (2012). A study of urban heat island and its association with particulate matter during winter months over Delhi. *Science of the Total Environment, 414*, 494–507.

Panofsky, H.A., & Dutton, J.A. (1984). *Atmospheric Turbulence - Models and Methods for Engineering Applications*. John Wiley and Sons.

Papachristodoulou, C., Ioannides, K., & Spathis, S. (2007). The effect of moisture content on radon diffusion through soil: assessment in laboratory and field experiments. *Health Physics*, *92*(3), 257–264.

Pasquill, F., & Smith, F. B. (1983). *Atmospheric diffusion: Study of the Dispersion of Windborne Material from Industrial and Other Sources*. 3rd ed. Ellis Horwood Ltd., Chichester.

Pasquill, F. (1961). The estimation of the dispersion of windborne material. *Meteorological Magazine*, *90*, 33–49.

Pearson, J. E., & Jones, G. E. (1965). Emanation of radon-222 from soils and its use as a tracer. *Journal of Geophysical Research*, *70*(20), 5279–5290.

Peled, R., Friger, M., Bolotin, A., Bibi, H., Epstein, L., Pilpel, D., & Scharf, S. (2005). Fine particles and meteorological conditions are associated with lung function in children with asthma living near two power plants. *Public Health*, *119*, 418–425.

Perrino, C., Pietrodangelo, A., & Febo, A. (2001). An atmospheric stability index based on radon progeny measurements for the evaluation of primary urban pollution. *Atmospheric Environment*, *35*, 5235–5244.

Petkovšek, Z. (1978). Relief meteorologically relevant characteristics of basins (air land interactions in quasi-closed system). *Zeitschrift Für Meteorologie*, *28*(6), 333–340.

Petkovšek, Z. (1985). The termination of air pollution periods in valley basins. *Zeitschrift Für Meteorologie*, *35*(6), 370–372.

Poberžnik, M., & Štrumbelj, E. (2016). The effects of air mass transport, seasonality, and meteorology on pollutant levels at the Iskrba regional background station (1996–2014). *Atmospheric Environment*, *134*, 138–146.

Podstawczyńska, A. (2016). Differences of near-ground atmospheric Rn-222 concentration between urban and rural area with reference to microclimate diversity. *Atmospheric Environment*, *126*, 225–234.

Podstawczyńska, A., & Chambers, S. D. (2018). Radon-based technique for the analysis of atmospheric stability – a case study from Central Poland. *Nukleonika*, *63*(2), 47–54.

Poje, D. (1992). Wind persistence in Croatia. *International Journal of Climatology*, *12*(6), 569–586.

Pope, C. A., & Dockery, D. W. (2006). Health effects of fine particulate air pollution: Lines that connect. *Journal of the Air and Waste Management Association*, *56*(6), 709–742.

Pucer, J. F., & Štrumbelj, E. (2018). Impact of changes in climate on air pollution in Slovenia between 2002 and 2017. *Environmental Pollution*, *242*, 398–406.

Querol, X., Alastuey, A., Reche, C., Orio, A., Pallares, M., Reina, F., Dieguez, J. J., Mantilla, E., Escudero, M., Alonso, L., Gangoiti, G., & Millán, M. (2016). On the origin of the highest ozone episodes in Spain. *Science of the Total Environment*, *572*, 379–389.

Querol, Xavier, Alastuey, A., Gangoiti, G., Perez, N., Lee, H. K., Eun, H. R., Park, Y., Mantilla, E., Escudero, M., Titos, G., Alonso, L., Temime-Roussel, B., Marchand, N., Moreta, J. R., Revuelta, M. A., Salvador, P., Artíñano, B., Dos Santos, S. G., Anguas, M., Alberto, N., Saiz-Lopez, A., Harrison, M., Millán, M., & Ahn, K. H. (2018). Phenomenology of summer ozone episodes over the Madrid Metropolitan Area, central Spain. *Atmospheric Chemistry and Physics*, *18*(9), 6511–6533.

Rakovec, J., Merše, J., Jernej, S., & Paradiž, B. (2002). Turbulent dissipation of the cold-air pool in a basin: Comparison of observed and simulated development. *Meteorology and Atmospheric Physics*, *79*(3–4), 195–213.

Rao, Y. P., & Desai, B. N. (1969). Monsoon circulation from observations of natural radon. *Earth and Planetary Science Letters*, *9*, 56–60.

Rodriguez-Villamizar, L. A., Magico, A., Osornio-Vargas, A., & Rowe, B. H. (2015). The effects of outdoor air pollution on the respiratory health of Canadian children: A systematic review of epidemiological studies. *Canadian Respiratory Journal*, *22*(5), 282–293.

Russo, A., Trigo, R. M., Martins, H., & Mendes, M. T. (2014). NO_2, PM_{10} and O_3 urban concentrations and its association with circulation weather types in Portugal. *Atmospheric Environment*, *89*(2), 768–785.

Saikawa, E., Naik, V., Horowitz, L. W., Liu, J., & Mauzerall, D. L. (2009). Present and potential future contributions of sulfate, black and organic carbon aerosols from China to global air quality, premature mortality and radiative forcing. *Atmospheric Environment*, *43*(17), 2814–2822.

Šajn, R., Gosar, M., Bidovec, M., Pirc, S., & Alijagić, J. (2011). Geochemical mapping of Ljubljana urban and suburban area, Slovenia. In *Mapping the Chemical Environment of Urban Areas* (pp. 375–392).

Sakoda, A., Hanamoto, K., Ishimori, Y., Kataoka, T., Kawabe, A., & Yamaoka, K. (2010b). First model of the effect of grain size on radon emanation. *Applied Radiation and Isotopes*, *68*(6), 1169–1172.

Sakoda, A., Nishiyama, Y., Hanamoto, K., Ishimori, Y., Yamamoto, Y., Kataoka, T., Kawabe, A., & Yamaoka, K. (2010a). Differences of natural radioactivity and radon emanation fraction among constituent minerals of rock or soil. *Applied Radiation and Isotopes*, *68*(6), 1180–1184.

Salvador, P., Pey, J., Artíñano, B., Bustos, J. J. De, Alastuey, A., & Querol, X. (2014). African dust outbreaks over the western Mediterranean Basin: 11-year characterization of atmospheric circulation patterns and dust source areas. *Atmospheric Chemistry and Physics*, *14*, 6759–6775.

Salzano, R., Pasini, A., Casasanta, G., Cacciani, M., & Perrino, C. (2016). Quantitative interpretation of air radon progeny fluctuations in terms of stability conditions in the atmospheric boundary layer. *Boundary-Layer Meteorology*, *160*(3), 529–550.

Salzano, R., Pasini, A., Ianniello, A., Mazzola, M., Traversi, R., & Udisti, R. (2018). High-time resolved radon-progeny measurements in the Arctic region (Svalbard Islands, Norway): results and potentialities. *Atmospheric Chemistry and Physics*, *18*, 6959–6969.

Sandradewi, J., Prévôt, A. S. H., Weingartner, E., Schmidhauser, R., Gysel, M., & Baltensperger, U. (2008). A study of wood burning and traffic aerosols in an Alpine valley using a multi-wavelength Aethalometer. *Atmospheric Environment*, *42*(1), 101–112.

Satterly, J. (1910). On the amount of radium emanation in the lower regions of the atmosphere and its variation with the weather. *The London, Edinburgh, and Dublin Philosophical Magazine and Journal of Science*, *20*(115), 1–36.

Saxena, P., & Sonwani, S. (2019). *Criteria Air Pollutants and their Impact on Environmental Health*. Springer Singapore.

Schery, S. D., & Huang, S. (2004). An estimate of the global distribution of radon emissions from the ocean. *Geophysical Research Letters*, *31*(19), L19104.

Schumann, R. R., & Gundersen, L. C. S. (1996). Geologic and climatic controls on the radon emanation coefficient. *Environment International*, *22*, 439–446.

Seinfeld, J. H., & Pandis, S. N. (2006). *Atmospheric Chemistry and Physics: From Air Pollution to Climate Change*. John Willey & Sons. Inc., New York.

Sesana, L., Caprioli, E., & Marcazzan, G. M. (2003). Long period study of outdoor radon concentration in Milan and correlation between its temporal variations and dispersion properties of atmosphere. *Journal of Environmental Radioactivity*, *65*(2), 147–160.

Sesana, L., Ottobrini, B., Polla, G., & Facchini, U. (2006). ^{222}Rn as indicator of atmospheric turbulence: Measurements at Lake Maggiore and on the pre-Alps. *Journal of Environmental Radioactivity*, *86*(2), 271–288.

Shindell, D., Shindell, D., Kuylenstierna, J. C. I., Vignati, E., Dingenen, R. Van, Amann, M., Klimont, Z., Anenberg, S. C., Muller, N., Janssens-maenhout, G., Raes, F., Schwartz, J., Faluvegi, G., Pozzoli, L., Kupiainen, K., Höglund-isaksson, L., Emberson, L., Streets, D., Ramanathan, V., Hicks, K., Oanh, N., Milly, G., Williams, M., Demkine, V., & Fowler, D. (2012). Simultaneously mitigating near-term climate change and improving human health and food security. *Science*, *335*, 183–188.

Silcox, G. D., Kelly, K. E., Crosman, E. T., Whiteman, C. D., & Allen, B. L. (2012). Wintertime $PM_{2.5}$ concentrations during persistent, multi-day cold-air pools in a mountain valley. *Atmospheric Environment*, *46*, 17–24.

Silva, R. A., West, J. J., Zhang, Y., C, A. S., Lamarque, J.-F., Shindell, D. T., Collins, W. J., Dalsoren, S., Faluvegi, G., Folberth, G., Horowitz, L. W., Nagashima9, T., Naik, V., Rumbold, S., Skeie, R., Sudo, K., Takemura, T., Bergmann, D., Cameron-Smith, P., Cionni, I., Doherty, R., Eyring, V., Josse, B., MacKenzie, I. A., Plummer, D., Righi, M., Stevenson, D., Strode, S., Sophie, S., & Zeng, G. (2013). Global premature mortality due to anthropogenic outdoor air pollution and the contribution of past climate change. *Environmental Research Letters*, *8*, 034005.

Smith, R. (1985). On severe downslope winds. *Journal of the Atmospheric Sciences*, *42*(23), 2597–2603.

Smith, S. J., Aardenne, J. Van, Klimont, Z., Andres, R. J., Volke, A., & Arias, S. D. (2011). Anthropogenic sulfur dioxide emissions: 1850–2005. *Atmospheric Measurment Techniques*, *11*, 1101–1116.

Stevenson, D. S., Dentener, F. J., Schultz, M. G., Ellingsen, K., Noije, T. P. C. Van, Wild, O., Zeng, G., Amann, M., Atherton, C. S., Bell, N., Bergmann, D. J., & Bey, I. (2006). Multimodel ensemble simulations of present-day and near-future tropospheric ozone. *Journal of Geophysical Research*, *111*, D08301.

Stevenson, D. S., Young, P. J., Naik, V., Lamarque, J., Shindell, D. T., Voulgarakis, A., & Skeie, R. B. (2013). Tropospheric ozone changes, radiative forcing and attribution to emissions in the Atmospheric Chemistry and Climate Model Intercomparison Project (ACCMIP). *Atmospheric Chemistry and Physics*, *13*, 3063–3085.

Stull, R. (1988). *An Introduction to Boundary Layer Meteorology.* Kluwer Academic Publishers.

Sun, J., Birmili, W., Hermann, M., Tuch, T., Weinhold, K., Spindler, G., Schladitz, A., Bastian, S., Löschau, G., Cyrys, J., Gu, J., Flentje, H., Briel, B., Asbach, C., Kaminski, H., Ries, L., Sohmer, R., Gerwig, H., Wirtz, K., … & Wiedensohler, A. (2019). Variability of black carbon mass concentrations, sub-micrometer particle number concentrations and size distributions: results of the German Ultrafine Aerosol Network ranging from city street to High Alpine locations. *Atmospheric Environment*, *202*, 256–268.

Szegvary, T., Conen, F., & Ciais, P. (2009). European ^{222}Rn inventory for applied atmospheric studies. *Atmospheric Environment*, *43*(8), 1536–1539.

Szegvary, T., Leuenberger, M. C., & Conen, F. (2007). Prediciting terrestrial ^{222}Rn flux using gamma dose rate as a proxy. *Atmospheric Chemistry and Physics*, 2789–2795.

Tanner, A. B. (1980). Radon migration in the ground: a supplementary review. *US Geological Survey Open-File Report*, *78*(1050), 61.

Thurston, D. (2008). Outdoor air pollution: sources, atmospheric transport, and human health effects. In H. Kris (Ed.), *International Encyclopedia of Public Health* (pp. 700–712). Academic Press, Oxford.

Tomasi, C., & Lupi, A. (2017). Primary and secondary sources of atmospheric aerosol. In C. Tomasi, S. Fuzzi, & G. R. Kim (Eds.), *Atmospheric Aerosols.* Wiley Online Library.

Tonne, C., Melly, S., Mittleman, M., Coull, B., Goldberg, R., & Schwartz, J. (2007). A case-control analysis of exposure to traffic and acute myocardial infarction. *Environmental Health Prespectives, 115*(1), 53–57.

Turekian, K. K., Nozaki, Y., & Benninger, L. K. (1977). Geochemistry of atmospheric radon and radon products. *Annual Review of Earth and Planetary Sciences*, *5*(1), 227–255.

Turner, B. (1964). A diffusion model for an urban area. *Journal of Applied Meteorology*, *3*, 83–91.

United Nations Economic Commission for Europe (UNECE). (2010). *Hemispheric transport of air pollution 2010. Part A: ozone and particulate matter, air pollution studies*. United Nations Publication, New York and Geneva.

Vaupotič, J., Kobal, I., & Križman, M. J. (2010). Background outdoor radon levels in Slovenia. *Nukleonika*, *55*, 579–582.

Vrhovec, T. (1990). Analysis of mesometeorological temperature fields. *Meteorology and Atmospheric Physics*, *43*(1–4), 235–240.

Wang, F., Chambers, S. D., Zhang, Z., Williams, A. G., Deng, X., Zhang, H., Lonati, G., Crawford, J., Griffiths, A. D., Ianniello, A., & Allegrini, I. (2016). Quantifying stability influences on air pollution in Lanzhou, China, using a radon-based "stability monitor": Seasonality and extreme events. *Atmospheric Environment*, *145*, 376–391.

Wang, L., Liu, J., Gao, Z., Li, Y., Huang, M., Fan, S., Zhang, X., & Yang, Y. (2019). Vertical observations of the atmospheric boundary layer structure over Beijing urban area during air pollution episodes. *Atmospheric Chemistry and Physics*, *19*(10), 6949–6967.

Whiteman, C. D. (1982). Breakup of temperature inversions in deep mountain valleys: Part I. Observations. *Journal of Applied Meteorology, 21,* 270–289.

Whiteman, C. D., Eisenbach, S., Pospichal, B., & Steinacker, R. (2004). Comparison of vertical soundings and sidewall air temperature measurements in a small Alpine Basin. *Journal of Applied Meteorology*, *43*(11), 1635–1647.

Whiteman, C. D., Hoch, S. W., Horel, J. D., & Charland, A. (2014). Relationship between particulate air pollution and meteorological variables in Utah's Salt Lake Valley. *Atmospheric Environment*, *94*, 742–753.

World Health Organization (WHO). (2003). *Health aspects of air pollution with particulate matter, ozone and nitrogen dioxide*. Geneva: World Health Organization.

World Health Organization (WHO). (2012). *Health effects of black carbon*. Geneva: World Health Organization.

World Health Organization (WHO). (2014). *Ambient (outdoor) air quality and health*. Geneva: World Health Organization.

Wilkening, M., & Clements, E. (1975). Radon-222 from the ocean surface. *Journal of Geophysical Research*, *80*(27), 3828–3830.

Williams, A. G., Chambers, S., & Griffiths, A. (2013). Bulk mixing and decoupling of the nocturnal stable boundary layer characterized using a ubiquitous natural tracer. *Boundary-Layer Meteorology*, *149*(3), 381–402.

Williams, Alastair G., Chambers, S. D., Conen, F., Reimann, S., Hill, M., Griffiths, A. D., & Crawford, J. (2016). Radon as a tracer of atmospheric influences on traffic-related air pollution in a small inland city. *Tellus, Series B: Chemical and Physical Meteorology*, *68*(1), 1–21.

Yao, W., & Zhong, S. (2009). Nocturnal temperature inversions in a small, enclosed basin and their relationship to ambient atmospheric conditions. *Meteorology and Atmospheric Physics*, *103*(1–4), 195–210.

Yoshino, M. (1976). *Local Wind Bora*. University of Tokyo Press.

Young, P. J., Archibald, A. T., Bowman, K. W., Lamarque, J., Naik, V., Stevenson, D. S., & Tilmes, S. (2013). Pre-industrial to end 21st century projections of tropospheric ozone from the Atmospheric Chemistry and Climate Model Intercomparison Project (ACCMIP). *Atmospheric Chemistry and Physics*, *13*, 2063–2090.

Zahorowski, W., Chambers, S. D., & Henderson-Sellers, A. (2004). Ground based radon-222 observations and their application to atmospheric studies. *Journal of Environmental Radioactivity*, *76*(1–2), 3–33.

Zahorowski, W., Chambers, S. D., Wang, T., Kang, C. H., Uno, I., Poon, S., Oh, S. N., Werczynski, S., Kim, J., & Henderson-Sellers, A. (2005). Radon-222 in boundary layer and free tropospheric continental outflow events at three ACE-Asia sites. *Tellus, Series B: Chemical and Physical Meteorology*, *57*(2), 124–140.

Zhang, Y., Li, C., Krotkov, N. A., Joiner, J., Fioletov, V., & Mclinden, C. (2017). Continuation of long-term global SO_2 pollution monitoring from OMI to OMPS. *Atmospheric Measurment Techniques*, *10*, 1495–1509.

Zhuo, W., Guo, Q., Chen, B., & Cheng, G. (2008). Estimating the amount and distribution of radon flux density from the soil surface in China. *Journal of Environmental Radioactivity*, *99*, 1143–1148.

Bibliography

Journal Articles

Kikaj, D., Chambers, S., Kobal, M., Crawford, J., & Vaupotič, J. (2020). Characterizing atmospheric controls on winter urban pollution in a topographic basin setting using Radon-222. *Atmospheric Research*, 327, 104838. doi: 10.1016/j.atmosres.2019.104838

Kikaj, D., Vaupotič, J., & Chambers, S. (2019). Identifying persistent temperature inversion events in a subalpine basin using radon-222. *Atmospheric Measurement Techniques*, 12, 4455–4477. doi:10.5194/amt-12-4455-2019

Kikaj, D., Chambers, S., & Vaupotič, J. (2019). Radon-based atmospheric stability classification in contrasting sub-Alpine and sub-Mediterranean environments. *Journal of Environmental Radioactivity*, 203, 125–134. doi:10.1016/j.jenvrad.2019.03.010

Kikaj, D., & Vaupotič, J., (2019). Effective doses due to outdoor and indoor radon at a Mediterranean site. *Radiation Protection Dosimetry*, 1–5. doi: 10.1093/rpd/ncz155

Kikaj, D., Kovács, T., & Vaupotič, J. (2019). Role of meteorology and lithology in the temporal variation of the outdoor radon level. *Radiation Protection Dosimetry*, 184, 474–478. doi:10.1093/rpd/ncz079

Kikaj, D., & Vaupotič, J. (2017) Parameters influencing deviation of radon concentration from its typical diurnal pattern in the winter and summer. *Geologica Macedonica*, 31, 157–170.

Conference Paper

Kikaj, D., Džerovski, S., Chambers, S. D., & Vaupotič, J. (2020). Radon-based atmospheric mixing classification: identifying uncertainties by application of machine learning methods. In *VII. Terrestrial Radioisotopes in Environment International Conference on Environmental Protection*. Veszprém, Hunagry. Social Organization for Radioecological Cleanliness.

Kikaj, D., & Vaupotič, J. (2019) Radon-based method to assess atmospheric stability under winter conditions in Ljubljana. In *11th Student Conference of the Jožef Stefan International Postgraduate School and the 13th Day of Young Researchers (KMBO Conference).*

Kikaj, D., Chambers, S., & Vaupotič, J. (2019). Assessing urban pollution variability using radon as a tracer of atmospheric dynamics. In *25th Annual Meeting of the Slovenian Chemical Society.* Maribor, Slovenia.

Kikaj, D., & Vaupotič, J. (2018). Role of meteorology and lithology in temporal variation of outdoor radon level. In *9th International Conference on High Level Environmental Radiation Areas, ICHLERA 2018.* Aomori, Japan. Hirosaki University.

Kikaj, D., & Vaupotič, J. (2018). Radon as an indicator of atmospheric stability over the Ljubljana Basin in the cold season. In *VI. Terrestrial Radioisotopes in Environment, International Conference on Environmental Protection.* Veszprém, Hunagry. Social Organization for Radioecological Cleanliness.

Kikaj, D., & Vaupotič, J. (2018). The impact of 'radon-based stability' on aerosol particle pollution at Ljubljana Basin. In *10th Jožef Stefan International Postgraduate School Students' Conference and 12th Young Researchers' Day.* Piran, Slovenia.

Wang, L., Bergant, K., Bervida, M., Drinovec, L., Eichinger, W., Gregorič, A., Kikaj, D. Močnik, G., Mole, M., Vaupotič, J., & Stanič, S. (2017). Long-term investigation of aerosol variability in the boundary layer over Vipava valley based on lidar observations and black carbon measurements. In *Fifth International Symposium on Atmospheric Light Scattering and Remote Sensing ISALSaRS'17.* Hefei, China.

Kikaj, D., Gregorič, A., & Vaupotič, J. (2017). Outdoor radon as a tracer for planetary boundary layer mixing. In *9th Jožef Stefan International Postgraduate School Students' Conference and 11th Young researchers' Day.* Ljubljana, Slovenia.

Other Publications (Invited Lectures)

Vaupotič, J., & Kikaj, D. (2018). Outdoor radon as a tracer in the stability of atmosphere: invited talk, 9 March 2018, Hokkaido University, Sapporo, Japan.

Kikaj, D., & Vaupotič, J. (2018). Stability of atmosphere observed by radon monitoring in outdoor air: invited talk, National Institutes for Quantum and Radiological Science and Technology, 13 March 2018, Inage, Chiba, Japan.

Biography

The author of this thesis, Dafina Kikaj, obtained the title Bachelor of Physics and Chemistry at the Faculty of Education, University of Prishtina. In the academic year 2016 she was awarded MSc degree in Ecotechnologies, Study Programme Ecotechnologies at the Jožef Stefan International Postgraduate School, Ljubljana, Slovenia. In October 2016, she was selected as a PhD candidate at the Jožef Stefan International Postgraduate School, Ljubljana, Slovenia, under the supervision of Prof. Dr. Janja Vaupotič at the Department of Environmental Sciences and Dr. Scott Dudley Chambers at the Australian Nuclear Science and Technology Organisation, Sydney, Australia. Her research focus on using radon as a tracer for atmospheric science, particularly on characterizing synoptic- and diurnal-timescale changes in the atmosphere mixing state.